VIBRATION-BASED DAMAGE DETECTION OF STRUCTURES USING SIGNAL ANALYSIS METHODS

by

Nader Cheraghi

Submitted
in partial fulfillment of the requirements
for the degree of

DOCTOR OF PHILOSOPHY

Major Subject: Civil Engineering
at

DALHOUSIE UNIVERSITY

Halifax, Nova Scotia July, 2006

Your file Votre référence
ISBN: 978-0-494-27639-6
Our file Notre référence
ISBN: 978-0-494-27639-6

DALHOUSIE UNIVERSITY

To comply with the Canadian Privacy Act the National Library of Canada has requested that the following pages be removed from this copy of the thesis:

Preliminary Pages
- Examiners Signature Page
- Dalhousie Library Copyright Agreement

Appendices
- Copyright Releases (if applicable)

DEDICATION

To My Wife

TABLE OF CONTENTS

Page
List of Tables....ix
List of Figures....x
List of Symbols and Abbreviations....xv
Acknowledgements....xix
Abstract....xx
Chapter 1 1
Introduction 1
1.1 Introduction 1
1.2 Thesis Organization 3
Chapter 2 5
Literature Review 5
2.1 Types of Damage Detection Techniques 5
2.2 Levels of Structural Health Monitoring 6
2.3 DAMAGE IDENTIFICATION TECHNIQUES: 6
2.3.1 Change in Modal Parameters: 7
2.3.1.1. Change in Natural Frequency 10
2.3.1.1.1 The Forward Problem 12
2.3.1.1.2 The Inverse Problem 13
2.3.1.2 Change in Mode Shape 15
2.3.1.2.1 Mode Shape Curvature Change 16
2.3.2 Methods Based on Dynamic Flexibility Measurements 17
2.3.3 Model Update Methods 19
2.3.4 Neural Network (NN) based Methods 20
2.3.5 Pattern Recognition Techniques 21
2.3.6 Kalman Filter Technique 21
2.3.7 Statistical Approach 22
2.3.8 SIGNAL PROCESSING METHODS 22
2.3.8.1 Fourier Analysis 23
2.3.8.2 Wavelet Analysis 24
2.3.8.2.1 Continuous Wavelet Transform 24
2.3.8.2.2 Discrete Wavelet Transform 25
2.3.8.3 Wavelet Packet Transform 27
2.3.8.4 Hilbert-Huang Analysis 28
Chapter 3 31
Piezoelectric Material Behaviour and Formulation 31
3.1 History of piezoelectricity 31
3.2 Constitutive equations 32
3.2.1 Piezoelectricity 32
3.3 The Finite element approach 33
3.3.1 History 34
3.3.2 Finite element formulation 39
Chapter 4 43

Signal Analysis Method 43
4.1 Fourier Analysis 43
4.1.1 Introduction 43
4.1.2 Fourier Transform 44
4.2 Wavelets 49
4.2.1 Introduction 49
4.2.2. Mathematical Properties of Wavelets 51
4.2.2.1 Background 1
4.2.3 Continuous Wavelet Transform (CWT) 54
4.2.4 Discrete Wavelet Transform (DWT) 57
4.3. The Empirical Mode Decomposition and Hilbert-Huang Transform 58
4.3.1 Instantaneous frequency 61
4.3.2 Intrinsic mode functions 63
4.3.3 The empirical mode decomposition method: the sifting process 66
Chapter 5 73
Application of Hilbert-Huang Transform for Evaluation of Vibration Characteristics of Plastic Pipes Using Piezoelectric Sensors 73
5.1 ABSTRACT 73
5.2 INTRODUCTION 74
5.3 Modeling and formulation of piezoelectric material 77
5.4 Experimental procedure AND set up 78
5.4.1 Test Setup and Instrumentation 78
5.4.2 Test Procedure 79
5.5 ESTIMATION OF DAMPING RATIO USING VARIOUS METHODS OF ANALYSIS 79
5.5.1 Evaluation of damping ratio by the logarithmic decrement analysis (LDA) 80
5.5.2 Evaluation of damping ratio by the Hilbert Transform Analysis (HTA) 81
5.5.2.1 Mathematical Description of HHT 85
5.5.2.2 Band-Pass Filtering and EMD 86
5.5.2.3 Evaluation of Damping Ratio By Hilbert-Huang Spectral Analysis 86
5.5.2.4 Evaluation of Natural Frequency Damping Ratio based on Hilbert-Huang Analysis (HHST) 90
5.5.3 Evaluation of damping ratio by the Moving Block Analysis (MBA) 91
5.5.4 Determination of damping ratio using the Half Power Bandwidth method 93
5.5.5 Evaluation of damping ratio by the Circle-Fitting Method 96
5.5.6 Finite Element Method for Calculation OF Natural Frequency of Structure 98
5.6 Evaluation of the Damping Ratio and Discussion of the Results 99
5.7 Conclusions 100
5.8 REFERENCES 104
Chapter 6 107
APPLICATION OF THE EMPIRICAL MODE DECOMPOSITION FOR SYSTEM IDENTIFICATION AND STRUCTURAL HEALTH MONITORING 107
6.1 Abstract 106
6.2 INTRODUCTION 108
6.3 Background to the Hilbert-Huang Transform (HHT) 110
6.3.1 Mathematical Description of the HHT 112

6.4 Modal Response of n-DOF Structures Due to Impulse Loading 114
6.5 Modal Response Using Empirical Mode Decomposition Baesd on Band Pass Filtering 118
6.5.1 Identification of natural frequencies and damping ratios 119
6.5.2 Identification of mode shapes, and mass, damping, and stiffness matrices... 120
6.6 Case Study # 1: a Healthy (Undamaged) Structure 121
6.7 Case Study # 2: a Damaged Structure 130
6.8 Intrinsic Mode Functions (IMFs) Based Damage Detection Methods 142
6.9 Conclusions 143
6.10 Acknowledgements 144
6.11 References 146
Chapter 7 148
Piezoelectric-Based Degradation Assessment of a Pipe Using Fourier and Wavelet Analyses 148
7.1 Abstract 148
7.2 Introduction 149
7.3 Modeling and formulation of piezoelectric material 151
7.4 FFT-based Damage Detection Methods 152
7.5 Wavelet transformation and damage index 153
7.5.1 THE DISCRETE WAVELET TRANSFORM 153
7.5.2 The Continuous Wavelet Transform and the Wavelet Series 154
7.5.3 Wavelet Families 155
7.6 Examples 157
7.6.1 Case 1: Dynamical response of piezoelectric sensors for different damage locations 157
7.6.2 Case 2: Detection of damage due to reduction in flexural rigidity 170
7.6.3 Case 3: Detection of partial damage around the circumference of the pipe .. 170
7.7 Conclusions 175
7.8 Acknowledgement 175
7.9 References 175
Chapter 8 178
A DAMAGE INDEX FOR STRUCTURAL HEALTH MONITORING BASED ON THE EMPIRICAL MODE DECOMPOSITION 178
8.1 Abstract 178
8.2 INTRODUCTION 179
8.3 MODELING AND FORMULATION OF THE PIEZOELECTRIC SENSORS. 180
8.4 FFT-BASED DAMAGE DETECTION METHOD 181
8.5 WAVELET TRANSFORMATION AND DAMAGE INDEX 183
8.5.1 The Discrete Wavelet Transform 183
8.5.2 WAVELET-BASED DAMAGE DETECTION METHOD 184
8.6 Mathematical Description of Hilbert-Huang Transform (HHT) 186
8.6.1 Band-pass filtering and EMD 189
8.7 Examples 189
8.7.1 Case 1: Dynamical response of piezoelectric sensors for different damage locations 193
8.7.2 Case 2: Detection of damage due to reduction in flexural rigidity 205

8.8 Conclusions 206
8.9 Acknowledgement 207
8.10 References 210

Chapter 9 212
A NOVEL APPROACH FOR DETECTION OF DAMAGE IN ADHESIVELY BONDED JOINTS IN PLASTIC PIPES BASED ON VIBRATION METHOD USING PIEZOELECTRIC SENSORS 212
9.1 ABSTRACT 212
9.2 Introduction 213
9.3 FFT-BASED DAMAGE DETECTION METHOD 218
9.4 WAVELET-BASED DAMAGE DETECTION METHOD 219
9.5 Mathematical Description of Hilbert Huang Transform (HHT) 221
9.6 Test Set-up and Instrumentation 222
9.6.1 Preliminary Investigation 224
9.6.2 Experimental Apparatus and Equipment 224
9.6.3 Experimental Procedure 225
9.6.4 Data Processing Methods 227
9.6.4.1 Removal of Non-Response Date 228
9.6.4.2 Response of Piezoelectric sensors for Fully Bonded Pipe 229
9.6.4.3 Impulse Hammer Response Processing 229
9.6.4.4 Evaluation of Frequency Response function 229
9.7 Experimental Results 230
9.7.1 Typical Responses 230
9.7.2 Influence of Sensor Location 231
9.7.3 Degree of Damage 232
9.7.3.1 Comparison of Damage Indices 232
9.7.4 Influence of Support Condition 234
9.8 Conclusions 234
9.9 References 239

Chapter 10
Conclusions 240
10.1 Conclusion 240
10.2 Recommendations for Future Work 242
References 243

LIST OF TABLES

Table 5.1. Basic properties of the materials 78

Table 5.3. Damping ratio evaluated based on the methods outlined.....92

Table 5.2. Natural frequency values obtained from the experimental and finite element analysis.....100

Table 6.1. Natural frequency and damping ratios of the healthy six DOF mechanical systems.....129

Table 6.2. Theoretical and Identified Mode Shapes of the healthy six DOF mechanical systems.....133

Table 6.3. Natural frequency and damping ratios of the damaged six DOF mechanical systems.....140

Table 6.4. Theoretical and Identified Mode Shapes of the damaged six DOF mechanical systems.....141

Table 6.5. Energy and damage indices of the first two modal responses based on the IMF energy.....145

Table 7.1. Geometry and material properties of pipe.....158

Table 7.2. Comparison of natural frequencies.....161

Table 7.3. Comparison of the energies for FFT, WT and WPT for the damage case DL2.....169

Table 8.1. Geometry and material properties of the pipe.....191

Table 8.2. Comparison of the computed natural frequencies.....191

Table 8.3. Comparison of the computed energies for FFT, WT and WPT for the damage case DL2.....195

Table 9.1. level of Damage in Test Specimens.....223

Table 9.2. Impulse Hammer Location.....227

Table 9.3. Support Fixture Tightness.....227

Table 9.4. Sensor/Debond Experimental Locations.....228

Table 9.5. Test Set-up Configurations (The Numbers are with reference to Tables 9.2 through 9.4).....228

LIST OF FIGURES

Figure 4.1. (a) A sample Signal (b) Reconstruction Using Fewer than 10% of the Coefficients from the coiflet 4 Wavelet Decomposition.....51

Figure 4.2. Schematic View of a 3-level decomposition of a function F by wavelet into an approximation space V3 and detail space W3 by a combination of low(H) and High(g) pass filter.....51

Figure 4.3. Schematic reconstruction of the function F from the 3-level decomposition. The approximation space V3 and the detail space W1, W2, W3 are all that are required.....52

Figure 4.4. An example signal for wavelet analysis, original from the calibration of a hydrophone.....54

Figure 4.5. Same example as figure 4.4 with zero added to pad the signal to have a length 2048 and create a discontinuity.....54

Figure 4.6. Example of effect of scaling and translation of the Mexican hat function. Note that (a) corresponds to a high frequency, whereas in (b), the function are at a lower frequency and are less localized.....56

Figure 4.7. A typical intrinsic mode function with the same numbers of zero crossings and extrema, and symmetry of the upper and lower envelopes with respect to zero.....65

Figure 4.8. Illustration of the sifting processes 69

Figure 4.9. Illustration of the effects of repeated sifting process: (*a*) after one more.....70

Figure 5.1. Schematic of test setup.....79

Figure 5.2. Typical responses obtained from the sensors, (a) Sensor #1 (b) Sensor #5....82

Figurer 5.3. Results obtained from the LDA method (a) Sensor # 2, (b) Sensor # 3, (c) Sensor # 4.....83

Figure 5.4. (a): Output voltage of Sensor #1 with its Envelope Function based on Hilbert transform, (b): plot of *ln* of Hilbert transform vs. time for data of sensor #1.....84

Figure 5.5. Output voltage of sensor #1 and the intrinsic mode function (IMFs) plots....94

Figure 5.6. Application of the HHSA method on data obtained from (a) sensor #1, (b) sensor #3, and (c) #4.....95

Figure 5.7. Plot of power spectrum vs. frequency obtained from the output voltage of (a) sensor #1, (b) sensor #2, and (c) #5.....97

Figure 5.8. Schematics of the formation of the (a) HPB and (b) CFM methods.....98

Figure 5.9. The calculated results of the CFM for (a) Sensor #1, (b) Sensor #2, (c) Sensor 3, (d) Sensor #4, (e) Sensor #5.....102

Figure 5.10.: Pipe's mode shapes determined by FEA (a) First mode, (b) Second Mode.....103

Figure 6.1. Schematic of the 6-DOF mechanical system.....122

Figure 6.2. Plots of (a) the displacement impulse response of mass # 3 of the damaged mechanical system, (b) the Fourier transform of displacement response of all masses of the healthy mechanical system.....125

Figure 6.3. Displacement and IMFs of mass #4 of the healthy mechanical system.....126

Figure 6.4. Plots of (a) the unwrapped phase angle of the first mass for the first modal response, (b) the unwrapped phase angle of the first mass for the sixth modal response of the healthy system.....127

Figure 6.5. Plots of (a) ln amplitude of the first mass for the first mode, (b) ln amplitude of the first mass for the sixth mode.....128

Figure 6.6. Plots of (a) the second modal response, (b) the third modal response of the mechanical system.....134

Figure 6.7. Plots of (a) the displacement impulse response of mass # 3 of the damaged mechanical system, (b) the Fourier transform of displacement response of all masses of the damaged mechanical system.....135

Figure 6.8. Displacement and IMFs of mass # 4 of the damaged mechanical system...136

Figure 6.9. Plots of (a) the unwrapped phase angle of the first mass for the first modal response, (b) the unwrapped phase angle of the first mass for the sixth modal response of the damaged system.....137

Figure 6.10. The third modal response of the damaged system.....138

Figure 6.11. Displacement and IMFs of mass #4 of the damaged mechanical system.....139
Figure 7.1. Schematics of (a) a typical FFT function; (b) a typical wavelet function.....154
Figure 7.2. Two different mother wavelet functions: (a) Haar and (b) Morlet Wavelet.....156
Figure 7.3. FEM dynamic response of the pipe; (a) FEM mesh, (b) First vibration mode, (c) second vibration mode.....162
Figure 7.4. Typical FRF response curves of sensor 5 for the healthy and damaged pipes.....163
Figure 7.5. Comparison of FRF response for sensor 5 at the damage cases DL1, DL2 and DL3.....164
Figure 7.6. Comparison of FRF response for sensors 2, 4 and 7 at the damage case of DL2.....165
Figure 7.7. Wavelet simulation of (a) healthy pipe, (b) damaged pipe (at DL2).....166
Figure 7.8. Wavelet packet simulation of (a) healthy pipe, (b) damaged pipe (at DL2).....167
Figure 7.9. Damage index at the damage location DL2 based on: (a) FFT energy; (b) FFT integration; (c) WT energy and (d) WPT energy.....168
Figure 7.10. Comparison of the FRF responses for the pipe with 10%, 30% and 50% reduction in its flexural rigidity.....171
Figure 7.11. Comparison of variation in damage indices (as a function of axial direction) for the pipe with 30% reduction in its flexure rigidity obtained by the FFT, FFT integration, WT and WPT methods (for case study #2).....172
Figure 7.12. Comparison of variation in damage indices in the form of variation in the damage indices as a function of various percentiles of degradation extent.....173
Figure 7.13. Comparison of variation in damage indices (as a function of axial direction) for the pipe with damage around a ¼, ½ and full circumference obtained by the FFT, FFT integration, WT and WPT methods.....174
Figure 8.1. Schematics of (a) a typical FFT function; (b) a typical wavelet function; (c) Two different mother wavelet functions: (a) Haar and (b) Morlet Wavelet.....184

Figure 8.2. Dynamic response of the pipe; (a) FEM mesh, (b) First vibration mode, (c) second vibration mode.....192

Figure 8.3. Typical FRF response curves of sensor 5 for the healthy and damaged pipes.....196

Figure 8.4. Comparison of FRF response for sensor 5 at the damage cases DL1, DL2 and DL3.....197

Figure 8.5. Comparison of FRF response for sensors 2, 4 and 7 at the damage case of DL2.....198

Figure 8.6. Empirical Mode Decomposition (EMD) for calculating first and second natural frequency based on first IMF.....199

Figure 8.7. Wavelet simulation of (a) healthy pipe, (b) damaged pipe (at DL2).....200

Figure 8.8. Wavelet packet simulation of (a) healthy pipe, (b) damaged pipe (at DL2).....201

Figure 8.9. Empirical Mode Decomposition (EMD) of (a) healthy pipe for sensor 3, (b) Sensor 6.....202

Figure 8.10. Damage indices for various percentiles of degradation based on the four methodologies (DL2).....203

Figure 8.11. (a) Damage index at the damage location DL1 based on EMD,WT and WPT (b) Damage index at the damage location DL2 based on EMD and WPT.....204

Figure 8.12. Comparison of the FRF responses for the pipe with 10%, 30% and 50% reduction in its flexural rigidity.....208

Figure 8.13. Comparison of variation in damage indices ((a) as a function of axial direction, and (b) as a function of sensor number) for the pipe with reduction in its flexure rigidity obtained by the FFT integration, WT and WPT methods (DL2).....209

Figure 9.1: Experimental Test Set-up for Adhesively Bonded Pipe Joints (a) Fully Bonded Joint, (b) ¾ Bonded Joint, (c) ½ Bonded Joint.....226

Figure 9.2: Support System for the Adhesively Bonded Pipe Joints.....226

Figure 9.3: Typical Top Surface Bonded Piezoelectric Sensor Time History Response.....230

Figure9.4: Typical Fourier Spectrum for Top Surface Bonded Piezoelectric Sensor.....230

Figure 9.5: Typical Frequency Response Function for Varying Degrees of Damage in Adhesively Bonded PVC Pipe Joint for Top Sensor.....231

Figure 9.6: Comparison of Damage Indices for Sensors 1 and 2 of the ¾ bonded Joint (a) FFT Index, (b) EMD Index, and (c) Wavelet Index.....233

Figure 9.7: Damage indices based on different method with different degree of debond.....236

Figure 9.8: Comparison of damage indices of bonded and debonded sensor with different method.....237

Figure 9.9: Comparison of damage indices of different support condition.....238

LIST OF SYMBOLS AND ABBREVIATIONS

Latin Alphabet

a	Scaling function
A_{kj} (t)	Instantaneous amplitude
b	Translation parameters
C	Damping matrix
C (a,b)	Wavelet coefficients
c(.)	Covariance function
C^E	Stiffness when the electric field is constant
C_j	Modal damping
$C_j(t)$	IMFs of measured signal
C_k	Fourier series coefficient
D	Dielectric Displacement
DI_{mn}	Damage index
e	Piezoelectric constant
E	Electric field
E(.)	Expected value defined as the ensemble average of quantity
E_{mn}	Energy of sensor number m and n is the mode shape number
$E_{xx}^{damaged}$	Equivalent energy of sensor's signal after damage
$E_{xx}^{Healthy}$	Equivalent energy of sensor's signal before damage
F(t)	Excitation force
F_0	Level of measured impact loading
f_a	Actual frequency
f_b	Body force
F_c	Concentrated force
$\{f_i\}$	Mechanical force vector
f_p (t)	Impact load applied at the p^{th} Dof
f_s	Sampling frequency
F_s	Surface force

g	High pass filter
$\{g_i\}$	Electrical force vector
g(k)	Discrete high pass filter
g[l]	Windowing function
H	Low pass filter
h(k)	Discrete low pass filter
$I_x^{damaged}$	Integration of output sensor's signal after damage
$I_x^{healthy}$	Integration of output sensor's signal before damage
K_j	Generalized modal stiffness
$[K_{uu}]$	Elastic stiffness matrix
M	Mass matrix
m_j	J^{th} modal mass
$[N_u]$	Displacement shape function
P	Polarization
q_c	Point charge
q_s	Surface charge
$r_n(t)$	Residual
S	Strain
S_1	Area where mechanical forces are applied
S_2	Area where electrical charges are applied
T	Stress
{u}	Displacement vector
$U_{f_l^{i,n}}^{damaged}$	Energy of output sensor's signal after damage
$U_{f_l^{i,n}}^{healthy}$	Energy of output sensor's signal before damage
$\{V_j\}$	Approximation tree
$\{W_j\}$	Detail tree
X(f)	Corresponding Fourier transform of x(t)
x(t)	Continuous function in time
x[n]	Discrete function

Greek Symbol

∇	Gradiant operator
$x(e^{2\pi jf})$	Corresponding Fourier transform
ψ	Mother wavelet function
$\overline{\psi}$	Complex conjugate of mother wavelet function
ω	Angular frequency
$\varphi_{kj,p}$	Phase difference between K^{th} element and P^{th} element in the J^{th} mode shape
$\beta_{kj}(t)$	Instantaneous phase angle
η_r	Hysteretic damping ratio
C_{jk}^{r}	Complex constant
$H(\omega,t)$	Hilbert transfom
θ'	Magnitude of the fitted line for phase angle curve
ρ	Mass density
$[\varepsilon]$	Dielectric matrix
$\psi(t)$	Mother wavelet
$\varphi(t)$	Scaling function
ω_{int}	Intermittency frequency
υ	Possion ratio
ξ	Viscouse-damping ratio
ω	Natural frequency
ω_D	Natural frequency of damped condition
ϕ	Mode shape
ω_j	J^{th} natural frequency
ξ_j	J^{th} damping ratio
ϕ_{pj}	P^{th} element of the J^{th} modal vector
ω_{dj}	J^{th} damped modal frequency
φ_j	Phase lag of the J^{th} mode

$\ddot{X}(t)$	Impulse acceleration response
$[N_\phi]$	Potential shape function
$[B_\phi]$	Derivative of potential shape function
$[K_{u\phi}]$	Piezoelectric coupling matrix
$[K_{\phi\phi}]$	Dielectric stiffness matrix
[Bu]	Derivative of displacement shape function
$\{\phi\}$	Electric potential vector
$\{\delta u_i\}$	Arbitrary variation of the displacement
$\{\delta\phi_i\}$	Arbitrary variation of the electric potential

ACKNOWLEDGEMENTS

I sincerely thank my wife for her love, devotion, and continued encouragement to gain further education and also my family for all their support.

I am very much thankful to Dr. Farid Taheri, the initiator of this project, for putting faith on me and giving me opportunity to work on this project, for all his encouragements and supports and for granting me a free will to explore the validity of my ideas.

I also thank all of my committee members, Dr. John Newhook, Dr. Tasos Georgiades and Dr. Rajamohan Ganesan for reading and evaluating the thesis.

I thank Dr.Zou, Mark Riley and Mark Macdonald for their technical support in setting-up the experiments.

My special thanks also go to all Iranian students in Halifax.

Killam trustees for their financial support are gratefully acknowledged. This study was also partly supported by Institutive of Research Material (IRM) and Atlantic Innovative Fund (AIF) which are thankfully acknowledged.

Finally, I like to thank to all those who gave me all co-operation especially all of graduate students of Dr. Farid Taheri.

ABSTRACT

This dissertation presents the strategies used for developing four damage indices, based on various signal analysis methods, used for locating and quantifying structural damage. The proposed damage indices demonstrate the effectiveness of a series of coupled mathematical/engineering approaches that enable us to detect damage in structures, reliably and accurately. The proposed health monitoring methodology is based on monitoring the vibration response of structures using piezoelectric sensors. The Fast Fourier transformation (FFT), FFT integration, wavelet transformation (WT), wavelet packet transformation (WPT) and the Empirical Mode Decomposition (EMD) methods are used to examine the structure's dynamic response signals caused by an impacting force. Novel "damage indices" expressions are developed based on the evaluation of the vibration induced energies. The proposed methodologies were verified both numerically and experimentally. Finite element analysis was used to simulate the response of healthy structures, as well as structures with various size damages with piezoelectric patches mounted on them. Various damage cases were studied to verify the proposed damage indices. The proposed formula was also used to assess the integrity of bonded joints. Experimental results demonstrated that the proposed methodologies could detect the integrity of adhesive bonded joints with the use of only a single sensor. A system identification technique was developed based on EMD and the Hilbert-Huang transform (HHT) and was verified numerically for a six degree freedom mass-spring system. Experimental investigation was also carried out for evaluation of damping of PVC pipes with equipped piezoelectric sensors with the various available techniques and the results were compared to that obtained through the proposed EMD/ HHT system identification method.

The proposed methods have been found to be successful in localizing the damage in the structure and in system identification application.

Chapter 1

Introduction

1.1 Introduction

Structural health monitoring has been an evolving area of research in the past two decades with increasing need of online monitoring the health of large structures. The damage detection by visual inspection of the structure can prove impractical, expensive and ineffective in case of large structures such as multi-storied buildings and bridges. This necessitates the development of a structural health monitoring (SHM) systems that can effectively detect the occurrence of damage in the structure and can provide information regarding the location as well as severity of damage and possibly the remaining life of the structure. The SHM system analyzes the structural response by excitation due to controlled or uncontrolled loading. The controlled loading may be attributed to impulse excitation whereas the uncontrolled loading may be attributed to the excitation by automobiles on bridge, a random excitation due to wind loads or due to earthquake excitation.

The terms "Smart Structures" and "Intelligent Material Systems" are fast becoming a common phrase among the engineering community. Although there is no agreed definition for intelligent material systems, Rogers (1992) proposed two definitions. The first one is based upon a technology paradigm: "the integration of actuators, sensors, and controls of a material or structural component." The second one is based upon a science paradigm and addresses the goal of intelligent material systems: "material systems with intelligence and life features integrated in the microstructure of the material system to reduce mass and energy and produce adaptive functionality."

An on-line structural health monitoring system should meet three requirements Rogers and Lalande (1996) : (i) it must be small, non-intrusive, and must offer the possibility of being located in inaccessible remote areas of the structure and, as such, it must be able to transmit information easily to a central processor;(ii) it must be as sensitive as conventional non-destructive evaluation (NDE) techniques, *i.e.* it must be

able to detect minor damages such as small cracks, delaminations or loose connections; and (iii) it must be able to monitor a certain minimum area of the structure as opposed to the point measurements offered by presently available NDE equipment.

Conventional NDE techniques such as ultrasonic testing and X-radiography can provide significant details about the nature of damage. However, these techniques usually require direct access to the structure being investigated and involve bulky equipment. Moreover, the structure should be scanned at every location to detect presence of any flaw. These techniques usually require the structure to be out of service during the inspection and this may cause major disruptions to the service. For these reasons, these techniques are not favored for on-line structural health monitoring.

The major goal of this thesis has been to develop and introduce novel energy based damage indices evaluated through the output of piezoelectric sensors to identify damage. Three new damage indices are introduced based on the Fast Fourier, Wavelet and Empirical Mode Decomposition (EMD) methods. It has been shown that the proposed damage indices can identify the presence and location of damage with a good accuracy and consistency.

The proposed piezoelectric based structural health monitoring technique along with the introduced damage indices investigated in this research provide an effective solution for on-line structural health monitoring. This technique utilizes the direct electromechanical properties of piezoelectric materials, for sensing the vibrational response of a structure. Physical changes in the structure cause changes in the structural mechanical properties and systems. Due to electromechanical coupling between the piezoelectric material and the structure, the change in structural mechanical property induces a change in the electrical output of the piezoelectric material. Hence, it is possible to determine when a structural damage occurs or is becoming imminent by monitoring the output voltage of the piezoelectric sensor.

This work involved numerical modeling and experimental investigation to verify the introduced damage indices. In the numerical modeling, two models were developed based on Finite Element Method (FEM) and an analytical solution. In the

experimental investigation two setups were also developed and investigated to verify first the integrity of the proposed system identification, and then the effectiveness of the proposed damage indices.

1.2 Thesis Organization

Chapter 2 presents thorough literatures review of current damage detection techniques and most structural health monitoring systems. The literature review focused on vibrational based methods for damage identification and location because it is believed that vibrational based SHM is an effective and efficient solution.

Chapter 3 provides details of piezoelectric materials and the associated formulation for the materials when used as sensors.

Chapter 4 introduces the Fast-Fourier, Wavelet and Hilbert-Huang mathematical formulations for processing the output signal of piezoelectric sensors and introduces the proposed damage indices derived based on these methods.

Chapters 5 to 9 are written in series paper format some of which have been published and some of them are under review for publication.

Chapter 5 outlines the experimental setup and procedures used to verify the integrity of the proposed system identification and damaged indices. The setup used a PVC pipe which had been instrumented with five piezoelectric patch sensors. This setup was developed to find the applicability of piezoelectric sensors to monitor vibration of the structure and to verify the applicability of the Hilbert-Huang based system identification method verification. For that the calculated damping coefficient of the structure was evaluated and compared with those obtained by most of the commonly used methods.

Chapter 6 presents two numerical models used to verify the integrity and accuracy of the proposed damaged indices and system identification method. The system is a 6-DOF mechanical system subjected to an impact load has been solved by an exact analytical solution, using MATLAB software, as well as with finite element method, using ANSYS program. The presence of damage was simulated by reducing the stiffness of the springs used to idealized the stiffness of the spring-mass system.

Chapter 7 outlines the numerical analysis which is provided to evaluate the integrity of the proposed damage indices in a pipe structure based on Fourier and Wavelet analysis. Finite element analysis was used to simulate the response of a healthy pipe, as well as pipes with various sizes of damages. The pipes' degradations (defects) were assumed to have existed in the form of local patches of corrosion, simulated by reducing the wall thickness in various areas around the circumference of pipes.

Chapter 8 presents the same numerical work of Chapter 7 which is provided to evaluate the integrity of the proposed damage indices in a pipe structures based on developed damage indices with Fourier, Wavelet and EMD analysis.

Chapter 9 outlines an experimental setup which was used to check and verify the proposed damage indices for two pipes joined by an adhesive. The aim of this setup was to detect any debonding of adhesive bonded structures. In this chapter all of the proposed damage indices have been used and compared to each other.

The conclusions and recommendations for the future studies are summarized in Chapter 10.

Chapter 2

Literature Review

The research in structural health monitoring and damage detection has recently become an area of interest for a large number of academic and commercial laboratories. Especially, a need to develop in-service and on-line health monitoring techniques is increasing. This kind of technique allows systems and structures to monitor their own structural integrity while in operation and throughout their life, such techniques are useful not only for improving reliability of the structures, but also reducing their maintenance and inspection cost.

Damage in a structure can be classified as linear and non-linear. Linear damage is the case when the initially linear-elastic structure remains linear-elastic after damage is created (Doebling, 1996a). This occurs, for example, when the structure is subjected to a sudden damage of relatively low intensity. The modal parameters change in this case, but the structure would still exhibit linear response after the damage. This facilitates the formation of a simple model of the structure, and to derive equations of motion based on an assumption of linear structural properties.

Non-linear damage is a case when the initially linear-elastic structure exhibits non-linear behavior after initiation of the damage. A fatigue crack initiated in a shaft subjected to cyclic loading can be called a non-linear damage case. In this case the crack opens and closes during every cycle, thereby making the shaft's stiffness non-linear. Most of the damage detection techniques assume linear damages when modeling the structure.

2.1 Types of Damage Detection Techniques

Current damage detection methods can be mainly categorized into local damage detection methods and global damage detection methods. In the case of local damage detection methods, the approximate location of damage in structure is generally known and the structure is analyzed locally to detect the damage. In this case, the

damaged region needs to be easily accessible to effectively detect its exact location, and severity. Some of the examples of the local damage detection techniques are eddy current technique, acoustic or ultrasonic damage detection techniques and radiographic technique.

Contrary to the local damage detection methods, the global methods do not require prior knowledge of the location of damage in the structure. The global methods monitor the changes in the vibration characteristics of the structure to detect the location and severity of a damage. The changes in dynamic properties of the structure may be attributed to the damage occurrence in the structure, as the modal parameters (comprising the natural frequencies, mode shapes and damping ratios) are functions of the physical properties i.e. (mass, damping and stiffness) of the structure. Any change in the physical properties would therefore change the modal parameters.

2.2 Levels of Structural Health Monitoring

Various global damage identification techniques have been developed to date. The effectiveness of each method can be evaluated by the extent of the information obtained about the damage. Rytter (1993) proposed a system of classification for damage-identification techniques, defining four levels of damage identification as follows:

Level 1: Determination of the presence of damage in the structure

Level 2: Determination of the geometric location of the damage

Level 3: Quantification of the severity of the damage

Level 4: Prediction of the remaining service life of the structure

According to above levels, damage identification techniques used in industrial machineries may be limited to Level 1, commonly known as fault identification technique. However most of the damage detection techniques implemented for SHM systems of civil infrastructures fall under the Level 3 and or Level 4.

2.3 DAMAGE IDENTIFICATION TECHNIQUES:

As stated, various damage identification methods, based on the measurement of the dynamic properties of structures have been developed to date. These methods can

be categorized based on the type of data collected when monitoring the structure, or the technique implemented to identify damage. Some of the methods worth mentioning are those monitoring the changes in the modal parameters, the matrix update methods, the neural network based methods, the pattern recognition methods, the Kalman filter based methods and those based on statistical approach. The following sections provide a summary of the above stated methods.

2.3.1 Change in Modal Parameters:

Any change in the dynamic properties of structure causes change in the modal properties of the structure, including change in the natural frequencies, mode shapes and modal damping values. These values can be tracked to get information about the damage present in the structure.

The idea that changes in vibration characteristics could provide information regarding damage in a structure is very intuitive; one may however ask the question: Why has it taken such a long time for the technology to be formally and generally recognized and adopted by the modern engineering community? The answer maybe that there are several confounding factors that make the vibration-based damage identification methods difficult to implement in practice. Firstly, the standard modal properties represent a form of data compression. Modal properties are estimated experimentally from measured time history responses. A typical time-history may have 1024 data points, and if measurements are made at 100 points, then there would be 102,400 pieces of information regarding the state of the structure.

Through the system identification procedure commonly referred to as experimental modal analysis (Ewins, 1984), the volume of data is converted into some number of resonant frequencies, mode shapes and modal damping values. This data compression is done because the modal quantities would be easier to visualize, and physically interpret, in terms of standard mathematical modeling of vibrating systems, than are the actual time-history data. As an example, if twenty real modes are identified, then the 102,400 pieces of information would have been reduced to 2020-2040 pieces of information (20 modes, each consisting of 1 resonant frequency value, 1 modal damping value and 100 modal amplitude values).

Intuitively, information about the current state of the structure may be lost in this data reduction and system identification process. The loss of information occurs primarily from the fact that for a linear system, the modal properties are independent of the excitation signal characteristics (amplitude and frequency content) and the location of the excitation, whereas the time histories are not. In addition, if the input excites response at frequencies greater than those that can be resolved with the specified data sampling parameters, the identified modes will not provide any information regarding the higher frequency response characteristics of the structure that are contributing to the measured time-history responses. Within the measured frequency range of the response, it is often difficult to identify all the modes contributing to the measured response, because of the coupling between the modes that are closely spaced in frequency. This difficulty is observed more commonly at the higher frequency portions of the spectrum, where the modal density is typically greater. Also, the introduction of bias (or systematic) errors, such as those that arise from windowing of the data, finite frequency resolution, and those arising from the changes in the ambient condition during the test, would tend to make the identified modal parameters less representative of the true dynamic properties of the structure.

Another confounding factor is the fact that a damage is typically a local phenomenon. Local response is captured by higher frequency modes, whereas lower frequency modes tend to capture the global response of the structure and are less sensitive to local changes in a structure. From the experimental prespective, it would be more difficult to excite the higher frequencies of a structure, as more energy would be required to produce measurable response at such higher frequencies than at the lower frequencies. These factors, coupled with the loss of information resulting from the necessary reduction of time-history measurements to modal properties, add further difficulties to the process of vibration-based damage identification. These factors have also limited this technology to the research area with only limited cases practiced by the engineering community.

A logical question then would be "why not examine the time-histories directly for indications of damage?"

The answer may be, despite the difficulties associated with damage detection based on changes in modal properties, it is even more difficult to identify damage by direct examination of the time histories responses. To identify that damage has occurred based on the changes in patterns of time histories, and to relate these changes to physical changes in the structure pose certain complexities. If the excitation sources and/or the environmental condition change, then this process becomes even further complicated. However, it should be pointed out that in a situation where the system response changes from linear to nonlinear, the time histories alone (actually their frequency domain power spectra) would not constitute sufficient information to identify the damage. Generally, an identification technique requires the knowledge of the location of the damage as *a priori*, as for instance is typically the case with loosening of bearings in rotating machinery. Detecting the onset of nonlinear vibration behavior in rotating machinery represents one of the most widely practiced forms of vibration-based damage identification (Wowk, (1991)).

Notwithstanding the difficulties mentioned above, the advances in vibration-based damage detection over the last 20-30 years have produced new methods utilizing dynamic data for indications of structural damage. These methods are seeing more widespread applications. One of the most prominent examples of this application is NASA's space shuttle modal inspection system (Hunt, 1990). A vibration-based damage detection system was developed because of the difficulties in accessing the exterior surface caused by the thermal protective system. This system could identify damage that would have eluded the traditional non-destructive testing methods because of inaccessibility to the damaged components. The methodology has then been adopted as a standard inspection tool for the Space Shuttle Orbiter structures.

It is the intent of this literature survey to provide an overview of the recent advances in vibration-based damage detection methodology. This literature survey is mainly based on a detailed review of the vibration-based damage detection literature (Doebling, 1996b).

As mentioned previously, the field of damage identification is very broad and encompasses both local and global methods. This literature review will be limited to

global methods that are used to infer damage from changes in vibration characteristics of structures. Many different issues are critical to the success of using the observed changes in mechanical vibration characteristics of a structure for damage identification and health monitoring. Among the important issues are the excitation and measurement considerations, including the selection of the type and location of sensors, and the type and location of the excitations. Another important topic is the issue of signal processing, which includes such methods as the Fourier analysis, time-frequency analysis and wavelet analysis. In this literature survey, these peripheral issues will not be directly addressed. The scope of this literature survey will be limited to the methods that use changes in modal properties (i.e. modal frequencies, modal damping ratios, and mode shapes) to infer changes in the mechanical properties and the application of these methods to engineering problems. The review includes both methods that are based solely on changes in the measured data, as well as those that use a finite element method in their formulation. The reader should note that methods based on identifying nonlinear response or non-parametric models (such as the neural network-based approaches) are only briefly noted in this review.

Most of the modern developments in vibration-based damage detection stemmed from studies performed in the 1970s and early 1980s by offshore oil industry. For more information the reader should review Vandiver (1975; and 1977), Begg (1976), Loland and Dodds (1976), Wojnarowski (1977), Coppolino and Rubin (1980), Duggan (1980), Kenley and Dodds (1980), Crohas and Lepert (1982), Nataraja (1983), and Whittome and Dodds (1983) for more details on these studies. However, in the view of this author, most of the proposed techniques were less than successful. Because of the lack of success, the oil industry mostly abandoned pursuit of this technology in the mid-1980s.

2.3.1.1 Change in Natural Frequency

The natural frequency of a structure is a function of the stiffness and mass of the structure. Any damage occurring in the structure would cause loss of stiffness, whereas the mass of the structural members remains unchanged resulting in the

reduction of the natural frequency of the structure. Thus a reduction in the natural frequency of the structure can be used as an indicator of damage in the structure.

The damage identification with this technique is implemented with two types of approaches. One of the approach models damage mathematically and predicts the frequency of the structure. The predicted natural frequency is compared with the measured natural frequency and the damage is hereby identified. The second approach evaluates damage parameters like crack length and location from the frequency shifts and thus measures the intensity and location of damage in addition to just identifying of the damage as observed in the first approach.

The amount of literature related to damage detection using shifts in resonant frequencies is quite large. Salawu (1997a) presented an excellent review on the use of modal frequency changes for damage diagnostics. The observation that changes in structural properties cause changes in vibration frequencies was the impetus for using modal methods for damage identification and health monitoring. Because of the large amount of literature, not all papers that the authors have reviewed on this subject are included in the reference list of this thesis. A more thorough review and reference list can be found in Doebling (1996a). An effort has been made to include some of the early works on the subject, some papers representative of the different types of work done in this area, and papers that are considered by the author to be significant contributions in this area.

It should be noted that frequency shifts have significant practical limitations for applications to the types of structures considered in this review, although ongoing and future work may help resolve these difficulties. The somewhat low sensitivity of frequency shifts to damage requires either very precise measurement sensors or large levels of damage. However, recent studies have shown that resonant frequencies have much less statistical variation from random error sources than other modal parameters (Farrar,1996; Doebling,1996b).

For example, in offshore platforms damage-induced frequency shifts are difficult to distinguish from the shifts resulting from increased mass due to marine growth. Tests conducted on the Interstate 40 highway bridge (Farrar,1994) also demonstrated that frequency shifts are not sensitive indicators of damage. In this

investigation when stiffness of the cross-sectional at the center of a main plate girder had been reduced by 96.4%, which reduced the bending stiffness of the overall bridge cross-section by 21%, still no significant reduction in the modal frequencies were observed. Currently, using frequency shifts to detect damage appears to be more practical in applications where such shifts can be measured very precisely under a controlled environment, such as for quality control in manufacturing. As an example, a method known as "resonant ultrasound spectroscopy", which uses homodyne detectors to make precise sine-sweep frequency measurements, has been used successfully to determine the out-of-roundness of ball bearings (Migliori, et al., 1993).

Also, because modal frequencies are a global property of the structure, it is not clear that shifts in this parameter can be used to identify more than Level 1 damage. In other words, the frequencies generally cannot provide spatial information about structural changes. An exception to this limitation occurs at higher modal frequencies, where the modes are associated with local responses. However, the practical limitations involved with the excitation and extraction of these local modes, caused in part by high modal density, can make them difficult to identify. Multiple frequency shifts can provide spatial information about structural damage because changes in the structure at different locations will cause different combinations of changes in the modal frequencies. However, as pointed out by several authors, there are often an insufficient number of frequencies with significant changes to uniquely determine the location of the damage.

2.3.1.1.1 The Forward Problem

The forward problem, which usually falls into the category of Level 1 damage identification, consists of calculating frequency shifts from a known type of damage. Typically, the damage is modeled mathematically, and then the predicted frequencies are compared to the measured frequencies to determine the damage. This method was used extensively by the previously mentioned offshore oil industry investigators.

As an example, Cawley and Adams (1979) gave a formulation for detecting damage in composite materials using the frequency shifts. They started with the ratio

between frequency shifts for two different modes in their procedure. A grid of possible damage points was considered and an error term was constructed that related the measured frequency shifts to those predicted by a model based on a local stiffness reduction. A number of mode pairs were considered for each potential damage location and the pair giving the lowest error indicated the location of the damage. The formulation did not account for multiple-damage locations.

Friswell (1994) presented the results of an attempt to identify damage based on a known catalog of likely damage scenarios. The authors used an existing model of the structure which was highly accurate. Using this model, they computed frequency shifts of the first several modes for both the undamaged structure and all the postulated damage scenarios. Then ratios of all the frequency shifts were computed. For the candidate structure, the same ratios were computed, and a power-law relation was fit to these two sets of numbers. When the body of data was noise-free, and when the candidate structure lay in the class of assumed damages, the correct type of damage would produce a fit that would be a line with unity slope. For all other types of damage the fit would be inexact. The likelihood of damage was keyed on the quality of the fit to each pattern of known damage. Two measures of fit were used: the first was related to the correlation coefficient; the second was a measure of how close the exponent and coefficient were to unity. Both measures were defined on a scale from 0 to 100. It was hypothesized that damage was present when both measures were near 100.

Juneja et al. (1994) presented a forward technique called the "contrast maximization", matching the response of the damaged structure to a database of structural responses, thus locating the damage. They also develop a predictive measure of the detectability of the damage. Gudmundson (1982), Tracy and Pardoen (1989), and Penny (1993) also presented other approaches to the forward problem.

2.3.1.1.2 The Inverse Problem

The inverse problem, which, is typically considered as Level 2 or 3 damage identification, consists of calculating the damage parameters (e.g., crack length and/or location) from the frequency shifts.

Lifshitz et al. (1969) presented probably the first journal article to propose damage detection technique via vibration measurements. They looked at the change in the dynamic moduli, which could be related to the frequency shift, as an indication of damage in particle-filled elastomers. The dynamic moduli, which are the slopes of the extensional and rotational stress-strain curves obtained under dynamic loading, were computed for the test articles from a curve-fit of the measured stress-strain relationships at various levels of filling.

Stubbs (1990a; 1990b) developed a damage detection method using the sensitivity of modal frequency changes that was based on work of Cawley and Adams (1979). In this method, an error function for each mode and each structural member was computed assuming that only one member was damaged. The member that minimized this error was determined to be the damaged member. This method was demonstrated to produce more accurate results than the previous ones in the case where the number of members is much greater than the number of measured modes. The authors also pointed out that this frequency-change sensitivity method relied on sensitivity matrices that were computed using finite element method. This requirement increased the computational burden of these methods and also increased the dependence on an accurate prior numerical model. To overcome this drawback, Stubbs (1992) developed a damage index method, which is presented in the section on methods that use mode shape curvature changes.

Morassi (1997) presented an inverse technique to localize notch effects in steel frames using changes in their modal frequency. This study focused particularly on the accuracy of the assumed reference (undamaged) structural configuration and the practicality of making vibration measurements in the field. Koh (1995) used a recursive method based on static condensation to locate damage based on measured modal frequencies.

Further examples of inverse methods for examining changes in the modal frequencies for indications of damage are presented by: Adams, et al. (1978), Wang and Zhang (1987), Stubbs et al. (1990), Hearn and Testa (1991), Richardson and Mannan (1992), Sanders et al. (1992), Narkis (1994), Brincker et al. (1995), Balis Crema et al. (1995), Skjaerbaek et al. (1996a), and Villemure et al. (1996).

As natural frequencies of a structure are global properties of a structure, they cannot provide spatial information about damage in the structure and thus only indicate the occurrence of damage and can only be used as a Level 1 damage detection technique. The exception to this is modal response at higher natural frequencies, because the mode shapes are associated with local responses at higher modal frequencies.

2.3.1.2 Change in Mode Shapes

Mode shape information can be utilized to locate damage in the structure and this technique can be implemented as Level 3 damage detection technique. Damage present in structure causes change in its mode shape and the relative change in the mode shape can be graphically monitored to locate damage in the structure. The mode shapes need to be normalized in order to effectively find the location of damage.

West (1984) presented what was possibly the first systematic use of mode shape information for the location of structural damage without the use of a prior FEA model. He used the modal assurance criteria (MAC) to determine the level of correlation between modes from the test of an undamaged Space Shuttle Orbiter body flap and the modes from the test of the flap after it had been exposed to acoustic loading. The mode shapes were partitioned using various schemes, and the change in MAC across the different partitioning techniques was used to localize the structural damage.

Fox (1992) showed that single-number measures of mode shape changes, as the MAC were relatively insensitive to damage in a beam with a saw cut. Again this highlights the problem that too much data compression can cause in a damage identification. "Node line MAC," a MAC based on measurement points close to node points for a particular mode, was found to be a more sensitive indicator of changes in the mode shape caused by damage. Graphical comparisons of relative changes in mode shapes proved to be the best way of detecting the damage location when only resonant frequencies and mode shapes were examined. A simple method of correlating node points in modes that showed relatively little change in resonant

frequencies with the corresponding peak amplitude points in modes that showed large changes in resonant frequencies was shown to locate the damage. The author also presented a method of scaling the relative changes in mode shape to better identify the location of the damage.

Mayes (1992) presented a method for model error localization based on the mode shape changes known as the structural translational and rotational error checking (STRECH). By taking ratios of relative modal displacements, STRECH can assess the accuracy of the structural stiffness between two different structural degrees of freedom (DOF). STRECH can also be applied to compare the results of a test with an original FEM or to compare the results of two tests.

Ratcliffe (1997) presented a technique for locating damage in a beam that used a finite difference approximation of a Laplacian operator on mode shape data. Cobb and Liebst (1997) presented a method for prioritizing sensor locations for structural damage identification based on an eigenvector sensitivity analysis. Skjaeraek et al. (1996b) examined the optimal sensor location issue for detecting structural damage based on changes in mode shapes and modal frequencies using a substructure iteration method.

Yuen (1985), Rizos et al. (1990), Osegueda et al. (1992), Kam and Lee (1992), Kim et al.(1992), Srinivasan and Kot (1992), Ko et al. (1994), Salawu and Williams (1994, 1995), Lam et al. (1995), Salawu (1995), Salawu (1997), and Saitoh and Takei (1996) also provided examples of other studies that examined changes in mode shapes. The studies focused primarily on MAC and coordinate MAC (COMAC) values to identify damage.

2.3.1.2.1 MODE SHAPE CURVATURE/STRAIN MODE SHAPE CHANGES

An alternative to using mode shapes to obtain spatial information about sources of vibration changes is using mode shape derivatives, such as the curvature. It is first noted that for beams, plates and shells there was a direct relationship between curvature and bending strain. Some researchers discuss the practical issues of measuring strain directly or computing them from displacements or accelerations.

Pandey et al. (1991) demonstrated that absolute changes in a mode shape curvature could be a good indicator of damage for the beam structures they considered. The curvature values were computed from the displacement mode shape using the central difference operator.

Stubbs et al. (1992) presented a method based on the decrease in modal strain energy between two structural DOF, as defined by the curvature of the measured mode shapes. Topole and Stubbs (1995a, 1995b) examined the feasibility of using a limited set of modal parameters for structural damage detection. In a more recent publication, Stubbs and Kim (1996) examined the feasibility of localizing damage using this technique without using the baseline modal parameters.

Chance, et al. (1994) found that numerically calculating curvature from mode shapes resulted in unacceptable errors. They used directly measured strains instead of measuring curvature directly, which dramatically improved the results.

Chen and Swamidas (1994), Dong et al. (1994), Kondo and Hamamoto (1994), Nwosu et al.(1995), and Yao and Chang (1995) presented other studies that identify damage from the changes in mode shape curvature or strain-based mode shapes.

2.3.2 Methods Based on Dynamic Flexibility Measurements

These methods use the dynamically measured stiffness matrix in order to detect damage. The flexibility matrix of the structure is defined as the inverse of stiffness matrix, and each column of the flexibility matrix of the structure corresponds to the displacement pattern of the structure when subjected to a unit force at a particular node. The flexibility matrix can be derived by calculating mass-normalized mode shapes and natural frequencies. In case of a structure having large number of degrees of freedom (DOF), due to limitations in calculating of all mode shapes and natural frequencies, only significant low- frequency modes and their corresponding natural frequencies are considered.

While implementing this technique, damage is detected by comparing a calculated flexibility matrix obtained by using the modes of the damaged structure to the flexibility matrix obtained with the modes obtained from the undamaged

structure. Sometimes, for a comparison of flexibility matrices, a flexibility matrix obtained by finite element model (FEM) of the undamaged structure may be used instead of a measured flexibility matrix of the undamaged structure. This technique is considered as a Level 3 damage detection technique.

Because the flexibility matrix is defined as the inverse of the static stiffness matrix, the flexibility matrix relates the applied static force and the resulting structural displacement. The measured flexibility matrix can also be estimated from the mass-normalized measured mode shapes and frequencies. The formulation of the flexibility matrix by this method is approximate due to the fact that only the first few modes of the structure (typically the lowest frequency modes) are measured. The synthesis of the complete static flexibility matrix would require the measurement of all of the mode shapes and frequencies.

Typically, damage is detected using flexibility matrices by comparing the flexibility matrix synthesized using the modes of the damaged structure to the flexibility matrix synthesized using the modes of the undamaged structure or the flexibility matrix from a FEM. Because of the inverse relationship to the square of the modal frequencies, the measured flexibility matrix is most sensitive to changes in the lower-frequency modes of the structure. Therefore, Aktan et al. (1994) proposed the use of measured flexibility as a "condition index" to indicate the relative integrity of a bridge. They applied this technique to two bridges and analyzed the accuracy of the flexibility measurements by comparing the measured flexibility to the static deflections induced by a set of truck-load tests.

Pandey and Biswas (1994, 1995) presented a damage-detection method based on changes in the measured flexibility of the structure. The method applied to several numerical examples and to an actual spliced beam where the damage was linear in nature. Results of the numerical and experimental examples showed that evaluation of the damage condition and its location of the damage could be obtained from just the first two measured modes of the structure.

Toksoy and Aktan (1994) computed the measured flexibility of a bridge and examined the cross hyphen sectional deflection profiles with and without a baseline

data set. They observed that anomalies in the deflection profile could indicate damage, even without access to a baseline data set.

Mayes (1995) used the measured flexibility to locate damage from the results of a modal test on a bridge. He also proposed a method for using the measured flexibility as the input for a damaged detection method (STRECH), which evaluated the changes in the load-deflection behavior of a spring-mass model of the structure.

Peterson et al. (1995) proposed a method for decomposing the measured flexibility matrix into elemental stiffness parameters for an assumed structural connectivity. This decomposition is accomplished by projecting the flexibility matrix onto an assemblage of the element-level static structural eigenvectors.

Zhang and Aktan (1995) suggested that changes in curvatures of a uniformly distributed load surface (deformed shape of the structure when subjected to a uniform load), calculated using the uniform load flexibilities, were sensitive indicators of local damage. The authors stated that changes in the load surface could also be used to identify uniform deterioration. A uniform load flexibility matrix was constructed by summing the columns of the measured flexibility matrix. The curvature is then calculated from the uniform load flexibilities using a central difference operator.

2.3.3 Model Update Methods

This type of technique uses a structural model and the structural model parameters (i.e. mass, stiffness and damping) are calculated from the equations of motion and the dynamic measurements. The matrices for mass, stiffness and damping in the model are formulated in such a way that the model response will be almost similar to the measured dynamic response of the structure. The matrices are updated with new dynamic measurements and the updated stiffness, as well as damping matrix, can be compared to the original stiffness and damping matrix, respectively, to detect the location and intensity of the damage in a structure.

Various other methods have also been developed, each with different approach for model updating. Those can be classified in different categories depending on the objective function for minimization problem, constraints placed on the model or numerical method used to accomplish the optimization. For more information about

the model update methods the reader is referred to Smith and Beattie (1991a) and Zimmerman and Smith (1992).

2.3.4 Neural Network (NN) based Methods

The neural network, a concept developed as generalization of mathematical models of human cognition or neural biology, has proven to be an efficient technique for damage detection. According to Haykin (1998), a neural network is a massively parallel distributed processor made of simple processing units, which has a natural propensity for storing experimental knowledge and making it available for use. With its capacity of performing accurate pattern recognition and classification, adaptivity, modeling non-linearity, and learning capabilities, neural networks can be used for SHM in different ways:

1. To model the dynamic behavior of a system or part of the system under control (Chen et al. 1995, and Adeli, 2001)

2. To model the restoring forces in civil structures (Liang et al., 1997 and Saadat, 2003)

3. To carry out pattern recognition for fault detection in rotating machinery, e.g., for gear box failure (Dellomo, 1999), turbo-machinery (Kerezsi and Howard, 1995), and bearing fault detection (Samanta et al., 2004).

Application of neural network model for SHM can also be found in Saadat (2003) where the author used an "Intelligent Parameter Varying" (IPV) technique for health monitoring and damage detection technique that accurately detects the existence, location, and time of damage occurrence without any assumptions about the constitutive nature of the structural non-linearity. The technique in Saadat (2003) was based on the concept of the "gray box", a concept which combines a linear time invariant dynamic model for a part of the structure with a neural network model used to model the restoring forces in a non-linear and time-varying system. The detailed information about the technique can be found in Nelles (2000).

Even if good results are obtained with NN techniques, one of the challenges in implementing it for a practical application in SHM is appropriate level of training and

avoiding over-training of the network. Recent work in integration of NN with other computational techniques to enhance their performance can be found in Adeli (2001).

2.3.5 Pattern Recognition Techniques

Damage present in the structure causes change in the modal parameters which in turn causes change in the pattern of the structural response. This pattern can be monitored to detect the time, location and intensity of damage. Hera & Hou (2003) successfully detected sudden damage in the ASCE benchmark structure by monitoring the spikes present in the higher level details of the acceleration response. A motivation behind this approach was that a sudden damage in structure causes singularity in the acceleration response and this singularity results in a spike in higher level details of the wavelet transform of the signal.

Another pattern recognition method, proposed by Los Alamos National Laboratory, is based on statistical considerations. A statistical pattern recognition framework was proposed which consisted of the assessment of structure's working environment, the acquisition of structural response, the extraction of features sensitive to damage and the development of statistical model that was used for feature discrimination. More information and application of this method can be found in Sohn and Farrar (2001), Sohn et al. (2001a & 2001b), Worden (2002) and Lei et al. (2003).

2.3.6 Kalman Filter Technique

Kalman filter technique is the model based technique that implements an optimal recursive data processing algorithm to estimate structural parameters necessary to identify damage in the structure. The parameters with which damage in a structure can be identified (i.e. stiffness and damping of the structure) cannot be measured directly, and in general practice, acceleration, velocity or displacement of the structure is measured. The Kalman filter technique uses a set of equations of motion that relates structural properties with the measured parameters. It works in a predictor-corrector manner (i.e. it estimates the value of the structural parameter based on the dynamic model and the previous measurements and then optimizes the estimated value by comparing it with the value obtained by a measurement model and

actual measurements). The optimization of the estimated value is done to minimize the square of the difference between the estimated and the measured value. This technique accounts for the effect of noise introduced during a measurement, as well as the effect of modeling errors. Kalman filter has been applied for damage detection (Lus et al.,1999).

2.3.7 Statistical Approach

This newly developed technique is fundamentally based on the Bayesian approach, a well known theorem in statistical theory. An important advantage of the Bayesian approach is that it can handle the non-uniqueness of a model that can appear in the cases with insufficient number of measurements. In order to take care of uncertainties, Beck and Katafygiotis (1998) developed a Bayesian statistical framework for system identification and structural health monitoring. The statistical model was developed to take care of the uncertainties introduced due to incomplete test data as a result of limited number of sensors, noise contaminated dynamic test data, modeling errors, insensitiveness of modal parameters to the changes in stiffness, and to describe the class of structural models that include as much prior information as possible to reduce the uncertainties and degree of non-uniqueness.

The method can be used for updating the system probability model to account for the above-mentioned uncertainties and to provide a quantitative assessment of the accuracy of results. The applications of the approach for modal identification can be found in Yuen et al., (2002), and Yuen and Katafygiotis (1998), whereas the methods application for an ASCE benchmark SHM problem can be found in Yuen et al., (2002), and Lam et al., (2004).

2.3.8 SIGNAL PROCESSING METHODS

A signal collected from the accelerometers mounted on a structure cannot be analyzed directly to draw useful conclusions about damage unless the damage intensity is very high. It needs to be processed in order to extract useful information about the structural parameters and damage. The signal is often transformed into different domains in order to better interpret the physical characteristics inherent to the original signal. The original signal can be reconstructed by performing inverse

operation on the transformed signal without any loss of data. The popular methods in signal processing for SHM applications include the Fourier, Wavelet Analysis and Hilbert-Huang Analysis. All of these methods can be distinguished from one another by a way in which it maps the signal and each has advantages over one another in terms of applicability for analyzing specific data type. A brief introduction of each method is given below.

2.3.8.1 Fourier Analysis

Fourier analysis of a signal converts the signal from time domain to frequency domain. Mathematically the Fourier transform of a signal *'f(t)'* can be represented

$$H(\omega) = \int_{-\infty}^{\infty} f(t) e^{-\omega t} \, dt \qquad (2.1)$$

where '$H(\omega)$' is the Fourier transform of signal *'f(t)'*. Fourier transform represents the signal in frequency domain and useful information about the frequency content in the signal can be extracted. The plot of the power of Fourier transform versus frequency exhibits peaks at the dominant frequencies present in the signal and the amplitude of the power indicates intensity of the frequency component.

Note that the Fourier transform of a signal integrates the product of the signal with a harmonic of infinite length; therefore the time information in the signal may be lost or become implicit. If the signal to be analyzed is a non-stationary signal i.e. (if the amplitude or frequency changes abruptly over time), then, with the Fourier transform of the signal, this abrupt change in time spreads over the whole frequency axis in '$H(\omega)$'. Therefore Fourier transform is more appropriate to analyze a stationary signal.

To cope with the deficiency of losing time information in Fourier transform, the Short-Time-Fourier-Transform (STFT) was developed. STFT uses a sinusoidal window of fixed width to analyze the signal and it shifts along the data to be analyzed in order to retain the time information in the signal. Thus in contrast to only frequency representation ($H(\omega)$ as in case of Fourier transform), STFT employs a

time-frequency representation, $H(\omega,\tau)$, of the signal '*f(t)*' as in the following equation 2.2.

$$H(\omega,t)=\int_{-\infty}^{\infty} f(t)\,g^{*}(t-\tau)\,e^{-\omega t}\,dt \qquad (2.2)$$

where $g(t-\tau)$ is a window function. Once the window width is chosen, then the time-frequency resolution obtained remains fixed over the entire time-frequency plane. Consequently, and one can either get good time resolution, or good frequency resolution in the analysis, but not both. More information about the STFT can be found in Allen and Rabiner (1977) and Rioul and Vetterli (1991).

Because of its ability to identify the frequency content and intensity of the frequency component of a signal, significant information about the modal parameters (i.e. natural frequency, mode shapes and damping) can be extracted from the Fourier transform of the structural response. Various methods of fault diagnosis and damage detection based on the Fourier transform of the vibration response of the structure can be found in Chiang et al., (2001).

2.3.8.2 Wavelet Analysis

Analyzing the response data of general transient nature without knowing the time at which the damage occurred, would result into inaccurate results if one uses the traditional Fourier analysis. This is due to the time integration conducted over the entire time span. Moreover, damage usually develops progressively (such as stiffness degradation due to mechanical fatigue and chemical corrosion); therefore a change in stiffness might never be detectable. As an extension of the traditional Fourier analysis, the wavelet analysis provides a multi-resolution and time-frequency analysis for non-stationary data; therefore, it can be effectively applied for structural health monitoring.

2.3.8.2.1 Continuous Wavelet Transform (CWT)

The Continuous Wavelet Transform (CWT) of a signal *f(t)*, $W_f(a,b)$, is defined as

$$W_f(a,b) = \frac{1}{\sqrt{a}} \int_{-\infty}^{\infty} f(t) * \overline{\psi}\left(\frac{t-b}{a}\right) dt \qquad (2.3)$$

Here $\overline{\psi}$ is the conjugate of a mother wavelet function ψ, 'a' and 'b' are called as the dilation parameter and the translation parameter, respectively. Both of the parameters are real and 'a' must be positive. The mother wavelet ψ needs to satisfy certain admissibility condition in order to ensure existence of the inverse wavelet transform.

The dilation parameter 'a' and the translation parameter 'b' are also referred as the scaling and shifting parameters, respectively; they play an important role in the wavelet analysis. By varying the value of translation parameter 'b', a signal is examined by the wavelet window piece by piece localized in the neighborhood of 't=b'; thus, the non-stationary nature of the data can be examined, in which case, it becomes similar to the Short Time Fourier Transform (STFT). By varying the value of the dilation parameter 'a', the data portion in the neighborhood of 'b' can be examined in different resolutions; thus, a time varying frequency content of the signal can be revealed by this multi-resolution analysis, a feature not available in the STFT. The continuous wavelet transform maps the signal on a Time-Scale plane. The concept of scale in Wavelet analysis is similar to the concept of frequency in Time-Frequency analysis; the scale is inversely proportional to the frequency. Performing the inverse wavelet transform on the wavelet transform of a signal, the original signal can be reconstructed without any loss of data. For detailed information of wavelet transform readers are referred to Rioul and Vetterli (1991) and Daubechies (1992). Early applications of wavelets for damage detection of mechanical systems were also summarized in Staszewski (1998).

2.3.8.2.2 Discrete Wavelet Transform (DWT)

The computational cost of performing continuous wavelet transform can be reduced by implementing Discrete Wavelet Transform (DWT). In DWT, the dilation parameter 'a' and the translation parameter 'b' are discretized by using the dyadic scale, i.e.,

$$a = 2^j \quad b = k.2^j \qquad j,k \in z \tag{2.4}$$

where z is a set of positive integers.

In the case of DWT, the wavelet plays a role of dyadic filter. The DWT analyzes the signal by implementing a wavelet filter of particular frequency band to shift along a time axis. The frequency band of the filter depends on the level of decomposition, and by shifting it in the time domain, the local examination of the signal becomes possible. As a result, the signal can be decomposed into a tree structure, with wavelet details and wavelet approximations at various levels as follows

$$f(t) = \sum_{i=1}^{i=j} D_i(t) + A_i(t) \tag{2.5}$$

where $D_i(t)$ denotes the wavelet detail and $A_i(t)$ stands for the wavelet approximation at the j^{th} level, respectively. A graphical representation of DWT of a signal is shown in Figure 2.1.

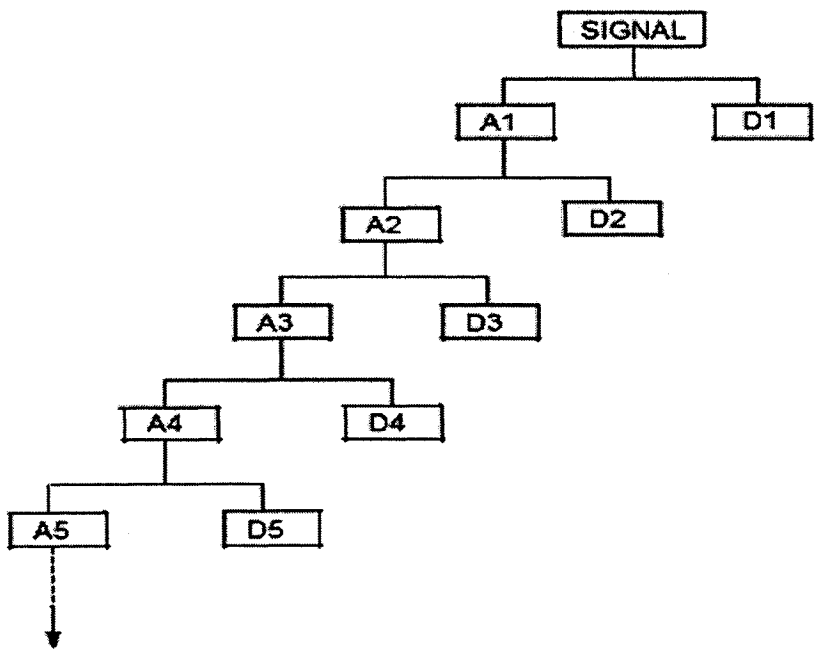

Figure 2.1 Schematic of the Discrete Wavelet Transform Decomposition Tree

The DWT decomposition of the signal with each level of decomposition results in halving the time resolution, but doubling the frequency resolution. The signal can be easily reconstructed as the dyadic wavelet filter family forms an orthonormal basis (Daubechies, 1999). Recent applications of discrete wavelet transform for structural health monitoring can be found in Hou et al. (2000) and Hera and Hou (2003).

2.3.8.3 Wavelet Packet Transform

As a result of decomposition of only the approximation component at each level using the dyadic filter bank, the frequency resolution in higher-level (e.g. A1 and D1), DWT decompositions in a regular wavelet analysis may be lower. It may therefore cause problems while applying DWT in certain applications, where the important information is located in higher frequency components. The frequency resolution of the decomposition filter may not be fine enough to extract necessary information from the decomposed component of the signal. The necessary frequency resolution can be achieved by implementing a wavelet packet transform to decompose a signal further (Goswami and Chan, 1999). The wavelet packet analysis is similar to the DWT with the only difference that in addition to the decomposition of only the wavelet approximation component at each level, a wavelet detail component is also further decomposed to obtain its own approximation and detail components as schematically shown in Figure 2.2.

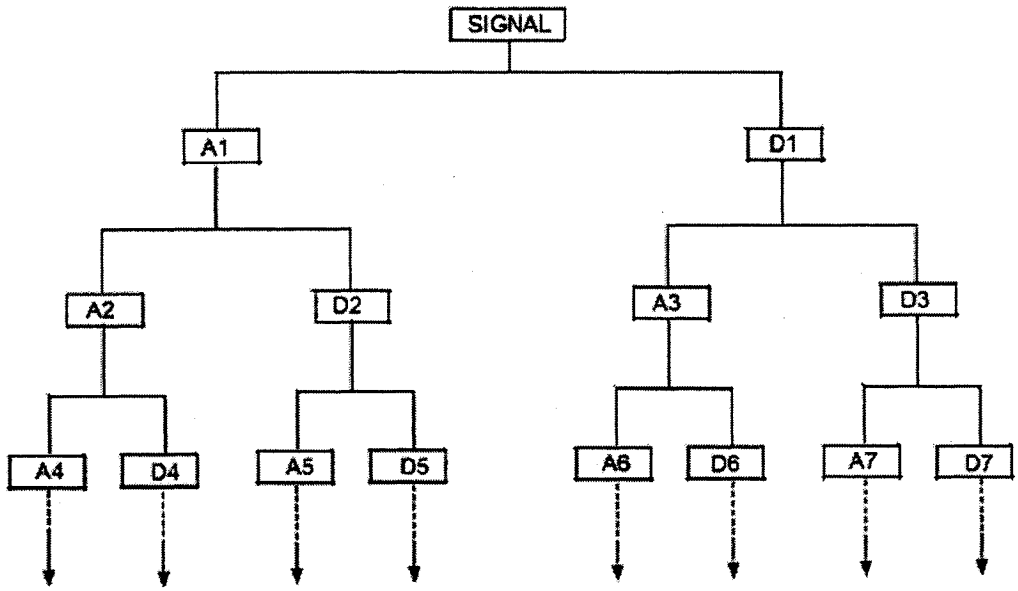

Figure 2.2 Wavelet Packet Decomposition Tree **Schematics**

Each component in this wavelet packet tree can be viewed as a filtered component with a bandwidth of a filter decreasing with increasing level of decomposition; one can then view the whole tree as a filter bank. At the top of the tree, the time resolution of the WP components is relatively good, but at the expense of poor frequency resolution. On the other hand, at the bottom of the tree, the frequency resolution is relatively good but at the expense of poor time resolution. Thus, with the use of wavelet packet analysis, the frequency resolution of the decomposed component with high frequency content can be increased. As a result, the wavelet packet analysis provides better control of frequency resolution for the decomposition of the signal.

2.3.8.4 Hilbert-Huang Analysis

NASA Goddard Space Flight Center (GSFC) developed a signal analysis method, known as the Empirical Mode Decomposition (EMD) method, which analyzes the signal by decomposing the signal into its monocomponents, called the Intrinsic Mode Functions (IMF) (Huang et al., 1998). The empirical nature of the

approach may be partially attributed to a subjective definition of the envelope and the intrinsic mode function involved in its sifting process. The EMD method used in conjunction with the Hilbert Transform is also known as the 'Hilbert-Huang Transform' (HHT). Because of its effectiveness in analyzing nonlinear, non-stationary signals, the HHT has been recognized as one of the most important discoveries in the field of applied mathematics in NASA's history. By the EMD method, the original signal *'f(t)'* can be represented in terms of the IMFs as:

$$f(t) = \sum_{i=1}^{n} c_i(t) + r_n \tag{2.6}$$

where $c_i(t)$ is the i^{th} Intrinsic Mode Function, and r_n is the residue.

A set of analytic functions can be constructed for these IMFs. The analytic function '*z(t)*' of a typical IMF '*c(t)*' is a complex signal having the original signal '*c(t)*' as the real part and its Hilbert transform of the signal as its imaginary part. By representing the signal in the polar coordinate form, one has

$$z(t) = c(t) + jH[c(t)] = a(t).e^{j\phi(t)} \tag{2.7}$$

where '*a(t)*' is the instantaneous amplitude and '$\phi(t)$' is the instantaneous phase function. The instantaneous amplitude '*a(t)*' and the instantaneous phase function '$\phi(t)$' can be calculated as

$$a(t) = \sqrt{\{c(t)\}^2 + \{H[c(t)]\}^2} \tag{2.8}$$

$$\phi(t) = \tan^{-1}\left\{\frac{H[c(t)]}{c(t)}\right\} \tag{2.9}$$

The instantaneous frequency of a signal at time *t* can be expressed as the rate of change of the phase angle function of the analytic function obtained by Hilbert Transform of the signal (Ville, 1948). The expression for the instantaneous frequency is given by:

$$\omega(t) = \frac{d\phi(t)}{dt} \tag{2.10}$$

Because of the capability of extracting the instantaneous amplitude *'a(t)'* and the instantaneous frequency $\omega(t)$ from the signal, this method can be used to analyze non-stationary vibration signals. In a special case of a single harmonic signal, the phase angle of its Hilbert transform is a linear function of time, and therefore, its instantaneous frequency is constant and is exactly equal to the frequency of the harmonic. In general, the concept of instantaneous frequency provides an insightful description as how the frequency content of the signal varies with the time. The method can be used for damage detection and system identification and the relevant applications can be found in Vincent et al., (1999), Yang and Lei (2000), Yang et al., (2003a, 2003b, 2004).

Chapter 3

Piezoelectric Material Behavior and Formulation

3.1 History of piezoelectricity

Centuries ago natives from Ceylan and India noticed a peculiar property of tourmaline crystals. Thrown in hot ashes, these crystals first attract them and then rejected them a few moments afterwards.

This observation came into Europe with the import of tourmaline by Dutch tradesmen at the beginning of the 18^{th} century. The tourmaline was called the Ceylan magnet.

In 1756, the electrical origin of that behavior was demonstrated by the German physicist, Aepinus (electrical capacitance's inventor). That behavior was named pyroelectricity by the Scottish physicist Brewster in 1824. The pyroelectric effect can be defined as the induction of polarization by thermal energy absorption; the induced polarization is proportional to the resulting temperature variation. The inverse property, of much less amplitude, is called the electro caloric effect.

The piezoelectric effect was first mentioned in 1817 by the French mineralogist Rene' Just Hauy. However, it was first demonstrated by Pierre and Jacques Curie in 1880. Their experiments led them to elaborate the early theory of piezoelectricity. This theory was complemented by the further work of G. Lippman, W.G. Hankel, Lord Kelvin and W. Voigt (beginning of 20^{th} century).

Until the beginning of the century, the piezoelectricity did not leave the laboratories. The first applications appeared during the first world war with the sonar in which piezoelectric quartz were used to produce ultrasonic waves (P.Langevin) and as sensors. In the twenties, the use of quartz to control the resonance frequency of oscillators was proposed by an American physicist: W. G. Cady. It is during the period following the first world war that most of the applications we are now familiar with (microphones, accelerometers, ultrasonic transducers, benders ...) were

conceived. However, the materials available at the time often limited device performance. The development of electronics, especially during the Second World War, and the discovery of ferroelectric ceramics increased the use of piezoelectric materials.

The direct piezoelectric effect describes of the ability of certain crystalline materials (i.e. ceramics) to generate an electrical charge in proportion to an externally applied force. The direct piezoelectric effect has been widely used in transducers design (accelerometers, force and pressure transducers, etc). According to the inverse piezoelectric effect, an electric field induces a deformation of the piezoelectric material. The inverse piezoelectric effect has been applied in actuator design.

The use of piezoelectric materials as actuators and sensors for noise and vibration control has been demonstrated extensively over the past few years (e.g. Forward, 1981; Crawley and de Luis, 1987). There are two classes of piezoelectric materials used in vibration control: ceramics and polymers. The best known piezoceramic is the Lead Zirconate Titanate (PZT); it has a recoverable strain of 0.1% and is widely used as actuator and sensor for a wide range of frequencies, including ultrasonic applications; it is well suited for high precision applications as well. Piezopolymers are mainly used as sensors; the best known is the Polyvinylidene Fluoride (PVDF). The PVDF were first studied by Kawai (end of the 60's) and were made commercially available in the early 80's.

3.2 Constitutive equations

In a first section, the unidimensional constitutive equations are established starting from the electrostatics point of view. The general thermo piezoelectric constitutive equations are derived from the laws of thermodynamics in the second section.

3.2.1 Piezoelectricity

In an unstressed one-dimensional dielectric medium, the dielectric displacement D (charge per unit area, expressed in Cb/m^2) is related to the electric field E (V/m) and the polarization P (Cb/m^2) by Equation.(3.1).

$$D = \varepsilon E = \varepsilon_0 E + P \tag{3.1}$$

$$P = (\varepsilon - \varepsilon_0)E \tag{3.2}$$

Similarly, in a one-dimensional elastic body placed in a zero electric field, the stress T (N/m2) and the strain S are related by

$$T = cS \tag{3.3}$$

where c is the stiffness of the material (the Young's modulus).

For a piezoelectric material, the electrical and mechanical constitutive equations are coupled. A strain S in the material induces a polarization eS by the direct piezoelectric effect. The total induced polarization is given by

$$P = (\varepsilon - \varepsilon_0)E + eS \tag{3.4}$$

Conversely, an applied electric field E tends to align the internal dipoles, inducing stresses –eE in the material by the inverse piezoelectric effect. The coupled equations finally become:

$$T = c^E S - eE \tag{3.5}$$

$$D = eS + \varepsilon^S E \tag{3.6}$$

In equation (3.5), the piezoelectric constant e relates the stress to the electric field E in the absence of mechanical strain and c^E refers to the stiffness when the electric field is constant. In equation (3.6), e relates the electric charge per unit area D to the strain under a zero electric field (short-circuited electrodes); e is expressed in $NV^{-1}m^{-1}$ or Cb/m^2. ε^S is the permittivity under constant strain.

Equation (3.5) is the starting point for the formulation of the equation of a piezoelectric actuator, while equation (3.6) is that for a sensor.

3.3 The Finite element approach

The study of physical systems frequently results in partial differential equations that either cannot be solved analytically or lack an exact analytic solution due to the complexity of the boundary conditions or domain. For a realistic and detailed study, a numerical method must be used to solve the problem. The finite element method is often found to be the most efficient numerical tool.

Over the years, with the development of modern computers, the finite element method has become one of the most important analysis tools in engineering. It has penetrated successfully many areas such as solid mechanics, heat transfer, fluid mechanics, electromagnetism, acoustics and fracture mechanics. Commercial finite element packages are now widely available on personal workstations.

Basically, the finite element method (Zienkiewicz, 1971; Reddy, 1984; Hughes, 1987) consists in a piecewise application of classical variational methods to smaller and simpler subdomains called finite elements connected to each other in a finite number of points called nodes. The fundamental principles of the finite element method (displacement based) are:

The continuum is divided in a finite number of elements of geometrically simple shape. These elements are connected in a finite number of nodes. The unknowns are the displacements of these nodes. Polynomial interpolation functions are chosen to describe the unknown displacement field at each point of the elements related to the corresponding field values at the nodes.

The forces applied to the structure are replaced by an equivalent system of forces applied to the nodes. The situation where they are nearly collocated is particularly critical, because the zeros of the frequency response function are dominated by local effects (See Preumont (1997); Loix et al. (1998)). These can easily be accounted for by finite elements (Piefort & Henrioulle, 2000).

A finite element formulation accounting for the coupling between the equations of electrostatics and elastodynamics becomes necessary when the piezoelectric material represents a non negligible fraction of the entire structure.

3.3.1 History

Following the early work of Eer Nisse (1967) and Tiersten (1967) who established variation principles for piezoelectric media, the finite element modeling of structures with embedded piezoelectrics has known important developments in recent years. Allik and Hughes (1970) proposed a tetrahedral volumic element accounting for the piezoelectricity. Starting from Hamilton's principle and the constitutive equations for piezoelectric media, a simple volumic element (tetrahedron)

taking into account the piezoelectric coupling is presented. The element has 4 nodes and 4 degrees of freedom per node (3 translations and the electric potential); it uses linear shape functions for both displacement and electrical fields.

Lerch (1990) developed a general formulation accounting for the piezoelectric coupling for two and three-dimensional finite element modeling of piezoelectric devices. Comparisons between numerical simulation and experiment are presented for the vibration of piezoceramic parallelepiped bars.

A higher order tetrahedral element was proposed by Moetakef et al. (1995). Interpolation functions of higher order were used; tetrahedron of 10 (linear strain element) and 20 nodes (quadratic strain element) were presented; brick elements were obtained by assembling tetrahedrons using a Guyan condensation of the resulting internal nodes to reduce the number of degrees of freedom; these elements were used to model a bimorph pointer (actuation), for which the results were compared to an analytical solution, and a cube under uniform pressure (sensing). An experiment consisting of generating an elastic wave in a cantilever beam was also described in Moetakef et al. (1996); results from the model are compared to experimental ones and shown good qualitative agreement.

With the increasing number of shell structures, the need for a finite element modeling tool for plates and shells with embedded distributed piezoelectric actuators and sensors has become more and more evident. Different approaches for modeling thin and thick shells have been proposed.

Tzou and Tseng (1990, 1991) derived a thin brick element for distributed dynamic measurement and active vibration control of a rectangular plate; the element consists of a thin solid piezo-electric brick having 8 structural nodes with 4 degrees of freedom per node (3 translations and the electric potential) and 3 internal nodes (condensed using a Guyan's reduction) to dissipate the excessive shear energy due to the small dimension in the thickness direction. A classic configuration for an intelligent structure is composed of a master structure sandwiched between 2 piezoelectric thin layers acting as the distributed sensor and actuator. Both bonded and embedded piezoelectric sensors and actuators result in a laminate; the multilayer structure is modeled by stacking the thin brick elements together and connecting the

corresponding nodes. The model was applied to the vibration control of a simply supported square plate. Mode shape and modal voltage distribution were obtained thanks to the model.

Ha et al. (1992) used a similar brick element, where the multilayer structure was taken into account; the element matrices were integrated over the thickness of each layer and summed. That element is used to model the cantilever plate described in (Crawley and Lazarus, 1991) (static case), to determine the step-response of a cantilever beam and to design the active damping of the first mode of sensor/actuator composite cantilever plate. The results were compared to the results found in (Crawley and Lazarus, 1991) and showed good agreement.

Rao and Sunar (1993) established a finite element formulation of thermopiezoelectric problems starting from the linear thermo piezoelectric constitutive equations established Mindlin (1974) and the Hamilton's principles. Sunar and Rao, (1996, 1997), used the quasi static equations of thermo piezoelectricity to develop heat, sensor and actuator equations; a finite element formulation was also presented. A distributed control system consisting of a cantilever beam sandwiched between a piezoelectric sensor/actuator pair was used to evaluate the proposed finite element approach on the static and dynamic behavior.

Tzou and Ye (1996) derived a 12-nodes triangular thin solid plane element with 4 degrees of freedom per node. The element uses shape functions quadratic in the two in-plane directions and linear in the transverse direction with the assumption of a layer wise constant shear angle (Mindlin hypothesis). A laminate can be composed of laminae which could be either elastic material or piezoelectric material; the laminated structure is obtained by stacking elements together and connecting the corresponding nodes; this element was validated by modeling the actuation of a bimorph pointer. To stress the influence of the piezoelectric coupling on the vibration characteristics, a semicircular ring shell was modeled using 60 triangular shell elements (20 for each layer and 10 element meshes along the length); the evolution of its Eigen frequencies with a growing number of short-circuited electrodes was examined. The number of short-circuited electrodes varies from 1 to 10 (fully short-circuited). This element has been extended later by K¨oppe et al. (1998) to isoparametric curved triangular and

quadrangular elements with shape functions of different polynomial degree for each layer; the model is applied to a rectangular plate of composite material with surface bonded piezo patches under static voltage load, simply supported on two edges.

The modeling of shells using solid elements results in an excessive shear strain energy in the thickness direction. By reducing one dimension compared to the others, the transverse shear stiffness term becomes excessively important (linked to the linear interpolation of the strain) leading to what is usually called the shear locking phenomenon. A commonly used solution to overcome this difficulty consists in adding internal degrees of freedom resulting in large problem size requiring techniques such as the Guyan's reduction (also known as static condensation) to reduce the number of degrees of freedom.

Lee and Saravanos (1996) derived a thermopiezoelectric multilayer beam element; it uses shape functions linear along the beam and linear through the thickness of each layer (layerwise linear).

A reduced integration scheme for the transverse shear stiffness was used; the element takes into account the effect of constant thermal load (constant gradient of temperature); A cantilever beam under thermal load was modeled. Heyliger et al. (1996) extended the layerwise linear formulation to a piezoelectric shell element and applied it to static and dynamic modeling of a simply supported plate and a cylindrical shell. Later, Saravanos (1997) presented a multilayer piezoelectric thin plate using the Kirchhoff-Love assumption (linear displacement field through the thickness) and bilinear shape functions; it has 1 electrical degree of freedom per piezoelectric layer per node, assuming a constant electric field through the thickness for each layer (layerwise linear transverse shape function for the electric potential). That shell element has been applied to the modeling of a simply supported plate and shown good agreement with exact solutions for moderately thin plates ($a/h \approx 50$), an actuated cylindrical panel to study the effect of the actuator placement through the thickness which exactly matched a Ritz solution. Cantilever cylindrical shell was used to show the effect of actuation and sensing, and of the difference between continuous and discontinuous transducers (4 across the length), as well as the effect of the curvature on the tip displacement and sensing. The element later used to evaluate the

passive damping of piezoelectric shells with integrated electrical network and the results were compared with experiments (Saravanos, 2000).

A pure bending (Kirchhoff assumption) plane rectangular plate element was proposed by (Hwang and Park, 1993); the main idea was the use of a multilayered plate element with a single electrical degree of freedom per piezoelectric layer, the voltage across the thickness of the layer, uniform on the element surface. This multilayer element has 4 nodes with 3 degrees of freedom per node (1 translation and 2 rotations) and 1 electrical degree of freedom for each piezoelectric layer (voltage across the layer). This element neglects the transverse shear and is therefore not suitable for modeling thick shells; it does not account for the extension, thus modeling only the bending behavior. The bimorph pointer was modeled numerically and the results were compared to an analytical solution, and showing a good agreement. Chen et al. (1997) used an isoparametric pure bending element to model a bimorph beam for vibration control design.

Samanta et al. (1996) used a cubic displacement field with an 8-node quadratic rectangular multilayer plate with 2 electrical degrees of freedom (constant voltage over the element across the only two piezoelectric outer layers) and 11 mechanical degrees of freedom per node (3 translations, 3 slopes and 5 higher order rotations). A simply supported plate was modeled; the fundamental natural frequencies and forced response were computed and showed good agreement with exact solutions.

Suleman and Venkayya (1995a) and Suleman and Goncalv`es (1995) proposed a 4 node plate element using bilinear shape functions and the Mindlin assumption (constant shear angle) to accommodate thick as well as thin shells; each node having 5 degrees of freedom (3 translations and 2 rotations), the element has also one additional electrical degree of freedom per piezoelectric layer (voltage across the thickness). It uses a reduced integration scheme for the transverse shear stiffness to avoid the shear locking phenomenon. This element was verified using the plate described by Crawley and Lazarus (1991), a bimorph pointer and panel flutter control; comparison with the work of Ha et al. (1992) was also made.

Chattopadhyay et al. (1999) developed a quasi-static coupled thermo piezoelectric model for a smart composite plate structure with surface bonded

piezoelectric materials using a variational approach. Linear piezoelectricity was assumed and a higher order transverse shear strain distribution was used (third order). A simply supported unidirectional graphite/epoxy laminate plate was modeled to verify the formulation. The influence of transverse shear and couplings were discussed. A shell finite element formulation was derived (Zhou et al., 2000) with the same transverse shear strain distribution and a higher order thermal field. A rectangular fiber-reinforced laminated plate with surface bonded piezoelectric patches is modeled; the influence of the couplings on the dynamics of piezo and thermo-actuated structures is discussed.

When plate's thickness becomes small, the behavior of the elements accounting for the transverse shear strain (e.g. Mindlin elements) is driven by transverse shear stiffness while the transverse shear strain should be negligible. This also leads to the shear locking phenomenon. Solutions to overcome this problem can be either using a reduced integration scheme for the transverse shear stiffness (Suleman and Venkayya, 1995b; Hong and Chopra, 1999), or to use different interpolation functions for the transverse shear strain.

3.3.2 Finite element formulation

The displacement field {u} and the electric potential ϕ over an element are related to the corresponding node values $\{u_i\}$ and $\{\phi_i\}$ by the mean of the shape functions $[N_u], [N_\phi]$

$$\{u\} = [N_u]\{u_i\} \qquad (3.7)$$
$$\phi = [N_\phi]\{\phi_i\}$$

And therefore, the strain field {S} and the electric field {E} are related to the nodal displacements and potential by the shape functions derivatives $[B_u]$ and $[B_\phi]$ defined by

$$\{S\} = [D][N_u]\{u_i\} = [B_u][u_i]$$
$$\{E\} = -\nabla[N_\phi]\{\phi_i\} = -[B_\phi]\{\phi_i\} \qquad (3.8)$$

where ∇ is the gradient operator and [D] is the derivation operator defined such as {S} = [D]{u}

$$[D]=\begin{bmatrix} \partial_x & 0 & 0 \\ 0 & \partial_y & 0 \\ 0 & 0 & \partial_z \\ 0 & \partial_z & \partial_y \\ \partial_z & 0 & \partial_x \\ \partial_y & \partial_x & 0 \end{bmatrix}$$

Substituting expressions (3.7) into the variational principle yields

$$\begin{aligned} 0 = &-\{\delta u_i\}^T \int_V \rho [N_u]^T [N_u] dV \{\ddot{u}\} - \{\delta u_i\}^T \int_V [B_u]^T [c^E] [B_u] dV \{u_i\} \\ &- \{\delta u_i\}^T \int_V [B_u]^T [e] [B_\phi] dV \{\phi_i\} - \{\delta \phi_i\}^T \int_V [B\phi]^T [e]^T [B_u] dV \{u_i\} \\ &+ \{\delta \phi_i\}^T \int_V [B_\phi]^T [\varepsilon^S] [B_\phi] dV \{\phi_i\} + \{\delta u_i\}^T \int_V [N_u]^T \{F_V\} dV \\ &+ \{\delta u_i\}^T \int_{\Omega_1} [N_u]^T \{F_\Omega\} d\Omega + \{\delta u_i\}^T [N_u] \{F_P\} \\ &- \{\delta \phi_i\}^T \int [N_\phi]^T \vartheta d\Omega - \{\delta \phi_i\}^T [N_\phi]^T Q \end{aligned} \tag{3.9}$$

which must be verified for any arbitrary variation of the displacements $\{\delta u_i\}$ and electrical potentials $\{\delta \phi_i\}$ compatible with the essential boundary conditions.

For an element, Equation (3.9) can be written under the form

$$[M]\{\ddot{u}_i\} + [K_{uu}]\{u_i\} + [K_{u\phi}]\{\phi_i\} = \{f_i\} \tag{3.10}$$

$$[K_{\phi u}]\{u_i\} + [K_{\phi\phi}]\{\phi_i\} = \{g_i\} \tag{3.11}$$

with

$$[M] = \int_V \rho \{N_u\}^T [N_u] dV \tag{3.12}$$

$$[K_{uu}] = \int_V [B_u]^T [c^E] [B_u] dV \tag{3.13}$$

$$[K_{u\phi}] = \int_V [B_u]^T [e]^T [B_\phi] dV \tag{3.14}$$

$$[K_{\phi\phi}] = -\int_V [B_\phi]^T [\varepsilon] [B_\phi] dV \tag{3.15}$$

$$[K_{\phi u}] = [K_{u\phi}]^T \tag{3.16}$$

or, the element mass, stiffness, piezoelectric coupling and capacitance matrix, respectively

$$\{f_i\} = \int_V [N_u]^T \{P_b\} dV + \int_{\Omega_1} [N_u]^T \{P_S\} d\Omega + [N_u]^T \{P_c\} \tag{3.17}$$

$$\{g_i\} = -\int_{\Omega_2} [N_\phi]^T \vartheta d\Omega - [N_\phi]^T Q \tag{3.18}$$

the external mechanical force and electric charge.

Each element k of the mesh is connected to its neighboring elements at the global nodes and the displacement is continuous from one element to the next. The element degrees of freedom (dof) $\left(\{u_i\}^{(k)}, \{\phi_i\}^{(k)}\right)$ are related to the global dof ({U}, $\{\phi\}$) by the mean of the localization matrices $[L_u]^{(k)}$ and $[L_\phi]^{(k)}$:

$$\{u_i\}^{(k)} = [L_u]^{(k)} \{U\} \tag{3.19}$$

$$\{\phi_i\}^{(k)} = [L_\phi]^{(k)} \{\phi\} \tag{3.20}$$

The element ij of $[L_u]^{(k)}$ is equal to 1 if the i^{th} mechanical dof of the finite element k corresponds to the j^{th} global dof and is zero otherwise. The element ij of $[L_\phi]^{(k)}$ is equal to 1 if the i^{th} electric dof of the finite element k is connected to the j^{th} global electric dof and is zero otherwise.

The Hamilton's principle must also be verified for the entire structure, which results in (by summation of the contribution from each finite element):

$$\begin{aligned} 0 = \{\delta U\}^T & \left[\left(\sum_k [L_u]^{(k)^T} [M]^{(k)} [L_u]^{(k)}\right)\{\ddot{U}\} + \left(\sum_k [L_u]^{(k)^T} [K_{uu}]^{(k)} [L_u]^{(k)}\right)\{U\}\right] \\ & + \left(\sum_k [L_u]^{(k)^T} [K_{u\phi}]^{(k)} [L_\phi]^{(k)}\right)\{\phi\} - \sum_k [L_u]^{(k)^T} [f_k] \\ & + \{\delta\phi\}^T \left[\left(\sum_k [L_\phi]^{(k)^T} [K_{\phi u}]^{(k)} [L_u]^{(k)}\right)\{U\} + \left(\sum_k [L_\phi]^{(k)^T} [K_{\phi\phi}]^{(k)} [L_\phi]^{(k)}\right)\{\phi\}\right] - \sum_k [L_\phi]^{(k)^T} [\vartheta_k] \end{aligned} \tag{3.21}$$

again for any arbitrary variation of the displacements $\{\delta U\}$ and electrical potentials $\{\delta\phi\}$, and verifying the essential boundary conditions.

Equation (3.21) can be rewritten in the form

$$[M]\{\ddot{U}\}+[K_{UU}]\{U\}+[K_{U\phi}]\{\phi\}=\{F\} \tag{3.22}$$

$$[K_{\phi U}]\{U\}+[K_{\phi\phi}]\{\phi\}=\{G\} \tag{3.23}$$

where the assembled matrices are given by:

$$[M]=\sum_i [L_{ui}]^T [M^{(i)}][L_{ui}] \tag{3.24}$$

$$[K_{UU}]=\sum_i [L_{ui}]^T [K_{uu}^{(i)}][L_{ui}] \tag{3.25}$$

$$[K_{U\phi}]=\sum_i [L_{ui}]^T [K_{u\phi}^{(i)}][L_{\phi i}] \tag{3.27}$$

$$[K_{\phi U}]=\sum_i [L_{\phi i}]^T [K_{\phi u}^{(i)}][L_{ui}] \tag{3.28}$$

$$[K_{\phi\phi}]=\sum_i [L_{\phi i}]^T [K_{\phi\phi}^{(i)}][L_{\phi i}] \tag{3.29}$$

$$\{F\}=\sum_i [L_{ui}]^T \{f_i\} \tag{3.30}$$

$$\{G\}=\sum_i [L_{\phi i}]^T \{g_i\} \tag{3.31}$$

Equations (3.23) and (3.24) couple the mechanical variables {U} and the electrical potentials $\{\phi\}$; {F} represents the external forces applied to the structure and {G} the electric charges brought to the electrodes.

Chapter 4

Signal Analysis Method

4.1 Fourier Analysis

4.1.1 Introduction

The Fourier transform has long been a principal analytical tool in such diverse fields as linear systems, optics, probability theory, quantum physics, antennas, and signal analysis. This mathematical tool originally was used for analysis of continuous signals and systems. Application of digital technology in signals and systems resulted in modifications and development of the Fourier transform for discrete signals and systems. Computational aspects of the Fourier transform were further developed to speed up the computation that is demanded for real applications. Further advances in digital hardware technology, along with high-speed computational algorithm for the Fourier transform, resulted in extensive application of this mathematical tool.

One of the areas that significantly benefited from this advancement is digital signal processing. With present day technology, it is possible to calculate the Fourier transform of a real-time discrete signal (e.g., speech signal or digital videos) and process the result in transform domain, and carry out the inverse transform all in real-time. Computational solutions for variety of hardware implementation of the Fourier transform are available. Most of these solutions are in public domain and are free.

The Fourier transform, with its wide range of applications, like many other mathematical tools, has its limitations. For example, this transformation cannot be applied to non-stationary signals. These signals (e.g. speech and image) have different characteristics at different time or space. Although the modified version of the Fourier transform, referred to as the short-time (or time-variable) Fourier transform can resolve some of the problems associated with non-stationary signals, t it does not address all issues of concern. The short-time Fourier transform is extensively used in speech signal processing, but rarely, if ever, used in image processing.

The wavelet transform, which was developed independently on different fronts, is gradually substituting the Fourier transform in some essential signal processing applications. Multi-resolution signal processing, used in computer vision; subband coding, developed for speech and image compression; and wavelet series expansions developed in applied mathematics, have been recognized as different views of a single theory.

Wavelet transform applies to both continuous and discrete signals. This transformation provides a general technique that is applicable to many tasks in signal processing.

The wavelet transform is successfully applied to non-stationary signals for analysis and processing and provides an alternative to the short-time Fourier transform (STFT). In contrast to STFT, which uses a single analysis window, the wavelet transform uses short windows at high frequencies and long windows at low frequencies. This flexibility is introduced in the spirit of so-called "*constant Q*" or constant relative bandwidth frequency analysis. For some applications it is desirable to obtain the wavelet transform as signal decomposition onto a set of basis functions, referred to as wavelets. These basis functions are obtained from a single prototype wavelet by dilations and contractions (scaling) as well as shifts. Recent surge in application of wavelet transform in various areas of signal processing resulted from the effectiveness of this mathematical tool for analysis and synthesis of signals.

In the following sections, first different formulations of the Fourier transform are presented. Details of discrete Fourier transform and time-dependent (short-time) Fourier transform are further discussed. Then, the wavelet transform is presented and its properties and characteristics for discrete signals are detailed.

4.1.2 Fourier Transform

The essence of the Fourier transform of a waveform is to decompose or separate the waveform into a sum of sinusoids of different frequencies. In other words, the Fourier transform identifies or distinguishes the different frequency sinusoids, and their respective amplitudes, which are combined to form an arbitrary waveform. The Fourier transform is then a frequency domain representation of a function. This

transform contains exactly the same information as that of the original function; they differ only in the manner of presentation of the information. Fourier analysis allows one to examine a function from another point of view, the transform domain.

Mathematically, this relationship is stated by a pair of equations denoting the forward and inverse transformation. In the case of continuous function, the transform pair, known as Fourier Transform (FT) is given by

$$\begin{aligned} &\textit{Forward FT}: && X(f) = \int_{-\infty}^{\infty} x(t) e^{-j2\pi ft}\, dt \\ &\textit{Inverse FT}: && x(t) = \int_{-\infty}^{\infty} X(f) e^{j2\pi ft}\, dt \end{aligned} \tag{4.1}$$

In above relations, $j = \sqrt{-1}$, $x(t)$ is the continuous function in time and $X(f)$ is its corresponding Fourier transform, which is a continuous function in frequency. This formula is mainly applied to functions with bounded energy. In other words, $x(t)$ should be an energy signal satisfying the following bound.

$$\int_{-\infty}^{\infty} \left|x(t)\right|^2 dt \prec \infty \tag{4.2}$$

This Fourier transform is mainly used for theoretical analysis and design of continuous signals and systems. For example, when designing an analog filter, the filter frequency response is obtained by applying the Fourier transform to the impulse response of the filter. Also when analyzing an energy signal, the signal spectrum is obtained by using the Fourier transform. This transformation is also used in many areas of applied mathematics such as solution of differential equations.

In the case of continuous periodic functions, the function does not have a finite energy. If $x(t)$ is periodic with a period of T and fundamental frequency of $f_0 = \frac{1}{T}$, $x(t)$ satisfies $x(t) = x(t+T)$ for all t 's, and if it has a finite power, the periodic function can then be expressed as a linear combination of harmonically related sinusoidal functions. The pair of equations, which defines the Fourier series (FS) of a periodic function, is stated by

$$\begin{aligned} &\textit{Forward} \quad FS: \quad c_k = \frac{1}{T}\int_{-T/2}^{T/2} x(t)e^{-j2\pi kf_o}dt \\ &\textit{Inverse} \quad FS: \quad x(t) = \sum_{k=-\infty}^{\infty} c_k\, e^{j2\pi kf_0} \end{aligned} \tag{4.3}$$

In the above relations, $c_k's$ are Fourier series coefficients of $x(t)$. The condition of having finite power for the periodic function $x(t)$ is stated by the following bound.

$$\frac{1}{T}\int_{-\infty}^{\infty}\left|x(t)\right|^2 dt \prec \infty \tag{4.4}$$

This transform converts a continuous periodic function to a sequence of complex numbers. In general, this sequence is infinite. However, in most practical cases, only finite number of $c_k's$ have significant values. The Fourier series expansion of periodic functions or functions with finite support, finite duration, allows analysis and design of signals and systems under some very special conditions. This transformation is also used in many areas of applied mathematics, like in solving partial differential equations.

Advances in computers and digital technology resulted in design of discrete signals and systems and modifications in the Fourier transform. The Fourier transform that is applied to discrete sequences and referred to as discrete time Fourier transform (DTFT) is defined by the following pair of equations.

$$\begin{aligned} &\textit{Forward} \quad DTFT: \quad X(e^{j2\pi f}) = \sum_{n=-\infty}^{\infty} x[n]e^{-j2\pi f} \\ &\textit{Inverse} \quad DTFT: \quad x[n] = \int_{-\pi}^{\pi} X(e^{j2\pi f})e^{j2\pi f}\, df \end{aligned} \tag{4.5}$$

In the above relations, $x[n]$ is the discrete function and $X(e^{j2\pi f})$ is its corresponding Fourier transform. The transform function is continuous and periodic in the frequency domain, with the period of 2π . In this formulation, the frequency variable, f, is normalized by the sampling frequency f_s . In other words, if f_a is the actual frequency in Hz, $f = f_a / f_s$ is the normalized frequency used in equation (4.5). This transformation is commonly used for analysis of discrete signals and systems.

Calculation of DTFT by computers can only be carried out for finite sequences and for discrete samples of in frequency domain. These requirements and constraints result in another formulation of the $X(e^{j2\pi f})$ Fourier transform that is defined for periodic discrete functions. Let $x[n]$ be a periodic sequence with a period of N; i.e., $x[n]=x[n+N]$ for all n 's, the pair of the Fourier transform relations, referred to as discrete Fourier transform (DFT), for $x[n]$, is defined by:

$$\begin{aligned} &\textit{Forward DFT}: \quad X[k]=\sum_{n=0}^{N-1} x[n]e^{-j2\pi nk/N} \quad \textit{for } k=0,1,2,...,N-1 \\ &\textit{Inverse DFT}: \quad x[n]=\frac{1}{N}\sum_{k=0}^{N-1} X[k]e^{j2\pi nk/N} \quad \textit{for } n=0,1,2,...,N-1 \end{aligned} \tag{4.6}$$

In above the relations, both discrete $x[n]$ functions and its DFT, $x[k]$, are periodic with the same period N . For graphical purposes and better visual representation of the signal spectrum, the forward DFT can be calculated for $M \succ\succ N$ points in frequency domain as follows.

$$X[k]=\sum_{n=0}^{N-1} x[n]e^{-j2\pi nk/M} \quad \textit{for} \quad k=0,1,2,...,M-1 \tag{4.7}$$

This formulation is obtained from the forward DTFT in (4.6) by using $\Delta f=\frac{1}{M}$ for the sampling of the normalized frequency.

Although different formulations of the Fourier transform have real applications in analyzing signals and systems, but only the last one, the DFT relations shown in (4.7), is practically used in real world computations. Some of the applications of DFT in signal processing are spectrum estimation, feature extraction, and frequency domain filtering. Due to advances in fast computation algorithms for DFT, known as Fast Fourier Transform (FFT), and high-speed hardware implementation, this approach is used for real-time digital signal processing (DSP). It is therefore necessary to address performance and limitation issues of DFT for various applications.

Let $x[n]$ for $n = 1,2,...,N-1$, be the sequence of real numbers obtained from sampling an analog temporal signal with sampling period of T seconds. The actual duration of this signal is therefore equal to $T_0 = NT$ seconds. When calculating the DFT of this sequence, the resultant sequence, $x[k]$, is in general a complex sequence in frequency domain. The actual distance between frequencies associated to the two consecutive samples of $x[k]$ is $1/(NT)$ Hertz (Hz). Due to the symmetry properties of $x[k]$ and sampling constraints, center of $x[k]$ sequence corresponds to the maximum frequency of the signal. This frequency is $f_{\max} = (N/2)\left(1/NT\right) = 1/2T$ Hz, which is determined by the sampling period T. Resolution of DFT is fixed at $\Delta f = 1/NT = 1/T_0$ Hz and is depended on the duration of the original analog signal. Increasing the number of samples by reducing the sampling period does not change the overall resolution.

One main assumption in using DFT for calculation of the spectrum of a discrete signal is that the observed signal is stationary during the observation time T_0 . In other words, the spectrum of the signal is assumed to remain the same during the observation time. For most practical signals, this assumption is not valid. For example, in speech signals, spectrum of the signal may vary significantly from one point to another. This depends on the contents of the speech and the sampling period. In this case and other similar cases, the Fourier transform is modified such that a two-dimensional time-frequency representation of the signal is obtained. The modified Fourier transform referred to as the short-time or time-dependent Fourier transform depends on a window function. For the discrete signals, this transformation, referred to as the discrete short time Fourier transform (DSTFT) is obtained by using a window function, $g[l]$, where

$$\begin{aligned} g[l] &\neq 0 \quad for \quad 0 \le l \le L-1 \\ g[l] &= 0 \quad for \quad l \prec 0 \ or \ l \ge L \end{aligned} \tag{4.8}$$

The pair of equations, which define the DSTFT of a discrete sequence, is stated by

$$\begin{aligned} &\textit{Forward} \quad DSTFT: \quad X[n,k] = \sum_{l=0}^{M-1} x[n+l]g[l]e^{-j2\pi lk/N} \\ &\textit{Inverse} \quad DSTFT: \quad x[n+l] = \frac{1}{Ng[l]} \sum_{k=0}^{N-1} X[n,k]e^{-j2\pi lk/N} \end{aligned} \tag{4.9}$$

The index k in equation (4.9) is similar to the frequency index in DFT given in equation (4.6). The resultant forward Fourier transform in this case provides estimates of the instantaneous frequency spectrum of the signal at any desired time. The window $g[l]$ has a stationary origin, and as n changes, the signal slides past the window so that, at each value of n, a different portion of the signal is viewed. The operation detailed in equation (4.9) can be carried out by using linear filtering. For example, the Kth component of the forward transform, $X[n,k]$, can be obtained by filtering $x[n]$ with an FIR filter whose impulse response is

$$h_k[n] = g[-n]e^{j2\pi kn/N} \tag{4.10}$$

The main purpose of the window in the time-dependent Fourier transform is to limit the extent of the transformed sequence, so that the spectral characteristics are reasonably stationary over the duration of the window function. The more rapidly the signal characteristics change, the shorter the window should be. Resolution in frequency depends on the duration of the window function. In the discrete case and for the uniform window, the actual frequency resolution, in terms of the sampling period T, equals to $\Delta f = \frac{1}{LT}$, which is the inverse of the actual size of the window. For other shaped windows (e.g. the raised cosine function), the resolution is obtained from $\Delta f \cong \frac{\alpha}{MT}$ in which, $0 \prec \alpha \leq 1$ depends on the shape of the window.

4.2 Wavelets

4.2.1 Introduction

Wavelets offer an alternative to traditional Fourier bases for representing functions. Wavelets may be thought of as oscillations that are localized in time (or

space) and in frequency. A representation of a function or signal based on these localized oscillations is attractive, because the coefficients associated with each wavelet convey details in time and frequency. A small coefficient means there is little variation in the function or signal in the vicinity of that particular small oscillation, whereas a large coefficient indicates that there is appreciable change in the signal or function. Analysis of the coefficients allows features in the function or signal to be identified.

Furthermore, because coefficients are identified with a localized frequency and time, small coefficients can be replaced by zeros, without greatly affecting the reconstruction of the signal. This strategy leads to the efficient representation of functions and algorithms for de-noising of general signals. In summary, the combination of the two localization properties makes wavelets attractive for the following applications:

- sparse representation of functions,
- feature detection in signals,
- de-noising of signals.

As an illustration of the de-noising and sparse representation properties, a signal arising from the calibration of a hydrophone has been plotted in Figure 4.1 (a)(see Harris 2005), and in Figure 4.1(b) the same signal reconstructed from a wavelet decomposition where over 90% of the coefficients have been replaced by zero. The horizontal axis shows the indices of the data points in the signal; the vertical axis is the voltage across the hydrophone (measured in volts).

In this introduction some of the fundamental mathematical properties of wavelets are discussed and the wavelet transforms analogous, to the Fourier and fast Fourier transforms are introduced. The aim is to introduce the reader to the basic concepts and terminologies associated with wavelets. For a more comprehensive review of the mathematics involved the reader is referred to (Daubechies (1992), DeVore et al (1991), and Jawerth et al (1994). There is also a great number of on-line resource pages for wavelets, containing information on the whole range of wavelet analyses, introductions to recent research papers and guides to available software.

Two good such sites are. http://www.wavelet.org, and http://www.mathsoft.com/wavelets.html).

4.2.2. Mathematical Properties of Wavelets

4.2.2.1 Background

From a signal processing point of view, a wavelet decomposition may be thought of as a combination of high and low pass filters that have particular properties. Let *g* be a high pass filter and *H* be a low pass filter and suppose function F is to be examined. Then a wavelet decomposition successively decomposes the function F using the filters into spaces of "approximations" {Vj} and "details" {Wj}. This process is illustrated in Figure 4.2. The high pass filter ,g, extracts "detail", whereas the low pass filter H smoothes the signal. The coefficients in the filters determine the properties of the decomposition.

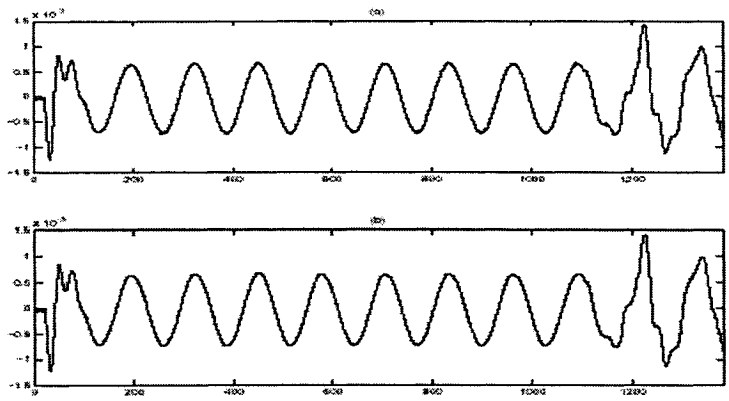

Figure 4.1. (a) A sample signal (b) Reconstruction Using Fewer than 10% of the Coefficients from the coiflet 4 Wavelet Decomposition

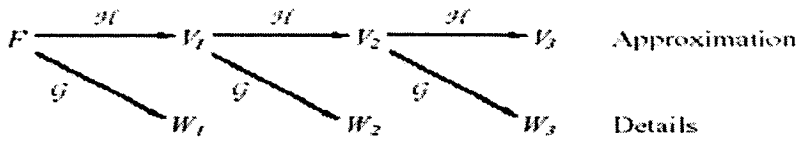

Figure 4.2. Schematic View of a 3-level decomposition of a function F by wavelet into an approximation space V3 and detail space W3 by a combination of low(H) and High(g) pass filter

An important consequence of this decomposition is that in order to reconstruct the function F, all that is required are the coefficients from the detail spaces {Wj ,j = 1, . . . , J, and the final approximation V_j . We can think of decomposition as taking us from a fine to a coarse approximation, while reconstruction takes us in the opposite direction. The reconstruction process is schematically shown in Figure 4.3, in which we see that to reconstruct F, all that is required are the detail spaces W_1, W_2, W_3 and the final approximation V_3.

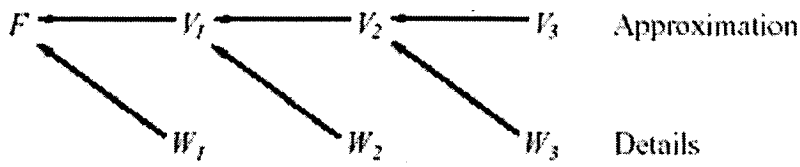

Figure 4.3. Schematic reconstruction of the function F from the 3-level decomposition. The approximation space V3 and the detail space W1,W2,W3 are all that are required

Another way to introduce wavelet decomposition is in terms of a wavelet basis and coefficients that convey information both about frequency and spatial/temporal position. To obtain such a basis we use dilations and translations of a wavelet function: these wavelet functions form a basis for the detail spaces $\{W_j\}$. There are associated scaling functions that form a basis for the approximation spaces $\{V_j\}$. Both wavelet and scaling functions will be discussed in subsequent sections.

Notation: Throughout this introduction we will use j to denote the level of scale of the details. Note, however, that there is no standard convention in the literature or computational packages as to whether j = 0 represents the finest or coarsest scale. Shifts in position are denoted throughout by k.

There are two important features about the wavelet coefficients that make wavelets so attractive:

1. Data Compression: A key to a good basis is being able to represent a function with as few basis functions as possible. For an arbitrary function, a large number of

the wavelet coefficients are either zero or very small. Since these coefficients contribute little to the reconstruction of the function, they can be replaced by zero and so good data compression is achieved. This suppression of near-zero coefficients can allow for effective de-noising of a function with noise.

2. Feature Extraction: We have seen above that wavelet decomposition is achieved by a combination of high and low pass filters. This decomposition will essentially identify high, medium and low scales in the function. In addition, the non-zero wavelet coefficients can be related to the size of the derivative of the function in a particular region. This relationship is useful for feature extraction, the large coefficients identifying where there are steep gradients or discontinuities in the function.

To help illustrate the use of wavelets, we will consider in the following sections the signal shown in Figure 4.1. This waveform arises from measurements made in a Reverberant tank of the response of an underwater electroacoustic transducer driven by a discrete-frequency tone-burst: Two transducers are suspended in a tank of finite size filled with water; one acts as a projector or transmitter and is driven by the tone-burst, the other as a receiver, used to record the response of the projector. We can observe in the waveform a number of important features of the measurement. The "turn-on" of the projector is followed immediately by an oscillation representing its resonant behavior. After three or four cycles of this oscillation, the resonant behavior is sufficiently damped to observe the steady-state response which takes the form of an undamped oscillation at the frequency of the drive signal. Finally, a change in the waveform results from the "turn-off" of the projector and the arrival at the receiver of reflections from the tank walls. Throughout, the measured waveform is contaminated by high-frequency noise. In what follows, instead of considering the signal in Figure 4.4 directly, we modify the waveform to include a discontinuity by padding the signal with zeros as in Figure 4.5. Note that in Figure 4.4, we plot the voltage (V) against the indices of the data points in the signal, while in Figure 4.5 the padded waveform is plotted against position in the signal.

4.2.3 Continuous Wavelet Transform (CWT)

Suppose we are given a time signal *f(t)*. A Fourier analysis of this signal extracts information about the frequencies contained in *f(t)*. The standard Fourier transform

$$f(\omega) = \frac{1}{\sqrt{2\pi}} \int e^{-i\omega t} f(t) dt \tag{4.11}$$

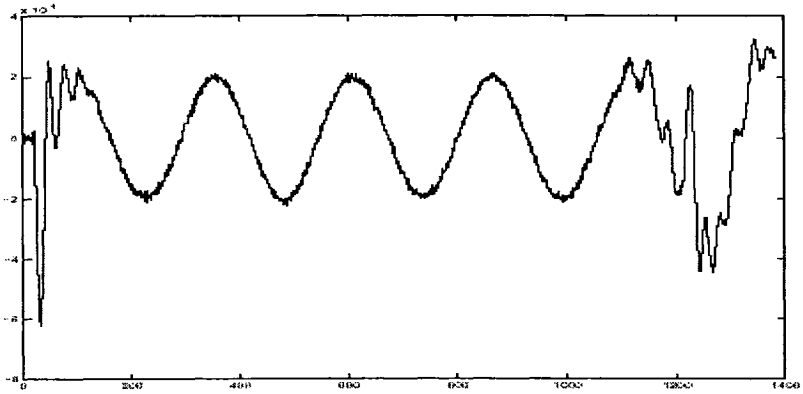

Figure 4.4. An example signal for wavelet analysis, original from the calibration of a hydrophone

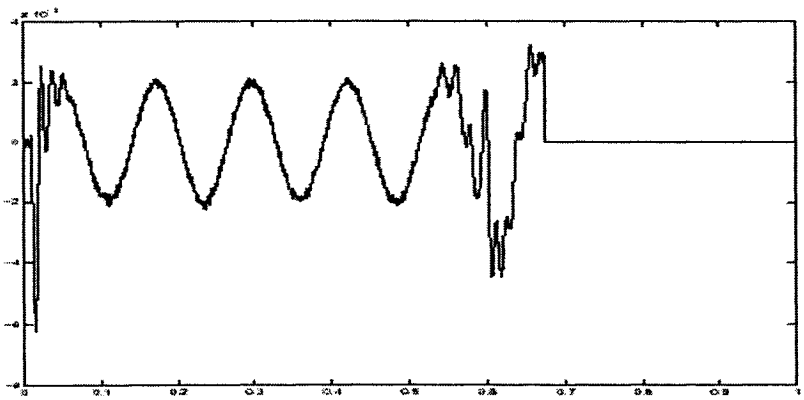

Figure 4.5. Same example as figure 4.4 with zero added to pad the signal to have a length 2048 and create a discontinuty

will give frequency information. However information concerning time-localization is more difficult to obtain from $f(\omega)$.Windowing the signal *f(t)* is a step towards obtaining such information. Here the signal is first restricted to an interval (with smoothed edges) by multiplying it by a fixed window function, before carrying out a Fourier analysis of the product. Repeating the process with shifted versions of the window function allows localized frequency information throughout the signal to be obtained.

$$(T^{win} f)(\omega,t) = \int f(s)g(s-t)e^{-i\omega s}ds \tag{4.12}$$

where g is the windowing function having compact support .

The continuous wavelet transform gives time-frequency decomposition by taking translations and dilations of a (real or complex) wavelet:

$$\psi_{a,b}(t) = \frac{1}{\sqrt{|a|}}\psi(\frac{t-b}{a}) \tag{4.13}$$

The continuous wavelet transform (CWT) of f is then given by

$$C(a,b) = \langle f, \psi_{a,b} \rangle = \frac{1}{\sqrt{|a|}} \int f(t)\overline{\psi(\frac{t-b}{a})}dt \tag{4.14}$$

where $\overline{\psi}$ denotes the complex conjugate of ψ which is mother wavelet function.

The {C(a, b)} are called the wavelet coefficients, with a and b referred to as the scale and translation parameters respectively. It is assumed that the wavelet has zero mean so that

$$\int \psi dt = 0 \tag{4.15}$$

A classical choice for $\psi(t)$ is the "Mexican hat" function, which is represented by:

$$\psi(t) = (1-t^2)e^{-\frac{t^2}{2}} \tag{4.16}$$

This function is localized both in time and frequency and satisfies the zero mean condition. The Mexican hat function with a = 1, b = 0 has been plotted in Figure

4.6(a) it can be seen that is centered about the origin. Figure 4.6(b) illustrated the two scaled and translated versions of the function with a = 2, and b = ±5.

In what follows, we will use the terms "high frequency" and "low frequency" to refer respectively to low and high values of the scale parameter. This"inverse relationship" between scale and frequency is quite intuitive: we can think of a low scale as corresponding to a compressed wavelet, where the details are changing rapidly, similar to the behaviour of a high frequency signal. We also talk about the resolution which is simply defined as the reciprocal of the scale parameter.

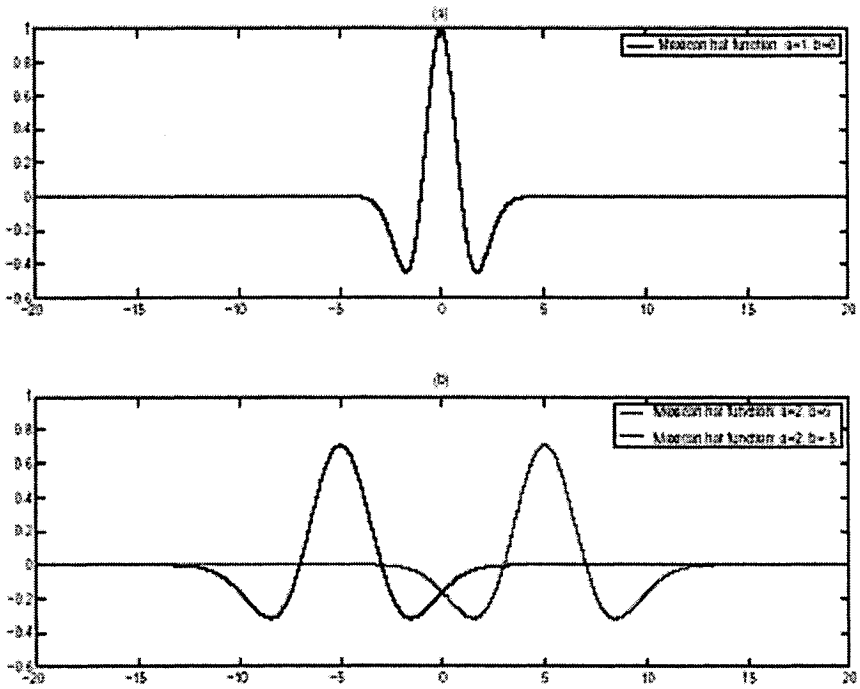

Figure 4.6. Example of effect of scaling and translation of the Mexican hat function. Note that (a) corresponds to a high frequency, whereas in (b), the function are at a lower frequency and are less localized.

The original function f can be reconstructed from its continuous wavelet transform by evaluating

$$f(t) = C_{\psi}^{-1} \int\int a^{-2} C(a,b) \psi_{a,b}(t) da db \tag{4.17}$$

where the constant C_ψ satisfies an admissibility condition given by

$$C_\psi = 2\pi \int |\xi|^{-1} |\psi(\xi)|^2 d\xi \prec \infty \tag{4.18}$$

This reconstruction formula (known as the inverse wavelet transform) was proven in Daubechies (1992); however, it is rarely used in practice.

4.2.4 Discrete Wavelet Transform (DWT)

The key difference in a discrete wavelet analysis is that the scale parameter (a) and translation parameter (b) in equation (4.11) are no longer continuous, but instead are integers. Indeed, in the majority of cases, the choice of (a) and (b) is limited to the following discrete set:

$(j,k) \in Z^2$

$a = 2^j$

$b = k * 2^j = ka$

The indices a and b in $\psi_{a,b}$ are replaced by j and k respectively, and so equation (4.18) becomes

$$\psi_{j,k}(t) = 2^{-j/2} \psi(2^{-j} t - k), j,k \in Z^2 \tag{4.19}$$

Reconstruction of a signal from its DWT is possible, provided that the wavelet satisfies certain conditions. The reconstruction formula is analogous to equation (4.14):

$$f(t) = \sum_{j,k} \langle f, \psi_{j,k} \rangle \psi_{j,k}(n), j,k \in Z^2 \tag{4.20}$$

4.3. The Empirical Mode Decomposition and Hilbert-Huang Transform

Data analysis is a necessary part in pure research and practical applications. Imperfect as some data might be, they represent the reality sensed by sensors; consequently, data analysis serves two main purposes: (i) to determine the parameters needed to construct the necessary model, and (ii) to conform the model we constructed to represent the phenomenon.

Unfortunately, the data, whether from physical measurements or numerical modeling, most likely will have one or more of the following problems: (*a*) the total data span is too short; (*b*) the data are non-stationary; and (*c*) the data represent nonlinear processes. Although each of the above problems can be real by itself, the first two are related. A data section shorter than the longest time scale of a stationary process can appear to be non-stationary. One has limited options to use such in data analysis.

Historically, the Fourier spectral analysis has provided a general method for examining the global energy–frequency distributions. As a result, the term 'spectrum' has become almost synonymous with the Fourier transform of the data. Partially because of its prowess and partially because of its simplicity, Fourier analysis has dominated the data analysis efforts since soon after its introduction, and has been applied to all kinds of data. Although the Fourier transform is valid under extremely general conditions (Titchmarsh 1948), there are some crucial restrictions of the Fourier spectral analysis: the system must be linear; and the data must be strictly periodic or stationary; otherwise, the resulting spectrum will make little physical sense.

The stationarity requirement is not particular to the Fourier spectral analysis; it is a general one for most of the available data analysis methods. Therefore, it behaves us to review the definitions of stationary here.

According to the traditional definition, a time series, $X(t)$, is stationary in the wide sense, if, for all t,

$$\begin{aligned} &E(|X(t)^2|) < \infty, \\ &E(X(t)) = m, \\ &C(X(t_1), X(t_2)) = C(X(t_1 + \tau), X(t_2 + \tau)) = C(t_1 - t_2), \end{aligned} \tag{4.21}$$

in which $E(\cdot)$ is the expected value defined as the ensemble average of the quantity (.), and $C(\cdot)$ is the covariance function. Stationarity in the wide sense is also known as weak stationarity, covariance stationarity or second-order stationarity (Brockwell & Davis 1991). A time series, $X(t)$, is strictly stationary, if the joint distribution of

$$[X(t_1), X(t_2), ..., X(t_n)] \quad \textit{and} \quad [X(t_1 + \tau), X(t_2 + \tau), ..., X(t_n + \tau)] \tag{4.22}$$

are the same for all t_i and τ . Thus, a strictly stationary process with finite second moments is also weakly stationary, but the inverse is not true. Both definitions are rigorous but idealized. Other less rigorous definitions for stationarity have also been used; for example, piecewise stationarity is for any random variable that is stationary within a limited time span, and asymptotically stationary is for any random variable that is stationary when τ in equations (4.21) or (4.22) approaches infinity. In practice, we can only have data for finite time spans; therefore, even to check these definitions, we have to make approximations. Few of the data sets, from either natural phenomena or artificial sources, can satisfy these definitions. It may be argued that the difficulty of invoking stationarity as well as ergodicity is not on principle but on practicality: we just cannot have enough data to cover all possible points in the phase plane; therefore, most of the cases facing us are transient in nature.

Other than stationarity, the Fourier spectral analysis also requires linearity. Although many natural phenomena can be approximated by linear systems, they also have the tendency to be nonlinear whenever their variations become finite in amplitude. Compounding these complications is the imperfection of our sensors and/or numerical schemes; the interactions of the imperfect sensors even with a perfect linear system can make the final data nonlinear. For the above reasons, the available data are usually of finite duration, non-stationary and from systems that are

frequently nonlinear, either intrinsically or through interactions with the imperfect sensors or numerical schemes. Under these conditions, the Fourier spectral analysis is of limited use. For lack of alternatives, however, the Fourier spectral analysis is still used to process such data. The uncritical use of Fourier spectral analysis and the insouciant adoption of the stationary and linear assumptions may give misleading results; some of those are described as follows.

First, the Fourier spectrum defines uniform harmonic components globally; therefore, it needs many additional harmonic components to simulate non-stationary data that are non-uniform globally. As a result, it spreads the energy over a wide frequency range. Here, many Fourier components are added to simulate the non-stationary nature of the data in the time domain, but their existence diverts energy to a much wider frequency domain. Constrained by the energy conservation, these spurious harmonics and the wide frequency spectrum cannot adequately represent the true energy density in the frequency space. More seriously, the Fourier representation also requires the existence of negative light intensity so that the components can cancel out one another to produce the final delta function. Thus, the Fourier components might make mathematical sense, but do not really make physical sense at all. Although no physical process can be represented exactly by a delta function, some data, such as the near field strong earthquake records, are of extremely short durations, lasting only a few seconds to tens of seconds at most. Such records almost approach a delta function, and they always give artificially wide Fourier spectra.

Second, Fourier spectral analysis uses linear superposition of trigonometric functions; therefore, it needs additional harmonic components to simulate the deformed wave-profiles. Such deformations, as will be shown later, are the direct consequence of nonlinear effects. Whenever the form of the data deviates from a pure sine or cosine function, the Fourier spectrum will contain harmonics. As explained above, both non-stationarity and nonlinearity can induce spurious harmonic components that cause energy spreading. The consequence is the misleading energy–frequency distribution for nonlinear and non-stationary data.

Hilbert Huang (1996) introduced new data analysis method based on the empirical mode decomposition (EMD) method, which will generate a collection of

intrinsic mode functions (IMF). The decomposition is based on the direct extraction of the energy associated with various intrinsic time scales, the most important parameters of the system. Expressed in IMFs, they have well-behaved Hilbert transforms, from which the instantaneous frequencies can be calculated. Thus, we can localize any event on the time as well as the frequency axis. The decomposition can also be viewed as an expansion of the data in terms of the IMFs. Then, these IMFs, based on and derived from the data, can serve as the basis of that expansion which can be linear or nonlinear as dictated by the data, and it is complete and almost orthogonal. Most important of all, it is adaptive. The principle of this basis construction is based on the physical time scales that characterize the oscillations of the phenomena. The local energy and the instantaneous frequency derived from the IMFs through the Hilbert transform can give us a full energy–frequency–time distribution of the data. Such a representation is designated as the Hilbert spectrum; it would be ideal for nonlinear and non-stationary data analysis. He has obtained good results and new insights by applying the combination of the EMD and Hilbert spectral analysis methods to various data: from the numerical results of the classical nonlinear equation systems to data representing natural phenomena.

The classical nonlinear systems serve to illustrate the roles played by the nonlinear effects in the energy frequency–time distribution. With the low degrees of freedom, they can train our eyes for more complicated cases.

4.3.1 Instantaneous frequency

The notion of the instantaneous energy or the instantaneous envelope of the signal is well accepted; the notion of the instantaneous frequency, on the other hand, has been highly controversial. Existing opinions range from editing it out of existence (Shekel 1953) to accepting it but only for special 'monocomponent' signals (Boashash 1992; Cohen 1995).

There are two basic difficulties with accepting the idea of an instantaneous frequency. The first one arises from the deeply entrenched influence of the Fourier spectral analysis. In the traditional Fourier analysis, the frequency is defined for the sine or cosine function spanning the whole data length with constant amplitude. As an

extension of this definition, the instantaneous frequencies also have to relate to either a sine or a cosine function. Thus, we need at least one full oscillation of a sine or a cosine wave to define the local frequency value. According to this logic, nothing shorter than a full wave will do. Such a definition would not make sense for non-stationary data for which the frequency has to change values from time to time. The second difficulty arises from the non-unique way in defining the instantaneous frequency. Nevertheless, this difficulty is no longer serious since the introduction of the means to make the data analytical through the Hilbert transform. Difficulties, however, still exist as 'paradoxes' discussed by Cohen (1995). For an arbitrary time series, $X(t)$, we can always have its Hilbert Transform, $Y(t)$, as

$$Y(t) = \frac{1}{\pi} P \int_{-\infty}^{\infty} \frac{X(t')}{t - t'} dt' \tag{4.23}$$

where P indicates the Cauchy principal value. This transform exists for all functions of class L^P (Titchmarsh 1948). With this definition, $X(t)$ and $Y(t)$ form the complex conjugate pair, so we can have an analytic signal, $Z(t)$, as

$$Z(t) = X(t) + iY(t) = a(t)e^{i\theta(t)} \tag{4.24}$$

in which

$$a(t) = \left[X^2(t) + Y^2(t)\right]^{1/2} \quad , \theta(t) = \arctan \left(\frac{Y(t)}{X(t)}\right). \tag{4.25}$$

Theoretically, there are infinitely many ways of defining the imaginary part, but the Hilbert transform provides a unique way of defining the imaginary part so that the result is an analytic function. A brief tutorial on the Hilbert transform with the emphasis on its physical interpretation can be found in Bendat & Piersol (1986). Essentially, Equation (4.23) defines the Hilbert transform as the convolution of $X(t)$ with $1/t$; therefore, it emphasizes the local properties of $X(t)$. In Equation (4.24), the polar coordinate expression further clarifies the local nature of this representation: it is the best local t of an amplitude and phase varying trigonometric function to $X(t)$. Even with the Hilbert transform, there is still considerable controversy in defining the instantaneous frequency as

$$\omega = \frac{d\theta(t)}{dt} \tag{4.26}$$

This led Cohen (1995) to introduce the term, 'monocomponent function'. In principle, some limitations on the data are necessary, for the instantaneous frequency given in Equation (4.26) is a single value function of time. At any given time, there is only one frequency value; therefore, it can only represent one component, hence monocomponent'. Unfortunately, no clear definition of the 'monocomponent' signal was given to judge whether a function is or is not 'monocomponent'. For lack of a precise definition, 'narrow band' was adopted as a limitation on the data for the instantaneous frequency to make sense (Schwartz et al. 1966).

4.3.2 Intrinsic mode functions

An intrinsic mode function (IMF) is a function that satisfies two conditions: (1) in the whole data set, the number of extrema and the number of zero crossings must either equal or differ at most by one; and (2) at any point, the mean value of the envelope defined by the local maxima and the envelope defined by the local minima is zero.

The first condition is obvious; it is similar to the traditional narrow band requirements for a stationary Gaussian process. The second condition is a new idea; it modifies the classical global requirement to a local one; it is necessary so that the instantaneous frequency will not have the unwanted fluctuations induced by asymmetric wave forms. Ideally, the requirement should be 'the local mean of the data being zero'. For non-stationary data, the 'local mean' involves a 'local time scale' to compute the mean, which is impossible to define. As a surrogate, we use the local mean of the envelopes defined by the local maxima and the local minima to force the local symmetry instead. This is a necessary approximation to avoid the definition of a local averaging time scale. Although it will introduce an alias in the instantaneous frequency for nonlinearly deformed waves. With the physical approach and the approximation adopted here, the method does not always guarantee a perfect instantaneous frequency under all conditions. Nevertheless, we will show that, even under the worst conditions, the instantaneous frequency so defined is still consistent with the physics of the system studied.

The name 'intrinsic mode function' is adopted because it represents the oscillation mode imbedded in the data. With this definition, the IMF in each cycle, defined by the zero crossings, involves only one mode of oscillation, no complex riding waves are allowed. With this definition, an IMF is not restricted to a narrow band signal, and it can be both amplitude and frequency modulated. In fact, it can be non-stationary. As discussed above, purely frequency or amplitude modulated functions can be IMFs even though they have finite bandwidth according to the traditional definition. A typical IMF is shown in Figure 4.7.

Having defined IMF, we will show that the definition given in equation (4.26) gives the best instantaneous frequency. An IMF after the Hilbert transform can be expressed as in equation (4.24). If we perform a Fourier transform on $Z(t)$, we would have:

$$W(\omega) = \int_{-\infty}^{\infty} a(t) e^{i\theta(t)} e^{-i\omega t}\, dt = \int_{-\infty}^{\infty} a(t) e^{i(\theta(t)-\omega t)}\, dt \tag{4.27}$$

Then by the stationary phase method (see, for example, Copson 1967), the maximum contribution to $W(\omega)$ is given by the frequency satisfying the condition

$$\frac{d}{dt}(\theta(t) - \omega t) = 0 \tag{4.28}$$

therefore, equation (4.26) follows. Although mathematically, the application of the stationary phase method requires a large parameter for the exponential function, the adoption here can be justified if the frequency, ω, is high compared with the inversed local time scale of the amplitude variation. Therefore, this definition fits the best for gradually changing amplitude. Even with this condition, this is still a much better definition for instantaneous frequency than the zero-crossing frequency; it is also better than the integral definition suggested by Cohen (1995). Furthermore, it agrees with the definition of frequency for the classic wave theory (Whitham 1975).

As given in Equation (4.28) and the simple analogy given in Equations (4.24)–(4.26), the frequency defined through the stationary phase approximation agrees also with the best fit sinusoidal function locally; therefore, we do not need a whole oscillatory period to define a frequency value. We can define it for every point with the value changing from point to point. In this sense, even a monotonic function can be treated

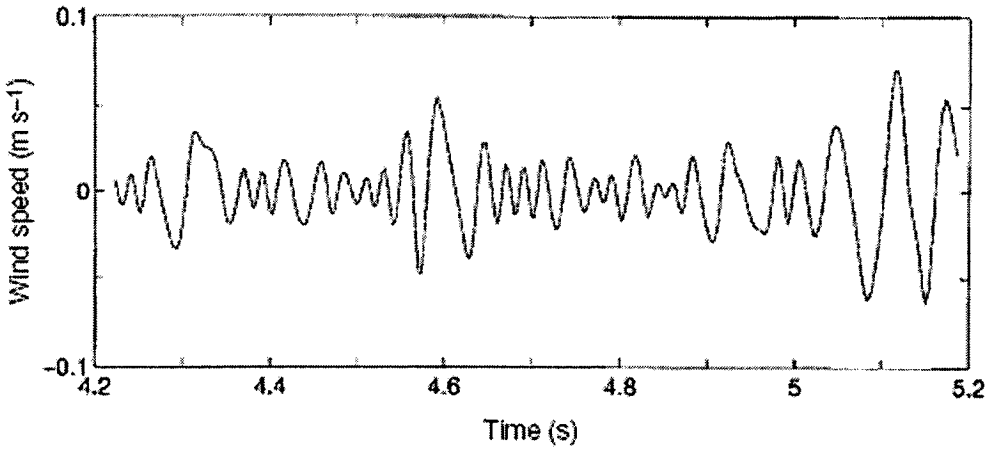

Figure 4.7. A typical intrinsic mode function with the same numbers of zero crossings and extrema, and symmetry of the upper and lower envelopes with respect to zero.

as part of an oscillatory function and have instantaneous frequency assigned according to equation (4.26). Any frequency variation is designated as frequency modulation. There are actually two types of frequency modulations: the interwave and the intrawave modulations. The first type is familiar to us; the frequency of the oscillation is gradually changing with the waves in a dispersive system. Technically, in the dispersive waves, the frequency is also changing within one wave, but that was not emphasized either for convenience, or for lack of a more precise frequency definition. The second type is less familiar, but it is also a common phenomenon. If the frequency changes from time to time within a wave, its profile can no longer be a simple sine or cosine function. Therefore, any wave-profile deformation from the simple sinusoidal form implies the intrawave frequency modulation. In the past such phenomena were treated as harmonic distortions. We will show in detail later that most such deformations are better viewed as intrawave frequency modulation, for the intrawave frequency modulation is more physical. In order to use this unique definition of instantaneous frequency, we have to reduce an arbitrary data set into IMF components from which an instantaneous frequency value can be assigned to each IMF component. Consequently, for complicated data, we can have more than one instantaneous frequency at a time locally. We will introduce the empirical mode decomposition method to reduce the data into the needed IMFs.

4.3.3 The empirical mode decomposition method: the sifting process

Knowing the well-behaved Hilbert transforms of the IMF components is only the starting point. Unfortunately, most of the data are not IMFs. At any given time, the data may involve more than one oscillatory mode; that is why the simple Hilbert transform cannot provide the full description of the frequency content for the general data as reported by Long *et al.* (1995). We have to decompose the data into IMF components. Here, we will introduce a new method to deal with both non-stationary and nonlinear data by decomposing the signal first, and discuss the physical meaning of this decomposition later. Contrary to almost all the previous methods, this new method is intuitive, direct, *a posteriori* and adaptive, with the basis of the decomposition based on, and derived from, the data.

The decomposition is based on the assumptions that: (1) the signal has at least two extrema one maximum and one minimum; (2) the characteristic time scale is defined by the time lapse between the extrema; and (3) if the data were totally devoid of extrema but contained only inflection points, then it can be differentiated once or more times to reveal the extrema. Final results can be obtained by integration(s) of the components.

The essence of the method is to identify the intrinsic oscillatory modes by their characteristic time scales in the data empirically, and then decompose the data accordingly. According to Drazin (1992), the first step of data analysis is to examine the data by eye. From this examination, one can immediately identify the different scales directly in two ways: by the time lapse between the successive alternations of local maxima and minima; and by the time lapse between the successive zero crossings. The interlaced local extrema and zero crossings give us the complicated data: one undulation is riding on top of another, and they, in turn, are riding on still other undulations, and so on. Each of these undulations defines a characteristic scale of the data; it is intrinsic to the process. We have decided to adopt the time lapse between successive extrema as the definition of the time scale for the intrinsic oscillatory mode, because it not only gives a much finer resolution of the oscillatory modes, but also can be applied to data with non-zero mean, either all positive or all

negative values, without zero crossings. A systematic way to extract them, designated as the sifting process, is described as follows.

This is still not an IMF, for there are negative local maxima and positive minima suggesting riding waves.

By virtue of the IMF definition, the decomposition method can simply use the envelopes defined by the local maxima and minima separately. Once the extrema are identified, all the local maxima are connected by a cubic spline line as the upper envelope. Repeat the procedure for the local minima to produce the lower envelope. The upper and lower envelopes should cover all the data between them. Their mean is designated as m_1, and the difference between the data and m_1 is the first component, h_1, i.e.

$$X(t) - m_1 = h_1 \tag{4.29}$$

The procedure is illustrated in Figures 4.8*a–c* (Figure 4.8*a* gives the data; Figure 4.8b gives the data in the thin solid line, the upper and the lower envelopes in the dot-dashed lines, and their mean in the thick solid line, which bisects the data very well; and Figure 4.8*c* gives the difference between the data and the local mean as in Equation (4.29).

Ideally, h_1 should be an IMF, since the construction of h_1 described above seems to have been made to satisfy all the requirements of IMF. In reality, however, overshoots and undershoots are common, which can also generate new extrema, and shift or exaggerate the existing ones. The imperfection of the overshoots and undershoots can be found at the 4.6 and 4.7 s points in Figure 4.8*b*. Their effects, however, are not direct, for it is the mean, not the envelopes, which will enter the sifting process. Nevertheless, the problem is real. Even if the fitting is perfect, a gentle hump on a slope can be amplified to become a local extremum in changing the local zero from a rectangular to a curvilinear coordinate system. An example can be found for the hump between the 4.5 and 4.6 s range in the data in Figure 4.8*a*. After the first round of sifting, the hump becomes a local maximum at the same time location as in Figure 4.8*c*. New extrema generated in this way actually recover the proper modes lost in the initial examination. In fact, the sifting process can recover low-amplitude riding waves with repeated siftings.

Still another complication is that the envelope mean may be different from the true local mean for nonlinear data; consequently, some asymmetric wave forms can still exist no matter how many times the data are sifted. We have to accept this approximation as discussed before.

Other than these theoretical difficulties, on the practical side, serious problems of the spline fitting can occur near the ends, where the cubic spline fitting can have large wings. Left by themselves, the end swings can eventually propagate inward and corrupt the whole data span especially in the low-frequency components. At any rate, improving the spline fitting is absolutely necessary. Even with these problems, the sifting process can still extract the essential scales from the data.

The sifting process serves two purposes: to eliminate riding waves; and to make the wave-profiles more symmetric. Toward this end, the sifting process has to be repeated more times. In the second sifting process, h_1 is treated as the data, then

$$h_1 - m_{11} = h_{11} \tag{4.30}$$

Figure 4.9*a* shows the much improved result after the second sifting, but there are still local maxima below the zero line. After another sifting, the result is given in Figure 4.9*b*. Now all the local maxima are positive, and all the local minima are negative, but many waves are still asymmetric. We can repeat this sifting procedure k times, until h_{1k} is an IMF, that is

$$h_{1(k-1)} - m_{1k} = h_{1k} \tag{4.31}$$

The result is shown in Figure 4.7 after nine siftings. Then, it is designated as:

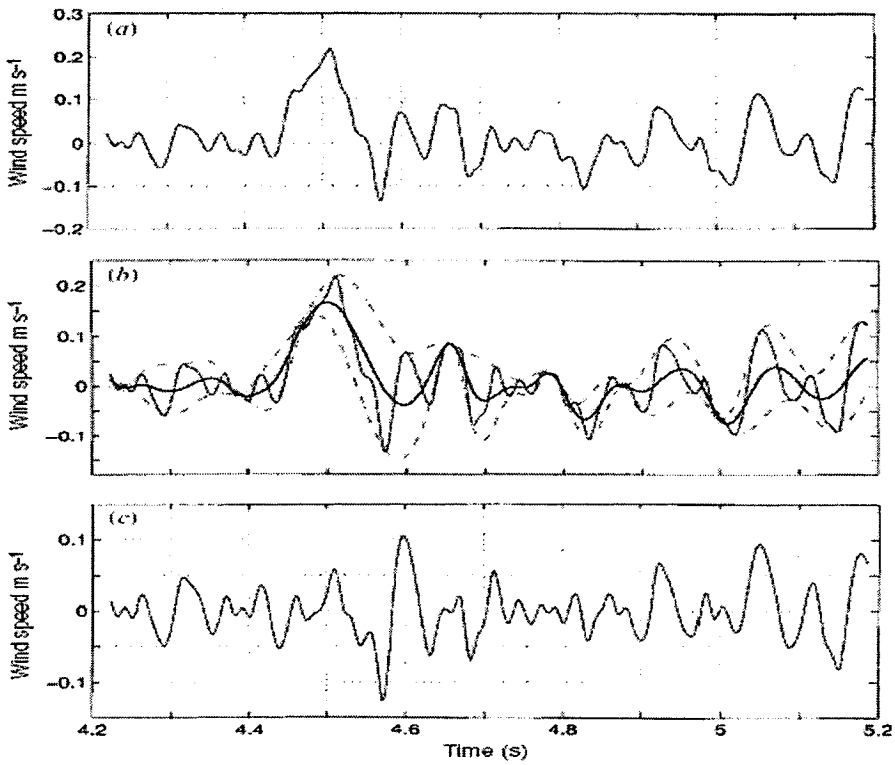

Figure 4.8. Illustration of the sifting processes: (*a*) the original data; (*b*) the data in thin solid line, with the upper and lower envelopes in dot-dashed lines and the mean in thick solid line; (*c*) the difference between the data and $m1$.

The final IMF is shown in Figure 4.7 after nine siftings.

$$c_1 = h_{1k} \tag{4.32}$$

the first IMF component from the data.

As described above, the process is indeed like sifting: to separate the finest local mode from the data first based only on the characteristic time scale. The sifting process, however, has two effects: (*a*) to eliminate riding waves; and (*b*) to smooth uneven amplitudes.

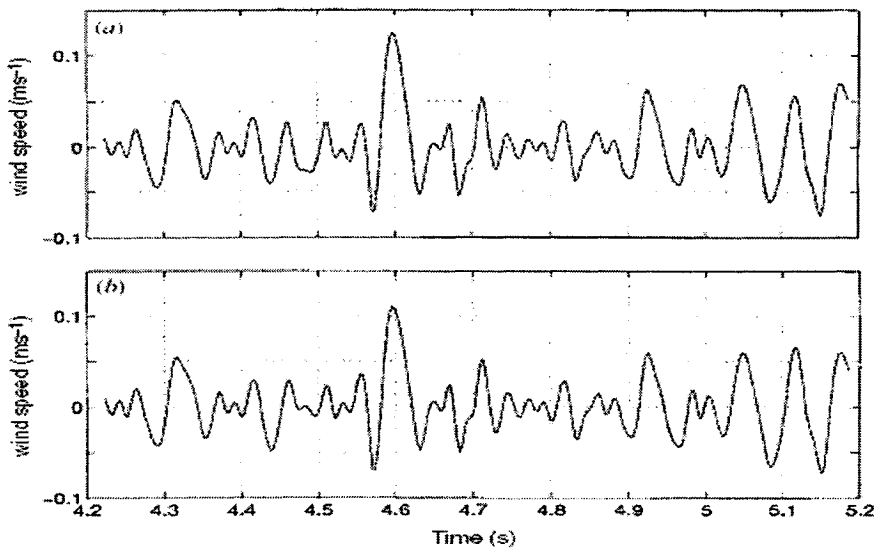

Figure 4.9. Illustration of the effects of repeated sifting process: (*a*) after one more sifting of the result in Figure 4.8*c*, the result is still asymmetric and still not an IMF; (*b*) after three siftings, the result is much improved, but more sifting needed to eliminate the asymmetry.

While the first condition is absolutely necessary for the instantaneous frequency to be meaningful, the second condition is also necessary in case the neighboring wave amplitudes have too large a disparity. Unfortunately, the second effect, when carried to the extreme, could obliterate the physically meaningful amplitude fluctuations. Therefore, the sifting process should be applied with care, for carrying the process to an extreme could make the resulting IMF a pure frequency modulated signal of constant amplitude. To guarantee that the IMF components retain enough physical sense of both amplitude and frequency modulations, we have to determine a criterion for the sifting process to stop. This can be accomplished by limiting the size of the standard deviation, SD, computed from the two consecutive sifting results as

$$SD = \sum_{t=0}^{T} \left[\frac{\left| \left(h_{1(k-1)}(t) - h_{1k}(t) \right) \right|^2}{h_{1(k-1)}^2(t)} \right] \tag{4.33}$$

A typical value for SD can be set between 0.2 and 0.3. This is based on the fact that the two Fourier spectra, computed by shifting only five out of 1024 points from the same data, can have an equivalent SD of 0.2–0.3 calculated point-by-point.

Therefore, a SD value of 0.2–0.3 for the sifting procedure is a very rigorous limitation for the difference between siftings.

Overall, c_1 should contain the .nest scale or the shortest period component of the signal. We can separate c_1 from the rest of the data by

$$X(t) - c_1 = r_1 \tag{4.34}$$

Since the residue, r_1, still contains information of longer period components, it is treated as the new data and subjected to the same sifting process as described above. This procedure can be repeated on all the subsequent r_j s, and the result is

$$r_1 - c_2 = r_2, \ldots\ldots, r_{n-1} - c_n = r_n \tag{4.35}$$

The sifting process can be stopped by any of the following predetermined criteria: either when the component, c_n, or the residue, r_n, becomes so small that it is less than the predetermined value of substantial consequence, or when the residue, r_n, becomes a monotonic function from which no more IMF can be extracted. Even for data with zero mean, the final residue can still be different from zero; for data with a trend, then the final residue should be that trend. By summing up equations (4.34) and (4.35), we finally obtain

$$X(t) = \sum_{i=1}^{n} c_i + r_n \tag{4.36}$$

Thus, we achieved a decomposition of the data into n-empirical modes, and a residue, r_n, which can be either the mean trend or a constant. As discussed here, to apply the EMD method, a mean or zero reference is not required; EMD only needs the locations of the local extrema. The zero references for each component will be generated by the sifting process.

Finally, let us examine the physical meaning of each IMF component. The components of the EMD are usually physical, for the characteristic scales are physical. Nevertheless, this is not strictly true, since there are cases when a certain scale of a phenomenon is intermittent. Then, the decomposed component could contain two scales in one IMF component. Therefore, the physical meaning of the decomposition comes only in the totality of the decomposed components in the Hilbert spectrum. Even with the entire set of decomposed components, sound physical interpretation is still not guaranteed for other decompositions such as Fourier

expansion. Because this decomposition is *a posteriori*, the check should also be *a posteriori*.

Chapter 5

Application of Hilbert-Huang Transform for Evaluation of Vibration Characteristics of Plastic Pipes Using Piezoelectric Sensors

N. Cheraghi, M.J. Riley, and F. Taheri*

Publication status: Submitted to Journal. of Structural Engineering and Mechanics, July 2005.

5.1 ABSTRACT

This paper discusses the application of piezoelectric sensors used for evaluation of damping ratio of PVC plastics. A systematic experimental and analytical investigation was carried out to demonstrate the integrity of several methods commonly used to evaluate the damping of materials based on a single degree freedom formulation. The influence of the sensors' location was also investigated.

Besides the commonly used methods, a newly emerging time-frequency method, namely the Empirical Mode decomposition, is also employed. Mathematical formulations based on the Hilbert-Huang formulation, and a frequency spacing technique were also developed for establishing the natural frequency and damping ratio based on the output voltage of a single piezoelectric sensor. A numerical investigation was also conducted and the results were compared and verified with experimental resultys, revealing good agreement.

Keywords: Plastics, Damping, FFT, Finite Element Analysis, Hilbert Transform, Frequency Spacing, Empirical Mode Decomposition (EMD).

5.2 INTRODUCTION

Characterization of damping forces in a vibrating structure has long been an active and challenging area of research in structural dynamics. The demands of modern engineering have led to a steady increase in the interest in recent years. Nonetheless, in spite of a large amount of research, the fundamental understanding of structural damping still requires further exploration. A major obstacle is that in comparison to the forces related to the inertia and strain energy of the body, it is not generally clear which state variables would be the most relevant for determining the damping force. By far the most common approach is to assume the so-called "viscous damping", a linear model in which it is assumed that the instantaneous generalized velocities are the only relevant state variables that affect damping. This approach was first introduced by Rayleigh (1945) via his famous "dissipation function", in which a quadratic expression was formulated to characterize the energy dissipation rate with a symmetric matrix of coefficients, also refereed to as the "damping matrix". A further idealization, also pointed out by Rayleigh, is to assume the damping matrix to be a linear combination of the mass and stiffness matrices.

Rayleigh was quite clear in stating that his proposed approach was solely based on mathematical convenience, because it allowed the damping matrix to be simultaneously diagonalized with the mass and stiffness matrices, thus preserving the simplicity of an uncoupled and real normal mode, as in an undamped case. Since its introduction, this method has been used extensively and is now usually referred to as the "Rayleigh damping", or the "proportional damping", or the "classical damping" method.

Imregun (1991) compared two different single-degree-of-freedom (SDOF) modal analysis techniques, as well as a global multi-degree-of freedom (MDOF) method applied to frequency response function measurements taken on a lightly damped linear structure. For the SDOF, the circle-fit and the line-fit that were used to identify the modal prosperities resulting in very similar outcomes in comparison to the other techniques considered. It was however noted that at times it was not possible to fit a reliable circle to the FRF data. Also, the weak and coupled modes were among the most difficult ones to analyze. He concluded that the circle-fit

method could provide reliable results so long as there are enough data points around the resonance and that damping is not too low. On the other hand, it was stated that the method should not be used when the data contains noise around the resonance. He found that the global MDOF identification method could produce more consistent set of modal properties and is much faster than the SDOF approach.

In another paper, Fahey and Pratt (1998a) also explained the use of SDOF and MDOF techniques for fitting the experimental data. The SDOF techniques used were the Half-Power and Finite Difference method. They stated that the aforementioned techniques would be suitable when performing quick field analysis or when wanting to provide initial estimates of the parameters for use in the more complex MDOF techniques. As for the MDOF techniques they considered the simultaneous frequency-domain method and the rational polynomial method. They also addressed the topic of refitting the data for evaluating the global modal parameters. But in another article (1998b), they compared different time-domain modal estimation techniques.

Iglesias (2000) reported the comparison of the Half Power Frequency Domain Method, the Hilbert Transform Method and the Half Power Frequency Domain Method based on the so-called "zoom" measurements. It was concluded that third method was time consuming and that it should be used only when it is absolutely necessary to improve the frequency resolution. It was also stated that for light damping the Hilbert Transform would give better results than the Half Power Frequency Domain Method. Moreover, the first method was shown to have produced better fast loss factor with faster calculation speed in cases where coherence was good with small frequency resolution.

In another study, Naghipour et al. (2005) used different methods based on SDOF to evaluate vibration damping of Glass Fiber Reinforced plastic (GRP) glulam composite cantilever beams. The GRP used to reinforce the beams had various lay ups. They showed that damping coefficient based on the SDOF methodologies could be obtained with reasonable accuracy.

Yang (2003) used EMD for system identification of four degrees of freedom mechanical system, and evaluated the natural frequencies and damping of an *in-situ* tall building. Based on an experimental investigation, Xu and Chen (2004) also used

EMD for damage detection of a three story shear-walled building. He concluded that damage location could be identified by the spatial distribution of the spikes (spikes in the curve of the sensor's quantity, i.e. voltage versus time), in the vicinity of the damage location in a building.

This paper outlines the details of six techniques used for determining the damping of a PVC material used in a pipe, based on time, frequency, and time-frequency domain methodologies. The methods considered in the time domain were Logarithmic Decrement Algorithm (LDA) and the Hilbert Transform Analysis (HTA). The method considered in the time-frequency domain was Hilbert-Huang spectral analysis based on Empirical Mode Decomposition (EMD). In the frequency method, the Moving Block Analysis (MBA), the Half Power Bandwidth (HPB), and the Circle fitting method were considered. The first two and the fourth methods were also used by Smith and Wereley (1997) for evaluation of damping ratio of composite rotorcraft flex beams reinforced with viscoelastic damping layers. For this, a PVC pipe with the length of 1531 mm and 159.1mm outer diameter and wall-thickness of 4.55 mm was considered. The pipe was then instrumented using piezoelectric sensors and tested, and their damping ratios were evaluated using the above-mentioned methods. Five piezoelectric sensors were mounted at different locations along the length of the pipes and the pipe was subjected to an induced displacement and vibrational data was collected.

The other main objectives of our investigation are as follows:

- To validate the Hilbert-Huang spectral analysis approach and its formulation for system identification by comparing the results obtained from this method to those of other commonly used methods.

- To evaluate the influence of the location of the piezoelectric sensors used for gathering data on the resulting damping ratios.

- To compare the results obtained based on the three different approaches (i.e., the time domain, frequency domain and time-frequency domain).

Based on our findings, discussions are provided outlining the strengths and shortfalls of the approaches.

To the best of our knowledge, the comparison of the methods considered within this work has not been reported in literature. Moreover, this is the first time that the Empirical Mode Decomposition (EMD) method has been applied to evaluate structural damping based on the data obtained from piezoelectric sensors.

5.3 Modeling and formulation of piezoelectric material

Various finite element formulations have been presented by several researchers for the assessment of dynamic response of piezoelectric materials. For instance, Tzou and Tseng (1990), and Rao and Sunar (1994) used the following equations to represent the dynamic response:

$$\begin{aligned} [M]\{\ddot{u}\} + [K_{uu}]\{u\} + [K_{u\phi}]\{\phi\} &= \{F\} \\ [K_{\phi u}]\{u\} + [K_{\phi\phi}]\{\phi\} &= \{Q\} \end{aligned} \tag{5.1}$$

where:

$[M] = \int_V \rho [N_u]^T [N_u] dV$ is the kinematically consistent mass matrix;

$[K_{uu}] = \int_V [B_u]^T [C^E] [B_u] dV$ is the elastic stiffness matrix;

$[K_{u\phi}] = \int_V [B_u]^T [e]^T [B_\phi] dV$ is the piezoelectric coupling matrix;

$[K_{\phi\phi}] = -\int_V [B_\phi]^T [\varepsilon] [B_\phi] dV$ is the dielectric stiffness matrix;

$\{F\} = \int_V [N_u]^T \{f_b\} dV + \int_{S_1} [N_u]^T \{f_S\} d\Omega + [N_u]^T \{f_c\}$ is the mechanical force vector, and

$\{Q\} = -\int_{S_2} [N_\phi]^T q_s d\Omega - [N_\phi]^T q_c$ is the electrical force vector.

In the above equations, [M] is the mass matrix, u is the displacement, ϕ is the electric potential, Q is the applied concentrated electric charges, ρ is the mass density, $[B_u]$ and $[B_\phi]$ are the derivatives of the shape functions, $[N_u]$ and $[N_\phi]$; [C^E], [ε], and [e] are the elasticity, dielectric, and piezoelectric matrices respectively; f_b denotes the body force, f_s is the surface force, f_c is the concentrated force, q_s is the surface charge, q_c is the point charge, S_1 is the region to which the surface forces are applied, and S_2

is the region where the electrical charges are applied. The above equations are presented in a partitioned form to reflect the coupling between the elastic and electric fields. Equation (5.1) can be condensed to represent the sensor's potential in terms of the sensor displacement in the form:

$$\{\phi_s\} = [K_{\phi\phi}]^{-1}(-[K_{u\phi}^T]\{u\}) \tag{5.2}$$

5.4 Experimental procedure and set up

5.4.1 Test Setup and Instrumentation

The test specimens used to determine the damping ratios were pipes made of PVC. A PVC pipe was instrumented by five piezoelectric sensors, as shown in Figure 5.1. These sensors were bonded to the surface of the pipes using a West System's two-part epoxy. Once the sensors were bonded, they were held in place for eight hours under 20" of mercury vacuum to remove air voids and to ensure a strong bond. The pipes were held by a rigid metallic collar fastened to a massive steel platform. The material properties of the PVC pipe and piezoelectric patches are tabulated in Table 5.1.

Table 5.1: Basic properties of the materials.

E	2800 MPa
ν	0.35
ρ	1150 Kg/m^3
Piezoelectric Patches	
E	69000 MPa
ν	0.35
d_{31}	-179E-12 m/V
K_3^T	1800
ρ	7700 Kg/m^3

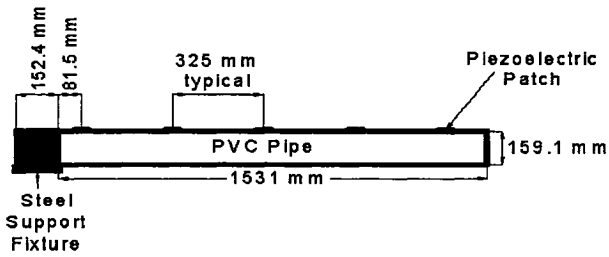

Figure 5.1. Schematic of test setup.

5.4.2 Test Procedure

As stated, the pipes were held in place as a cantilever beams. The rigid metallic collar was then secured in place under a 500 lb force using a 440,000 lb capacity Tinus-Olsen Universal Testing machine. Loading of the specimen was performed by hanging a known mass from a plastic strap on its free end, thus displacing the pipe's free end by a predetermined value. The strap was then cut, and the resulting vibration was monitored by the five piezoelectric patches.

The responses of the piezoelectric patches were simultaneously monitored with a differential channel set-up using a multi-purpose DT3010 data acquisition card manufactured by Data Translation (MA, USA). A C++ program was developed in-house to collect and process the data, using a sampling frequency of 1500 Hz.

5.5 ESTIMATION OF DAMPING RATIO USING VARIOUS METHODS OF ANALYSIS

As stated, several methods of analysis, based on the time, frequency, and time-frequency domains were considered in our investigation. The following sections provide the details of each methodology.

5.5.1 Evaluation of damping ratio by the logarithmic decrement analysis (LDA)

The true damping characteristic of a typical structural system is quite complex and rather difficult to define. However, it is a common practice to express the damping of a real system in terms of an equivalent viscous-damping ratio, ξ, which exhibits a similar decay rate under free-vibration condition. Consider any two successive positive peak amplitudes v_n and v_{n+1}, occurring at times $n\left(\frac{2\pi}{\omega_D}\right)$ and $(n+1)\left(\frac{2\pi}{\omega_D}\right)$, respectively. For a critically damped system, the ratio of these two successive values can be represented by:

$$v_n / v_{n+1} = \exp(2\pi\xi\, \omega / \omega_D) \tag{5.3}$$

where ω is the natural frequency, and subscript D indicates the damped condition.

Taking the natural logarithm (ln) of both sides of the above equation and substituting $\omega_D = \omega\sqrt{1-\xi^2}$, one obtains the so-called "logarithmic decrement" of damping, δ, by:

$$\delta = \ln\frac{v_n}{v_{n+1}} = \frac{2\pi\xi}{\sqrt{1-\xi^2}} \tag{5.4}$$

The logarithm of the ratio of the amplitude of two oscillations that are n cycles apart from each other, on the decaying transient of a single degree freedom system is defined by:

$$\ln\frac{v_m}{v_{n+m}} = \frac{2n\pi\xi}{\sqrt{1-\xi^2}} \tag{5.5}$$

where the peak amplitude of the m^{th} cycle and that of the n^{th} cycles apart from it can be calculated by the transient signal of an under critically- damped system equation:

$$v(t) = e^{-\xi\omega_n t}\sin(\sqrt{1-\xi^2}\,\omega_n t + \beta) \tag{5.6}$$

For low values of damping, Equation (5.3) can be simplified to:

$$\delta \doteq 2\pi n\xi \tag{5.7}$$

The damping ratio can thus be determined from the slope of the best-fitted line to the natural logarithm of each peak magnitude. Mathematically, the slope is equal to $-\xi\omega_n$.

Here we use output results of the piezoelectric sensors, which would be voltage versus time instead of using the usual displacement-time result. Typical output results of the piezoelectric sensors #1 and #5 are illustrated in Figures (5.2a, b), and the data sensors #2, #3, and #4 was processed by the LDA methods, as illustrated in Figures (5.3a, b, c).

5.5.2 Evaluation of damping ratio by the Hilbert Transform Analysis (HTA)

The Hilbert transforms are linear operators that can be defined for a time domain, x (t), by a convolution integral (Bracewell, 1999):

$$y(t)=\frac{1}{\pi}\int_{-\infty}^{\infty}\delta(\tau)\frac{x(\tau)}{(t-\tau)}d\tau \quad where \begin{cases} \delta=-1 & for \quad \tau<0 \\ \delta=0 & for \quad \tau=0 \\ \delta=+1 & for \quad \tau>0 \end{cases} \tag{5.8}$$

The Hilbert transform computes the so-called discrete-time analytic signal $x = x_r + ix_i$ such that x_i is the Hilbert transform of the real vector x_r.

For a discrete-time analytic signal x, the last half of FFT(x) is zero, and the first (DC) and center (Nyquist) elements of FFT(x) are purely real. Moreover, an analytical signal represented by $\left[z(t)=x(t)+iy(t)=A(t)e^{i\theta(t)}\right]$, consists of a real part (the original data) and an imaginary part (the Hilbert transform portion). One of the most useful properties of this transformation scheme relative to the Fourier transform is that when x(t) passes through the Hilbert Transformation, it leaves the magnitude of X(f) unchanged (where X(f) is the Fast Fourier transform of x(t)), but rotates the phase angle by $\frac{\pi}{2}$. The Hilbert transform is therefore useful in calculating the instantaneous of a time domain, especially the amplitude and frequency.

Based on the above introductory background, the damping analysis can be performed by calculating the envelope signals for the transient output data of the

piezoelectric sensors using the Hilbert transformation. This method was also applied by Smith and Wereley (1997) to evaluate the damping properties of a composite beam. For the transient response of a typical viscously damped system, the envelope signal, A(t), and the instantaneous damping ratio $\xi(t)$ can be expressed by:

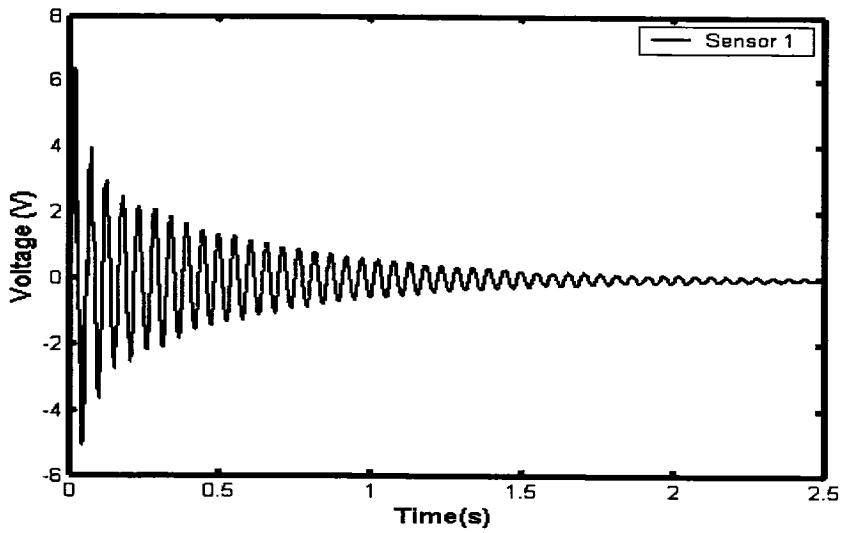

(a)

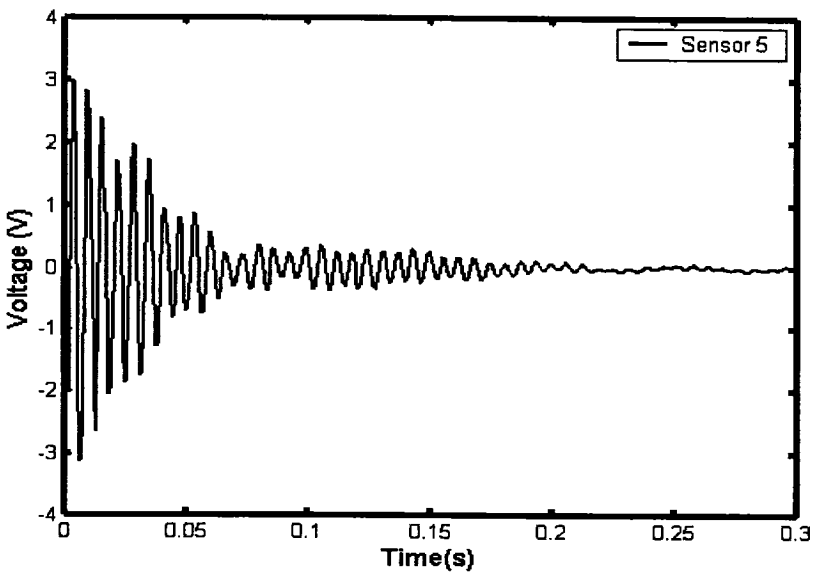

(b)

Figure 5.2. Typical responses obtained from the sensors, (a) Sensor #1 (b) Sensor #5.

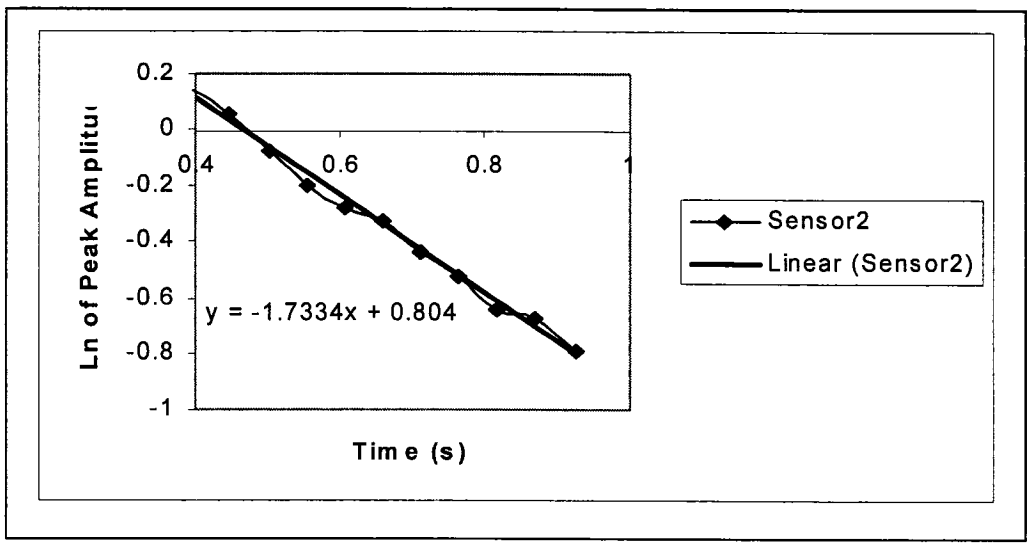

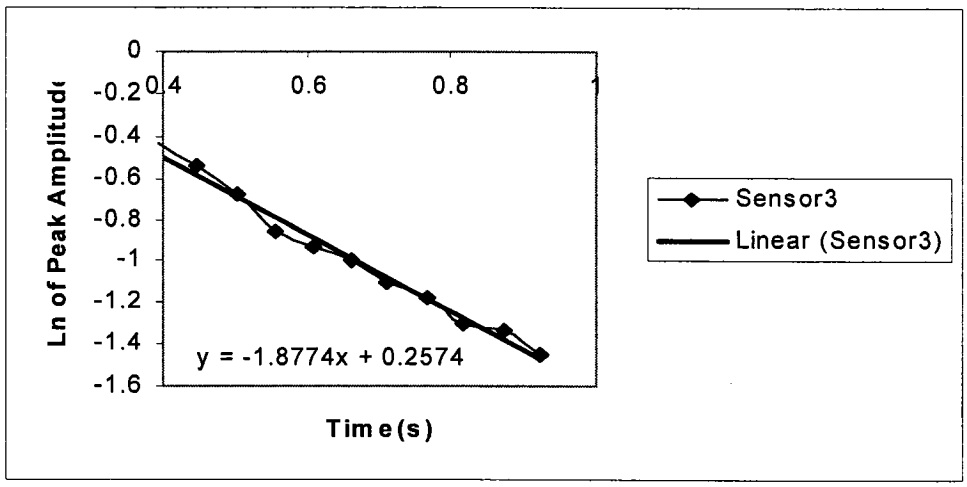

(b)

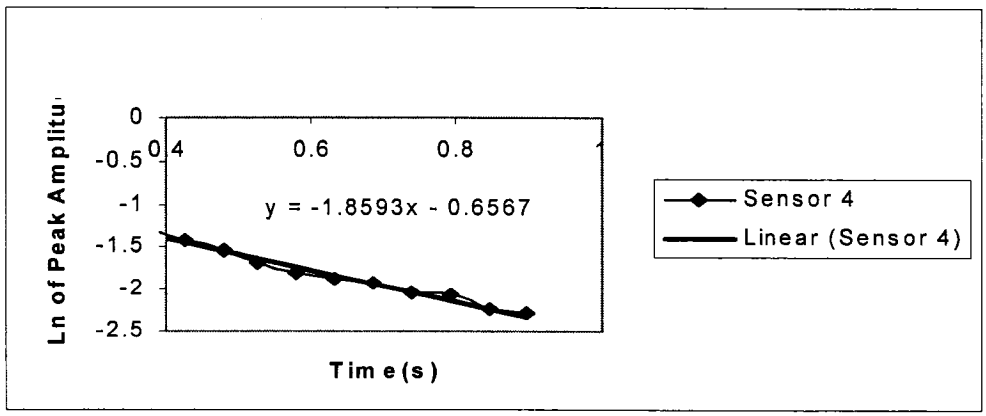

(c)

Figurer 5.3. Results obtained from the LDA method (a) Sensor # 2, (b) Sensor # 3, (c) Sensor # 4.

$$A(t) = e^{-\xi\omega_n t} \qquad \text{and} \qquad \xi(t) = -\frac{d(\ln A(t))}{\omega_n dt} = \xi \tag{9}$$

A line can therefore be fitted through the logarithm of the envelope, and the slope of this line, $-\xi\omega_n$, would be equivalent to the damping ratio. Typical results of the HHT method for sensor # 1 is illustrated in Figures (5.4a, b)

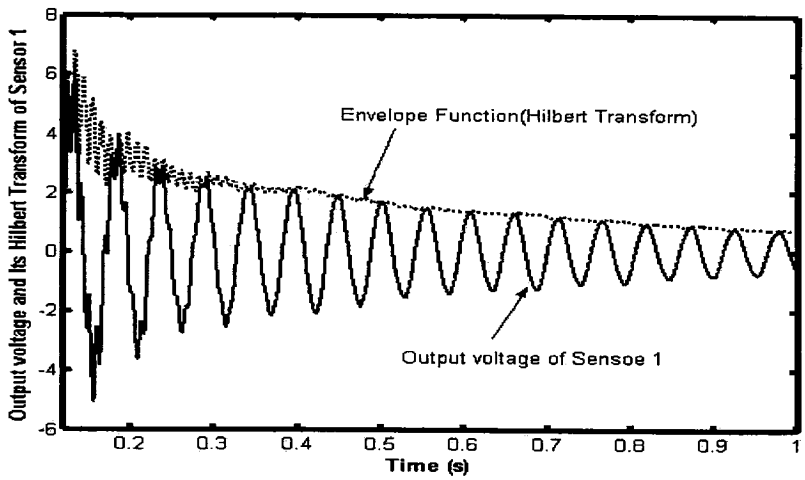

(a)

(b)

Figure 5.4. (a): Output voltage of Sensor #1 with its Envelope Function based on Hilbert transform, (b): plot of *ln* of Hilbert transform vs. time for data of sensor #1.

5.5.2.1 Mathematical Description of HHT

The Hilbert-Huang Transform (HHT) method was proposed by Huang et al. (1998). It consists of two parts: (i) the Empirical Mode Decomposition (EMD), and (ii) the Hilbert Spectral Analysis. With EMD, any complicated data set can be decomposed into a finite and often a smaller number of intrinsic mode functions.

The method is based on decomposing a signal into intrinsic mode functions (IMFs) using the empirical mode decomposition (EMD) method, where each IMF admits a well-behaved Hilbert transform. Then, the Hilbert transform is applied to each intrinsic mode function to obtain a decomposition of the signal in the frequency-time domain. This approach is also referred to as the Hilbert-Huang spectral analysis (HHSA) and it is applicable to any non-stationary signal (Huang et al., 1998; Huang et al., 1999). In this paper, the EMD method proposed by Huang (1998) and Huang et al. (1999), and will be used to decompose the measured response signal (output voltage of the piezoelectric sensors) into IMFs that would admit a well-behaved Hilbert transform. Based on the EMD, the modal response of each mode can be extracted from output voltage of a piezoelectric sensor.

The EMD procedure involves construction of the upper and lower envelopes of the signal by spline fitting, and then the average of both envelopes is computed. Then, the signal is subtracted from the mean. This process is referred to as the"sifting" process. The sifting process is repeated until the resulting signal becomes a monocomponent. The resulting monocomponent signal admits a well-behaved Hilbert transform; it is therefore referred to as an IMF. The original signal is then subtracted from IMF, and the repeated sifting process is applied to the remaining signals to obtain other IMFs. The process is iterated until m IMFs are obtained. The IMFs extracted from the sifting process may contain more than one frequency, which may not be the modal response of the output signal. During the sifting process in EMD, one can also impose an intermittency frequency, denoted by ω_{int} so that the resulting IMF will not contain any frequency components smaller than ω_{iut}. This is accomplished by removing data that have frequencies lower than ω_{iut}, from the IMF by a straightforward counting process. This process was also implemented in the EMD procedures used by several others (Huang et al., 1998; Huang et al., 1999).

A code produced in MATLAB language was developed for carrying out the EMD procedure for the output voltages of the piezoelectric sensors.

5.5.2.2 Band-pass filtering and EMD

The isolation of modal responses using the EMD method presented above has an advantage in that the frequency content of the signal at each time instant can be presented. However, the numerical computation based on this approach may be quite involved, in particular when the modal frequencies are high, and/or when the signal is polluted by an elevated noise level. In these cases, in order to obtain accurate modal responses, one should increase the number of siftings in the EMD. To simplify and decrease the computational efforts, an alternative approach based on the band-pass filter method was proposed by Yang et al. (2003). With Yang et al's proposed method, one can determine the approximate frequency range for each natural frequency from the Fourier spectrum of the output voltage. For example, if one considers the power spectrum analysis of sensor 1, as illustrated in Figure 5.7a, one would see that the first mode is between 18 to 20 Hz. Each signal is then processed through the band-pass filters with a set frequency band. The time history obtained from the jth band-pass filter (jth natural frequency) is then processed through EMD. In this way, the first resulting IMF would be quite close to the jth modal response. By repeating the above procedure for the other natural frequencies, one can then obtain *n* modal responses.

5.5.2.3 Evaluation of damping ratio by Hilbert-Huang Spectral Analysis (HHSA)

The equation of motion for an n-DOF structure can be expressed by (Yang et al., 2003):

$$M\ddot{X}(t) + C\dot{X}(t) + KX(t) = F(t) \tag{5.10}$$

in which $X(t) = [x_1, x_2, ..., x_n]$ represents the displacement vectors, *F(t)* is the excitation vector and *M, C* and *K* are the (n×n) mass, damping, and stiffness matrices, respectively. With the assumption of the existence of normal modes, the displacement and acceleration responses can be decomposed into n real modes:

$$X(t) = \sum_{j=1}^{n} \phi_j Y_j(t); \quad \ddot{X}(t) = \sum_{j=1}^{n} \phi_j \ddot{Y}(t) \tag{5.11}$$

From the above equations, it is apparent that the $n \times n$ mode-shape matrix ϕ serves to transform the generalized coordinate vector Y to the geometric coordinate vector X. The generalized components in vector Y are called the "normal coordinates" of the structure.

By substituting Equation (5.11) into Equation (5.10) and using the orthogonal properties of the mode shapes, one can decouple Equation (5.10) into n modes:

$$\ddot{Y}_j + 2\xi_j \omega_j \dot{Y} + \omega_j^2 Y = \phi_j^T F(t)/m_j \tag{5.12}$$

where ω_j is the jth modal frequency, ξ_j is the jth modal damping ratio, and m_j is the jth modal mass. Now, let's consider an impact load applied at the pth DOF (i.e. $f_p(t) = F_0\delta(t)$ and $f_j(t) = 0$ for all $j \neq p$, where $f_j(t)$ is the jth element of $F(t)$). Then, the acceleration response of the jth generalized modal co-ordinate is given by:

$$\ddot{Y}_j(t) = \frac{F_0 \phi_{pj} \omega_j}{m_j \sqrt{1-\xi_j^2}} e^{-\xi_j \omega_j t} \cos(\omega_{dj} t + \varphi_j + \frac{\pi}{2}) \tag{5.13}$$

where ϕ_{pj} is the pth element of the jth modal vector ϕ_j, $\omega_{dj} = \omega_j(1-\xi_j^2)^{0.5}$, is the jth damped modal frequency, and $\varphi_j = \tan^{-1}(2\xi_j\sqrt{1-\xi_j^2}/(1-2\xi_j^2))$ is the phase lag of the jth mode. The impulse acceleration response $\ddot{x}_k(t)$ of the structure at k (k=1,. . . , n) DOF is given by:

$$\ddot{x}_k(t) = \sum_{j=1}^{n} \phi_{kj} \ddot{Y}_j(t) = \sum_{j=1}^{n} \ddot{x}_{kj}(t) \tag{5.14}$$

where:

$$\ddot{x}_{kj}(t) = \phi_{kj} \ddot{Y}_j(t) = B_{kj,p} e^{-\xi_j \omega_j t} \cos(\omega_{dj} t + \varphi_j + \frac{\pi}{2} + \varphi_{kj,p}) \tag{5.15}$$

in which:

$$B_{kj,p} = \frac{F_0 |\phi_{kj}| |\phi_{pj}| \omega_j}{m_j \sqrt{1-\xi_j^2}} \tag{16}$$

$$x_{kj}(t) = B_{kj,p} \frac{e^{-\xi_j \omega_j t}}{(\xi_j^{\,2}\omega_j^{\,2} + \omega_{dj}^{\,2})^2} * \left[\begin{array}{l} \xi_j^{\,2}\omega_j^{\,2} \sin(\omega_{dj} t + \varphi_j + \frac{\pi}{2} + \varphi_{kj,p}) + \\ 2\xi_j \omega_j \omega_{dj} \cos(\omega_{dj} t + \varphi_j + \frac{\pi}{2} + \varphi_{kj,p}) - \varpi_{dj}^{\,2} \sin(\omega_{dj} t + \varphi_j + \frac{\pi}{2} + \varphi_{kj,p}) \end{array} \right] \tag{5.17}$$

$$x_{kj}(t) = B_{kj,p} \frac{e^{-\xi_j \omega_j t}}{(\xi_j^{\,2}\omega_j^{\,2} + \omega_{dj}^{\,2})^2} * \left[\sqrt{(\xi_j^{\,2}\omega_j^{\,2} - \omega_{dj}^{\,2})^2 + 4\xi_j^{\,2}\omega_j^{\,2}\omega_{dj}^{\,2}} \cos(\omega_{dj} t + \varphi_j + \frac{\pi}{2} + \varphi_{kj,p} - \theta) \right]$$

where:

$$\theta = tg^{-1}\left(\frac{\xi_j^{\,2}\omega_j^{\,2} - \omega_{dj}^{\,2}}{2\xi_j \omega_j \omega_{dj}}\right) \tag{5.18}$$

In Equations (5.15, 5.17, and 5.18), $\varphi_{kj,p}$ is the phase difference between the k^{th} element and the p^{th} element in the j^{th} mode shape. With the existence of normal modes, all the mode shapes are real and hence $\varphi_{kj,p}$ is either $\pm 2m\pi$ or $\pm(2m+1)\pi$, where m is an integer, i.e.

$\varphi_{kj} / \varphi_{pj} \succ 0$ when $\varphi_{kj,p} = \pm 2m\pi$

$\varphi_{kj} / \varphi_{pj} \prec 0$ when $\varphi_{kj,p} = \pm(2m+1)\pi$

The Hilbert transform $x_{kj}(t)$ in Equation (5.18) can be obtained using the Bedrosian's theorem (Hahn, 1996), as follows:

$$\tilde{x}_{kj}(t) = \frac{F_0 |\phi_{kj}| |\phi_{pj}| \omega_j}{m_j \sqrt{1-\xi_j^{\,2}}} \frac{e^{-\xi_j \omega_j t}\left(\sqrt{(\xi_j^{\,2}\omega_j^{\,2} + \omega_{dj}^{\,2})^2 + 4\xi_j^{\,2}\omega_j^{\,2}\omega_{dj}^{\,2}}\right)}{\left(\xi_j^{\,2}\omega_j^{\,2} + \omega_{dj}^{\,2}\right)^2} * \tag{5.19}$$

$$\left[a_{LK,j} \sin(\omega_{dj} t + \varphi_j + \frac{\pi}{2} + \varphi_{kj,p} - \theta) + \tilde{a}_{HK,j} \cos(\omega_{dj} t + \varphi_j + \frac{\pi}{2} + \varphi_{kj,p} - \theta) \right]$$

where:

$$a_{LK,j} = \frac{1}{\pi} \int_0^{\omega_{dj}} \frac{2\xi_j \omega_j}{\xi_j^{\,2}\omega_j^{\,2} + \omega^2} \cos(\omega t) d\omega \tag{5.20}$$

$$\tilde{a}_{HK,j} = \frac{1}{\pi} \int_{\omega_{dj}}^{\infty} \frac{2\xi_j \omega_j}{\xi_j^{\,2}\omega_j^{\,2} + \omega^2} \sin(\omega t) d\omega \tag{5.21}$$

The analytical signal $Z_{kj}(t)$ of the j^{th} mode is given by:

$$Z_{kj}(t) = x_{kj}(t) + i\tilde{x}_{kj}(t) = A_{kj}(t)e^{i\beta_{kj}(t)} \tag{5.22}$$

In which the instantaneous amplitude $A_{kj}(t)$ and instantaneous phase angle $\beta_{kj}(t)$ are represented by:

$$A_{kj}(t) = B_{kj,p}\frac{\sqrt{(\xi_j{}^2\omega_j{}^2 + \omega_{dj}{}^2)^2 + 4\xi_j{}^2\omega_j{}^2\omega_{dj}{}^2}}{(\xi_j{}^2\omega_j{}^2 + \omega_{dj}{}^2)^2}\left\{\begin{array}{l} e^{-2\xi_j\omega_j t}\cos^2(\omega_{dj}t + \varphi_j + \frac{\pi}{2} + \varphi_{kj,p} - \theta) + \\ \left[a_{LK,j}(t)\sin(\omega_{dj}t + \varphi_j + \frac{\pi}{2} + \varphi_{kj,p} - \theta) + \right.\\ \left.\tilde{a}_{HK,j(t)}\cos(\omega_{dj}t + \varphi_j + \frac{\pi}{2} + \varphi_{kj,p} - \theta)\right]^2 \end{array}\right\}^{1/2} \tag{5.23}$$

$$\beta_{kj}(t) = \tan^{-1}\left\{e^{\xi_j\omega_j t}\left[a_{LK,j}(t)\tan(\omega_{dj}t + \varphi_j + \frac{\pi}{2} + \varphi_{kj,p} - \theta) + \tilde{a}_{HK,j}(t)\right]\right\} \tag{5.24}$$

For a special case in which ξ_j is very small (less than 10%) and ω_j is large, Equations 5.20 and 5.21 yield:

$$a_{LK,j} \approx \frac{1}{\pi}\int_0^\infty \frac{2\xi_j\omega_j}{\xi_j{}^2\omega_j{}^2 + \omega^2}\cos(\omega t)d\omega = e^{-\xi_j\omega_j t} \tag{5.25}$$

$$\tilde{a}_{HK,j} = \frac{1}{\pi}\int_{\omega_{dj}}^\infty \frac{2\xi_j\omega_j}{\xi_j{}^2\omega_j{}^2 + \omega^2}\sin(\omega t)d\omega \approx 0 \tag{5.26}$$

Thus, Equation (19) becomes:

$$\tilde{x}_{kj}(t) = \frac{F_0|\phi_{kj}\|\phi_{pj}|\omega_j}{m_j\sqrt{1-\xi_j{}^2}}\frac{e^{-\xi_j\omega_j t}\left(\sqrt{(\xi_j{}^2\omega_j{}^2 + \omega_{dj}{}^2)^2 + 4\xi_j{}^2\omega_j{}^2\omega_{dj}{}^2}\right)}{\left(\xi_j{}^2\omega_j{}^2 + \omega_{dj}{}^2\right)^2} * \sin(\omega_{dj}t + \varphi_j + \frac{\pi}{2} + \varphi_{kj,p} - \theta) \tag{5.27}$$

and the amplitude $A_{kj}(t)$ and phase angle $\beta_{kj}(t)$ in Equation (5.22) are given by:

$$A_{kj}(t) = \frac{F_0|\phi_{kj}\|\phi_{pj}|\omega_j}{m_j\sqrt{1-\xi_j{}^2}}\frac{e^{-\xi_j\omega_j t}\left(\sqrt{(\xi_j{}^2\omega_j{}^2 + \omega_{dj}{}^2)^2 + 4\xi_j{}^2\omega_j{}^2\omega_{dj}{}^2}\right)}{\left(\xi_j{}^2\omega_j{}^2 + \omega_{dj}{}^2\right)^2} \tag{5.28}$$

$$\beta_{kj}(t) = \omega_{dj}t + \varphi_j + \frac{\pi}{2} + \varphi_{kj,p} - \theta \tag{5.29}$$

From Equations (5.28) and (5.29), one can obtain:

$$\ln A_{kj}(t) = -\xi_j \omega_j t + \ln\left(\frac{F_0 |\phi_{kj}| |\phi_{pj}| \omega_j}{m_j \sqrt{1-\xi_j^2}} \frac{\left(\sqrt{(\xi_j^2 \omega_j^2 + \omega_{dj}^2)^2 + 4\xi_j^2 \omega_j^2 \omega_{dj}^2}\right)}{\left(\xi_j^2 \omega_j^2 + \omega_{dj}^2\right)^2}\right) \tag{5.30}$$

$$\omega_j(t) = d\beta_{kj}(t)/dt = \omega_{dj} \tag{5.31}$$

With the measured output voltage of piezoelectric sensors, the EMD method can be used to decompose each measurement signal into *n* modal responses. Then, each modal response can be processed through the Hilbert transform to determine the signal's instantaneous amplitude and phase angle. Finally, the system identification can be conducted to evaluate the natural frequencies and damping ratios by the process described below.

It should be noted that for the sake of generality, the formulation presented in the above was developed based on the displacement data; alternatively, the above formulation can be developed based on the data obtained from another type of sensor, such as accelerometers or strain gauges.

The advantage of the outlined approach used for evaluating the damping and natural frequency is that it is not sensitive to the choice of sensor used to collect the data. In principle, signals obtained through any suitable sensors can be used for evaluation of the parameters of interest. For instance, one can directly input the output voltage of a piezoelectric sensor in Equation (5.29) to start the calculations. In this paper we have used the output voltage of piezoelectric sensors for evaluating the damping of a PVC pipe.

5.5.2.4 Evaluation of natural frequencies and damping ratios Based on Hilbert-Huang spectral analysis (HHST)

As stated, the advantage of the HHST method is that one needs data from only a single sensor (in our case, from one piezoelectric sensor), in order to evaluate the frequencies ω_j and damping ratios ξ_j for a structure with j=1, 2, ..., n DOF. The measured output voltage response of the piezoelectric sensor contains sufficient information about ω_j and ξ_j (j=1, 2,..., n). The procedure is described as follows:

For a ξ_j (less than 10%), it follows from Equation (5.13) that the damped natural frequency ω_{dj} can be obtained from the slope of the plot of phase angle $\theta_{pj}(t)$ versus time, t, for which $-\xi_j\omega_j$ can be estimated from the slope of the plot of the decaying amplitude $\ln A_{pj}(t)$ versus time t, obtained from Equation (5.30).

- For the general case in which ξ_j is not small, $A_{pj}(t)$ and $\theta_{pj}(t)$ are obtained from Equations (5.28) and (5.29). In this case, both $\theta_{pj}(t)$ and $\ln A_{pj}(t)$ would not be a linear functions of time t. Theoretically, ξ_j and ω_{dj} can be determined from the non-linear Equation (5.28). However, examination of the numerical results of Equation (5.28) would reveal that the variation of amplitude $A_{pj}(t)$ introduces an instantaneous frequency modulation. This frequency modulation is referred to as "intra-wave modulation" by Huang et al. (1998). It was shown that the amplitude variation could cause a frequency fluctuation around the mean value of a carrier frequency, but not a change of its mean value (Huang et al., 1998). Consequently, we propose the use of linear least-square fit procedures to estimate the mean values of the natural frequencies and damping ratios for general case.

Figure 5.5 illustrates a typical sensor (output voltage of sensor #1) with its IMFs. As stated, one can determine the frequencies of the system from data obtained from any of the sensors. For the sake of illustration, the first natural frequency was derived from the date obtained from sensor # 4 (the slope of the curve) and illustrated in Figure (5.6c). It should be noted that alternatively the data from other sensors could have been used to produce the same frequency. Moreover, to demonstrate the strength of this method, the data obtained from sensors 1 and 3 are used to construct the curves of $\ln A_{pj}(t)$ versus t (Figures 5.6(a) and (b)). The damping ratio is extracted from the slope of the curves, which are shown to be very similar in values (see Table 5.3).

5.5.3 Evaluation of damping ratio by the Moving Block Analysis (MBA)

The Moving Block Analysis was introduced by Hammond and Doggett (1975), who investigated the response of a rotating model-scale rotor system. Tasker and

Chopra (1990) showed that this method of damping analysis could be used to identify the stability characteristics of a high-level noise system. It was demonstrated that this method of analysis could effectively estimate the damping ratio for a variety of vibrating systems. This method was also used by Smith and Wereley (1997) for characterizing the dynamic response of a cantilevered composite beam hosting viscoelastic damping layers, excited by piezoelectric actuators.

In brief, the MBA is based on the calculation of the discrete approximation of the FFT of transient response data. This was presented by Tasker and Chopra (1990) in mathematical form as:

$$X(\omega) = \sum_{r=0}^{N-1} x(r\Delta t) e^{-i\omega r\Delta t} \qquad T = N\Delta t \tag{5.32}$$

For a damped transient response, the above could be represented by:

$$X(\omega, t_0) = \int_0^{T+t_0} A e^{-\omega_n t} \sin(\sqrt{1-\xi^2}\,\omega_n t + \phi) e^{-i\omega t} dt \tag{5.33}$$

where T is the block length and t_0 is the initial time of FFT.

Hammond and Doggett (1975) showed that the plot of the natural logarithm of the magnitude of FFT (i.e., $\ln|X(\omega_n, t|$) versus time would be the superposition of a straight line with a slope of $-\xi\omega_n$.

Table 5.3. Damping ratio evaluated based on the methods outlined.

Sensor Number	LDA	HTA	HHT (EMD)	MB A	Circle Fitted Method	HPB
1	1.47	1.39	1.42	1.36	1.37	1.86
2	1.55	1.36	1.38	1.32	1.27	1.86
3	1.56	1.33	1.35	1.25	1.22	1.86
4	1.55	1.30	1.32	1.22	1.21	1.94
5	Not acceptable*	.94	1.62	.96	1.00	1.74

5.5.4 Determination of damping ratio using the Half Power Bandwidth method

According to Richart et al. (1970), material damping (ξ) for each vibration mode can be determined from the respective resonant curve (see Figure (5.8a)), by means of the following expression:

$$\frac{2\pi\xi}{\sqrt{1-\xi^2}} = \frac{\pi}{2}\frac{(f_2^2 - f_1^2)}{f_m^2}\sqrt{\frac{A^2}{A_m^2 - A^2}}\frac{\sqrt{1-2\xi^2}}{1-\xi^2} \tag{5.34}$$

where A_m is the maximum amplitude and A is the amplitude at frequencies f_1 and f_2 at both sides of the resonant frequency f_m. For the case of a low damping ratio (less than 10%), Equation (5.33) can be simplified to:

$$\xi = A\frac{f_2^2 - f_1^2}{\sqrt{A^2 f_2^4 - 2A^2 f_2^2 f_1^2 + A^2 f_1^4 + 16 f_m^4 (A_m^2 - A^2)}} \tag{5.35}$$

Further simplification of Equation (5.34) is obtained if the amplitude A is taken at $\frac{A_m}{\sqrt{2}}$ with the resonant curve being symmetric with respect to f_m:

$$\xi = \frac{f_2 - f_1}{2f_m} \tag{5.36}$$

The above HPB formulation is one of the frequency domain methods usually admissible for materials that have small damping (Lanzan, 1968). Karnopp et al. (2000) showed that when considering the plot of the frequency response function versus frequency, the bandwidth at point corresponding to $\frac{1}{\sqrt{2}}$ of the maximum amplitude would be approximately twice the product of the damping ratio and natural frequency. Some typical power spectrum results of the output voltage of some of the piezoelectric sensors# 1, 2, and 5 have been illustrated in Figures (5.7a, b, c).

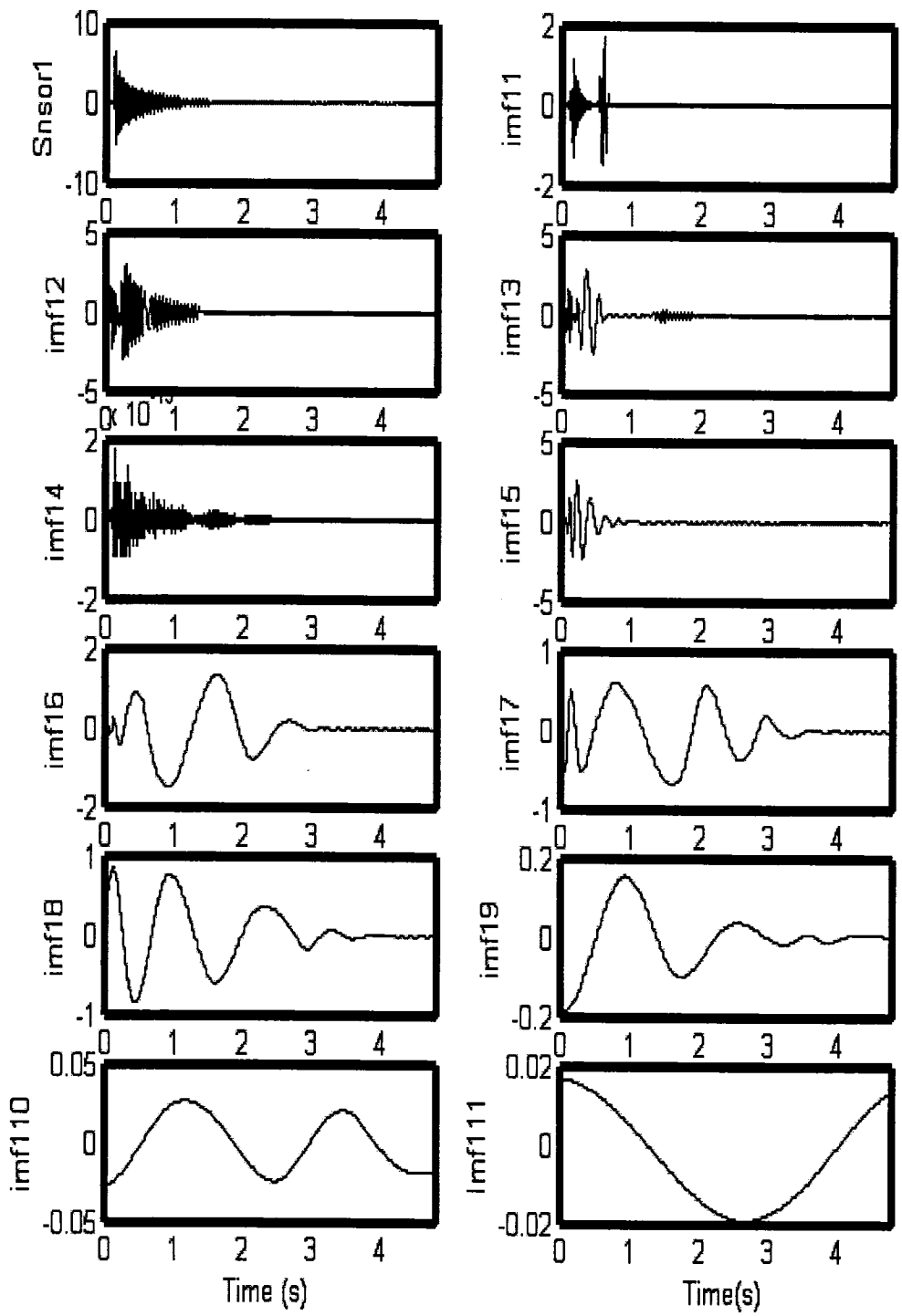

Figure 5.5. Output voltage of sensor #1 and the intrinsic mode function (IMFs) plots.

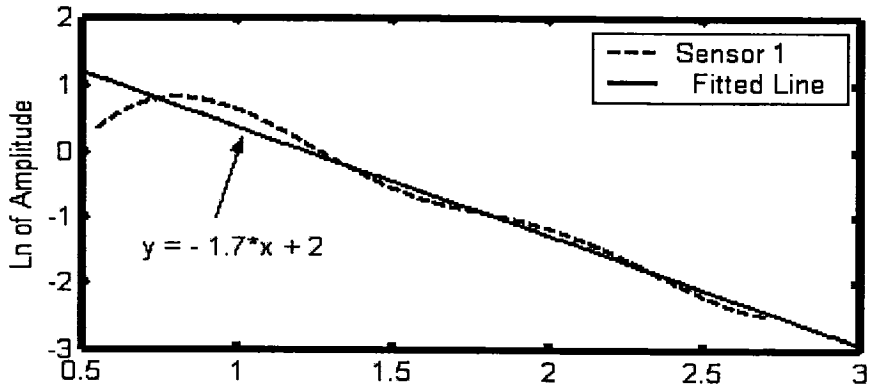

(a)

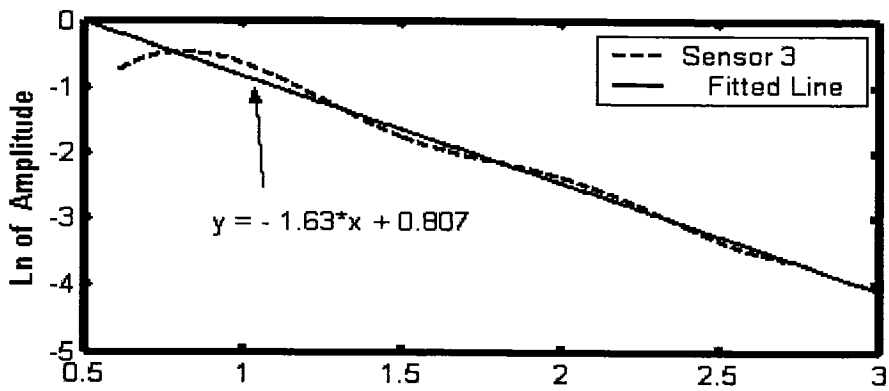

(b)

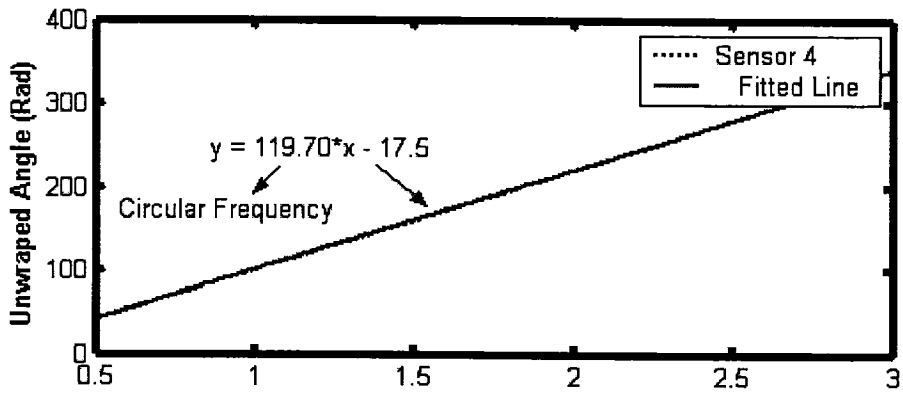

(c)

Figure 5.6. Application of the HHSA method on data obtained from (a) sensor #1, (b) sensor #3, and (c) #4.

5.5.5 Evaluation of damping ratio by the Circle-Fitting Method

This method, first introduced by Kennedy and Pancu, uses the Argand plane to display the real and imaginary parts of the receptance frequency response function (FRF). In this manner, in the vicinity of each natural frequency, the FRF curve approaches a circle; the natural frequency can then be located at the point where the rate of change of the arc length of frequency attains a maximum. The model assumed that the damping is the hysteretic one and the damping factor could be evaluated from a simplified half-power point calculation, and the mode shapes could be calculated from the ratios of the diameters of the circles fitted around each natural frequency for the various output response. In the present study, the circle-fitting method has been implemented as a mathematical solution, which accurately predicts the natural frequency ω_n and the damping factor η. Based on the vibration theory (Ewins, 1984), the receptance FRF of an N degree of freedom system with hysteretic damping can be evaluated by the following equation:

$$\alpha_{jk} = \sum_{r=1}^{N} \frac{C_{jk}^{r}}{\omega_r^2 - \omega^2 + i\eta_r\omega_r^2} \tag{5.37}$$

where η_r, ω_r and C_{jk}^{r} are the hysteretic damping ratio, natural frequency, and complex constant, respectively, associated with each mode r. The Nyquist plot of $(\omega_r^2 - \omega^2 + i\eta_r\omega_r^2)^{-1}$ is a circle. Thus, multiplication by the complex constant C_{jk}^{r} means a magnification or reduction of the circle radius, as well as giving a certain degree of rotation. In practice, the complex curve will not be exactly a circle around each natural frequency, but the curve will have circular arcs around those frequencies, especially when the modal frequencies are very similar.

The location and determination of the natural frequency are usually based on a frequency spacing technique. For a given mode, and apart from the effect of the complex modal constant, the phase angle θ_r associated with the dynamic response is given by Equation (5.38) from which the resonant frequency ω_r can be extracted at a location where $d\omega^2/d\theta_r$ is a minimum. The phase angle can also be evaluated by:

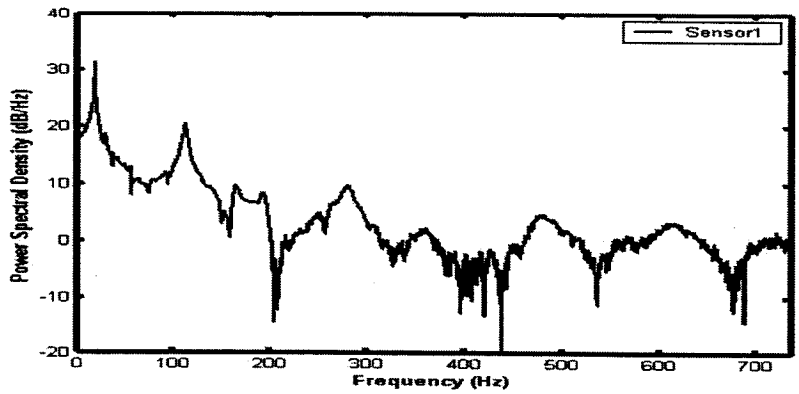

(a)

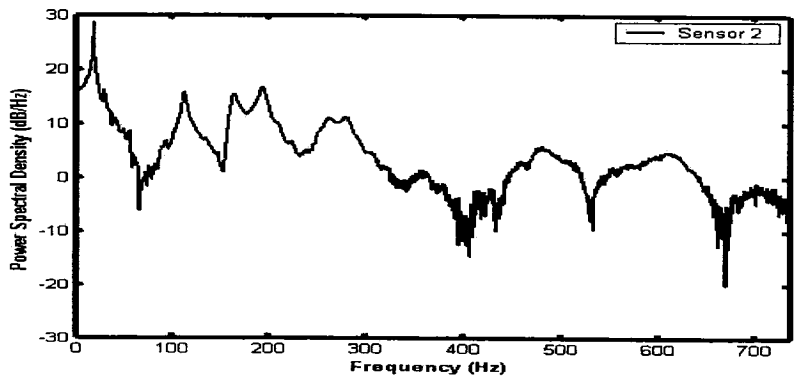

(b)

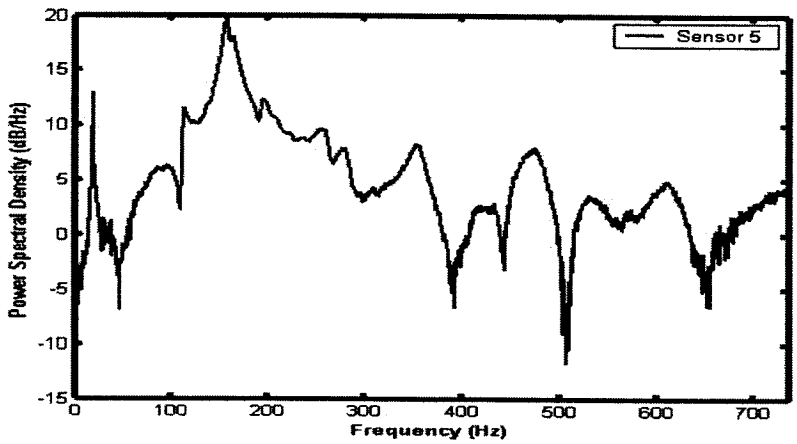

(c)

Figure 5.7. Plot of power spectrum vs. frequency obtained from the output voltage of (a) sensor #1, (b) sensor #2, and (c) #5.

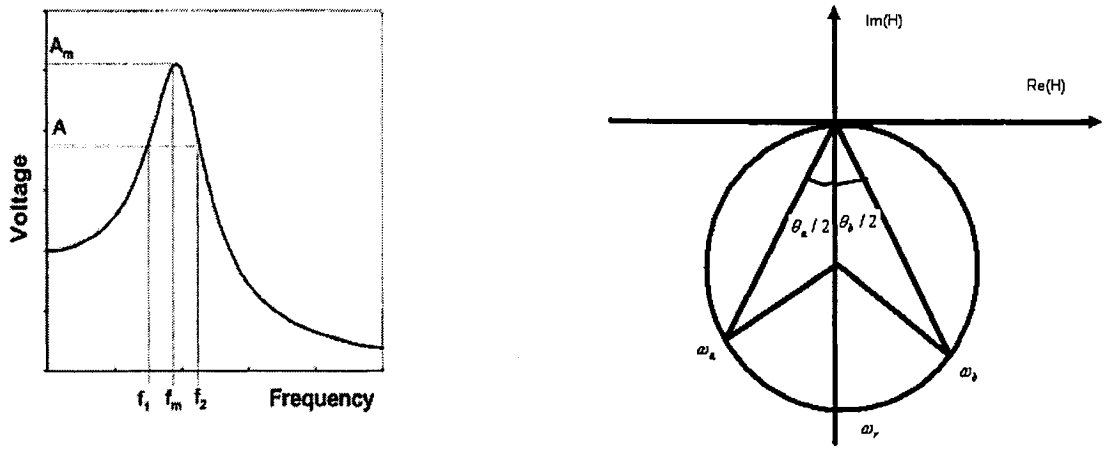

(a) (b)

Figure 5.8. Schematics of the formation of the (a) HPB and (b) CFM methods.

$$\theta_r = \tan^{-1}[\eta_r(1-\frac{\omega}{\omega_r})^{-2}] \tag{5.38}$$

It is evident that calculating the minimum of $d\omega^2/d\gamma_r$ is equivalent to $d\omega^2/d\theta_r$. Thus, with reference to Figure (5.8b), by taking two points, *a* and *b* on the circle, one corresponding to a frequency slightly below the natural frequency (ω_b), and the other corresponding to a frequency slightly above the natural frequency (ω_a), one can express the damping factor η_r by:

$$\eta_r = \frac{\omega_a^2 - \omega_b^2}{\omega_r^2} \frac{1}{\tan(\Delta\theta_a) + \tan(\Delta\theta_b)}, \eta_r = 2\xi_r \tag{5.39}$$

An optimization program was developed for establishing the location of the centre of the circle. Figure (5.9) illustrates the circles plotted based on the vibration data obtained through all piezoelectric sensors.

5.5.6 Finite Element Method for Calculation of Natural Frequency of Structure

To further verify the integrity of the approaches used here, a finite element analysis (FEA) was also conducted to evaluate the first two natural frequencies of the

PVC pipes. NISA finite element software (NISA, 2004) was used for this task. The Solid 8-node element of NISA with 3 DOF per node (translational DOF) was used to model the pipes. NISA's solid 8-node piezoelectric element with 4 DOF per node (3 translational and one electric DOF (ϕ in Equation (5.1)) was also used to model each piezoelectric patch. All displacements at the fixed end of the pipe were restricted in order to simulate the clamping of the pipe. The mesh that was used to model the pipe consisted of 242 elements in the axial direction and 80 in the circumferential direction, with 2 layers of elements through the thickness. Each piezoelectric patch was modeled with 8x4x1 piezo elements (length x width x thickness, respectively).

The Lanczos method was used for extracting the eigen-values of the system with a consistent mass formulation and a frontal solver. The results from the eigen-value and the Fast Fourier analysis are tabulated in Table 5.2.

5.6 Evaluation of the Damping Ratio and Discussion of the Results

As stated earlier, the main objective of this paper was to validate the Hilbert-Huang spectral analysis and formulation for system identification by comparing the results obtained from this method to those of other commonly used methods found in the literature.

Moreover, we also wanted to investigate the influence of location of the sensors on the dynamic response of the pipe. For this, we used the power spectrum method to establish the basic dynamic response of the pipe.

The mechanical material properties of the PVC pipe are tabulated in Table 5.1. The natural frequencies of the pipes were obtained based on the Fast Fourier analysis. The time history was collected using the five piezoelectric sensors. These results were considered as the time domain data for conducting the Fast Fourier analysis.

The natural frequencies of the pipes were calculated, by FEA, and by the EMD method. The FEA results are tabulated in Table 5.2. As can be seen, the experimental results are in good agreement with the FEA results. The first and second vibration mode shapes of the pipe are also illustrated in Figure (5.10a and b).

Moreover, using the LDA method, the natural logarithm of each peak (the absolute value of response obtained through each piezoelectric sensor) was calculated and plotted versus time (see Figure (5.3)). A line was fitted through the resulting data using a least-mean-squares approach. The damping ratio was obtained through the slope of the best-fit line, as illustrated in Figure (5.3). A summary of the results is tabulated in Table 5.3. A similar procedure was also followed for obtaining the damping ratio using the HTA, MBA, HPB, EMD and the circle-fitted methods, with the results also reported in Table 5.3. As it can be seen, all methods are capable of producing acceptable results, however, it is noted that the mixed time-frequency methods (i.e., HTA, EMD and MBA) could produce more consistent results than the other two methods. Therefore, the time-frequency domain approaches summarized above are recommended when evaluating the damping property of such damped materials.

Moreover, it is also noted that the results reported in the last row of Table 5.3 (i.e., the 5^{th} sensor's results) are comparatively inconsistent with the results obtained form the other sensors. The data gathered through the 5^{th} sensor exhibited some dual peaks in some of the first half cycles. This is believed to be due to the interference of loading induced high frequencies at the location of the sensor which was very close to the loading point.

Table 5.2. Natural frequency values obtained from the experimental and finite element analysis.

Bending Mode	Natural Frequency (Hz) (FEA)	Natural Frequency HZ) Experiment (FFT)	Natural Frequency (Hz) Experiment (EMD)
1	19.01	19.07	19.05
2	109.17	112.7	111.3

5.7 Conclusions

Our experimental and analytical investigations considered two important dynamic issues governing the dynamic characteristics of plastic (PVC) pipes. Firstly,

the integrity of five different admissible analytical methods for evaluating the damping ratio of plastic pipes was systematically examined both experimentally (through free vibration tests) as well as computationally (using finite element analysis). Secondly, the influence of the location of the piezoelectric sensors used for sensing the pipes' vibration was also investigated. Thirdly, the results obtained through the time domain analysis were compared to those obtained through the frequency domain methods.

An important aspect of the work presented here is the application of the Empirical Mode Decomposition (EMD) for evaluating the structural damping based on the data obtained from piezoelectric sensors. The advantage of this method was observed to be the fact that the approach requires data from only a single sensor; therefore, it is an effective and efficient approach.

The results clearly showed that the time domain results (i.e., the LDA method) obtained from the data from sensors positioned at various locations along the pipe's length were not consistent. It is believed that the discrepancy is due to the loading system used. It was also observed that some of the first half cycles in the response domain had dual peaks, which is believed to have occurred due to the nature of the applied loading and the adopted clamping mechanism. Nevertheless, results obtained through the frequency domain methods were found to be more consistent.

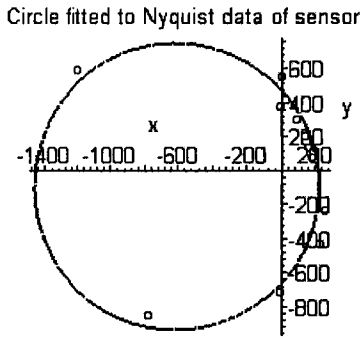

$$\mathrm{Im}(x)^2 + \mathrm{Re}(x)^2 + 1242.04x + 227.19y - 305419.37 = 0 \quad \text{(a)}$$
$$x_c = -621.02, y_c = -113.59, R = 839.04$$

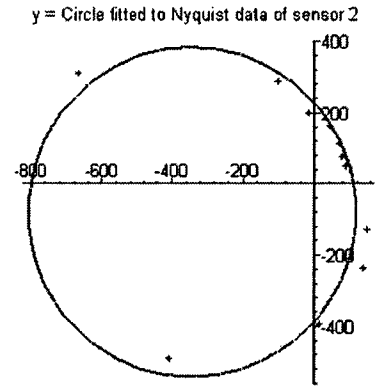

$$\mathrm{Im}(x)^2 + \mathrm{Re}(x)^2 + 692.57x + 158.74y - 89376.27 = 0 \quad \text{(b)}$$
$$x_c = -346.28, y_c = -79.37, R = 464.31$$

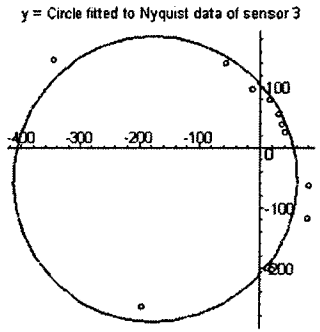

$$\mathrm{Im}(x)^2 + \mathrm{Re}(x)^2 + 353.53x + 105.73y - 22621.28 = 0 \quad \text{(c)}$$
$$x_c = -176.77, y_c = -52.86, R = 238.04$$

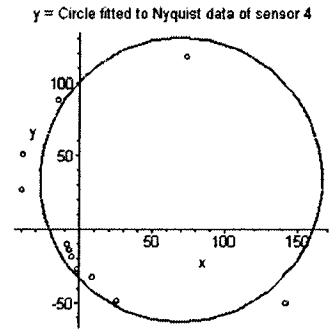

$$\mathrm{Im}(x)^2 + \mathrm{Re}(x)^2 - 139.23x - 67.33y - 3446.05 = 0 \quad \text{(d)}$$
$$x_c = 69.61, y_c = 33.67, R = 97.08$$

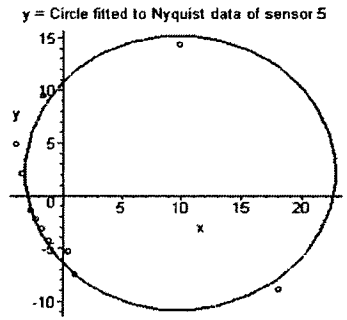

$$\mathrm{Im}(x)^2 + \mathrm{Re}(x)^2 - 19.54x - 4.36y - 70.36 = 0$$
$$x_c = 9.77, y_c = 2.18, R = 13.06$$

(e)

Figure 5.9. The calculated results of the CFM for (a) Sensor #1, (b) Sensor #2, (c) Sensor 3, (d) Sensor #4, (e) Sensor #5.

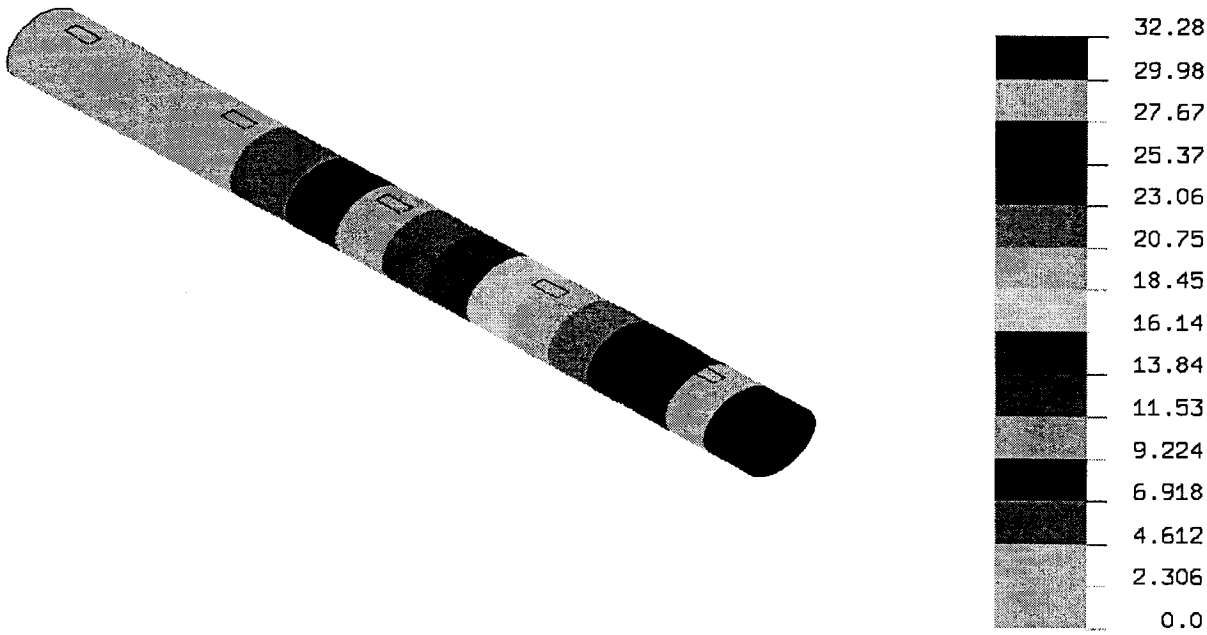

(a)

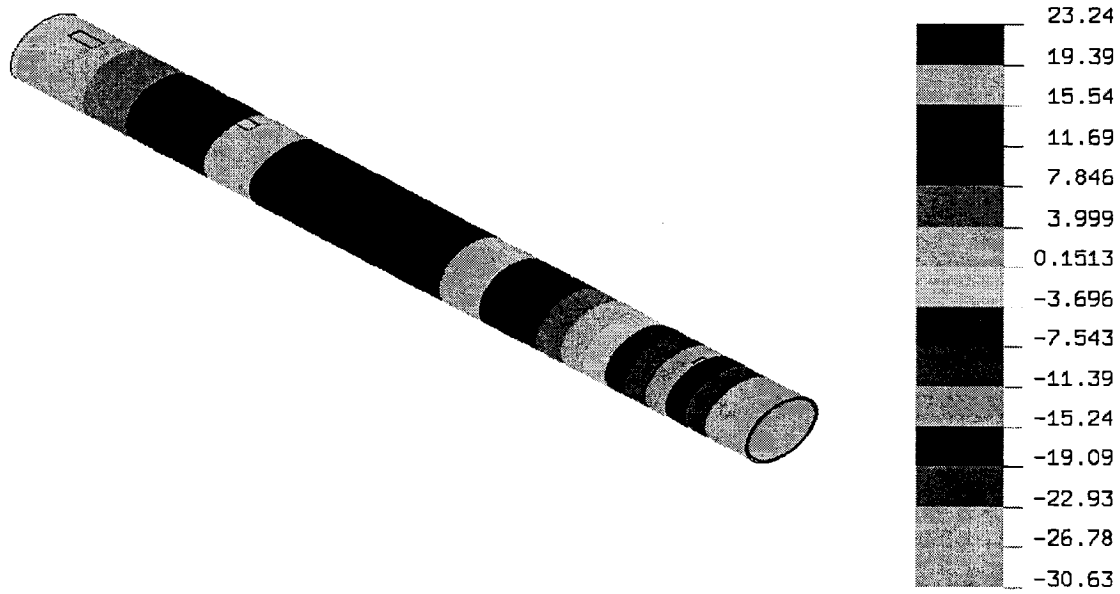

(b)

Figure 5.10.: Pipe's mode shapes determined by FEA (a) First mode, (b) Second Mode.

Therefore, the frequency domain approaches summarized above are recommended when evaluating the damping property of such damped materials.

An important aspect of the work presented here is the application of the Empirical Mode Decomposition (EMD) for evaluating the structural damping based on the data obtained from piezoelectric sensors.

It is noted that although both pure time-domain method (i.e., LDA) and pure frequency-domain method (i.e., HPB) could produce consistent and acceptable results. It appears that the mixed time-frequency methods (i.e., HTA, EMD and MBA) produced more consistent results. Therefore, the time-frequency domain approaches summarized above are recommended when evaluating the damping property of such damped materials.

5.8 REFERENCES

Bracewell, R. (1999) *The Fourier Transform and Its Applications,* 3rd ed. McGraw-Hill, New York:.

Ewins, D.J. (1984) *Modal Testing: theory and Application*, Research Studies Press. New York.

Fahey S. O'F and Pratt J. (1998a) "Frequency Domain Modal Estimation Techniques", Experimental Techniques, 33-37, September/October.

Fahey S. O'F. and Pratt J. (1998b) "Time Domain Modal Estimation Techniques", Experimental Techniques, 45-49, November/December.

Hahn, S.J. (1996) "The Hilbert transform of the product $a(t)\cos(\omega_0 t + \phi_0)$" Bulletin of the Polish Academy of Science, 1996, **44**(1), 75–80.

Hammond, C.E. and Doggett, R.V. (1975) "Determination of Subcritical Damping by Moving-Block/ Random Applications" National Aeronautics and Space administration symposium on Flutter Testing Techniques, NASA **CP-415**, 59-76.

Huang N.E., Shen Z., and Long S.R. (1999) "A new view of nonlinear water waves: the Hilbert spectrum". Annual Review of Fluid Mechanics, **31,** 417– 457.

Huang, K. (1998) "A nondestructive instrument bridge safety inspection system (NIBSIS) using a transient load". US patent No. 09=210.693.

Huang, N.E, Shen, Z., Long, S.R., Wu, M.C., Shih H.H., Zheng Q., Yen N-C, Tung C.C., and Liu H.H. (1998) "The empirical mode decomposition and Hilbert spectrum for nonlinear and non-stationary time series analysis". Proceedings of the Royal Society of London—Series A, **454**, 903–995.

Iglasias, A.M. (2000) *Investigating Various Modal Analysis Extraction Techniques to Estimate Damping Ratio.* Masters thesis, Department of Mechanical Engineering, Virginia Polytechnic Institute and State University, Blacksburg, Virginia.

Imregun M. (1991) "A Comparison of SDOF and Global MDOF Modal Analysis Techniques when applied to a Lightly-Damped Linear Structure", Proceedings of the International Modal Analysis Conference, 435-441.

Karnopp, D.C., Margolis, D.L., and Rosenberg, R.C. (2000) *System Dynamics: Modeling and Simulation Of Mechatronic Systems*, Third Edition, John Wiley & Sons, Inc., Canada.

Lazan, B.J. (1968) *Damping of Materials and Members in Structural Mechanics*, Pergamon Press, Oxford, UK.

Naghipour M., Zou GP. and Taheri F. (2005) "Evaluation of Vibration Damping of GRP reinforced Glulam Composite Beams". ASCE Journal of Engineering Mechanics, in press.

NISA (2004) V.12, Engineering Mechanics Research Corporation, Troy, MI.

Rao, S.S., and Sunar, M. (1994) "Piezoelectricity and its use in disturbance sensoring and control of flexible structures: a survey." Appl. Mech. Rev., **47**, 113-136.

Ra yleigh L. (1945) *Theory of sounds* (two volumes). New York: Dover Publications, re-issue, second edition.

Richart, F.E. Jr., Hall, J.R., and Woods, R.D. (1970) *Vibration of Soils and Foundation.* Prentice-Hall, Inc., Englewood Cliffs, N. J.

Smith, C.B., and Wereley, N.M. (1997). "Composite Rotorcraft flexbeams with Viscoelastic Damping Layers for Aeromechanical Stability Augmentation,"

Mechanics and mechanisms of Material Damping, ASTM STP 1304, Wolfenden, A. and Kinra, V.K., Eds., 62-67.

Tasker, F.A. and Chopra, I. (1990) "Assessment of Transient Analysis Techniques for Rotor Stability Testing" Journal of the American Helicopter Society, **35** (1), 39-50.

Tzou, H.S. and Tseng, C.I. (1990) "Distributed piezoelectric sensor/acyuatoractuator design for dynamic measurement/control of distributed parameter systems: A piezoelectric finite element approach." Journal of Sound and Vibration, 1990, **138**(1), 17-34.

Xu Y.L., and Chen J. (2004) "Structural Damage Detection Using Empirical Mode Decomposition: Experimental Investigation", Journal of engineering mechanics, **130**, 1279-1288.

Yang J.N., Lei Y., Pan S., and Huang N. (2003) "System identification of linear structures based on Hilbert-Huang spectral analysis. Part 1: normal modes", Earthquake engineering and structural dynamics, **32**, 1443-1467.

Chapter 6

APPLICATION OF THE EMPIRICAL MODE DECOMPOSITION FOR SYSTEM IDENTIFICATION AND STRUCTURAL HEALTH MONITORING

N. Cheraghi, and F. Taheri*

Publication Status: Accepted to Publish at International Journal of Applied Mathematics and Engineering Sciences, May 2006

6.1 Abstract

When measured vibration data of a structural response contains damage related data, it is crucial to extract as much damage related information as possible. This paper presents an analytical and numerical investigation into the applicability of the empirical mode decomposition (EMD) for structural damage detection caused by a sudden change of structural stiffness, in conjunction with a novel idea based on energy of *intrinsic mode functions (IMFs)*. A 6-DOF mechanical system was modeled and analyzed subject to an impact load by exact solution, using MATLAB software, as well as with the finite element method, using the ANSYS program. The presence of damage was simulated by reducing the stiffness of the springs of the idealized spring-mass system. Dynamic responses including displacements and accelerations were calculated. With this method, the measured response data was first decomposed into modal response using the empirical mode decomposition (EMD) approach employing the band-pass intermittency criterion. Then, the Hilbert transform was applied to each modal response to obtain the instantaneous amplitude and phase angle time history. A linear least-square fit procedure was used to identify the system's natural frequency and damping ratio from the instantaneous amplitude

* Corresponding author, 1360 Barrington Street, Halifax, Nova Scotia, B3J 1Z1
Tel: (902) 494-3935 Fax: (484-6635) email: farid.Taheri@dal.ca

and phase angle for each modal response. Then the structural mode shapes, and subsequently the stiffness and damping matrices, were identified. It will be shown that the proposed damage index could effectively detect the presence of the damage. Moreover, the location of damage was also determined by comparing the stiffness matrix of the system before and after damage.

6.2 INTRODUCTION

Vibration-based structural damage detection methods have attracted considerable attention in recent years for health monitoring of large civil structures (Xu et al., 2004). Most of the currently used vibration-based structural damage detection methods are formulated based on the idea that the measured modal parameters, or the properties derived from these modal parameters, are functions of the physical properties of the structure. As a result, changes in the physical properties will cause noticeable and detectable changes in the modal parameters (Dowbling et al. 1998). Although these methods have demonstrated a certain degree of success in damage detection of small structures, there are several confounding factors that make the applicability and effectiveness of these methods for health monitoring of larger structures rather questionable. One issue of primary concern is that these methods presume access to a set of data extracted from the structure at its undamaged (healthy) state; however, such information is not usually readily available in the case of most existing civil structures. Another factor is that most of these methods operate based on the data recorded before and after the occurrence of the damage. Moreover, often a linear structural behavior is assumed for the structure during the data collection. On the contrary, the identified modal parameters (the damage indices) in fact represent the average characteristics of the structure over the duration of the data collection, thus they may not be accurately sensitive to damage, since damage is typically a local phenomenon. Consequently, if a damage event suddenly occurs during the measurement period, the time of the occurrence of the damage cannot be determined by these methods.

In contrast to a large number of publications pertaining to damage indices using the average modal characteristics, there is a paucity of research works addressing instantaneous damage indices. It is believed that the application of time–frequency data processing would be necessary to detect a damage event, including characterization of the event time. The logical candidates for such a task would be the wavelet method, and the recently emerged signal processing technique, as well as the empirical mode decomposition (EMD), introduced by Huang et al. (1998, 1999).

In 2002, Sun and Chang (2002) proposed a wavelet packet transform-based method for damage assessment. The transient signals measured from a structure were first decomposed into wavelet packet components in the time domain. The component energies were then calculated and used as inputs into neural network models developed for damage assessment purposes. Hou et al. (1999, 2000) also proposed a wavelet-based approach to identify the time of damage and its location in a simple structural model with breakage springs. The basic concept of their approach is that the sudden breakage of a structural element would cause discontinuity in the response signals measured in the vicinity of the damage location. By decomposing the vibration signals in the time-domain using the wavelet analysis, the discontinuity would form a specific signal feature (termed the "damage spike") among the wavelet details. The damage time instant could then be identified in terms of the occurrence time of the spike, and the damage location could be determined by the spatial distribution of the observed spikes. The same idea was adopted by Vincent et al. (1999) and Yang et al. (2001), however EMD was used to decompose the vibration signal to capture the signal discontinuity. Numerical simulations carried out in their studies showed that the EMD approach could also identify the instant at which the damage occurred, and of course its location by using a signal feature of the damage spike. Yang at al. (2003, 2004) further used EMD for system identification of a four degree of freedom (DOF) mechanical system and identified the natural frequencies and damping of a tall building. Xu et al. (2004) also used EMD for damage detection of a three-story shear walled building based on experimental (acceleration) data. He concluded that damage location could be identified by the spatial distribution of the spikes around the building. Compared with the wavelet-based approach for which a

proper mother wavelet, as well as a decomposition level should be decided before decomposition, the EMD approach provides a more attractive possibility, because it decomposes the signal based on the time scale of the signal itself with an adaptive mean. Nevertheless, the aforementioned studies using either the wavelet analysis or the EMD approach are based on numerical simulations. Several important assumptions made through such analyses will require further investigation and verification. It is therefore desirable to verify the integrity of these approaches by laboratory-scale experimental investigations before their application in large structures could be fully justified.

6.3 Background to the Hilbert-Huang Transform (HHT)

One of the most widely used dynamic data processing tools is the Fourier Transform (FT) and its digital analogue, the Fast Fourier Transform (FFT). The FT (developed decades ago) and its fairly recently developed counter-part, the FFT carry strong *a-priori* assumptions about the source of data, such as linearity and stationary properties. Natural phenomena responses are essentially nonlinear and non-stationary. The accommodation of this fact in FFT-based analysis often involves using more data samples to assure acceptable convergence and non-algorithmic procedural steps in the interpretation of FFT results. Therefore they cannot be considered as the most optimum methods for studying non-linear waves and other nonlinear phenomena. Wavelet-based analysis yields some improvement over the FFT, because it can handle non-stationary data, but the limitation of a linear data set remains constant. Wavelet methods may also prove inadequate because although being well suited for analyzing data with gradual frequency changes, its non-locally adaptive nature causes leakage. This leakage can spread frequency energy over a wider range, removing the details of data and thus giving it an overly smooth appearance.

To overcome these shortfalls, the Empirical Mode Decomposition method was recently proposed (Huang et al. (1998, 1999)). This method is based on the use of the Hilbert-Huang Transform (HHT), and provides a novel approach to the solution of the nonlinear class of problems. The initial application of the method was used to

analyze hydrospheric processes. The HHT allowed direct algorithmic analysis of nonlinear and non-stationary data functions by using an engineering and *a posteriori* data processing method, namely an Empirical Mode Decomposition method (EMD). EMD can decompose any complicated transient data into a finite (often smaller) number of *intrinsic mode functions (IMFs),* which in turn could admit well-behaved Hilbert transforms. With the Hilbert transform, the IMFs yield instantaneous frequencies as functions of time. The final presentation of the results is a time-frequency-energy distribution, designated as the Hilbert spectrum. Being different from the Fourier and wavelet decompositions, EMD has no specified "basis"; it is an adaptive procedure applied to the signal itself, offering high decomposition efficiency, sharp frequencies, and time localization.

A key feature of the signal analysis based on HHT is its physical attributes, which has made the method popular to a wide range of researchers and experts in signal processing and other related fields. Several works based on the framework of HHT theory have been reported in the recent years (Deng et al., (2001), and Flandrin et al., (2004)). Its application for signal analysis have spread into earthquake research (Loh et al. (2001), ocean science (Huang, 1999, biomedicine (Huang et al., 1998, 1999), Zhihua et al., (2004), and Phillips (2003)), speech signal analysis (Yang et al., 2004), and image analysis and processing (Han et al. 2003.

Nunes et al. (2003) further extended the EMD method from one-dimension to developing a decomposition algorithm for two-dimensional data, referred to as "Bidimensional Empirical Mode Deposition" (BEMD). The algorithm was used to extract texture features at multiple scales or spatial frequencies (Nunes, 2003) and for other applications. For an approximately periodic signal containing rich high frequency components, the relation between its period and its main frequencies is found by analyzing the influence of the signal's non-linearity on the distribution of the main frequency. It is used to estimate the period according to the main frequency distribution (MFD) of a signal.

6.3.1 Mathematical Description of the HHT

The HHT method consists of two parts: (1) the *Empirical Mode Decomposition (EMD)*, and (2) the *Hilbert Spectral Analysis*. As stated earlier, with EMD, one can decompose any complicated data set into a finite and often less *intrinsic mode functions (IMFs)*. An IMF is defined as a function satisfying the following conditions:

(a) The number of extrema and the number of zero-crossings must either equal or differ by at most one in the signal function being considered;

(b) At any point, the mean value of the envelope defined by the local maxima and the envelope defined by the local minima should be zero.

The resulting IMF then would admit a well-behaved Hilbert transform. In this way, EMD decomposes signals adaptively and is applicable to nonlinear and non-stationary data (the fundamental theory on nonlinear time series can be found in Huang et al., (1998). In this section, only a brief introduction is given to make this paper somewhat self-contained. The readers are referred to Huang et al. (1998) for details.

The Hilbert transform, $Y(t)$, of an arbitrary function, $X(t)$, in Lp-class (Titchmarsh et al.,1948), is defined by:

$$Y(t) = \frac{1}{\pi} P \int_{-\infty}^{\infty} \frac{X(t')}{t - t'} dt' \tag{6.1}$$

where P indicates the Cauchy principal value. Consequently an analytic signal, $Z(t)$, can be produced by:

$$Z(t) = X(t) + iY(t) = a(t)e^{i\theta(t)} \tag{6.2}$$

where

$$a(t) = [X^2(t) + Y^2(t)]^{\frac{1}{2}}, \qquad \theta(t) = \arctan(\frac{Y(t)}{X(t)}) \tag{6.3}$$

are the instantaneous amplitude and phase angle of $X(t)$.

Since Hilbert transform $Y(t)$ is defined as the convolution of $X(t)$ and $1/t$ by Equation(6.1), it emphasizes the local properties of $X(t)$, even though the transform is global. In Equation (6.2), the polar coordinate expression further clarifies the local

nature of this representation. With Equation (6.2), the instantaneous frequency of $X(t)$ can be defined by:

$$\omega(t) = \frac{d\theta(t)}{dt} \tag{6.4}$$

However, there is still considerable controversy on this definition. A detailed discussion and justification of the above definition can be found in Huang et al., (1998).

EMD is a necessary pre-processing of the data before the Hilbert transform can be applied. It reduces the data into a collection of *IMF*s and each *IMF*, which represents a simple oscillatory mode, is a counterpart to a simple harmonic function, yet is more general.

Moreover, by the application of EMD, any signal $X(t)$ can be decomposed into a series of finite IMFs, or $\text{imf}_j(t)$ ($j = 1; \ldots; n$), and a residue, $r(t)$, where n is a nonnegative integer depending on $X(t)$; that is,

$$X(t) = \sum_{j=1}^{n} imf_j(t) + r(t) \tag{6.5}$$

Let $Xj(t) = \text{imf}_j(t)$, whose corresponding instantaneous amplitude, $a_j(t)$, and frequency, $\omega_j(t)$, can be computed by Equations (6.3) and (6.4). Through Equations (6.2) and (6.4), the $\text{imf}_j(t)$ can be expressed as the real part (RP), in the following form:

$$imf_j(t) = RP[a_j(t)\exp(i\int\omega_j(t)dt] \tag{6.6}$$

Therefore, using Equations (6.5) and (6.6), $X(t)$ can be expressed as the IMF expansion as follows:

$$X(t) = RP\sum_{j=1}^{n} a_j(t)\exp(i\int\omega_j(t)dt) + r(t) \tag{6.7}$$

which generalizes the following Fourier expansion by admitting variable amplitudes and frequencies

$$X(t) = \sum_{j=1}^{\infty} a_j e^{i\omega_j t} \tag{6.8}$$

Consequently, the main advantage of EMD over FFT is that it could effectively accommodate nonlinear and non-stationary data. Equation (6.7) thus enables one to represent the amplitude and the instantaneous frequency as a function of time in a three-dimensional plot, in which the amplitude is contoured on the time-frequency plane. The time-frequency distribution of amplitude is designated as the Hilbert amplitude spectrum or simply the Hilbert spectrum, denoted by $H(\omega,t)$. Having obtained the Hilbert spectrum, the marginal spectrum can be easily determined by:

$$h(\omega) = \int_0^T H(\omega,t)dt \tag{6.9}$$

This marginal spectrum offers a measure of the total amplitude (or energy) contribution from each frequency value.

6.4 Modal Response of n-DOF Structures Due to Impulse Loading

The equation of motion of an n-DOF structure can be expressed as

$$M\ddot{X}(t) + C\dot{X}(t) + KX(t) = F(t) \tag{6.10}$$

in which $X(t) = [x_1, x_2, ..., x_n]$ is the displacement vector, $F(t)$ is the excitation vector and M, C, and K are the mass, damping, and stiffness matrices, respectively. With the assumption of the existence of normal modes, the displacement and acceleration responses can be decomposed into n real modes

$$X(t) = \sum_{j=1}^{n} \phi_j Y_j(t); \quad \ddot{X}(t) = \sum_{j=1}^{n} \phi_j \ddot{Y}(t) \tag{6.11}$$

In the above equation, it is apparent that the $n \times n$ mode-shape matrix ϕ serves to transform the generalized coordinate vector Y to the geometric coordinate vector X. The generalized components in vector Y are called the normal coordinates of the structures.

Substituting Equation (6.11) into Equation (6.10) and using the orthogonal properties of the mode shapes, one can decouple Equation (10) into n modes

$$\ddot{Y}_j + 2\xi_j \omega_j \dot{Y} + \omega_j^2 Y = \phi_j^T F(t)/m_j \tag{6.12}$$

in which ω_j is the j[th] modal frequency, ξ_j is the j[th] modal damping ratio, and m_j is the j[th] modal mass. Consider an impact loading applied to the p[th] DOF of the system, i.e. $f_p(t) = F_0\delta(t)$ and $f_j(t) = 0$ for all $j \neq p$, where $f_j(t)$ is the jth element of $F(t)$. Then, the acceleration response of the jth generalized modal co-ordinate is given by:

$$\ddot{Y}_j(t) = \frac{F_0\phi_{pj}\omega_j}{m_j\sqrt{1-\xi_j^2}} e^{-\xi_j\omega_j t}\cos(\omega_{dj}t + \varphi_j + \frac{\pi}{2}) \tag{6.13}$$

in which ϕ_{pj} is the pth element of the jth modal vector ϕ_j, $\omega_{dj} = \omega_j(1-\xi_j^2)^{0.5}$ is the jth damped modal frequency, and $\varphi_j = \tan^{-1}(2\xi_j\sqrt{1-\xi_j^2}/(1-2\xi_j^2))$ is the phase lag of the jth mode. The impulse acceleration response $\ddot{x}_k(t)$ of the structure at k (k=1,. . . ,n) DOF is given by:

$$\ddot{x}_k(t) = \sum_{j=1}^{n}\phi_{kj}\ddot{Y}_j(t) = \sum_{j=1}^{n}\ddot{x}_{kj}(t) \tag{6.14}$$

where

$$\ddot{x}_{kj}(t) = \phi_{kj}\ddot{Y}_j(t) = B_{kj,p}e^{-\xi_j\omega_j t}\cos(\omega_{dj}t + \varphi_j + \frac{\pi}{2} + \varphi_{kj,p}) \tag{6.15}$$

$$B_{kj,p} = \frac{F_0|\phi_{kj}||\phi_{pj}|\omega_j}{m_j\sqrt{1-\xi_j^2}} \tag{6.16}$$

$$x_{kj}(t) = B_{kj,p}\frac{e^{-\xi_j\omega_j t}}{(\xi_j^2\omega_j^2 + \omega_{dj}^2)^2} * \left[\begin{array}{l} \xi_j^2\omega_j^2\sin(\omega_{dj}t + \varphi_j + \frac{\pi}{2} + \varphi_{kj,p}) + \\ 2\xi_j\omega_j\omega_{dj}\cos(\omega_{dj}t + \varphi_j + \frac{\pi}{2} + \varphi_{kj,p}) - \varpi_{dj}^2\sin(\omega_{dj}t + \varphi_j + \frac{\pi}{2} + \varphi \end{array}\right. \tag{6.17a}$$

$$x_{kj}(t) = B_{kj,p}\frac{e^{-\xi_j\omega_j t}}{(\xi_j^2\omega_j^2 + \omega_{dj}^2)^2} * \left[\sqrt{(\xi_j^2\omega_j^2 - \omega_{dj}^2)^2 + 4\xi_j^2\omega_j^2\omega_{dj}^2}\cos(\omega_{dj}t + \varphi_j + \frac{\pi}{2} + \varphi_{kj,p} - \theta)\right] \tag{6.17b}$$

where

$$\theta = tg^{-1}(\frac{\xi_j^2\omega_j^2 - \omega_{dj}^2}{2\xi_j\omega_j\omega_{dj}}) \tag{6.18}$$

In Equations (6.15) to (6.18), $\varphi_{kj,p}$ is the phase difference between the kth element and the pth element in the jth mode shape. With the existence of normal modes, all the mode shapes are real and hence $\varphi_{kj,p}$ is either $\pm 2m\pi$ or $\pm(2m+1)\pi$ where m is an integer, i.e.

$\varphi_{kj} / \varphi_{pj} \succ 0$ when $\varphi_{kj,p} = \pm 2m\pi$

$\varphi_{kj} / \varphi_{pj} \prec 0$ when $\varphi_{kj,p} = \pm(2m+1)\pi$

The Hilbert transform $x_{kj}(t)$ in Equation (6.9) can be obtained using Bedrosian's theorem (Hahn, 1996)

$$\tilde{x}_{kj}(t) = \frac{F_0 |\phi_{kj}| |\phi_{pj}| \omega_j}{m_j \sqrt{1-\xi_j^2}} \frac{\left(\sqrt{(\xi_j^2 \omega_j^2 + \omega_{dj}^2)^2 + 4\xi_j^2 \omega_j^2 \omega_{dj}^2}\right)}{\left(\xi_j^2 \omega_j^2 + \omega_{dj}^2\right)^2} * \left[a_{LK,j} \sin(\omega_{dj} t + \varphi_j + \frac{\pi}{2} + \varphi_{kj,p} - \theta) + \tilde{a}_{HK,j} \cos(\omega_{dj} t + \varphi_j + \frac{\pi}{2} + \varphi_{kj,p} - \theta) \right] \tag{6.19}$$

where

$$a_{LK,j} = \frac{1}{\pi} \int_0^{\omega_{dj}} \frac{2\xi_j \omega_j}{\xi_j^2 \omega_j^2 + \omega^2} \cos(\omega t) d\omega \tag{6.20}$$

$$\tilde{a}_{HK,j} = \frac{1}{\pi} \int_{\omega_{dj}}^{\infty} \frac{2\xi_j \omega_j}{\xi_j^2 \omega_j^2 + \omega^2} \sin(\omega t) d\omega \tag{6.21}$$

The analytical signal $Z_{kj}(t)$ of the jth mode is given by:

$$Z_{kj}(t) = x_{kj}(t) + i\tilde{x}_{kj}(t) = A_{kj}(t) e^{i\beta_{kj}(t)} \tag{6.22}$$

In which the instantaneous amplitude $A_{kj}(t)$ and instantaneous phase angle $\beta_{kj}(t)$ are:

$$A_{kj}(t) = B_{kj,p} \frac{\sqrt{(\xi_j^2 \omega_j^2 + \omega_{dj}^2)^2 + 4\xi_j^2 \omega_j^2 \omega_{dj}^2}}{(\xi_j^2 \omega_j^2 + \omega_{dj}^2)^2} \left\{ \begin{array}{l} e^{-2\xi_j \omega_j t} \cos^2(\omega_{dj} t + \varphi_j + \frac{\pi}{2} + \varphi_{kj,p} - \theta) + \\ \left[a_{LK,j}(t) \sin(\omega_{dj} t + \varphi_j + \frac{\pi}{2} + \varphi_{kj,p} - \theta) + \right. \\ \left. \tilde{a}_{HK,j(t)} \cos(\omega_{dj} t + \varphi_j + \frac{\pi}{2} + \varphi_{kj,p} - \theta) \right]^2 \end{array} \right\}^{1/2} \tag{6.23}$$

$$\beta_{kj}(t) = \tan^{-1}\left\{e^{\xi_j \omega_j t}\left[a_{LK,j}(t)\tan(\omega_{dj}t + \varphi_j + \frac{\pi}{2} + \varphi_{kj,p} - \theta) + \tilde{a}_{HK,j}(t)\right]\right\}$$

(6.24)

For a special case in which ξ_j is very small and ω_j is large, one obtains from Equations (6.20, 6.21)

$$a_{LK,j} \approx \frac{1}{\pi}\int_0^{\infty} \frac{2\xi_j \omega_j}{\xi_j^{\,2}\omega_j^{\,2} + \omega^2}\cos(\omega t)d\omega = e^{-\xi_j \omega_j t} \tag{6.25}$$

$$\tilde{a}_{HK,j} = \frac{1}{\pi}\int_{\omega_{dj}}^{\infty} \frac{2\xi_j \omega_j}{\xi_j^{\,2}\omega_j^{\,2} + \omega^2}\sin(\omega t)d\omega \approx 0 \tag{6.26}$$

Thus, Equation (6.19) becomes:

$$\tilde{x}_{kj}(t) = \frac{F_0|\phi_{kj}\|\phi_{pj}|\omega_j}{m_j\sqrt{1-\xi_j^{\,2}}} \frac{e^{-\xi_j\omega_j t}\left(\sqrt{(\xi_j^{\,2}\omega_j^{\,2} + \omega_{dj}^{\,2})^2 + 4\xi_j^{\,2}\omega_j^{\,2}\omega_{dj}^{\,2}}\right)}{\left(\xi_j^{\,2}\omega_j^{\,2} + \omega_{dj}^{\,2}\right)^2} * \sin(\omega_{dj}t + \varphi_j + \frac{\pi}{2} + \varphi_{kj,p} - \theta)$$

(6.27)

and the amplitude $A_{kj}(t)$ and phase angle $\beta_{kj}(t)$ in Equation (6.22) are given by:

$$A_{kj}(t) = \frac{F_0|\phi_{kj}\|\phi_{pj}|\omega_j}{m_j\sqrt{1-\xi_j^{\,2}}} \frac{e^{-\xi_j\omega_j t}\left(\sqrt{(\xi_j^{\,2}\omega_j^{\,2} + \omega_{dj}^{\,2})^2 + 4\xi_j^{\,2}\omega_j^{\,2}\omega_{dj}^{\,2}}\right)}{\left(\xi_j^{\,2}\omega_j^{\,2} + \omega_{dj}^{\,2}\right)^2} \tag{6.28}$$

$$\beta_{kj}(t) = \omega_{dj}t + \varphi_j + \frac{\pi}{2} + \varphi_{kj,p} - \theta \tag{6.29}$$

From Equations (6.28) and (6.29), one can obtain

$$\ln A_{kj}(t) = -\xi_j\omega_j t + \ln\left(\frac{F_0|\phi_{kj}\|\phi_{pj}|\omega_j}{m_j\sqrt{1-\xi_j^{\,2}}} \frac{\left(\sqrt{(\xi_j^{\,2}\omega_j^{\,2} + \omega_{dj}^{\,2})^2 + 4\xi_j^{\,2}\omega_j^{\,2}\omega_{dj}^{\,2}}\right)}{\left(\xi_j^{\,2}\omega_j^{\,2} + \omega_{dj}^{\,2}\right)^2}\right)$$

(6.30)

$$\omega_j(t) = d\beta_{kj}(t)/dt = \omega_{dj} \tag{6.31}$$

As seen with the measured impulse response vector, the EMD method can be used to decompose each measurement into n modal responses. Then, each modal

response can be processed through the Hilbert transform to determine the instantaneous amplitude and phase angle. Finally, the system identification can be completed, including natural frequencies, damping ratios, mode shapes, mass matrix, damping matrix, and stiffness matrix, as follows.

6.5 Modal Response Using Empirical Mode Decomposition Baesd on Band Pass Filtering

There is a disadvantage in the way the modal response gets isolated in the EMD method. This is because the frequency content of the signal at each time instant (t) is preserved. Moreover, the numerical computation based on this approach may be quite involved, particularly when: (i) the modal frequencies are high, and (ii) the signal is polluted by a high noise level. In such cases the only means of obtaining accurate modal response is by applying a large number of siftings in the EMD. To simplify the computational efforts, therefore, an alternative approach based on the band-pass filter and EMD has been proposed; the procedure for which is as follows:

- Determine the approximate frequency range for each natural frequency, i.e. $\omega_{jL} \prec \omega_j \prec \omega_{jH}$ (j=1, 2, . . . ,n), from the Fourier spectrum of the acceleration response $\ddot{X}_k(t)$.

- Process the signal $\ddot{X}_k(t)$ through the band-pass filters each with a frequency band $\omega_{jL} \prec \omega_j \prec \omega_{jH}$. The time history obtained from the jth band-pass filter is then processed through EMD, and the resulting first IMF would be quite close to the j^{th} modal response.

- Repeat the same procedures for j=1, 2... n, to obtain the n modal responses.

This approach enables one to extract the modal response $\ddot{X}_{pj}(t)$ easily and removes all the noises outside the frequency range, $\omega_{jL} \prec \omega_j \prec \omega_{jH}$. It is important to note that the phase shift of the band-pass filter used should be as small as possible. To ensure this criterion is fulfilled, it would be sometimes necessary to pass the signal through the band-pass filter, two or three times. The approaches presented above for

obtaining the modal responses will be demonstrated later through numerical simulations.

6.5.1 Identification of natural frequencies and damping ratios

It should be noted that for the identification of natural frequencies ω_j and damping ratios ξ_j for j=1, 2 ..., n, only one measurement (i.e. from one sensor), say $\ddot{X}_p(t)$, would be sufficient, so long as that signal contains all the information ω_j and ξ_j (j=1, 2, e measured response is ..., n) of the system (this issue will be clarified later). The procedure is as follows:

o For a small ξ_j , it follows from Equation (6.13) that the damped natural frequency ω_{dj} can be obtained from the slope of the plot of the phase angle $\theta_{pj}(t)$ versus time, whereas $-\xi_j\omega_j$ (hence, damping ratio) can be estimated from the slope of the decaying amplitude of the '$\ln A_{pj}(t)$ versus time' plot (see Equation (6.26)). For the general case in which ξ_j is not too small, $A_{pj}(t)$ and $\theta_{pj}(t)$ are given by Equation (6.22). In this case, both $\theta_{pj}(t)$ and $\ln A_{pj}(t)$ are not linear functions of time, t. Theoretically, ξ_j and ω_{dj} can be determined from the non-linear equation represented by Equation (6.22). However, it is observed from the numerical results of Equation (6.22) that the amplitude variation $A_{pj}(t)$ introduces an instantaneous frequency modulation. This frequency modulation is referred to as the "intra-wave modulation" by Huang et al. 1998. It was shown that the amplitude variation could cause a frequency fluctuation around the mean value of a carrier frequency, but not a change of its mean value (Huang et al., 1998). Consequently, a linear least-square fit procedure is used to estimate the mean values of the natural frequencies and damping ratios for the general case.

6.5.2 Identification of mode shapes, and mass, damping, and stiffness matrices

As stated previously, only one measurement, at one location of the impulse response function $X_k(t)$ is needed to determine all the natural frequencies and damping ratios of a given system. However, to identify mode shapes and mass, damping, and stiffness matrices, the response time histories at all DOF should be measured. It follows from Equations (6.16) and (6.26) that the ratio of the absolute value of the modal elements ϕ_{mj} to ϕ_{nj} (m, n=1, 2...) can be determined by:

$$\left|\phi_{mj}\right| / \left|\phi_{nj}\right| = \exp(A'_{mj}(t_0) - A'_{nj}(t_0)) \tag{6.32}$$

in which $A'_{mj}(t_0)$ and $A'_{nj}(t_0)$ are the magnitude of the fitted line for the decaying amplitude $\ln A_{mj}(t)$ and $\ln A_{nj}(t)$, at the arbitrary time $t = t_0$, respectively. Moreover, the difference between the phase angle of the modal element ϕ_{mj} and that of ϕ_{nj} follows from Equation (6.25) as:

$$\phi_{mj,n} = \theta'_{mj}(t_0) - \theta'_{nj}(t_0) \tag{6.33}$$

in which $\theta'_{mj}(t_0)$ and $\theta'_{nj}(t_0)$ are the magnitudes of the fitted line for the phase angle $\theta_{mj}(t)$ and $\theta_{nj}(t)$ at the arbitrary time $t = t_0$.

Another method which one can use for mode shape identification is based on the modal response. In fact, mode shape specification can be identified by comparing the first IMF of every degree of freedom of the structure in the time domain data. The phase angle and amplitude of the mode shape can be calculated through dividing the amplitude response of the first IMF of one degree freedom, at a specific time, to those of another degree of freedom taken at the same time. If the quantities have the same sign (positive or negative), it would indicate that there is no phase angle.

After identifying the modal frequency ω_j, the damping ratios ξ_j, and mode shapes vector ϕ_j for $j = 1,2,....$, the mass, damping, and stiffness matrices of the structure can be determined using the following procedure.

♦ The generalized modal mass can be evaluated by substituting Equation (6.25) at $t = t_0$ into Equation (6.27), that is:

$$m_j = \frac{F_0 |\phi_{kj}| |\phi_{pj}| \omega_j}{A_{kj}(0)\sqrt{1-\xi_j^2}} \frac{\left(\sqrt{(\xi_j^2\omega_j^2 + \omega_{dj}^2)^2 + 4\xi_j^2\omega_j^2\omega_{dj}^2}\right)}{\left(\xi_j^2\omega_j^2 + \omega_{dj}^2\right)^2} \tag{6.34}$$

in which F_0 is the level of the measured impact loading. The generalized modal stiffness, k_j, and modal damping. c_j, are obtained from the following relations:

$$k_j = m_j\omega_j^2;\ c_j = 2\xi_j m_j \omega_j \tag{6.35}$$

Noting the following orthogonal properties:

$$\Phi^T M \Phi = diag[m_j];\ \ \Phi^T K \Phi = diag[k_j];\ \ \Phi^T C \Phi = diag[c_j] \tag{6.36}$$

in which Φ is the $n \times n$ modal matrix with the jth modal vector ϕ_j as the jth column. Hence, the mass, stiffness, and damping matrices can be represented as follows:

$$M = \Phi^{-T} diag[m_j]\Phi^{-1};\ K = \Phi^{-T} diag[k_j]\Phi^{-1}\ ; C = \Phi^{-T} diag[c_j]\Phi^{-1} \tag{6.37}$$

6.6 Case Study # 1: a Healthy (Undamaged) Structure

To investigate the effectiveness and integrity of the application of the proposed system identification for damage detection methodology in a structural system, the integrity of the Hilbert-Huang approach is investigated by applying it onto a 6-DOF mechanical system. Later, the same system will be investigated bearing a damage.

Consider the 6-DOF mechanical system, as shown in Figure (6.1), with the following properties:

$$m_1 = m_2 = m_3 = m_4 = m_5 = m_6 = 1kg$$
$$k_1 = k_2 = k_3 = k_4 = k_5 = k_6 = k_7 = 7500N/m,$$
$$c_1 = c_2 = c_3 = c_4 = c_5 = c_6 = c_7 = .75Ns/m$$

The Hilbert-Huang spectral approach, with its procedure outlined as above, will be applied to the system. In this problem, the displacement impulse responses of all

masses in response to an impact load applied to the third mass are measured. ANSYS finite element software was used to model the system, and modal and transient dynamic analyses were conducted. The results of the finite element analyses were compared to those reached through the exact solution, which were obtained using MATLAB software. The measured displacement $X_3(t)$, is shown in Figure (6.2a). The Fourier transforms of

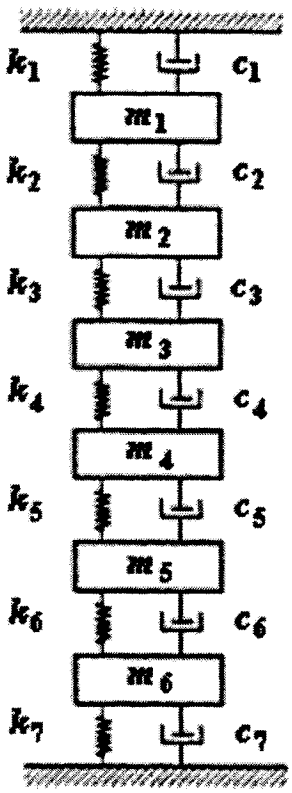

Figure 6.1. Schematic of the 6-DOF mechanical system.

the displacement responses of all degrees of freedom of the system ($X_1(t)$ through $X_6(t)$) are shown in Figure (6.2b). The modal frequency ranges are summarized in below:

(1) $5.38Hz = \omega_{1L} \prec \omega_1 \prec \omega_{1H} = 6.88Hz$ for the first mode

(2) $11.21 = \omega_{2L} \prec \omega_2 \prec \omega_{2H} = 12.71$ for the second mode

(3) $16.44 = \omega_{3L} \prec \omega_3 \prec \omega_{3H} = 17.94$ for the third mode

(4) $20.8 = \omega_{4L} \prec \omega_4 \prec \omega_{4H} = 22.3$ for the fourth mode

(5) $24.08 = \omega_{5L} \prec \omega_5 \prec \omega_{5H} = 25.58$ for the fifth mode

(6) $26.12 = \omega_{6L} \prec \omega_6 \prec \omega_{6H} = 27.62$ for the sixth mode

Subsequently, the band-pass method was used to carry out the EMD calculations and to extract the IMFs. The procedure is as follows:

- The signal for each DOF ($X(t)$, shown in Figure 6.2a was passed through a fourth-order band-pass filter, each within the frequency band noted above. The resulting six time histories from each DOF are denoted by $X_{mj}(j = 1,2,3,4,5,6)$ for each corresponding mass number.

- Then, all of the resulting X_{mj} were processed through EMD and the first IMF is used to identify the modal response of X_{mj}. As an illustration, the signature of the 4th DOF (mass) and its IMF is illustrated in Figure (6.3). It is important to note that the band-pass filter used for the operation should have the smallest possible phase shift to produce the best results. It should be noted that due to the phase shift, a segment of the modal response near t=0 is not a decaying function. Such a segment should be discarded prior to the application of the Hilber transform.

- After removing this segment, the modal responses illustrated in Figure (6.4) are processed through the Hilbert transform and the instantaneous phase angles $\theta_{mj}(t)$ and $a_{mj}(t)$ are obtained. The plots of θ_{11} and θ_{16} versus time t for the first mass are illustrated as the dotted curves in Figures (6.4a) and (6.4b), respectively.

- Slopes of these curves represent the first and sixth natural frequencies of the system. Figures (6.5a) and (6.5b) illustrate the plots of logarithm of the amplitude of the first and sixth DOF ($\ln a_{11}$ and $\ln a_{16}$) versus time. The linear least-square fits of the curves are also shown in the above noted figures by the solid lines. The natural frequencies ω_1 and ω_6, and the damping ratios ξ_1 and ξ_6 can be extracted from the slopes of the least square lines, as outlined earlier.

- The above process was repeated for all six DOF, and the natural frequencies and damping ratios of all DOF were obtained. The results are outlined in Table (6.1).

It is observed from this table that the correlation between the theoretical values (frequencies and damping) and the identified results is excellent. The efficiency of the procedure can be better appreciated by noting that only one response (displacement or acceleration), measured through only one sensor, was used to generate all the natural frequencies and damping ratios of the system. It should also be noted that the results presented in Table (6.1) are based averaging the mass of the system per segment.

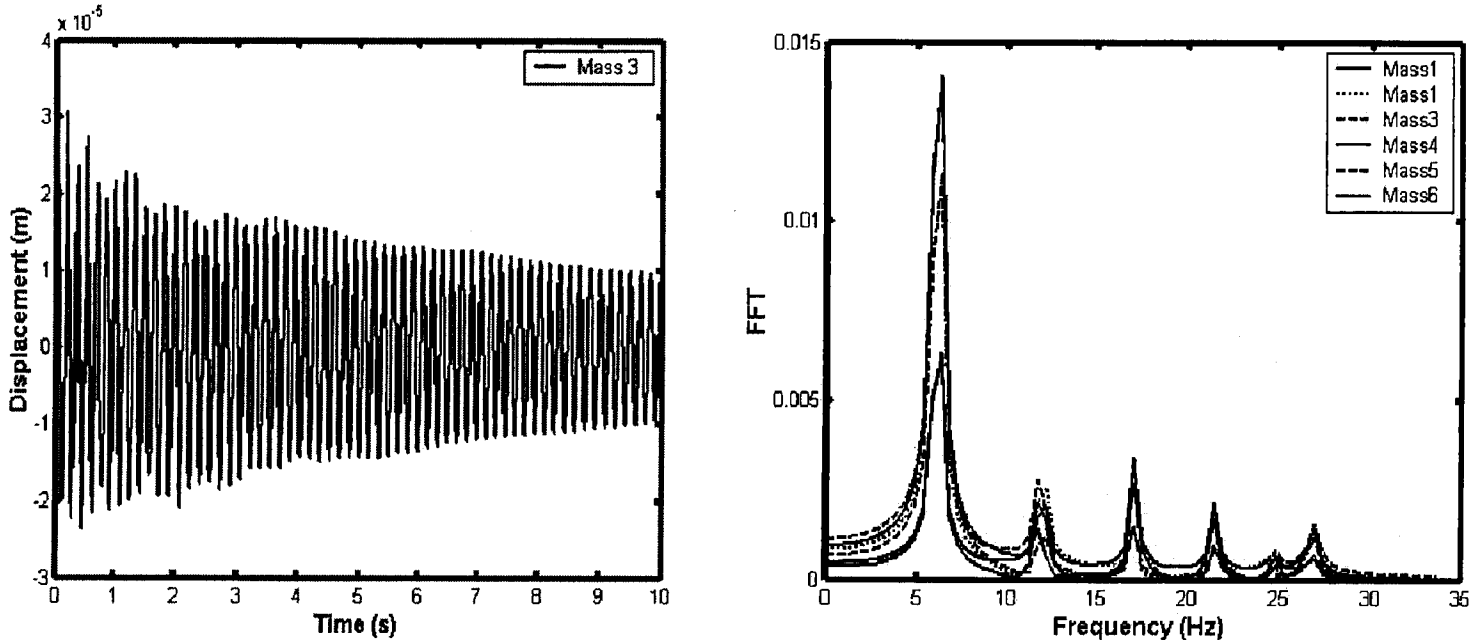

(a) (b)

Figure 6.2. Plots of (a) the displacement impulse response of mass # 3 of the damaged mechanical system, (b) the Fourier transform of displacement response of all masses of the healthy mechanical system.

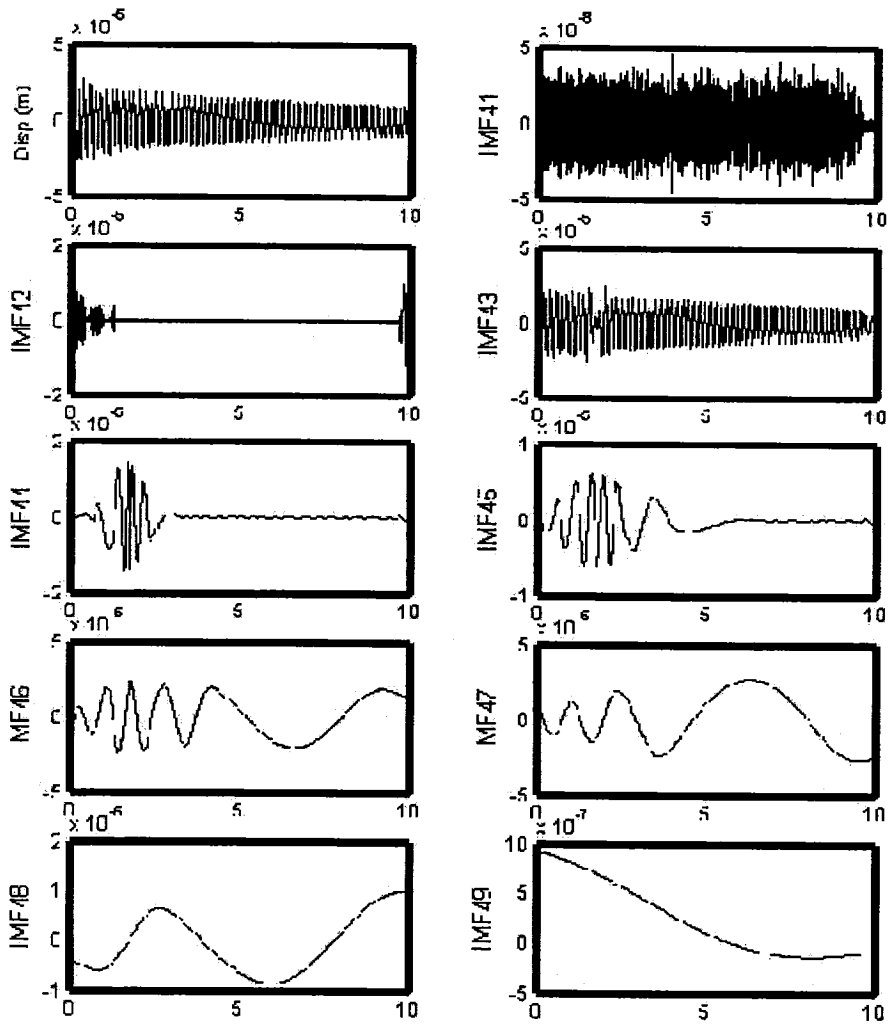

Figure 6.3. Displacement and IMFs of mass #4 of the healthy mechanical system.

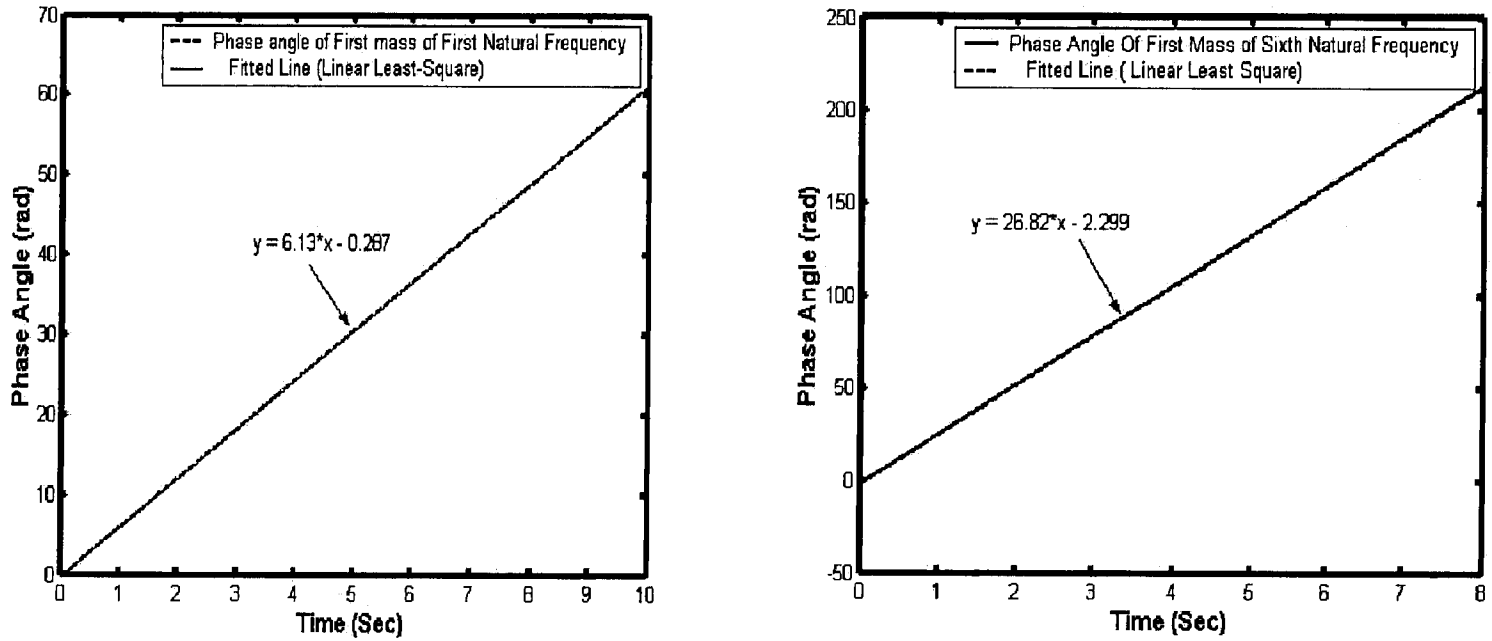

(a) *(b)*

Figure 6.4. Plots of (a) the unwrapped phase angle of the first mass for the first modal response, (b) the unwrapped phase angle of the first mass for the sixth modal response of the healthy system.

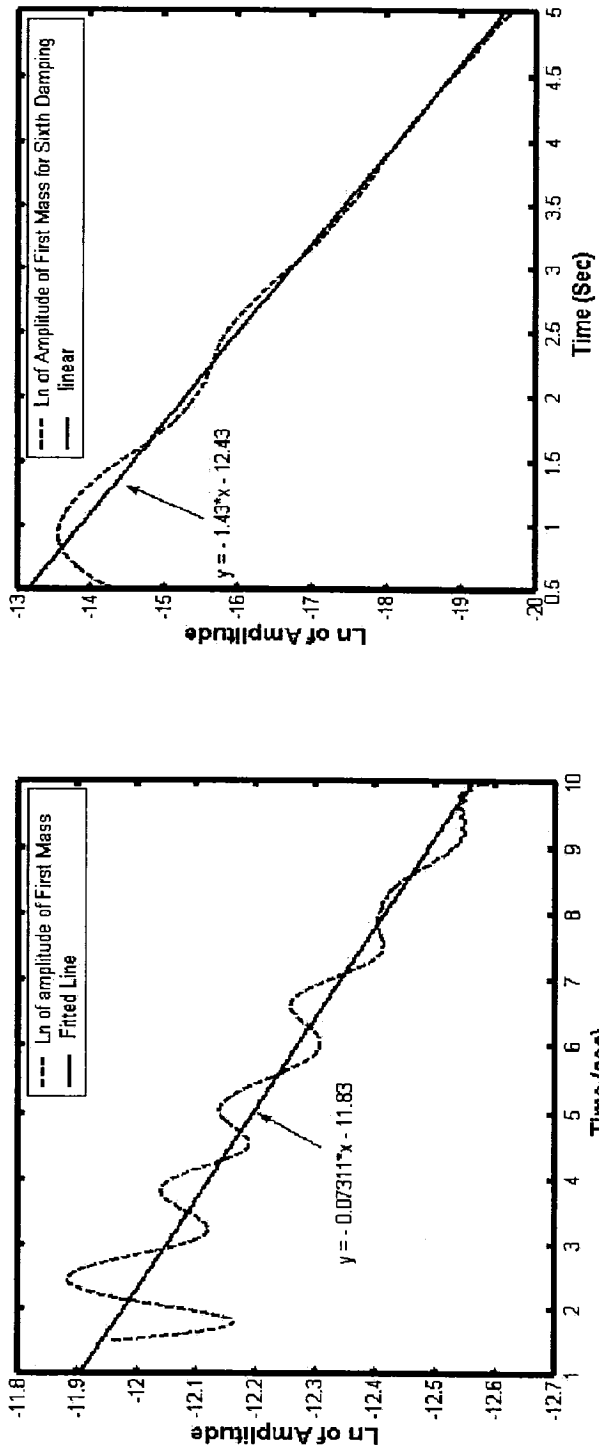

(a) (b)

Figure 6.5. Plots of (a) ln amplitude of the first mass for the first mode, (b) ln amplitude of the first mass for the sixth mode.

Table 6.1. Natural frequency and damping ratios of the healthy six DOF mechanical systems.

Theoretical Values			Identified Values	
Mode	Frequency Hz)	Damping ratio	Frequency Hz)	Damping ratio
1	6.13	0.19	6.13	0.19
2	11.96	0.38	11.95	0.38
3	17.18	0.54	17.17	0.54
4	21.55	0.68	21.50	0.68
5	24.84	0.78	24.81	0.79
6	26.87	0.84	26.70	0.85

Moreover, the complete mass matrix of the system can be calculated by repeating the above procedures for each DOF of the system. For illustration, the calculated mode shapes and their comparison with those obtained through the closed-form solution are tabulated in Table (6.2). The second and third modal responses are illustrated graphically in Figures (6.6a) and (6.6b). The identified stiffness matrix and damping matrices, as well as those obtained theoretically are listed below:

The identified modal mass:

$$[\Phi_{perfect}]\times[M]\times[\Phi'_{perfect}] = \begin{bmatrix} 18.16 & 0.04 & -0.14 & 0.03 & 0.12 & 0.01 \\ 0.04 & 5.71 & 0 & 0.01 & 0.05 & 0 \\ -0.14 & 0 & 3.69 & -0.01 & 0.10 & -0.03 \\ 0.03 & 0.01 & -0.01 & 3.67 & 0.04 & -0.01 \\ 0.12 & 0.05 & 0.10 & 0.04 & 5.32 & 0.02 \\ 0.01 & 0 & -0.03 & -0.01 & 0.02 & 18.73 \end{bmatrix}$$

The identified stiffness matrix:

$$K_{perfect} = \Phi^{-1}\times diag[K_j]\times[\Phi^{-1}]' = \begin{bmatrix} 14684 & -7327 & -128 & -153 & 131 & -188 \\ -7327 & 15176 & -7381 & -56 & 418 & -3 \\ -128 & -7381 & 14743 & -7537 & -139 & 13 \\ -153 & -56 & -7537 & 14744 & -7443 & -4 \\ 131 & 418 & -139 & -7443 & 15229 & -7430 \\ -188 & -3 & 13 & -4 & -7430 & 14885 \end{bmatrix}$$

The theoretical stiffness matrix:

$$K_{theory} = \begin{bmatrix} 15000 & -7500 & 0 & 0 & 0 & 0 \\ -7500 & 15000 & -7500 & 0 & 0 & 0 \\ 0 & -7500 & 15000 & -7500 & 0 & 0 \\ 0 & 0 & -7500 & 15000 & -7500 & 0 \\ 0 & 0 & 0 & -7500 & 15000 & -7500 \\ 0 & 0 & 0 & 0 & -7500 & 15000 \end{bmatrix}$$

The identified damping matrix:

$$C = \Phi^{-1} \times diag[c_j] \times [\Phi^{-1}]' = \begin{bmatrix} 1.4739 & -0.7331 & -0.0148 & -0.0151 & 0.0133 & -0.022 \\ -0.7331 & 1.5213 & -0.7382 & -0.0074 & 0.0389 & -0.0001 \\ -0.0148 & -0.7382 & 1.4781 & -0.7571 & -0.0158 & 0.0016 \\ -0.0151 & -0.0074 & -0.7571 & 1.4781 & -0.7445 & -0.0023 \\ 0.0133 & 0.0389 & -0.0158 & -0.7445 & 1.5266 & -0.7435 \\ -0.022 & -0.0001 & 0.0016 & -0.0023 & -0.7435 & 1.4941 \end{bmatrix}$$

The theoretical damping matrix:

$$C_{theory} = \begin{bmatrix} 1.5 & -0.75 & 0 & 0 & 0 & 0 \\ -0.75 & 1.5 & -0.75 & 0 & 0 & 0 \\ 0 & -0.75 & 1.5 & -0.75 & 0 & 0 \\ 0 & 0 & -0.75 & 1.5 & -0.75 & 0 \\ 0 & 0 & 0 & -0.75 & 1.5 & -0.75 \\ 0 & 0 & 0 & 0 & -0.75 & 1.5 \end{bmatrix}$$

As can be seen, there is good agreement between the identified and theoretically obtained results.

6.7 Case Study # 2: a Damaged Structure

In this section we consider the above mechanical system with only one difference. In this case, the stiffness of the fourth DOF (k_4) has been reduced from 7500 KN/m to 2500 KN/m (i.e. representing the presence of a damage in that region). The Hilbert-Huang spectral analysis presented above has also been applied to the new (damaged) system.

The measured displacement at the location corresponding to the third DOF ($X_{3d}(t)$) is shown in Figure (6.7a). The Fourier transforms of all DOF (i.e.,

$X_{1d}(t)$ through $X_{6d}(t)$ are illustrated in Figure (6.7b). The frequencies of the DOF fall in the following ranges:

(1) $5.38Hz = \omega_{1dL} \prec \omega_{1d} \prec \omega_{1dH} = 6.88Hz$ for the first mode

(2) $8.88 = \omega_{2dL} \prec \omega_{2d} \prec \omega_{2dH} = 10.39$ for the second mode

(3) $16.44 = \omega_{3dL} \prec \omega_{3d} \prec \omega_{3dH} = 17.94$ for the third mode

(4) $18 = \omega_{4dL} \prec \omega_{4d} \prec \omega_{4dH} = 19.42$ for the fourth mode

(5) $24 = \omega_{5dL} \prec \omega_{5d} \prec \omega_{5dH} = 25$ for the fifth mode

(6) $25 = \omega_{6dL} \prec \omega_{6d} \prec \omega_{6dH} = 27.95$ for the sixth mode

Figure 6.8 illustrates the signature of the fourth DOF of the damaged structure, as well as the signature's (signal's) IMF. The plots of for θ_{13} and θ_{14} versus time t for the first DOF (mass) are illustrated as dotted curves in Figures 6.9a and b, respectively. It can be seen that curves are quite straight and consequently, their least square fits are indistinguishable. Moreover, the third modal response of the damaged system in a certain portion of time domain has been illustrated in Figure (6.10). As an illustration, the signature of displacement of the 4th DOF (mass 4) and its IMFs in the damaged system is shown in Figure (6.11).

All natural frequencies and damping ratios of the damaged structure evaluated based on the presented approach, as well as the theoretical ones, are tabulated in Table (6.3). Similarly, the theoretically calculated mode shapes and those identified by the proposed approach are tabulated in Table (6.4).

The identified stiffness matrix and damping ratios of the damaged system, as well as those calculated by theoretical methods are listed below.

The identified modal mass:

$$[\Phi_{damaged}]\times[M]\times[\Phi'_{damaged}] = \begin{bmatrix} 18.16 & 0 & -0.14 & 0.04 & 0.27 & 0.06 \\ 0 & 9.88 & -0.01 & 0.01 & -0.02 & 0.01 \\ -0.14 & -0.01 & 3.6873 & -0.05 & 0.06 & -0.06 \\ 0.04 & 0.01 & -0.05 & 4.02 & 0 & 0.01 \\ 0.27 & -0.02 & 0.06 & 0 & 5.59 & 0.01 \\ 0.06 & 0.01 & -0.06 & 0.01 & 0.01 & 7.01 \end{bmatrix}$$

The identified stiffness matrix:

$$K_{damaged} = \Phi_{damaged}^{-1} \times diag[K_{j(damaged)}] \times [\Phi_{damaged}^{-1}]' =$$

$$\begin{bmatrix} 14900 & -7403 & -176 & -174 & 88 & -81 \\ -7403 & 15251 & -7435 & 89 & 288 & 35 \\ -176 & -7435 & 9844 & -2648 & -44 & -88 \\ -174 & 89 & -2648 & 9786 & -7505 & 10 \\ 88 & 288 & -44 & -7505 & 15347 & -7415 \\ -81 & 35 & -88 & 10 & -7415 & 14661 \end{bmatrix}$$

The theoretical stiffness matrix:

$$K_{theory} = \begin{bmatrix} 15000 & -7500 & 0 & 0 & 0 & 0 \\ -7500 & 15000 & -7500 & 0 & 0 & 0 \\ 0 & -7500 & 10000 & -2500 & 0 & 0 \\ 0 & 0 & -2500 & 10000 & -7500 & 0 \\ 0 & 0 & 0 & -7500 & 15000 & -7500 \\ 0 & 0 & 0 & 0 & -7500 & 15000 \end{bmatrix}$$

The identified damping matrix:

$$C_{damaged} = \begin{bmatrix} 1.6795 & -0.714 & -0.0687 & -0.0377 & -0.0347 & -0.1846 \\ -0.71 & 1.6656 & -0.7315 & -0.0133 & -0.0913 & -0.0392 \\ -0.0687 & -0.7315 & 1.1761 & -0.453 & -0.026 & 0.0564 \\ 0.0377 & -0.0133 & -0.453 & 1.1689 & -0.7383 & -0.0478 \\ -0.0347 & -0.0913 & -0.026 & -0.7383 & 1.6754 & -0.7147 \\ -0.1846 & -0.0392 & 0.564 & -0.0478 & -0.7147 & 1.6547 \end{bmatrix}$$

By examining the identified stiffness and damping matrices, one can clearly distinguish the damage location of the system. Otherwise, it is seen that the stiffness of the structure between DOFs three and four have been changed.

Table 6.2. Theoretical and Identified Mode Shapes of the healthy six DOF mechanical systems.

	Theoretical values of the mode shapes						Identified values of the mode shapes					
DOF	First	Second	Third	Fourth	Fifth	Sixth	First	Second	Third	Fourth	Fifth	Sixth
1	1	1	1	1	1	1	1	1	1	1	1	1
2	1.80	1.25	0.44	-0.44	-1.25	-1.80	1.72	1.25	0.44	-0.44	-1.20	-1.80
3	2.25	0.55	-0.80	-0.80	0.55	2.25	2.27	0.55	-0.80	-0.80	0.51	2.26
4	2.25	-0.55	-0.80	0.80	0.55	-2.25	2.27	-0.55	-0.80	0.80	-0.51	2.26
5	1.80	-1.25	0.44	0.44	-1.25	1.80	1.72	-1.25	0.44	0.44	1.20	1.80
6	1	-1	1	-1	1	-1	0.97	-0.99	1.01	-1	0.96	-1.02

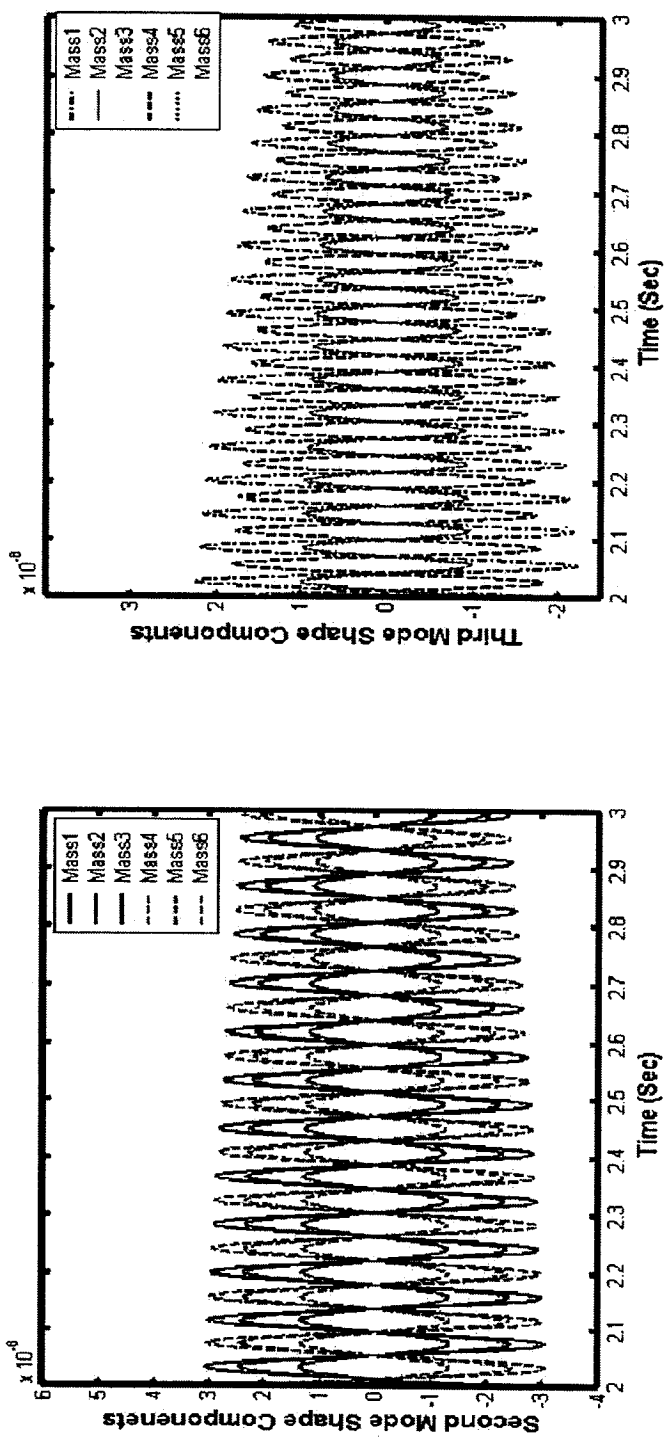

(a) (b)

Figure 6.6. Plots of (a) the second modal response, (b) the third modal response of the mechanical system.

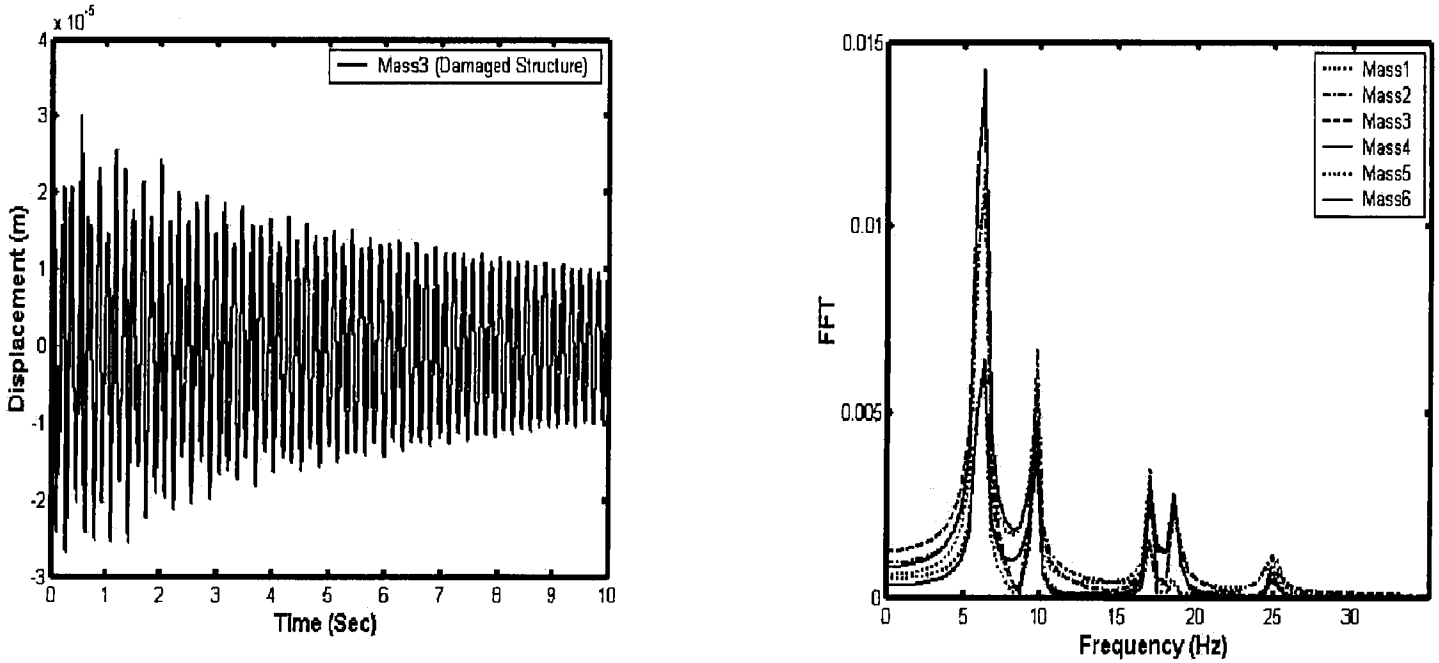

Figure 6.7. Plots of (a) the displacement impulse response of mass # 3 of the damaged mechanical system, (b) the Fourier transform of displacement response of all masses of the damaged mechanical system.

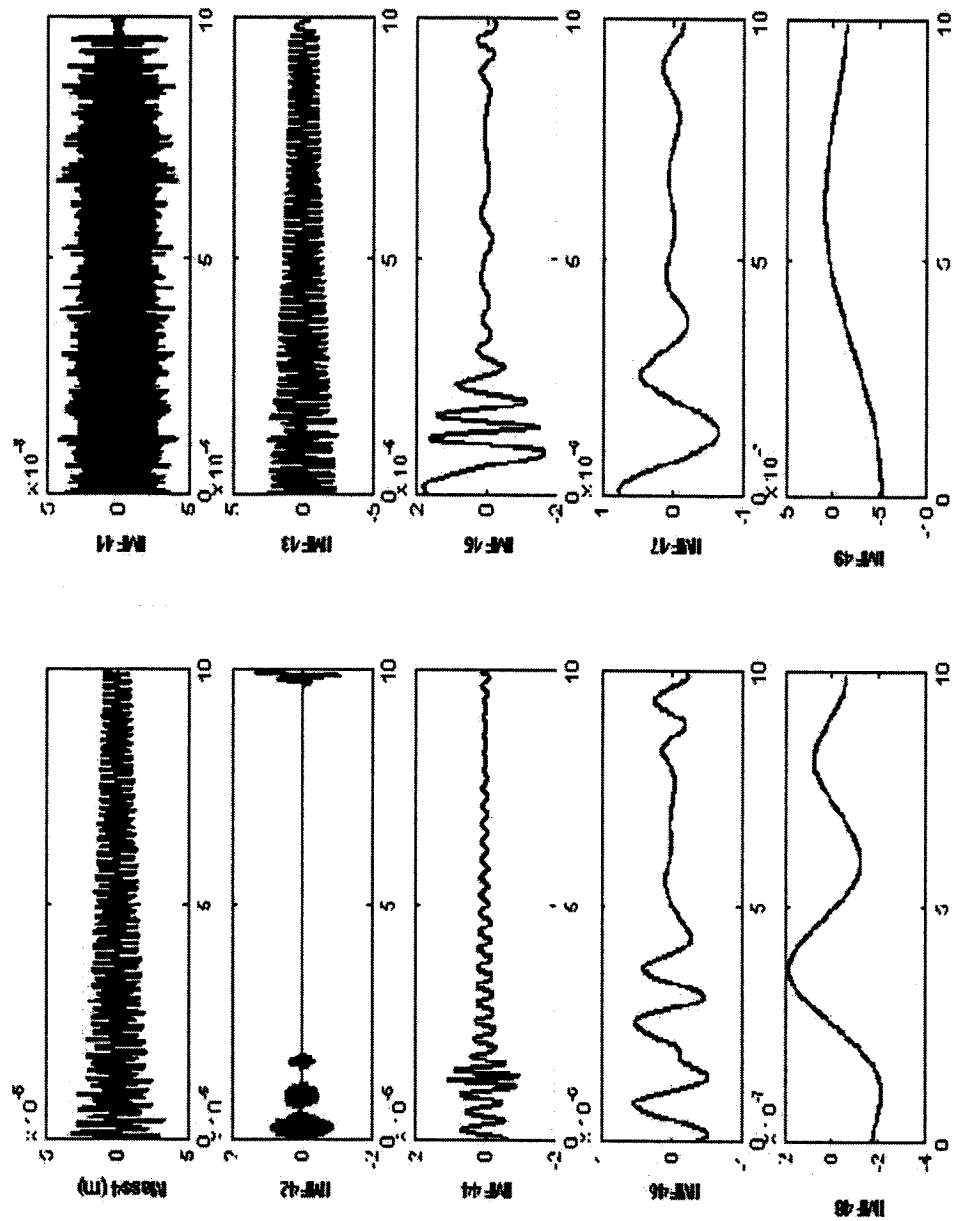

Figure 6.8. Displacement and IMFs of mass # 4 of the damaged mechanical system.

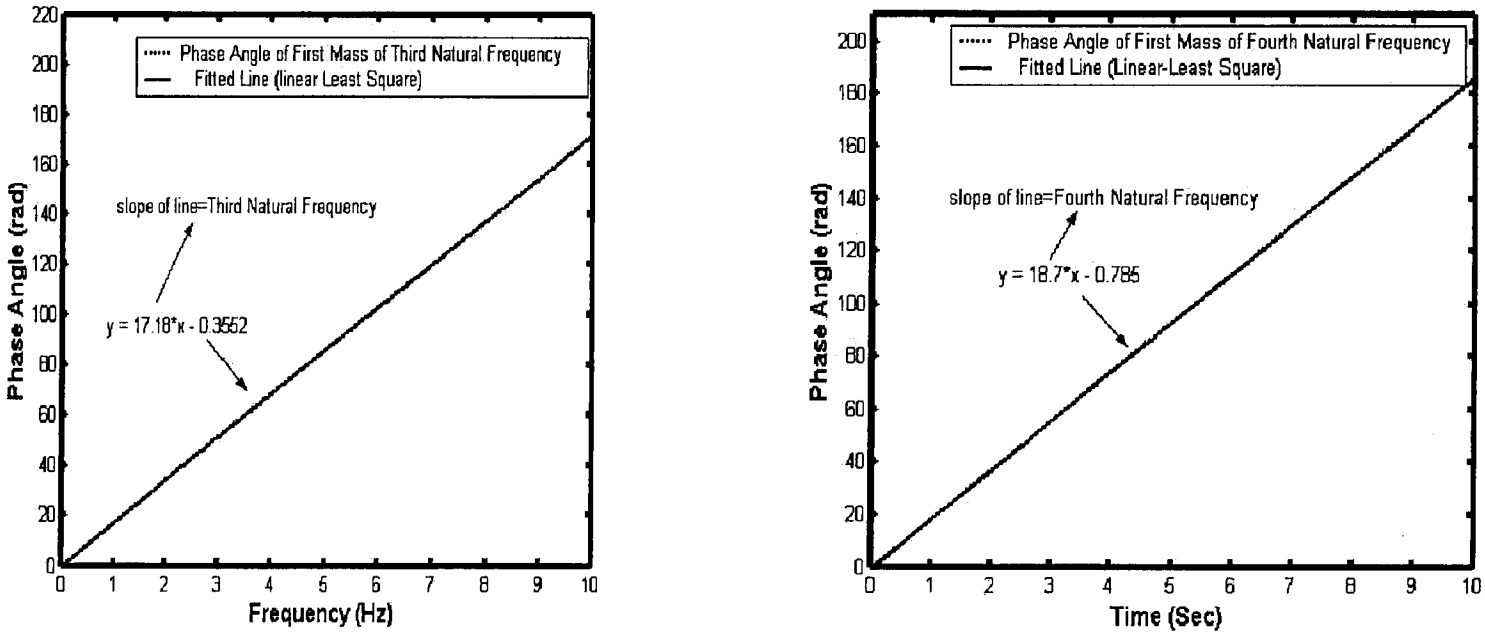

(a) (b)

Figure 6.9. Plots of (a) the unwrapped phase angle of the first mass for the first modal response, (b) the unwrapped phase angle of the first mass for the sixth modal response of the damaged system.

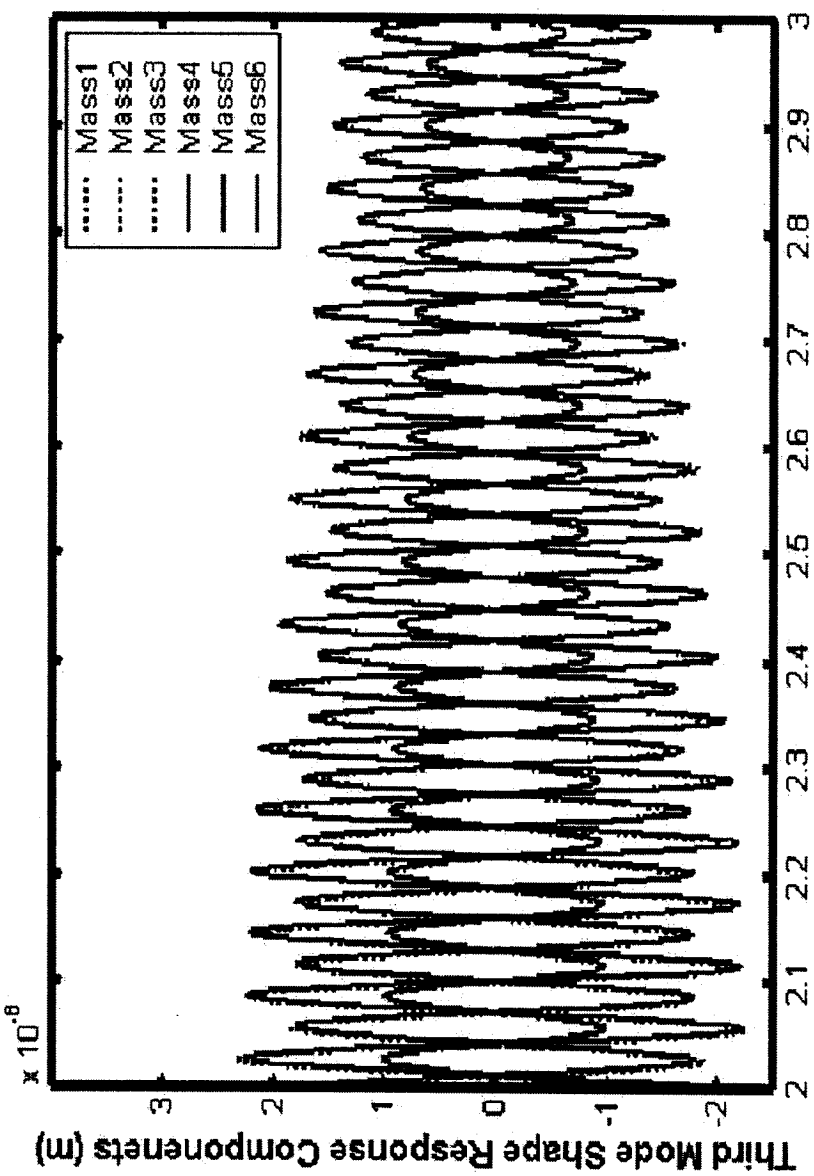

Figure 6.10. The third modal response of the damaged system.

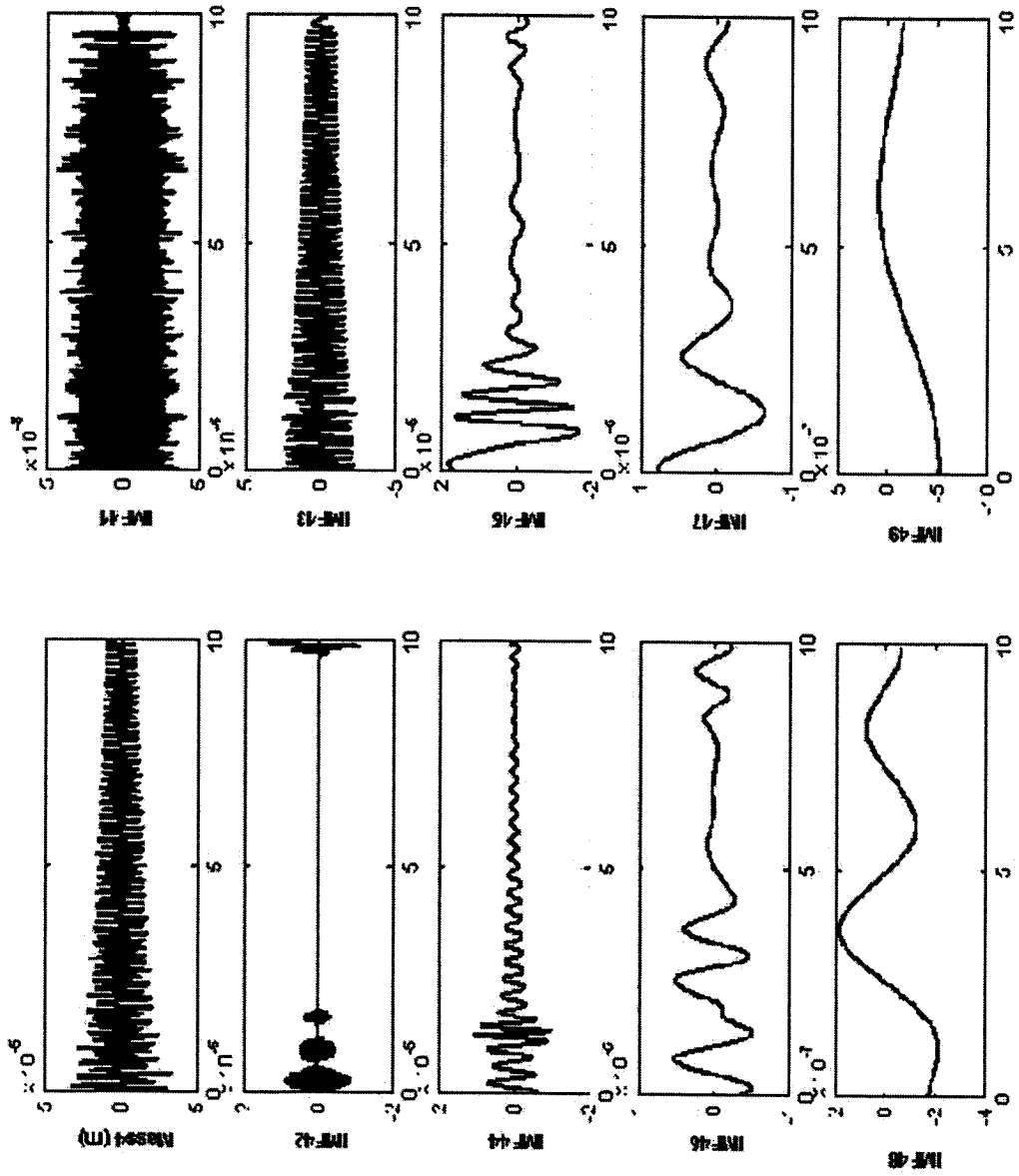

Figure 6.11. Displacement and IMFs of mass #4 of the damaged mechanical system.

Table 6.3. Natural frequency and damping ratios of the damaged sox DOF mechanical systems.

Theoretical Values			Identified Values	
Mode	Frequency (Hz)	Damping ratio	Frequency (Hz)	Damping ratio
1	6.13	0.19	6.13	0.19
2	9.63	0.58	9.63	0.60
3	17.18	0.54	17.17	0.54
4	18.67	0.79	18.60	0.78
5	24.84	0.78	24.81	0.79
6	25.19	0.84	25.16	0.85

Table 6.4. Theoretical and Identified Mode Shapes of the damaged six DOF mechanical systems.

	Theoretical values of the mode shapes						Identified values of the mode shapes					
DOF	First	Secon d	Third	Fourth	Fifth	Sixth	First	Secon d	Thir d	Fourth	Fifth	Sixth
1	1	1	1	1	1	1	1	1	1	1	1	1
2	1.80	1.51	0.44	0.16	-1.25	-1.34	1.72	1.51	0.44	0.16	-1.22	-1.36
3	2.25	1.28	-0.80	-0.97	0.55	0.80	2.27	1.28	-0.80	-0.97	0.55	0.82
4	2.25	-1.28	-0.80	0.97	0.55	-0.80	2.27	-1.29	-0.80	0.99	-0.55	-0.79
5	1.80	-1.51	0.44	-0.16	-1.25	-1.34	1.72	-1.51	0.44	-0.17	1.22	1.35
6	1	-1	1	-1	1	-1	0.97	-1.01	1.01	-1.02	1	-1.02

6.8 Intrinsic Mode Functions (IMFs) Based Damage Detection Methods

Having demonstrated the ability of the Hilbert Transform approach in evaluating the vibration response of damage and undamaged structures, in this paper we also propose a damage index for identifying damage in a given structure. This index is based on the first IMF of the filtered signal, which is indeed very close to the modal response of the structure. The energy of the first IMF can be evaluated by:

$$E_{mn} = \int_0^{t_0} (IMF)_{mn}^2 \, dt \tag{6.38}$$

In the above equation, m is the sensor number or the degree of freedom of the structure being considered, n is the mode shapes number and (IMF) is the first calculated intrinsic mode function of the signal, which has been passed through the aforementioned band-pass process. The damage index is therefore defined as:

$$DI_{mn} = \left| \frac{E_{mn}^{Healthy} - E_{mn}^{Damaged}}{E_{mn}^{Healthy}} \right| \times 100 \tag{6.39}$$

The advantage of the proposed damage detection approach is that the approach does not require significant computational effort, since the same procedure used for establishing the stiffness and damping matrices are effectively used to establish the damage index and location. Another advantage is that only the first few modal responses of (IMFs) are required for establishing the damage location.

To illustrate the capability of the proposed approach, the same 6-DOF mechanical systems (damaged and undamaged) are again considered. The energy terms calculated based on the IMFs, and the corresponding damage indices

are evaluated and tabulated in Table (6.5). Note that for the purpose of establishing the existence of the damage, only the first two frequencies have been used. It can be clearly seen that the energy terms corresponding to the first mode of the system have remained stationary for the undamaged and the damaged system. However, the results of Table (6.5) indicate that the energy terms corresponding to the second mode shape have significantly changed. Moreover, the maximum difference in the energy terms is in the vicinity of DOF three and four.

Table 6.5. Energy and damage indices of the first two modal responses based on the IMF energy.

Mass Number	IMF Energy of the healthy system		IMF Energy of the damaged system		Damaged Indices	
	First Mode	Second Mode	First Mode	Second Mode	First Mode	Second Mode
1	1.3562	.12167	1.3728	.23541	1.22	93.48
2	4.3844	.18827	4.4029	.5358	0.42	186.64
3	6.853	.036594	6.8652	.38273	0.18	**945.88**
4	6.9479	.038671	6.8919	.39534	0.81	**922.32**
5	4.4425	.18963	4.4302	.5416	0.28	185.60
6	1.3565	.12149	1.361	.23685	0.33	94.95

6.9 Conclusions

A theoretical investigation was carried out to investigate the vibration characteristics of a six degree freedom mechanical system. The investigation was carried out to demonstrate the integrity of Empirical Modal Decomposition (EMD). Moreover, the integrity of EMD in detecting the vibrational changes of the system as a result of sudden changes in stiffness at a particular location in the structure was also examined. The identification of the change in the stiffness of the structure due to a local change in the structural stiffness was used in the development of a damage index, by which the system's health could be monitored. The damage index was developed based on the energy of the first intrinsic mode function (IMFs). Some of the more significant observations from this study are summarized below:

1.The Hilbert-Huang spectral analysis method could be effectively used for the identification of the dynamic characteristics of multi-DOF structural systems. The formulation for evaluating stiffness and damping matrices was developed based on the measured free vibration-time histories of displacement of all degrees of freedom (though any measured quantity, such as acceleration could also be used).

2.The natural frequencies and damping ratios of the system could be effectively calculated based on the data collected through only one single sensor used for measuring the free vibration-time history of the system (more importantly, only at one single location).

3.If the time history responses are evaluated at all degrees of freedom of the system, one can effectively evaluate the mode shapes, as well as the mass, stiffness, and damping matrices of the structure.

4.Establishing the above information for a healthy system, as well as a damaged system can also effectively establish the presence of damage and its location by way of the proposed damage index. The developed damage index is based on the first intrinsic mode function.

Two case studies were used to demonstrate the integrity of the proposed identification system, as well as the developed damage index.

6.10 Acknowledgements

The financial support of the Atlantic Innovation Fund, as well as National Science and Engineering Reasearch Council granted to the second author in support of this work is gratefully acknowledged. The Killam Scholarship awarded to the first author is also acknowledged and appreciated.

6.11 References

Deng, Y., Wang W., Qian C., and Dai, D. (2001) Boundary-processing technique in EMD method and Hilbert transform. *Chinese Science Bulletin*, 46(3):954–961.

Flandrin, P., Rilling, G. and Goncalves, P. (2004) Empirical mode decomposition as a filter bank. IEEE Signal Processing Letters, 11(2):112–114.

Hahn, S.J. (1996) The Hilbert transform of the product a(t) cos(ω t + '0). Bulletin of the Polish Academy of Science 44(1):75–80.

Han, C., Guo, H., Wang, C , Fan. D, and Sang,. H. (2003) Multiscale edge detection based on EMD. *High technology letters (Chinese version)*, 6:13–17.

Hilbert-Huang Transform to the analysis of molecular dynamic simulations. *J. Phys. Chem.*, A (107): 4869–4876.

Huang, N.E., Shen, Z., Long, S.R., Wu, M.C., and Shih, H.H. (1998). The empirical mode decomposition and Hilbert spectrum for nonlinear and non-stationary time series analysis. Proceedings of the Royal Society of London—Series A 454: 903–995.

Huang, N.E., Shen, Z., and Long, S.R. (1999) A new view of nonlinear water waves: the Hilbert spectrum. *Ann Rev Fluid Mech*, 31:417–457.

Huang, N.E., Shen, Z., and Long, S.R. (1998). The empirical mode decomposition and the Hilbert spectrum for nonlinear and non-stationary time series analysis. *Proc. R. Soc. Lond. A*, pages 903–995.

Huang, W., Shen, Z., Huang, N.E., and Fung, Y.C. (1998) Engineering analysis of biological variables: An example of blood pressure over 1 day. *Proc. Natl. Acad. Sci. USA*, 95:4816–4821.

Huang, W., Shen, Z., Huang, N.E., and Fung,Y.C. (1999) Nonlinear indicial response of complex nonstationary oscillationsas pulmonary hypertension responding to step hypoxia. *Proc. Natl. Acad. Sci. USA*, 96:1834–1839.

Issue of Chi-Chi Earthquake, 91(5):1339–1357.

Loh, C.H., Wu, T.C., and Huang, N.E. (2001) Application of EMD+HHT method to identify near-fault ground motion characteristics and structural responses. *BSSA, Special.*

Nunes, J.C., Bouaoune, Y., Delechelle, E., Niang, O., and Bunel,P.H. (2003) Image analysis by bidimensional empirical mode decomposition. *Image and Vision Computing*, 21:1019–1026.

Phillips, S.C., Gledhill, R.G., Essex, J.W., and Edge, C.M. (2003) Application of theTitchmarsh. EC (1948) *Introduction to the Theory of Fourier Integrals*. Oxford University Press.

Xu, Y.L., Asce , M., and Chen, J. (2004) Structural Damage Detection Using Empirical Mode Decomposition: Experimental Investigation, Journal of engineering mechanics, November, 130: 1279-1288.

Yang, J.N. and Lei, Y. (2000) Identification of civil structures with non-proportional damping In Smart Structures and Materials 2000: Smart Systems for Bridges, Structures and Highways. Proceedings of SPIE, 3988, Newport Beach, CA, 284–294.

Yang, J.N., Lei, Y., Lin, S., and Huang, N.E. (2004) Identification of natural frequencies and damping of in situ tall buildings using ambient wind vibration data, Journal of engineering mechanics, 130:570-577.

Yang, J.N., Lei, Y., Pan, S., and Huang, N.E. (2003) System identification of linear structures based on Hilbert-Huang spectral analysis. Part 1: normal modes, Earthquake engineering and structural dynamics, 32: 1443-1467.

Yang, Z., Qi, D., and Yang, L. (2004) A novel automated detection of spindles from seepages based on Hilbert-Huang transform. *Technical Report, Sun Yat-sen University.*

Yang, Z., Qi, D., and Yang, L. (2004) A novel approach for detecting pitch based on Hilbert-Huang Transform. *Technical Report, Sun Yat-sen University.*

Yoshida, I. (2001) Damage detection using Monte Carlo filter based on non-Gaussian noises. Proceedings of the 8th International Conference on Structural Safety and Reliability, CD ROM. Royal Swet & Zeitling: the Netherlands, 8pp

Chapter 7

Piezoelectric-Based Degradation Assessment of a Pipe Using Fourier and Wavelet Analyses

N. Cheraghi, G. P. Zou and F. Taheri

Publication Status: Published at Journal of Computer-Aided Civil and Infrastructure Engineering, Volume 20 (5), September 2005.

7.1 Abstract

One of the most important issues in today's oil and gas industry is access to an effective and reliable damage detection system for health monitoring of pipeline systems. Vibration-based damage detection systems have been contemplated in the past with varying success. This paper demonstrates the effectiveness of a series of coupled mathematical/engineering approaches that are used to detect damage in pipes, reliably and accurately. The proposed health monitoring methodology is based on monitoring the vibration response of pipes using piezoelectric sensors. Finite element analysis is used to simulate the response of a healthy pipe, as well as pipes with various size damages. The degradations (defects) have been assumed to exist on the pipes in the form of local corrosion, simulated by reducing the wall thickness in various areas around the circumference of pipes. Fast Fourier transformation (FFT), FFT integration, wavelet transformation (WT) and wavelet packet transformation (WPT) methods are used to examine the pipe's dynamic response to an impacting force. Novel "Damage Indices" expressions are developed based on the evaluation of vibration signal induced energies. As it will be seen, the damage indices can effectively establish the existence of defects. Moreover, the energy indices can distinguish the differences among various size defects. It was observed that all the approaches considered could essentially establish the existence of the defects with good accuracy; however, incorporation of the WT and WPT energy components yielded a more precise identification of damage in the pipes examined.

7.2 Introduction

Pipelines are essential structural systems for transportation of natural gases, crude oils, and other refined oil by-products on and offshore. They are also used for both separation and transportation of bitumen in oil sand. Reliable and low-cost operation of pipelines is an important and critical aspect for the energy industry. As pipes age, their integrity deteriorates. Many factors such as corrosion, damage caused by excavation equipment, bending/buckling/wrinkling caused by earth and subsidence movement, cracks, and defective welds can impact the integrity of pipelines. Various non-destructive and in-line inspection methodologies have been developed and used with some success to detect the factors that can threaten the integrity of pipelines at the early stages of their development, thus preventing the resulting leakage and/or accidents and costly shutdowns. Most in-line inspection tools that are available today use either the magnetic flux leakage (MFL) method (Reber et al. 2002) or the ultrasonic guided wave method (Wilkie et al. 2002). Experimental works have also demonstrated the potential of piezoceramic actuators for controlling vibration in cylindrical shell applications (Fuller et al. 1990 and Silcox et al. 1992).

In comparison, piezoelectric sensors are light, can easily be adhered to components, use little power and are sensitive to small changes in strain and vibration, and are less sensitive to noise, thus are ideal for pipeline applications. Sun et al. (1995) and later Ayres et al. (1998) reported the use of PZT transducers for damage detection on a laboratory sized truss structure and a prototype truss joint, respectively. The proposed damage detection method is based on the principle of electromechanical coupling between the host structure and the bonded PZT transducer. The change in structural impedance due to the occurrence of damage modified the effective electrical impedance of the PZT adhered to the structure. This effected change in the driving point impedance of the PZT transducer was used to identify the onset of damage in the hosting structure (Giurgiutiu and Rogers 1997, 1998). Soh et al. (2000), Tseng et al. (2000) and Bhalla (2000) have reported some successful applications of the above method on concrete and other civil engineering structures. Tseng and Naidu (2002) and Jian et al. (1997) used piezoelectric patches for damage detection of composite structures, based on the non-parameter

characterization method. Hu and Fukunaga (2001) proposed a two-stage damage identification method based on the piezoelectric sensors for damage detection in composite structures. A proposed on-line damage diagnostic technique was successfully applied by Keilers and Chang (1993 and 1995b) for predicting delamination with piezoelectric sensors and actuators adhered to the top and bottom surfaces of a beam. The methodology was also validated experimentally (Keilers and Chang, 1995a). The diagnostic scheme was a search-based technique with an iterative damage identification algorithm combined with a wave response and a frequency domain method. Majumdar and Suryanarayan (1988) used the electromechanical effect of piezoelectric material for predicting the output voltages from the sensors when a delaminated beam was excited by the actuators. The presence of damage was identified by the difference between the output voltage obtained from the sensors attached to the damaged and undamaged structure. A review of damage detection methods using piezoelectric sensors and actuators can be found in Zou et al. (2000).

In this paper, a three-dimensional finite element model (FEM) is employed to characterize the vibration response of a pipe hosting piezoelectric sensors. The fundamental electrostatic equations governing the piezoelectric media are solved numerically by FEM. The piezoelectric sensors voltages are extracted from the dynamic response due to impact (much like an excitation induced by an impact hammer or a pendulum). Then, the Fast Fourier transformation (FFT), wavelet transformation (WT) and wavelet packet transformation (WPT) methods are used for analyzing the time-dependent piezoelectric voltage signals. Specifically, the FFT, the integral of the amplitude of the FRF, the WT and WPT equivalent energies over various ranges are taken as means of developing damage indices for establishing the presence and intensity of defects in cantilever pipes.

The motivation for the development of the damage detection methodology was prompted by a failure that occurred, in 2000, in one of Nova Scotia's offshore oil and gas facilities. The initial application of the method was therefore targeted toward exposed pipes on offshore facilities and refineries.

Our analysis indicated that although damages could be successfully detected by all the proposed methodologies, nevertheless, comparison of the energy components

obtained by WT and WPT yields a clearer means for identification of damage in comparison to those obtained through the FFT and the integral of FRF over the frequency ranges. These proposed algorithms can also distinguish the difference between different defect sizes.

7.3 Modeling and formulation of piezoelectric material

Various finite element formulations have been presented by several researchers for the assessment of dynamic response of piezoelectric materials. For instance, Tzou and Tseng (1990), and Rao and Sunar (1994) used the following equations to represent the dynamic response:

$$\begin{aligned} [M]\{\ddot{u}\}+[K_{uu}]\{u\}+[K_{u\phi}]\{\phi\} &= \{F\} \\ [K_{\phi u}]\{u\}+[K_{\phi\phi}]\{\phi\} &= \{Q\} \end{aligned} \tag{7.1}$$

where

$[M]=\int_V \rho[N_u]^T[N_u]dV$ is the kinematically consistent mass matrix;

$[K_{uu}]=\int_V [B_u]^T[C^E][B_u]dV$ is the elastic stiffness matrix;

$[K_{u\phi}]=\int_V [B_u]^T[e]^T[B_\phi]dV$ is the piezoelectric coupling matrix;

$[K_{\phi\phi}]=-\int_V [B_\phi]^T[\varepsilon][B_\phi]dV$ is the dielectric stiffness matrix;

$\{F\}=\int_V [N_u]^T\{f_b\}dV+\int_{S_1}[N_u]^T\{f_S\}d\Omega+[N_u]^T\{f_c\}$ is the mechanical force vector, and

$\{Q\}=-\int_{S_2}[N_\phi]^T q_s d\Omega-[N_\phi]^T q_c$ is the electrical force vector.

In the above equations, [M] is the mass matrix, u is the displacement, ϕ is the electric potential, Q is the applied concentrated electric charges, ρ is the mass density, $[B_u]$ and $[B_\phi]$ are the derivatives of the shape functions, $[N_u]$ and $[N_\phi]$; $[C^E]$, $[\varepsilon]$ and $[e]$ are the elasticity, dielectric and piezoelectric matrices, respectively; f_b denotes the body force, f_s is the surface force, f_c is the concentrated force, q_s is the surface charge, q_c is the

point charge, S_1 is the area where mechanical forces are applied at, and S_2 is the area where electrical charges are applied. The above matrix equations are written in partitioned form to reflect the coupling between the elastic and electric fields. Equation (7.1) can be condensed to represent the sensor's potential in terms of the sensor displacement in the form:

$$\{\phi_s\} = [K_{\phi\phi}]^{-1}(-[K_{u\phi}^T]\{u\}) \tag{7.2}$$

7.4 FFT-based Damage Detection Methods

All the methods presented here for comparison purposes are based on the assumption that damage is located between the points where the change in damage index is the greatest. The selection of these points is arbitrary. The methodology relies on vibration data obtained through the sensors located on these points. If more than one defect is located in between two sensors, the methodologies, at their present form, cannot detect that there are more than one defect. However, the methodologies can detect muti-defects, as long as each defect is located in between a pair of sensors.

The calculation of discrete approximation of FFT of the transient response data can be represented by (Santamarina and Dante 1998):

$$X(\omega) = \sum_{r=0}^{N-1} x(r\Delta t)e^{-i\omega r\Delta t}\Delta t \qquad \Delta t = \frac{T}{N} \tag{7.3}$$

The equivalent energy can be represented by:

$$E_{xx} = \int_{-\infty}^{+\infty} |X(\omega)|^2 d\omega \tag{7.4}$$

The equivalent FFT energy index is assumed to be:

$$FRF\_E_{\omega} = \sum_{\omega} \left| \frac{E_{xx}^{Damaged}}{E_{xx}^{Healthy}} \right| \frac{2}{N} \times 100 \tag{7.5}$$

where $E_{xx}^{Damaged}$ and $E_{xx}^{Healthy}$ are the before and after damage energies in the pipe, respectively.

This research proposes the integral of the amplitude of the FRF evaluated over various frequency ranges as a damage index. The selected frequency intervals should be such that their limits bound the natural frequencies of the original undamaged

system, because these are the regions most sensitive to the changes in response to the damage causing parameters.

It should be noted that if one looks at the time-domain data, there is not any noticeable change in the signal; there is, however, a slight shift in the natural frequency when considering the frequency domain data. Nevertheless, the observation of the behaviour of this integration quantity would enable one to detect damage in pipes. This integral is defined by:

$$I_x = \int_{-\infty}^{+\infty} |X(\omega)| d\omega \tag{7.6}$$

The damage index of FFT integration is defined as

$$FRF\ I_\omega = \left| \frac{I_x^{Damaged} - I_x^{Healthy}}{I_x^{Healthy}} \right| \times 100 \tag{7.7}$$

where $I_x^{Damaged}$ and $I_x^{Healthy}$ are the integral of pipe's signals at the damaged and undamaged state, respectively.

7.5 Wavelet transformation and damage index

7.5.1 THE DISCRETE WAVELET TRANSFORM

The following paragraphs briefly review wavelets and wavelet transformation methodologies with the aim of providing the reader with a better perspective of the work carried out in this paper.

Transformation of a signal is just another form of representing a signal, and it does not change the content present in the signal. In the context of the work presented here, the Wavelet Transform (WT) provides a time-frequency representation of a signal. This method was developed to overcome the short coming of the Short Time Fourier Transform (STFT), which is commonly used to analyze non-stationary signals. While STFT gives a constant resolution at all frequencies, WT uses multi-resolution technique by which different frequencies are analyzed with different resolutions.

A wave is an oscillating function of time or space, and periodic in nature, and wavelets are localized waves. They have their energies concentrated in time or space and are suited for analysis of transient signals. Fourier Transform and STFT use waves of regular shapes to analyze signals. The Wavelet Transform uses wavelets of finite energy to do the same. Figure 7.1 illustrates schematics of a FFT and Wavelet waves.

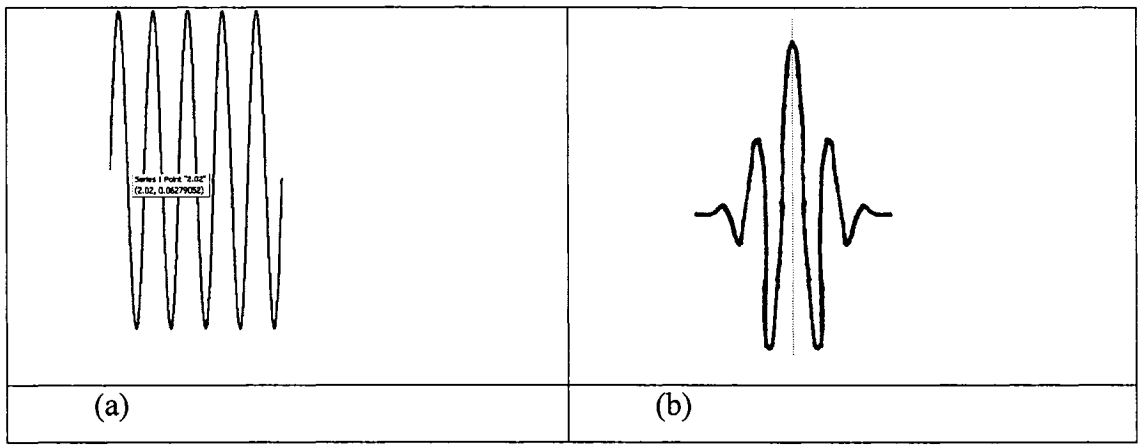

(a) (b)

Figure 7.1. Schematics of (a) a typical FFT function; (b) a typical wavelet function

A wavelet analysis is very similar to a STFT analysis. In STFT analysis the signal to be analyzed is multiplied by a window function, while in wavelet analysis, the function is multiplied with a wavelet function. However, as shown in the Figure 7.1, unlike the STFT, in WT, the width of the wavelet function changes with each spectral component. As a rule of thumb, the WT provides good time resolution and poor frequency resolution at high frequencies, but it conversely results in good frequency resolution and poor time resolution when used at low frequencies.

7.5.2 The Continuous Wavelet Transform and the Wavelet Series

A continuous wavelet transform of a function f(t) is defined by Newland (1993):

$$W_f(a,b) = \frac{1}{\sqrt{|a|}} \int_{-\infty}^{\infty} f(t)\psi^*\left(\frac{t-b}{a}\right)dt \qquad (7.8)$$

where W_f is the calculated wavelet coefficient, which can be used to recompose the original function f(t) (where f(t) itself is the function (signal) to be transformed); b is the translation parameter; a is the scale parameter; $\psi^*(t)$ is the transforming function (the so called "mother wavelet" or the "basis function"). All wavelet functions used in a given transformation are derived from the mother wavelet through translation (shifting) and scaling (dilation or compression).

The mother wavelet used to generate the basis functions is selected based on some desired characteristics associated with that function. The translation parameter b relates to the location of the wavelet function as it is shifted through the signal; thus, it corresponds to the time information in the WT. The scale parameter a is analogous to |1/frequency|, corresponding to the frequency information. By scaling the function, one may either dilate (expand) or contract (compress) a signal. Large scales can be used (at low frequencies) to dilate the signal and provide detailed information hidden in the signal, while small scales (used at high frequencies) can compress the signal and provide global information about the signal. It is important to note that the WT merely convolutes the signal and the basis function. This is quite useful, as in most practical applications, the high frequencies (at low scales) do not last for a long duration, but instead, appear as short bursts. Conversely, low frequencies (high scales), usually last for entire duration of the signal.

On the other hand, the recomposition equation can be expressed by:

$$f(t) = \frac{1}{c_\psi} \int_{-\infty}^{\infty} \int_{-\infty}^{\infty} \frac{1}{a^2} W_f(a,b) \psi^*\left(\frac{t-b}{a}\right) da db \tag{7.9}$$

where $c_\psi = 2\pi \int_0^\infty \left(|\psi(r)|\right)^2 (dr/r) < \infty$, in which $\psi(r)$ is the wavelet base function of r.

7.5.3 Wavelet Families

There are a number of Mother Wavelets or basis functions that can be used in WT. Common Wavelet families are Haar, Daubechies4, Coiflet1, Symlet2, Meyer, Morlet, and the Mexican Hat. These families represent various shapes, from simple shape (as in the Haar shown in Figure 7.2(a)), to more complex shape (such as the

Morlet shown in Figure 7.2(b)). For more information on these families, see the text book by Mallat (1999).

Since the mother wavelet produces all wavelet functions used in the transformation through translation and scaling, it determines the characteristics of the resulting wavelet Transform. Therefore, the details of the particular application should be taken into account and the appropriate mother wavelet should be selected so that the Wavelet Transform is accomplished effectively.

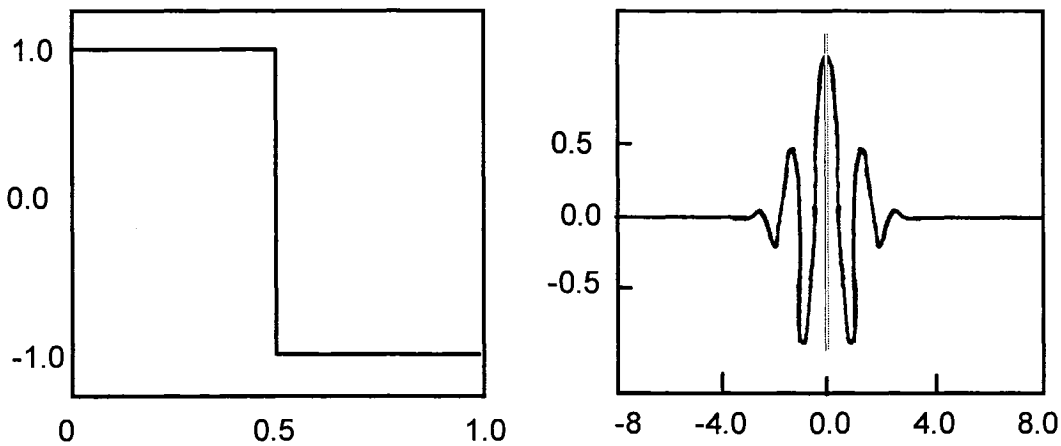

Figure 7.2. Two different mother wavelet functions: (a) Haar and (b) Morlet Wavelet

One of the most useful methods in practice is the wavelet packet analysis (WPT) (Sun and Chang 2002). Here, the WPT algorithm is briefly discussed.

Let $g_j^n(t) \in U_l^n$, then $g_j^n(t)$ can be expressed as

$$g_j^n(t) = \sum_l d_l^{j,n} \psi_n(2^j t - l) \tag{7.10}$$

in which ψ_n is the wavelet base, t is the time, and:

$$\begin{cases} d_l^{j+1,2n-1} = \sum_k a_{k-2} d_k^{j,n} \\ d_l^{j+1,2n} = \sum_k b_{k-2} d_k^{j,n} \end{cases} \tag{7.11}$$

where the recomposing $\left\{d_l^{j,n}\right\}$ can be calculated by:

$$d_l^{j,n} = \sum_k \left[h_{l-2k} d_k^{j+1,2n-1} + g_{l-2k} d_k^{j+1,2n} \right] \tag{7.12}$$

where *h(k)* and *g(k)* are the discrete filters (Wickerhauser 1994). Defining the signal energy U_f by:

where the wavelet packet component energy $U_{f_l^{k,n}}$ can be considered to be the energy stored in the component signal $d_l^{i,n}(t)$ as

$$U_{f_l^{k,n}} = \int_{-\infty}^{+\infty} d_l^{i,n}(t)^2 \, dt \tag{7.14}$$

The WPT damage index introduced in this analysis is therefore defined as:

$$WPT\_U = \sum_{i=1}^{2^l} \left| \frac{U_{f_l^{i,n}}^{Damaged} - U_{f_l^{i,n}}^{Healthy}}{U_{f_l^{i,n}}^{Healthy}} \right| \times 100 \tag{7.15}$$

where $U_{f_l^{i,n}}^{Damaged}$ and $U_{f_l^{i,n}}^{Healthy}$ are the energies of the pipe before and after the damage, respectively.

In summary, the wavelet-based approaches can be considered as adaptive, while the FFT-based approaches are non-adaptive.

7.6 Examples

To investigate the effectiveness of the proposed piezoelectric-based vibrational sensing damage detection methodology for assessing health of pipes, we investigate the response of aluminum pipes bearing various levels of damage. In each analysis, the pipe hosts nine piezoelectric patches bonded onto it. The physical and material properties of the pipes which are made of aluminum are provided in Table 7.1. Nine PZT BM500 patches with dimensions of 0.05 m long and 0.05 m wide and thickness of 1 mm, with mass density of 7650 kg/m^3 were used in this analysis. The material properties of PZT BM500 piezoceramic from Sensor Technology Limited (2001) are given as:

$$[C^E] = \begin{bmatrix} 12.1 & 7.54 & 7.52 & 0 & 0 & 0 \\ 7.54 & 12.1 & 7.52 & 0 & 0 & 0 \\ 7.52 & 7.52 & 11.1 & 0 & 0 & 0 \\ 0 & 0 & 0 & 2.11 & 0 & 0 \\ 0 & 0 & 0 & 0 & 2.26 & 0 \\ 0 & 0 & 0 & 0 & 0 & 2.26 \end{bmatrix} \times 10^{10} \left[N/m^2 \right] \tag{7.16}$$

$$[e]=\begin{bmatrix} 0 & 0 & 0 & 0 & 0 & 12.3 \\ 0 & 0 & 0 & 0 & 12.3 & 0 \\ -5.4 & -5.4 & 15.1 & 0 & 0 & 0 \end{bmatrix} \left[C/m^2\right] \quad (7.17)$$

$$\left[\varepsilon^S\right]=\begin{bmatrix} 8.11 & 0 & 0 \\ 0 & 8.11 & 0 \\ 0 & 0 & 7.349 \end{bmatrix} \times 10^{-9} \left[F/m\right] \quad (7.18)$$

where $[C^E]$ is the elasticity matrix, $[e]$ is the piezoelectric matrix and $[\varepsilon^S]$ is the dielectric matrix. The commercial finite element program ANSYS is employed for modeling the response of pipes and the piezoelectric sensors. The three-dimensional coupled element (SOLID5) of ANSYS is used for modeling. The pipes are cantilevered (fully supported in one end, and free at the other end). The mesh density has 40 rows of element along the axial direction, 18 elements along the pipe's circumference, in each row, and two layers through the thickness, as shown in Figure 7.3(a). The pipe is assumed to be impacted at its free end by pendulum, which is simulated by applying a concentrated load with magnitude of 1000N applied in a time interval of 2.5 μs. Different damage locations, sizes and stiffness reductions (as a damage form) are considered, as described in the following sections.

Table 7.1. Geometry and material properties of pipe

Outside diameter	273.5 mm
Wall thickness	9.3 mm
Length	2000 mm
Young's modulus	67×10^3 N/mm^2
Poisson ratio	ν=0.33
Mass density	2730 kg/m^3

7.6.1 Case 1: Dynamical response of piezoelectric sensors for different damage locations

To evaluate the integrity of the proposed methodologies, three different cantilevered aluminum pipes, each having damage at different locations along their length, were considered. This form of damage is assumed to result from corrosion,

and the subsequent reduction of material at that location. This is simulated by removing one layer (interior layers) element within two rows (i.e., a 100 mm width) from the mesh forming the pipe. The defects are assumed to be located in mid-distance between sensors 2 and 3, sensors 5 and 6, and sensors 7 and 8. These damage locations are referenced as DL1, DL2 and DL3, hereafter. The comparison of the natural frequencies obtained by the FEM (eigenvalue) analysis with those obtained from the frequency response function (FRF) analysis of the sensors for the healthy and damaged pipes (DL2) are provided in Table 7.2. Moreover, the first and second mode shapes for the healthy pipe are shown in Figures 7.3(b) and (c). As indicated in Table 7.2, a relatively close agreement between the two approaches is obtained. Typical FRF response curves of one of the sensors (sensor 5) for the healthy and damaged pipes are shown in Figure 7.4. Figure 7.5 illustrates the FRF response curves of sensor 5 for the pipes having damage at three locations (DL1, DL2 and DL3). The response of sensors 2, 4 and 7 for damage located in location 2 (DL2) is illustrated in Figure 7.6. Careful examination of the FRF responses shown in Figures 7.5 and 7.6 indicates that identical piezoelectric sensors, mounted under a similar condition on a pipe respond differently depending on the presence and location of damage in the substrate. This is a significant observation, in that health monitoring of pipes could be effectively achieved by using an array of piezoelectric transducers. The following section will provide justification for this statement.

Furthermore, wavelet analysis was also applied to the three cases. Specifically, the db3 wavelet (Daubechies3 Wavelet) and wavelet packet were used to conduct the analyses. Detailed wavelet responses obtained through the analysis of sensor 4 for the healthy and DL2 damaged pipe cases are shown in Figures 7.7(a) and 7.7(b), respectively; similarly, the information obtained for the wavelet packet analysis is shown in Figures 7.8(a) and 7.8(b). Notice that the wavelet methodology adopted here involves a multi-resolution analysis for a piece of data windowed by shifted and scaled wavelets generated from, or the so-called "mother wavelet" (Wickerhauser, 1994). Only the higher-resolution details were used to make the above observation. Therefore, to detect a potential damage at a particular point in time would only

require a small portion of data neighboring that particular time. This is an attractive feature of this approach and an effective mean for on-line heath monitoring of pipes.

The component of energies obtained by the FFT, WT and WPT are tabulated in Table 7.3. In this table, the WT and WPT energy components are evaluated based on the db3 wavelet at the 4^{th} level decomposition. In the case of the WT approach, the $d_4^a(t)$ and $d_4^d(t)$ component of energies shows sensitivity to damage. However, in the case of the WPT approach, the $d_4^1(t)$ component of energy exhibits more sensitivity to damage.

Figure 7.9 illustrates the damage signatures (damage energy indices evaluated based on the FFT, FFT integration, WT and WPT methodologies at the damage locations) as a function of the sensor number mounted along the axial direction of the pipe for the case where the damage is located in location 2 (DL2). It is observed that all four approaches can detect the defect locations within the range of a pair of sensors. However, it is noted that the WT and WPT methodologies can predict the damage location more accurately than the FFT methods (i.e. the differences in the energy indices from the sensors have much larger margin in WT and WPT than in the other methods). The results also confirm the suitability of PZT sensors and their sensitivity in detecting damage in pipes.

Moreover, the influence of noise on the data was also investigated. In general, piezoelectric sensors produce excellent response, with minimal noise. Nevertheless, it is instructive to examine the influence of noise on the results obtained through the four methods.

The results are illustrated in Figure 7.9. The comparison of the results reveals that only FFT method gets marginally affected by the noise, and the results obtained from the other methodology are not affected.

Table 7.2. Comparison of natural frequencies

Pipe Condition	Modes	FE (eigenvalue) solution (Hz)	FRF solution (Hz)
Healthy pipe	1	62.4	63.8
	2	339.1	332.1
	3	379.2	380.1
Damaged pipe (DL2)	1	62.3	63.7
	2	333.1	326.6
	3	377.1	376.3

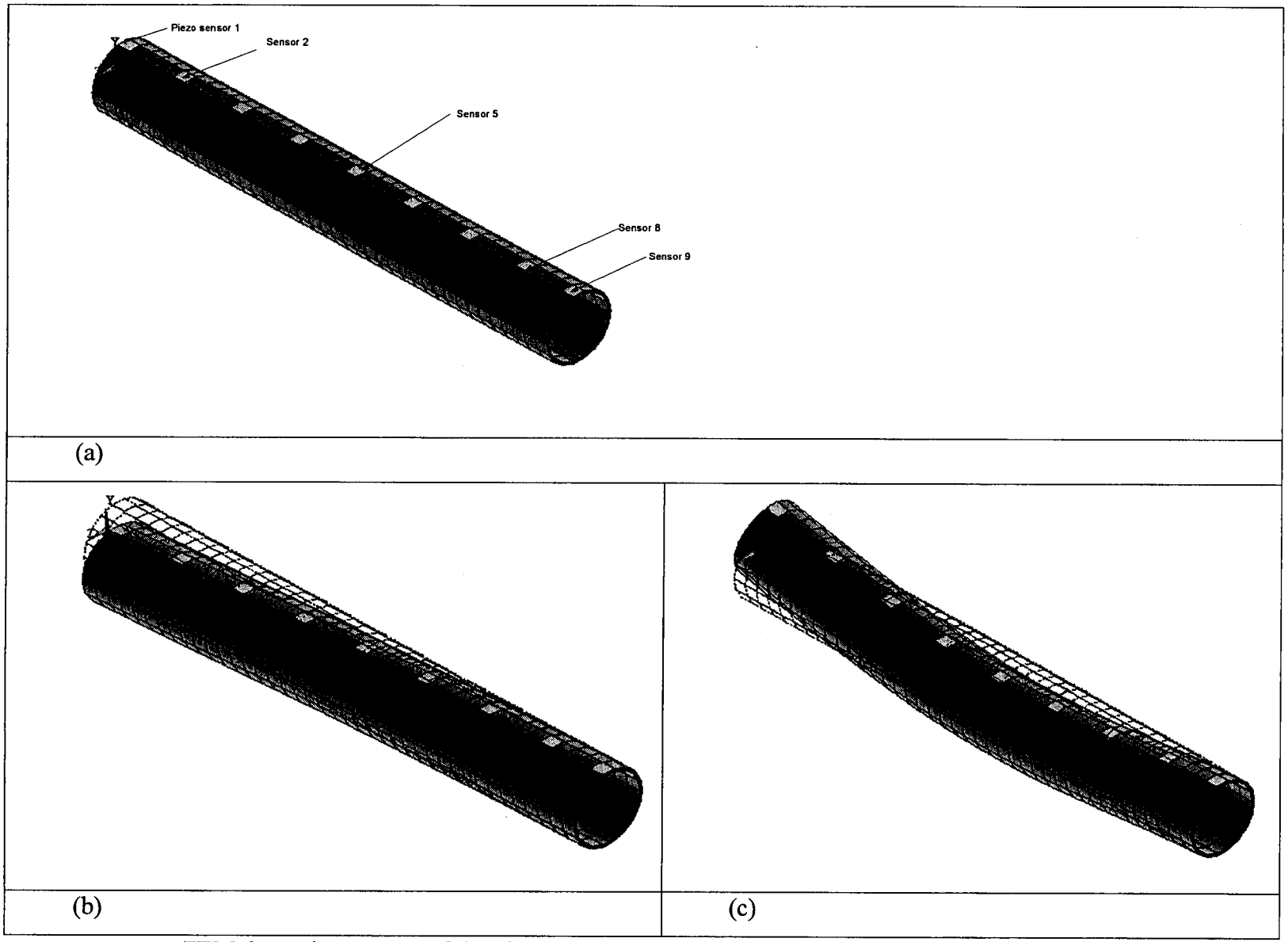

Figure 7.3. FEM dynamic response of the pipe; (a) FEM mesh, (b) First vibration mode, (c) second vibration mode.

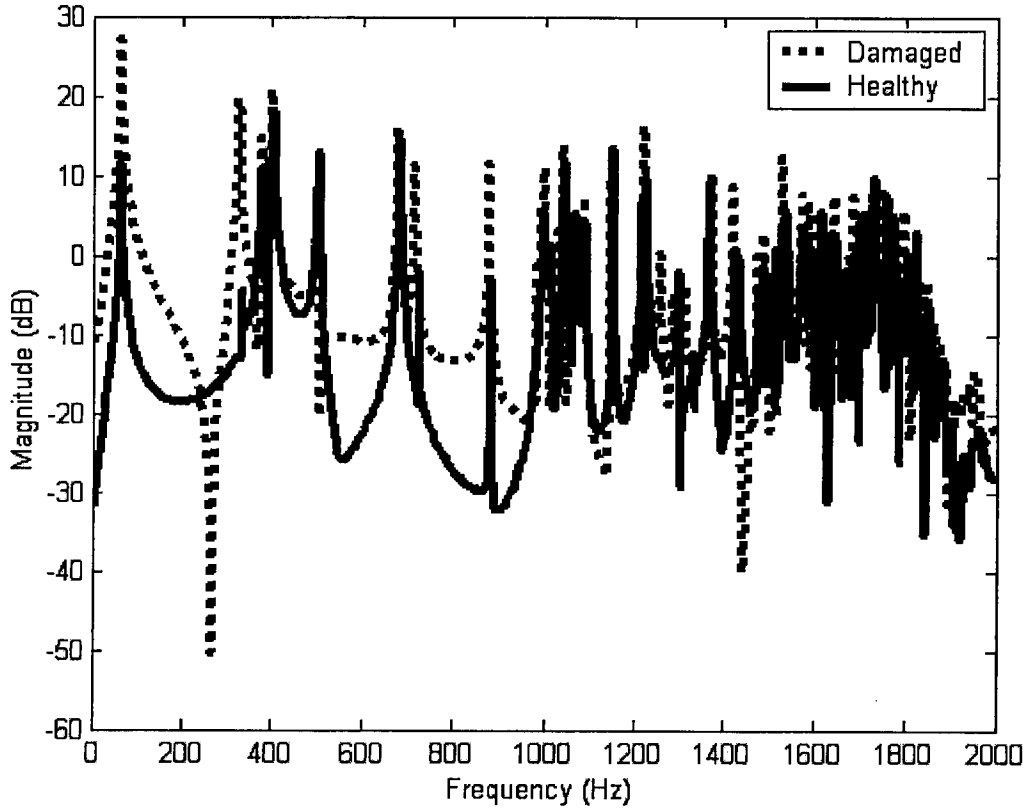

Figure 7.4. Typical FRF response curves of sensor 5 for the healthy and damaged pipes.

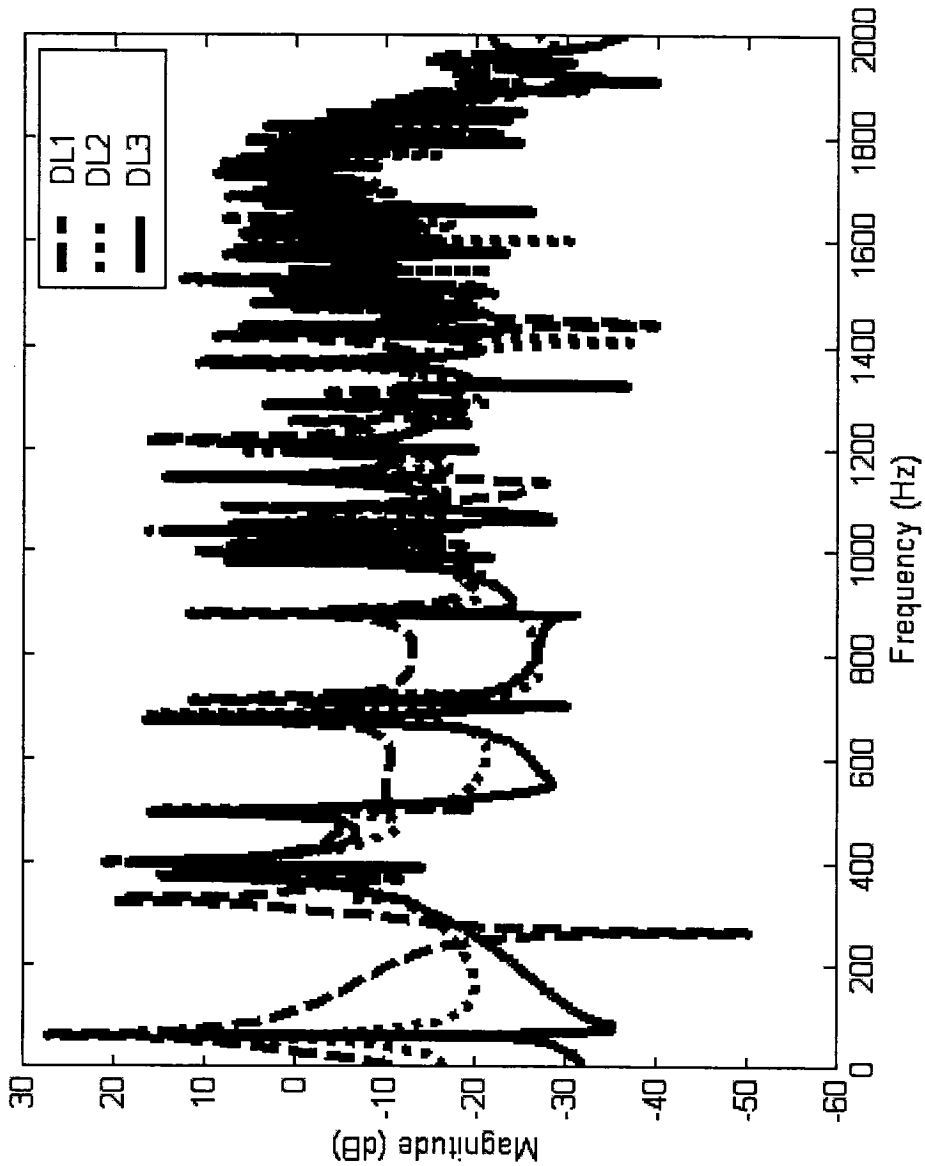

Figure 7.5. Comparison of FRF response for sensor 5 at the damage cases DL1, DL2 and DL3.

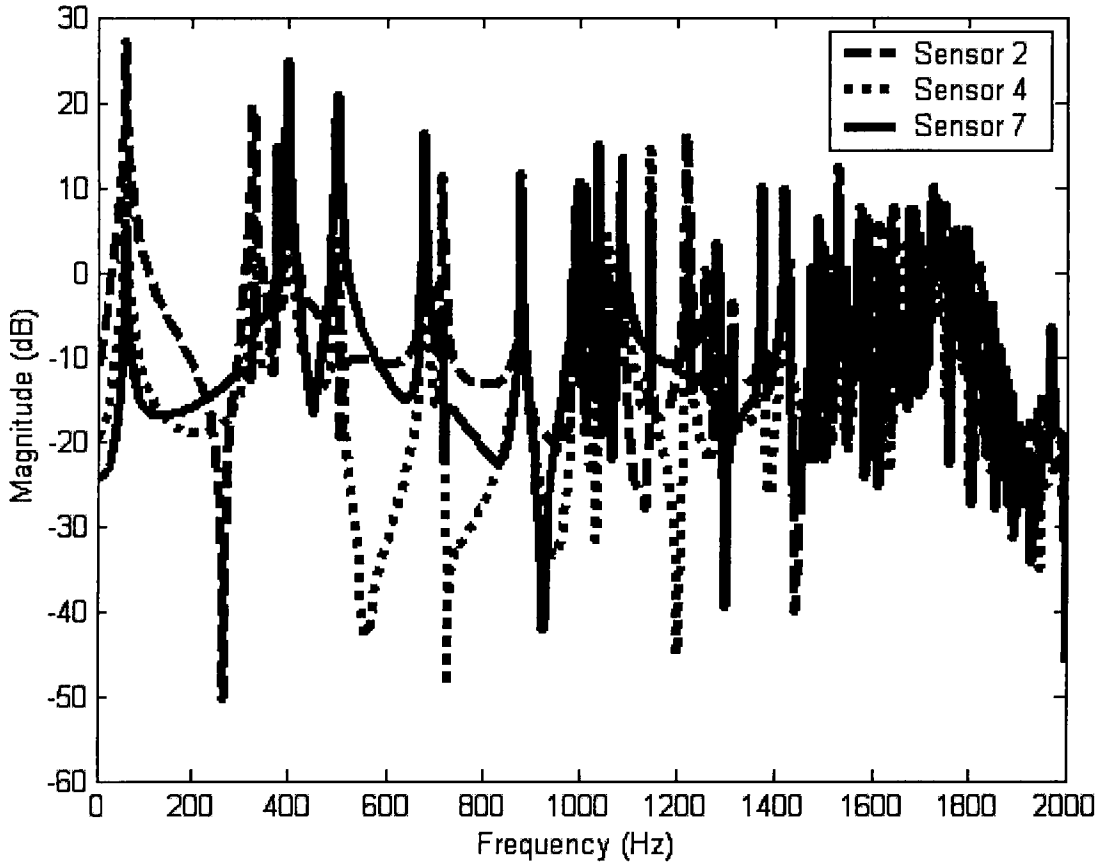

Figure 7.6. Comparison of FRF response for sensors 2, 4 and 7 at the damage case of DL2.

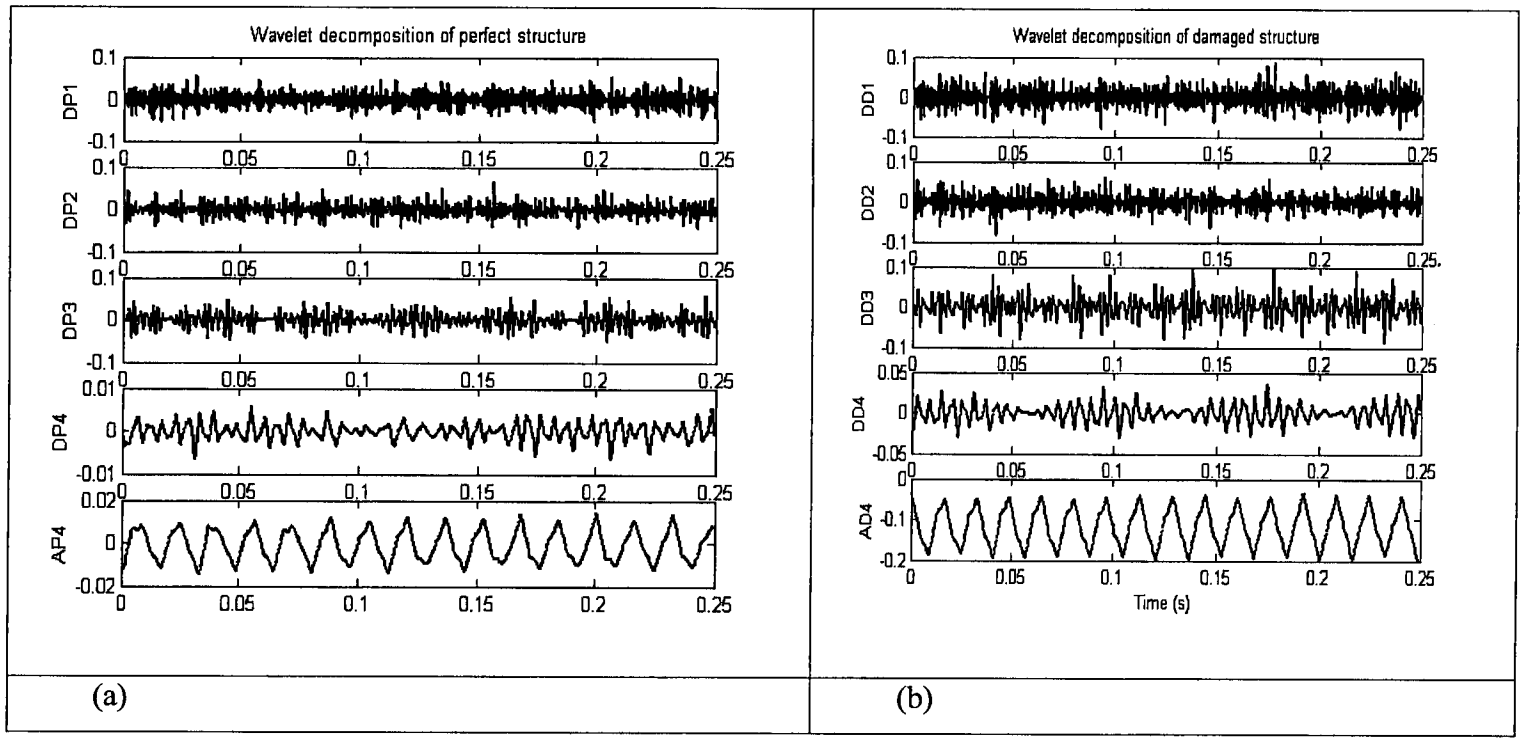

Figure 7.7. Wavelet simulation of (a) healthy pipe, (b) damaged pipe (at DL2).

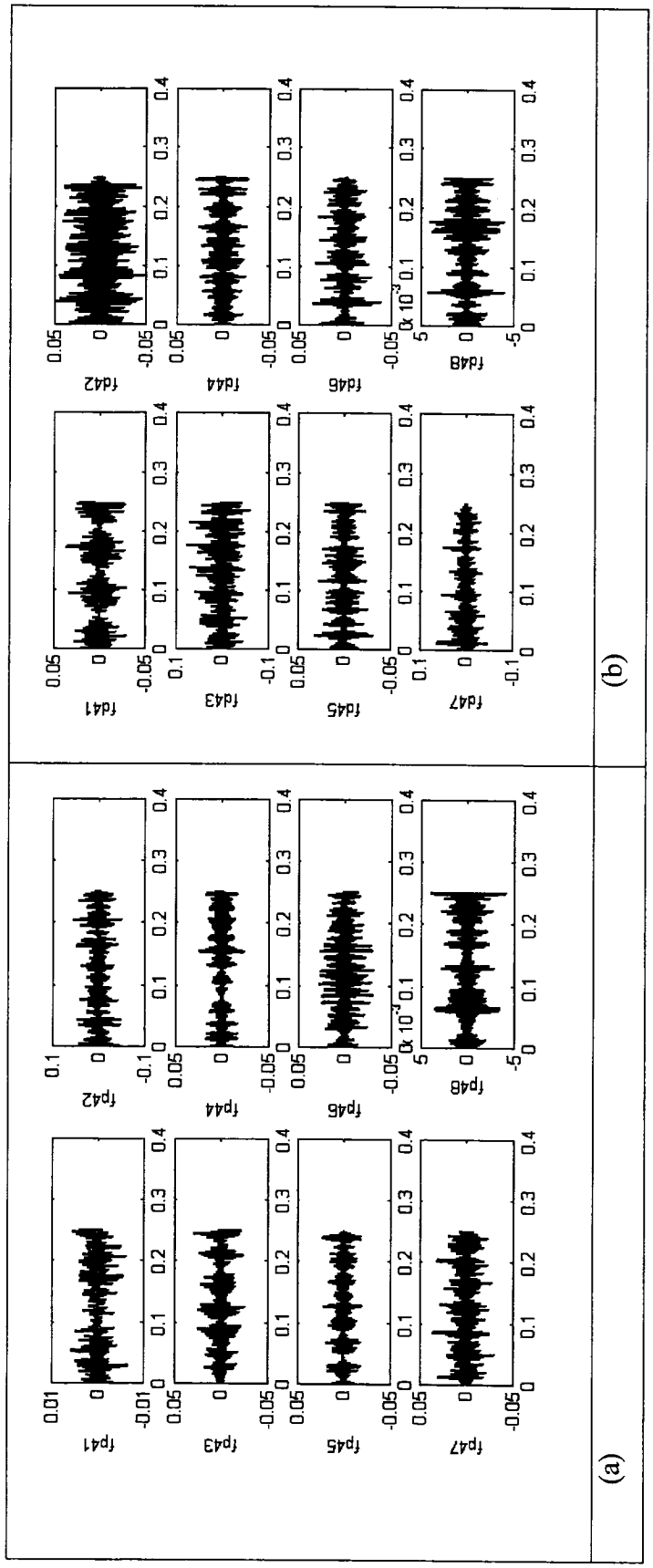

Figure 7.8. Wavelet packet simulation of (a) healthy pipe, (b) damaged pipe (at DL2).

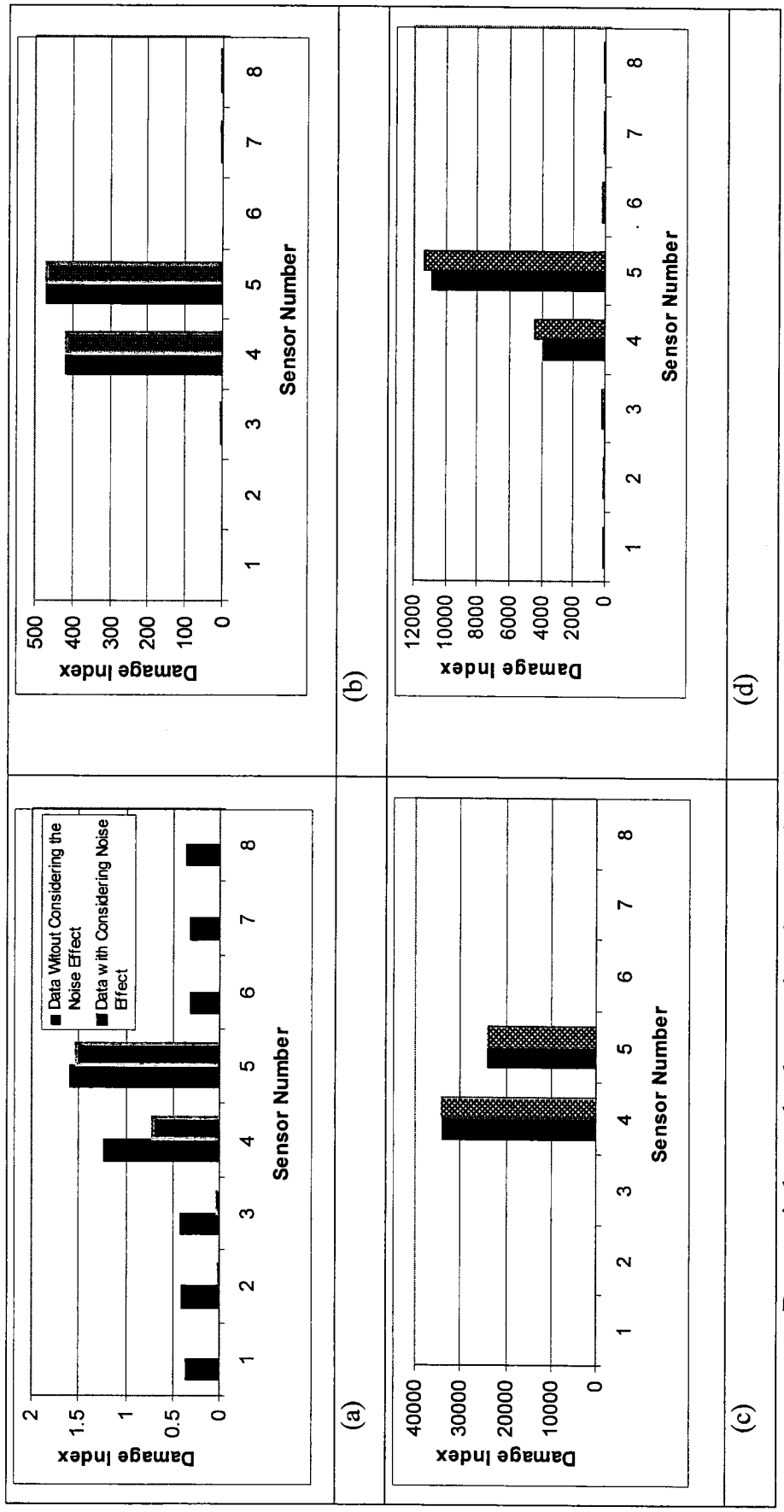

Figure 7.9. Damage index at the damage location DL2 based on: (a) FFT energy; (b) FFT integration; (c) WT energy and (d) WPT energy

Table 7.3. Comparison of the energies for FFT, WT and WPT for the damage case DL2

Method	Components	$E_{healthy}$ (0-0.25 s)	$E_{damaged}$ (0-0.25 s)	Change (%)
FFT	—	394.2	2426.2	515.5
WT	$d_4^a(t)$	1.2687×10^{-5}	3.9225×10^{-3}	30816.7
	$d_4^d(t)$	8.6086×10^{-7}	2.5979×10^{-5}	2917.8
	$d_3^d(t)$	6.0146×10^{-5}	1.5819×10^{-4}	163.0
	$d_2^d(t)$	5.0762×10^{-5}	8.3846×10^{-5}	65.2
	$d_1^d(t)$	7.2237×10^{-5}	1.2242×10^{-4}	69.5
WPT	$d_4^1(t)$	8.6086×10^{-7}	2.5979×10^{-5}	2917.8
	$d_4^2(t)$	4.6565×10^{-5}	5.9677×10^{-5}	28.2
	$d_4^3(t)$	1.3367×10^{-5}	9.8914×10^{-5}	640.0
	$d_4^4(t)$	8.7762×10^{-6}	1.6786×10^{-5}	91.3
	$d_4^5(t)$	6.8594×10^{-6}	1.3166×10^{-5}	91.9
	$d_4^6(t)$	1.7970×10^{-5}	1.7382×10^{-5}	3.3
	$d_4^7(t)$	1.6655×10^{-5}	3.6173×10^{-5}	117.2
	$d_4^8(t)$	2.8572×10^{-7}	3.6739×10^{-7}	28.6

7.6.2 Case 2: Detection of damage due to reduction in flexural rigidity

To further examine the integrity and sensitivity of the selected methodologies, this case study examines a pipe having reduced flexural rigidity in its mid-span, between sensors 4 and 5. This effect was simulated by reducing the Young's modulus of two rows of elements at the pipe's mid-span. The reduction in flexural rigidity ranges from 10% to 50% to represent different intensities of damage. The comparison of FRF response for the cases of 10%, 30% and 50% reduction in rigidity is plotted in Figure 7.10. The comparison of the damage indices evaluated by FFT, FFT integration, WT and WPT methodologies for the case of 30% damage are illustrated in Figure 7.11. The damage indices are clearly increased near the location where the pipe's rigidity is decreased. At a first glance, the reader may not appreciate the difference in the indices obtained by the various methods. However, if for example, we plot the indices obtained from the FFT (as shown in the insert of Figure 7.11), the difference between the indices can be seen more clearly. Furthermore, the slight difference (the shift) between the results from WPT and Wavelet is due to the nature of the tree structures in WT and WPT. Otherwise, the locations of the baby wavelets within the trees create the difference. Figure 7.12 also presents the summary of the results in the form of variation in the damage indices as a function of various percentiles of degradation extent, as predicted by the four methodologies.

7.6.3 Case 3: Detection of partial damage around the circumference of the pipe

To date, most research works (Melhem and Kimhas, 2003; Wei *et al.*, 2004; Qin and Zhong, 2004) have considered the effect of damage within the full depth of a beam or around the entire circumference of a pipe, since most approaches cannot easily detect relatively small defects (with respect to the overall size of the structure hosting the defect). The purpose of this case study is to demonstrate the ability of the proposed approaches in detecting partial damage around the pipe's circumference. For this, three different pipes, each having a different size defect, are examined. The first pipe has a defect around the entire circumference, in the second pipe the defect

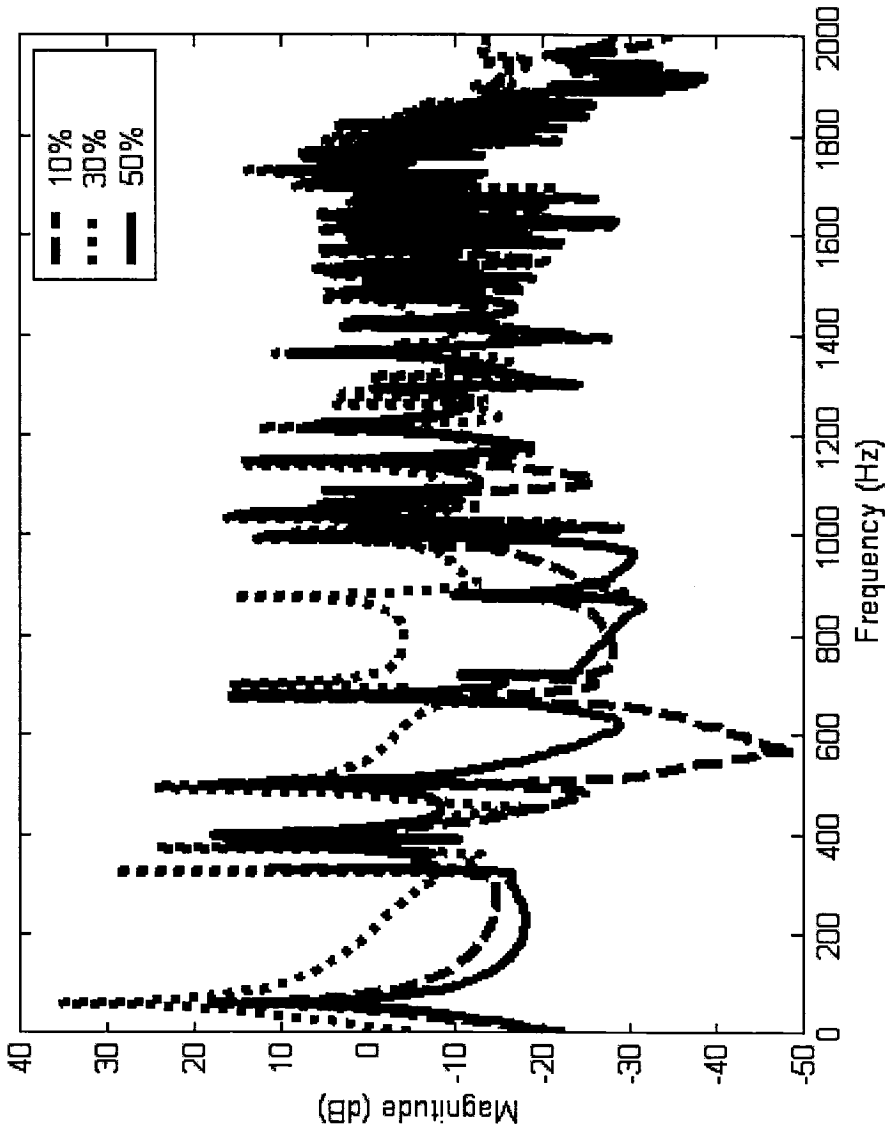

Figure 7.10. Comparison of the FRF responses for the pipe with 10%, 30% and 50% reduction in its flexural rigidity.

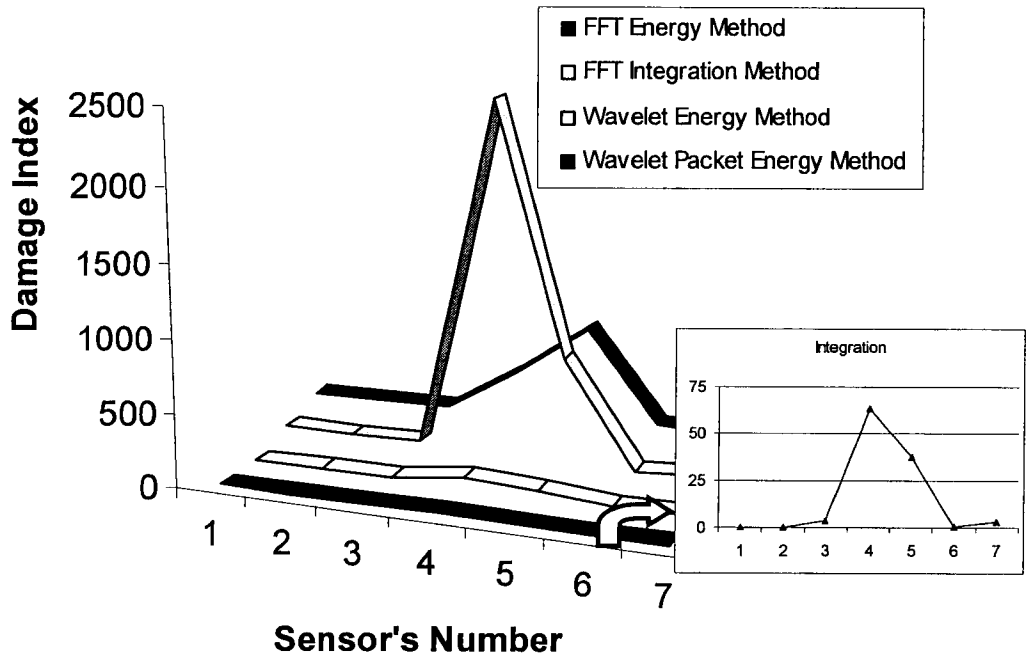

Figure 7.11. Comparison of variation in damage indices (as a function of axial direction) for the pipe with 30% reduction in its flexure rigidity obtained by the FFT, FFT integration, WT and WPT methods (for case study #2).

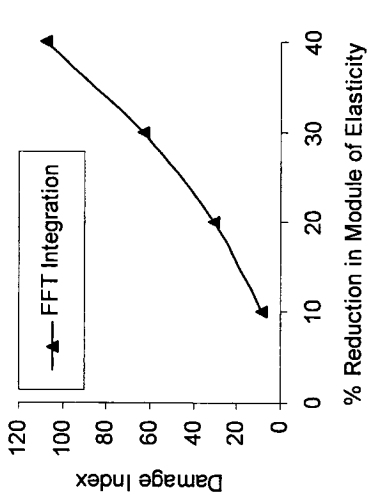
FFT Integration
Damage Index
% Reduction in Module of Elasticity
0
20
40
60
80
100
120
0
10
20
30
40

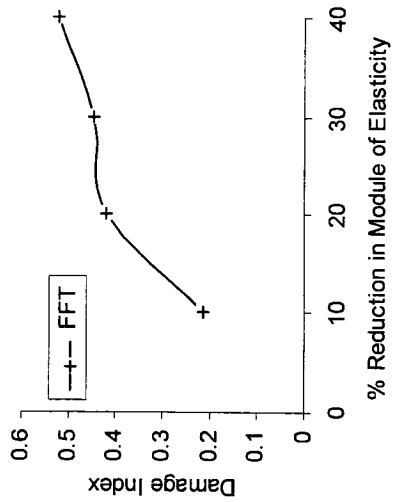
FFT
Damage Index
% Reduction in Module of Elasticity
0
0.1
0.2
0.3
0.4
0.5
0.6
0
10
20
30
40

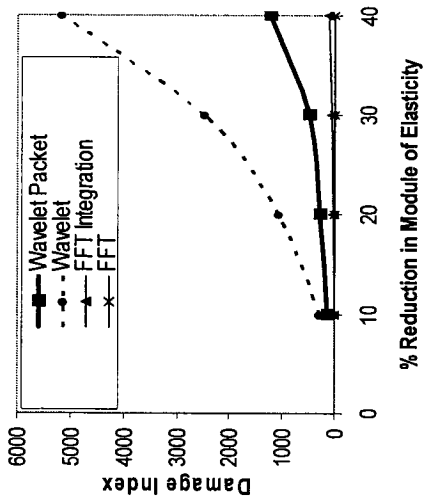
Wavelet Packet
Wavelet
FFT Integration
FFT
Damage Index
% Reduction in Module of Elasticity
0
1000
2000
3000
4000
5000
6000
0
10
20
30
40

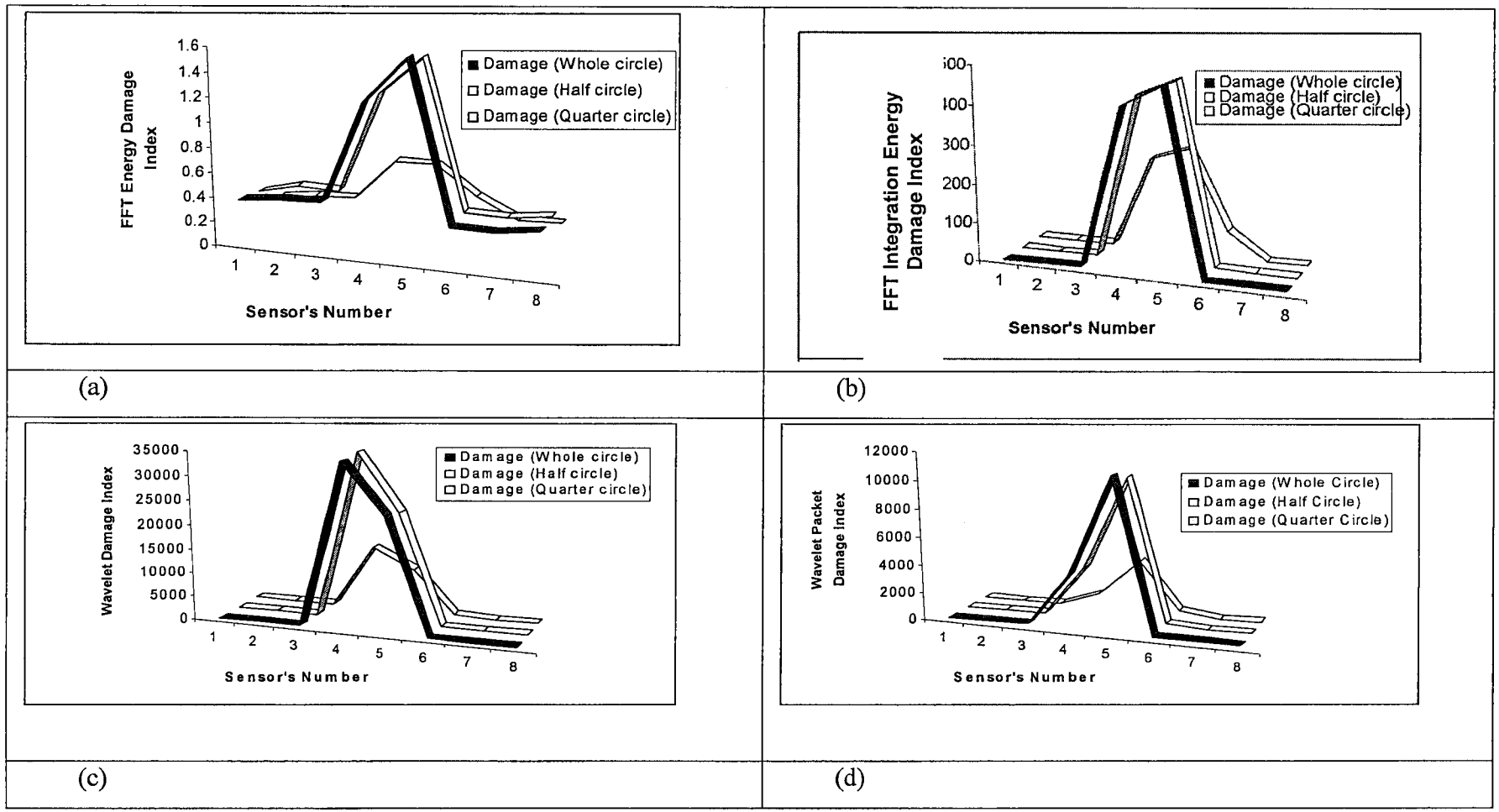

Figure 7.13. Comparison of variation in damage indices (as a function of axial direction) for the pipe with damage around a ¼, ½ and full circumference obtained by the FFT, FFT integration, WT and WPT methods.

7.7 Conclusions

Access to an effective health monitoring system is an important aspect of pipeline maintenance. The availability of an accurate and reliable damage detection system can significantly reduce the life-cycle cost of a pipeline system. This research introduced a new health monitoring approach based on sensing of vibration response of a pipe using smart piezoelectric transducers, and then evaluating the vibration response of the pipe using the data obtained by the transducers. In conjunction with the use of three-dimensional piezoelectric FE analysis, a novel approach was proposed for evaluating the "damage energy indices" established based on the Fast Fourier transform and wavelet transform methodologies. The damage indices can reveal the location of the defect. Case studies were considered to evaluate the integrity of the proposed methodologies. For this, cantilevered pipes having various forms of defects were examined. The defects were assumed to be at various locations, having different intensities (i.e., in the form of reduction of wall thickness to simulate a reduction in stiffness due to presence of corrosion). The numerical results confirm that the proposed approaches could effectively identify the existence and intensity of defects in the pipes. Among the FFT energy, FFT integration, wavelet energy and wavelet packet energy methodologies, the wavelet transform proved to be the most sensitive methods in detecting the location and intensity of the damage.

7.8 Acknowledgement

The financial support of the Atlantic Innovation fund, as well as NSERC granted to the third author in support of this work, is gratefully acknowledged.

7.9 References

Ayres, J. W., Lalande, F., Chaudhry, Z. and Rogers, C. A., 1998. "Qualitative impedance-based health monitoring of civil infrastructures", Smart Mater. Struct. 7, 599-605.

Bhalla, 2000. "Smart system based automated health monitoring of structure", Master of Engineering Dissertation Nanyang Technological University, Singapore.

Fuller, C. R., Snyder, S. D., Hansen, C. H. and Silcox, R. J., 1990. "Active control of interior noise in model aircraft elegies using piezocermatic actuators", Paper 90-3922, AIAA 13th Aeroacoustics Conference, Tallahassee, FL

Giurgiutiu, V. and Rogers, C. A., 1997. "Electromechanical (E/M) impedence method for structural health monitoring and non-destructive evaluation", Proc. 1st Int. Workshop on Structural Health Monitoring (California: Stanford University), 433-44.

Giurgiutiu, V. and Rogers, C. A., 1998. "Recent advancements in the electro-mechanical (E/M) mpedance method for structural health monitoring and NDE", Smart Structures and Materials Conf. (San Diego, California), Proc. SPIE 3329, 536-47.

Hu, N. and Fukunaga, H., (2001). "Structural damage identification using piezoelectric sensors", Advanced Nondestructive Evaluation for Structural and Biological Health Monitoring, Proc. of SPIE, 4335,371-382.

Jian, X. H., Tzou, H. S., Lissenden, C. J. and Penn, L. S., (1997). "Damage detection by piezoelectric patches in a free vibration method", Journal of Composite Materials, 31(4), 345-359.

Keilers, C. H. J. and Chang, F. K., (1995a). "Identifying delamination in composite beams using built-in piezoelectrics: Part I-experiments and analysis", Journal of Intelligent Materials Systems and Structures, 6, 649-663.

Keilers, C. H. J. and Chang, F. K., (1995b). "Identifying delamination in composite beams using built-in piezoelectrics: Part II-an identification method", Journal of Intelligent Materials Systems and Structures, 6, 664-672.

Keilers, C. H. J. and Chang, F. K., 1993. "Damage detection and diagnosis of composite using bull-in piezoceramics", Proceeding of SPIE-The International Society for Optical Engineering Smart Structures and Intelligent Systems, 1917, 1009-1015.

Majumdar, P.M. and Suryanarayan, 1988. "Flexural vibrations of beams with delaminations", Journal of Sound and Vibration 195, 977-993.

Mallat S., 1999. Wavelet Tour of Signal Processing (Wavelet Analysis & Its Applications), 2nd Edition, Academic Press, California, USA.

Melhem, H. and Kim, H., 2003. "Damage detection in concrete by Fourier and wavelet analysis", ASCE Journal of Engineering Mechanics, 129(5), 571-577.

Newland, D. E., 1993. An Introduction to Random vibrations, spectral and wavelet analysis, John Wiley & Sons, Inc., New York.

Paget, C. A., Grondel, S. and Delebarre, C., 2003. "Damage assessment in composites by Lamb waves and wavelet coefficients", Smart Materials and Struct., 12, 393-402.

Qin, S. R. and Zhong, Y. M., 2004. "Research on the unified mathematical model for FT, STFT and WT and its applications", Mechanical Systems and Signal Processing, 18, 1335-1347.

Rao, S.S., and Sunar, M., (1994). "Piezoelectricity and its use in disturbance sensoring and control of flexible structures: a survey." Appl. Mech. Rev., 47, 113-136.

Reber, K., Beller, M. and Uzelac, N. I., 2002. "How do defect assessment methods influence the choice and construction of in-line inspection tools", Proceeding of the 4th International Pipeline Conference, Calgary, Alberta

Santamarina, J. C., and Dante, F., 1998. Introduction to Discrete Signal and Inverse Problems in Civil Engineering. ASCE Press, Virginia, USA.

Sensor Technology Limited, www.sensortech.ca, 2001

Silcox, R. J., Lefebvre, S., Metcalf, V. L., Beyer, T. B. and Fuller, C. R., 1992. "Evaluation of piezoceramic actuators for control of aircraft interior noise", Proceedings of the DGLR/AIAA 14th Aeroacoustics Conference, Aachen, Germany

Soh, C. K., Tseng, K. K. H, Bhalla, S. and Gupta, A., 2000. "Performance of smart piezoceramic transducers in health monitoring of RC bridge", Smart Mater. Struct. 9, 553-42.

Sonti, V. R. and Jones, J. D., 1996. "Dynamic effects of piezoactuators on the cylindrical shell response", AIAA Journal, 34(4), 795-801.

Sun, F. P., Chaudhry, Z., Rogers, C. A., Majumdar, M. and Liang, C., (1995). "Automated real-time structure health monitoring via signature pattern recognition", Smart Structures and Material Conference (San Diego, California), Proc. SPIE 2443, 236-47.

Chapter 8

A DAMAGE INDEX FOR STRUCTURAL HEALTH MONITORING BASED ON THE EMPIRICAL MODE DECOMPOSITION

N. Cheraghi and F. Taheri*

Publication Status: Accepted to Publish at Journal of Mechanics of Material and Structures, June 2006.

8.1 Abstract

This paper presents two novel damage indices based on the empirical mode decomposition (EMD) and Fast-Fourier integration for identifying structural damage caused by a change in structural stiffness. The paper also demonstrates the effectiveness of proposed damage indices formulated based on a series of coupled mathematical/engineering approaches that are used to reliably and accurately detect damage in pipes. The main approach is based on monitoring the vibration response of pipes using piezoelectric sensors and the first intrinsic mode functions (IMFs). Finite element analysis is used to simulate the response of a healthy pipe, as well as pipes with various size damages. The damages are meant to represent the outcome of local corrosion (damage) with varying reduction in area around the circumference of the pipe. The evaluated damage indices could effectively establish the location of the defects. Moreover, the evaluated energy indices could also distinguish various size defects. To further demonstrate the effectiveness of our proposed damage indices, the results are compared with other effective indices based on wavelet packet and other statistical methods reported in the literature.

* Corresponding author, 1360 Barrington Street, Halifax, Nova Scotia, B3J 1Z1
Tel: (902) 494-3935 Fax: (484-6635) email: farid.Taheri@dal.ca

Keywords:

Damage detection, Empirical Mode Decomposition, Wavelet, Vibration based, health monitoring.

8.2 INTRODUCTION

Today's vital energy resources like oil and gas are transported through pipelines that span through various terrains. Therefore, pipelines are critical elements, and their health and reliability through their designed service life is an important issue for design and maintenance engineers. Ground movement, resulting from natural and unavoidable circumstances, could significantly change the supporting condition of pipelines, thus subjecting them to loads and boundary conditions that would not have been considered during the design phase. Moreover, as pipes age, their materials deteriorate. Therefore, many factors such as corrosion, damage caused by excavation equipment, cracks, and defective welds could severely impact the integrity of pipelines. There are several ramifications resulting from such changes to the original status of the pipe, thus causing massive costly dilemmas for industry stakeholders, including the producers, pipeline operators, regulatory agencies and public. Therefore, establishment of a safe and reliable method for detecting damage in pipeline is an important issue for not one, but several parties.

There are currently several industrially established non-destructive and in-line inspection methodologies available with some success to detect the factors that affect the safe performance of pipelines. Most in-line inspection tools that are available today use either the magnetic flux leakage (MFL) method (Reber et al. 2002) or the ultrasonic guided wave method (Wilkie et al. 2002). On the other hand, Experimental works have also demonstrated the potential of piezoceramic actuators for controlling vibration in cylindrical shell applications (Fuller et al. 1990 and Silcox et al. 1992).

Some of the reasons for using piezoelectric sensors are that they are lightweight, can easily be adhered to components, use little power and are sensitive to small changes in strain and vibration, and are less sensitive to noise, thus are ideal for pipeline applications. Sun et al. (1995) and later Ayres et al. (1998) reported the use of PZT transducers for damage detection on a laboratory sized truss structure and a

prototype truss joint, respectively. The proposed damage detection methods are based on the principle of electromechanical coupling between the host structure and the bonded PZT transducer. Several other workers have also explored the use of piezoelectric patches for detecting damage in structures. A review of damage detection methods using piezoelectric sensors and actuators can be found in Zou et al. (2000), and also in the recent article of Cheraghi et al (2005).

The present work follows the work done earlier (Cheraghi et al., 2005), with its main objective to demonstrate the effectiveness and integrity of two novel damage indices that were developed based on the empirical mode decomposition (EMD) and Fast-Fourier integration for identifying structural damage caused by a change in structural stiffness. A series of coupled mathematical/engineering approaches were used in the development of these indices, which as will be seen, would reliably and accurately detect damage in pipes. The demonstration will be based on the simulation of the response of a healthy pipe, as well as pipes with various size damages by Finite element method. Our cases studies will also demonstrate that the proposed indices could also establish the location of the defects, as well as the relative sizes of the defects.

Comparison will also be made by the results reported in the literature that were established based on the wavelet packet and other statistical methods.

8.3 MODELING AND FORMULATION OF THE PIEZOELECTRIC SENSORS

Various finite element formulations have been presented by several researchers for the assessment of dynamic response of piezoelectric materials. For instance, Tzou and Tseng (1990), and Rao and Sunar (1994) used the following equations to represent the dynamic response:

$$\begin{aligned} [M]\{\ddot{u}\} + [K_{uu}]\{u\} + [K_{u\phi}]\{\phi\} &= \{F\} \\ [K_{\phi u}]\{u\} + [K_{\phi\phi}]\{\phi\} &= \{Q\} \end{aligned} \tag{8.1}$$

where

$[M] = \int_V \rho [N_u]^T [N_u] dV$ is the kinematically consistent mass matrix;

$[K_{uu}] = \int_V [B_u]^T [C^E] [B_u] dV$ is the elastic stiffness matrix;

$[K_{u\phi}] = \int_V [B_u]^T [e]^T [B_\phi] dV$ is the piezoelectric coupling matrix;

$[K_{\phi\phi}] = -\int_V [B_\phi]^T [\varepsilon] [B_\phi] dV$ is the dielectric stiffness matrix;

$\{F\} = \int_V [N_u]^T \{f_b\} dV + \int_{S_1} [N_u]^T \{f_S\} d\Omega + [N_u]^T \{f_c\}$ is the mechanical force vector, and

$\{Q\} = -\int_{S_2} [N_\phi]^T q_s d\Omega - [N_\phi]^T q_c$ is the electrical force vector.

In the above equations, *[M]* is the mass matrix, u is the displacement, ϕ is the electric potential, Q is the applied concentrated electric charges, ρ is the mass density, $[B_u]$ and $[B_\phi]$ are the derivatives of the shape functions, $[N_u]$ and $[N_\phi]$; $[C^E]$, $[\varepsilon]$ and $[e]$ are the elasticity, dielectric and piezoelectric matrices, respectively; f_b denotes the body force, f_s is the surface force, f_c is the concentrated force, q_s is the surface charge, q_c is the point charge, S_1 is the area where mechanical forces are applied, and S_2 is the area where electrical charges are applied. The above matrix equations are written in partitioned form to reflect the coupling between the elastic and electric fields. Equation (8.1) can be condensed to represent the sensor's potential in terms of the sensor displacement in the form:

$$\{\phi_s\} = [K_{\phi\phi}]^{-1} \left(-[K_{u\phi}^T]\{u\}\right) \tag{8.2}$$

8.4 FFT-BASED DAMAGE DETECTION METHOD

All the methods presented here for comparison purposes are based on the assumption that damage is located between two locations that exhibit the greatest damage indices. The selection of these locations is arbitrary. The methodology relies on vibration data obtained through the sensors located on these points. If more than one defect is located in between two sensors, then the methodologies in their present

form could not indicate the existence of more than one defect. However, the methodologies could detect muti-defects, as long as each defect is located in-between a pair of sensors.

The calculation of discrete approximation of FFT of the transient response data can be represented by (Santamarina and Dante 1998):

$$X(\omega)=\sum_{r=0}^{N-1}x(r\Delta t)e^{-i\omega r\Delta t}\Delta t \qquad \Delta t=\frac{T}{N} \tag{8.3}$$

In above Equation, *x(t)* is a periodic function (containing the output of the piezoelectric sensors) with a period of T, N is the total number of samples, $X(\omega)$ is the frequency response of x(t).

The equivalent energy can be represented by:

$$E_{xx}=\int_{-\infty}^{+\infty}|X(\omega)|^2\,d\omega \tag{8.4}$$

The equivalent FFT energy index is assumed to be:

$$FRF\_E_{\omega}=\sum_{\omega}\left|\frac{E_{xx}^{Damaged}}{E_{xx}^{Healthy}}\right|\frac{2}{N}\times 100 \tag{8.5}$$

where $E_{xx}^{Damaged}$ and $E_{xx}^{Healthy}$ are the before and after damage energies in the pipeline, respectively.

This research proposes the integral of the amplitude of the frequency response function (FRF) evaluated over various frequency ranges as a novel quantity, i.e., damage index. The selected frequency intervals should be such that their limits bound the natural frequencies of the original undamaged system, because these are the regions most sensitive to the changes in response to the damage causing parameters.

This integral is then defined by:

$$I_x=\int_{-\infty}^{+\infty}|X(\omega)|d\omega \tag{8.6}$$

The damage index of FFT integration is defined as

$$FRF\ I_{\omega}=\left|\frac{I_x^{Damaged}-I_x^{Healthy}}{I_x^{Healthy}}\right|\times 100 \tag{8.7}$$

where $I_x^{Damaged}$ and $I_x^{Healthy}$ are the integral of pipe's signals at the damaged and undamaged state, respectively.

8.5 WAVELET TRANSFORMATION AND DAMAGE INDEX

8.5.1 The Discrete Wavelet Transform

The following paragraphs provide brief reviews of wavelets and wavelet transformation methodologies with the aim of offering the reader a better perspective of the work carried out in this paper.

Transformation of a signal is just another form of representing a signal; such a transformation, however, would not alter the content of a given signal. In the context of the work presented here, the Wavelet Transform (WT) provides a time-frequency representation of a signal. It was developed to overcome the limitations of the Short Time Fourier Transform (STFT), which is commonly used to analyze non-stationary signals. While STFT provides a constant resolution at all frequencies, WT uses a multi-resolution technique by which different frequencies are analyzed with different resolutions.

While a wave is an oscillating function of time or space and is periodic, wavelets are localized waves. They have their energies concentrated in time or space and are suited for analysis of transient signals. The Fourier Transform and STFT use waves of regular shapes to analyze signals, while the Wavelet Transform uses wavelets of finite energy to do the same. Figure 8.1 schematically illustrates typical FFT and Wavelet waves.

A wavelet analysis is very similar to a STFT analysis. In STFT analysis the signal to be analyzed is multiplied by a window function, while in wavelet analysis the function is multiplied with a wavelet function. However, as shown in the above figure, unlike the STFT, in WT, the width of the wavelet function changes with each spectral component. As a rule of thumb, the WT provides good time resolution but relatively poor frequency resolution at high frequencies; however, when used at low

frequencies, it provides good frequency resolution, but relatively poor time resolution.

8.5.2 WAVELET-BASED DAMAGE DETECTION METHOD

Wavelet packets consist of a set of linearly combined usual wavelet functions. A wavelet packet function has three indices, $\psi^i_{j,k}(t)$, where integers i , j and k are the modulation, the scale and translation parameters, respectively,

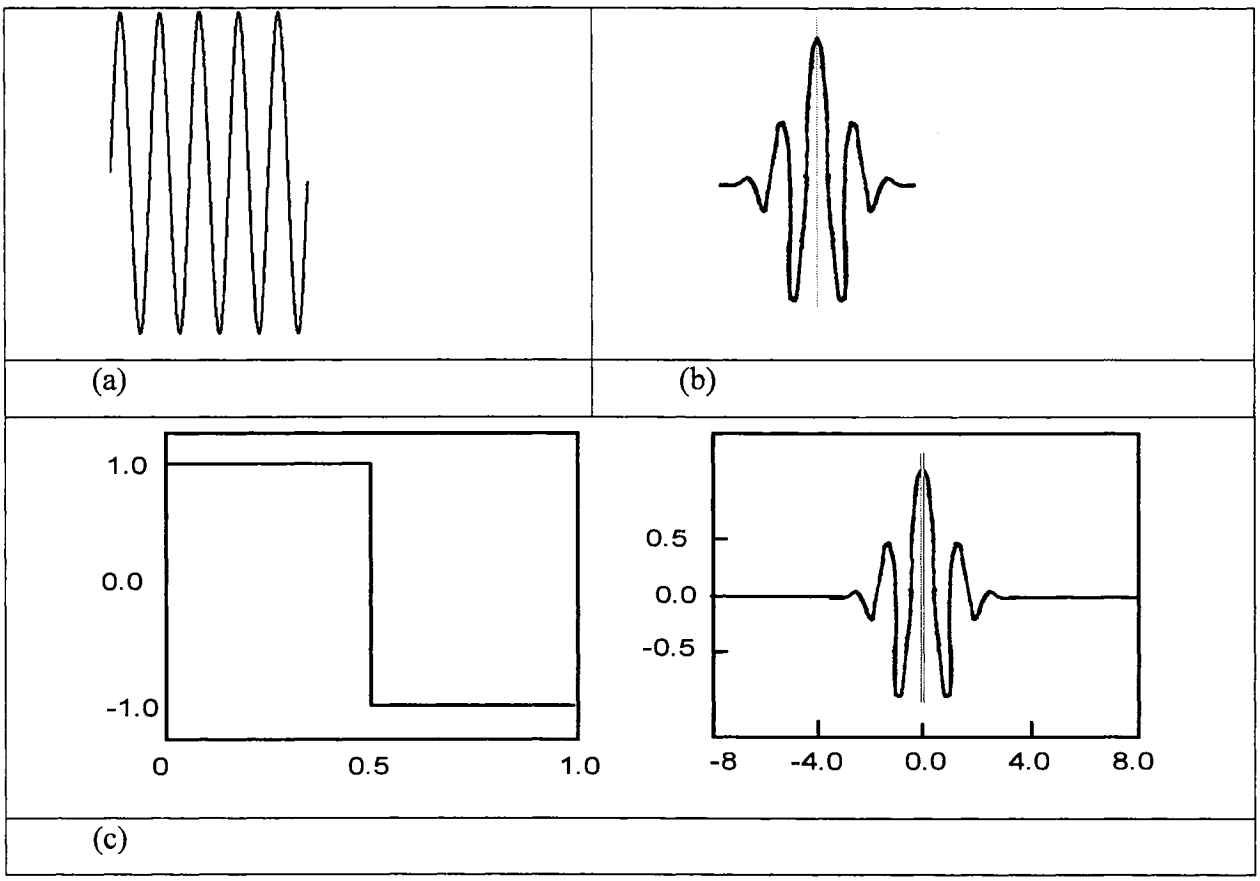

Figure 8.1. Schematics of (a) a typical FFT function; (b) a typical wavelet function; (c) Two different mother wavelet functions: (a) Haar and (b) Morlet Wavelet.

$$\psi^i_{j,k}(t) = 2^{j/2}\psi^i(2^j t - k) \tag{8.8}$$

The wavelets ψ^i are obtained from the following recursive relationships,

$$\psi^{2i}(t) = \sqrt{2}\sum_{k=-\infty}^{\infty} h(k)\psi^{i}(2t-k)$$
$$\psi^{2i+1}(t) = \sqrt{2}\sum_{k=-\infty}^{\infty} g(k)\psi^{i}(2t-k) \tag{8.9}$$

Note that the first wavelet is the so-called mother wavelet function,

$$\psi^{0}(t) = \varphi(t),\ \psi^{1}(t) = \psi(t) \tag{8.10}$$

The discrete filters $h(k)$ and $g(k)$ are the quadrature mirror filters associated with the scaling function $\varphi(t)$ and the mother wavelet function $\psi(t)$. Any measurable and square-integratable function can be decomposed into wavelet packet component functions. The decomposition process is a recursive filter-decimation operation. The decomposed wavelet packet component signals $f_j^i(t)$ can be expressed by a linear combination of wavelet packet functions $\psi_{j,k}^i(t)$ as follows,

$$f_j^i(t) = \sum_{k=-\infty}^{\infty} c_{j,k}^i \psi_{j,k}^i(t) \tag{8.11}$$

The wavelet packet coefficients $c_{j,k}^i(t)$ can be obtained from,

$$c_{j,k}^i = \int_{-\infty}^{\infty} f(t)\psi_{j,k}^i(t) \tag{8.12}$$

Each component in the wavelet packet decomposition (WPD) tree can be viewed as the output of a filter tuned to a particular basis function, thus the whole tree can be regarded as a filter bank. At the top of the WPD tree (lower decomposition level), the WPD yields a good resolution in time domain but a poor resolution in the frequency domain. On the other hand, at the bottom of the WPD tree (higher decomposition level), the WPD results in a good resolution in the frequency domain yet a poor resolution in the time domain. For the purpose of structural health monitoring, frequency domain information tends to be more important and thus a high level of the WPD is often required to detect the minute changes in the signals.

After understanding the basis of WPD, the methodologies used to utilize these signals for structural condition assessment are briefly summarized.

Sun and Chang (2002a) demonstrated numerically, using a three-span bridge, that wavelet packet component energies were sensitive parameters and could be used as structural condition signatures. These component energies were defined as,

$$E_j^i = \int_{-\infty}^{\infty} f_j^i(t)^2 dt \tag{8.13}$$

It can be shown that, when the mother wavelet is semi-orthogonal or orthogonal, the signal energy E_f would be the summation of the j^{th} level component energies as follows:

$$E_f = \int_{-\infty}^{\infty} f^2(t)dt = \sum_{i=1}^{2^j} E_j^i \tag{8.14}$$

Since each wavelet packet component contains information of the signal in a specific time-frequency window, the magnitude of the component energy could therefore vary quite significantly.

8.6 Mathematical Description of Hilbert-Huang Transform (HHT)

The Hilbert transform, $Y(t)$, of an arbitrary function, $X(t)$, in Lp-class (Titchmarsh et al.,1948), is defined by:

$$Y(t) = \frac{1}{\pi} P \int_{-\infty}^{\infty} \frac{X(t')}{t-t'} dt' \tag{8.15}$$

where P indicates the Cauchy principal value. Consequently an analytic signal, $Z(t)$, can be produced by:

$$Z(t) = X(t) + iY(t) = a(t)e^{i\theta(t)} \tag{8.16}$$

where

$$a(t) = [X^2(t) + Y^2(t)]^{\frac{1}{2}}, \qquad \theta(t) = \arctan(\frac{Y(t)}{X(t)}) \tag{8.17}$$

are the instantaneous amplitude and phase angle of $X(t)$.

Since Hilbert transform $Y(t)$ is defined as the convolution of $X(t)$ and $1/t$ by Eq. (8.15), it emphasizes the local properties of $X(t)$, even though the transform is global. In Eq. (8.16), the polar coordinate expression further clarifies the local nature

of this representation. With Eq. (8.16), the instantaneous frequency of $X(t)$ can be defined by:

$$\omega(t) = \frac{d\theta(t)}{dt} \tag{8.18}$$

The method of EMD was recently proposed by Huang (1998b) to decompose a measured response signal $x(t)$ into "intrinsic mode functions" (IMFs) that would admit well-behaved Hilbert transforms. The procedure of EMD is to construct the upper and lower envelopes of the signal by spline-fitting and the average (mean) of both envelopes are computed. Then the signal is subtracted from the mean (the process is referred to as the sifting process). By repeating the sifting process until the resulting signal becomes a monocomponent (i.e., one up-crossing or down-crossing) of zero, it will result in one local peak or (trough), indicating that the number of up-crossings (or down-crossings) of zero is equal to the number of peaks (or troughs). Such a monocomponent signal would then admit a well-behaved Hilbert transform and is referred to as an "IMF". The original signal is then subtracted from the IMF and the repeated sifting process is applied to the remaining signal to obtain another IMF. The process is repeated to obtain n IMFs, that is:

$$x(t) = \sum_{j=1}^{n} c_j(t) + r_n(t) \tag{8.19}$$

in which $c_j(t)$ (j= 1,2, . . . ,n) are the IMFs of the measured signal $x(t)$, and $r_n(t)$ are the residues that could be viewed as the mean trend of the signal or a constant.

The above set of operations is referred to as the EMD method, which has been patented by Huang and his co-workers (1998b, 1999). It has been shown by Huang et al. (1998b, 1999) that the characteristics of the signal could be extracted through the behavior of the IMFs, and that the EMD is applicable to nonstationary or nonlinear signals. Based on the EMD approach described above, the first IMF has the highest frequency contents of the signal. During the EMD process, a specified frequency is referred to as the intermittency frequency ω_{int}, which can be imposed so that the resulting IMF will have frequencies higher than ω_{int} see Huang (1998a). This is

accomplished by removing the data that have frequencies lower than ω_{int} from the IMFs by a straightforward counting process.

The Hilbert-Huang Transform (HHT) method was also proposed by Huang (1998a). It consists of two parts: (i) an Empirical Mode Decomposition (EMD), and (ii) a Hilbert Spectral Analysis. The method is based on decomposing a signal into intrinsic mode functions (IMFs) using the described empirical mode decomposition (EMD) method, with the condition that each IMF admits a well-behaved Hilbert transform. Then, the Hilbert transform is applied to each intrinsic mode function to obtain a decomposition of the signal in the frequency-time domain. This approach is also referred to as the Hilbert-Huang spectral analysis (HHSA) and it is applicable to a non-stationary signal (Huang (1998b), Huang et al. (1999)).

In this paper, the EMD method proposed by Huang (1998a) will be used to decompose the measured response signal (output voltage of the piezoelectric sensors) into IMFs that would admit a well-behaved Hilbert transform. Based on the EMD, the modal response of each mode can then be extracted from the output voltage of a piezoelectric sensor (or any other similar sensors). The key advantage of using the Hilbert Transform with Empirical Mode decomposition (EMD), rather than FFT or wavelet methodologies is that one is enabled to use the instantaneous frequency to display the data in a "time-frequency-energy" format. This would produce a more accurate "real-life" representation of the data, thereby eliminating the artifacts associated with the non-local and adaptive limitations imposed by the FFT or wavelet methodologies. Moreover, the conventional Fourier-based methods are designed to work with linear data or linear representations of nonlinear data; therefore, they are not efficient for studying nonlinear waves and other nonlinear phenomena.

In this paper, a damage index is also introduced that is based on the first (IMFs) of the output voltages obtained through piezoelectric sensors, which are passed through the band pass filter to ensure that they only contain the first natural frequency of the system. The energy of the first (IMFs) is defined as:

$$E = \int_0^{t_0} (IMF)^2 dt \tag{8.20}$$

The damage index is therefore defined as:

$$DI_{mn} = \left| \frac{E_{mn}^{Healthy} - E_{mn}^{Damaged}}{E_{mn}^{Healthy}} \right| \times 100 \qquad (8.21)$$

In the above equation, m is the sensor's number or the considered degree of freedom of structure, n is the mode shape and (IMF) is the first calculated intrinsic mode function of the signal which has been passed through the band-pass criterion.

8.6.1 Band-pass filtering and EMD

The isolation of the modal responses using the EMD method presented above has an advantage in that the frequency content of the signal at each time instant can be effectively obtained. However, the associated computation could be quite involved, in particular when the modal frequencies are high, and/or when the signal is polluted by an elevated noise level. In these cases, in order to obtain accurate modal responses, one should increase the number of siftings in the EMD procedure. Therefore, in order to simplify and decrease the computational efforts, an alternative approach based on the band-pass filter was proposed by Yang et al. (2003). With their proposed method, one could determine the approximate frequency range for each natural frequency from the Fourier spectrum of the output voltage. For example, if one looks at the power spectrum analysis of sensor 3, as illustrated in Figure 8.3, one would see that the first mode is between 60 to 65 Hz. Each signal is then processed through the band-pass filters with a set frequency band. The time history obtained from the jth band-pass filter (jth natural frequency) is then processed through EMD. In this way, the first resulting IMF would be quite close to the jth modal response. By repeating the above procedure for the other natural frequencies, one could then obtain *n* modal responses. In Table 8.2 the result of calculating natural frequency based on EMD method is tabulated. Here we pass all of the output signals of piezoelectric sensors through band pass filter which only has a first natural frequency because our damage index is based on first IMFs of first natural frequency.

8.7 Examples

To investigate the effectiveness of the proposed piezoelectric-based vibrational sensing damage detection methodology for assessing the health of pipeline systems, we investigate the response of aluminum pipes bearing various levels of damage. In

each analysis, the pipe hosts nine piezoelectric patches bonded onto it. The physical and material properties of the pipes, which are made of aluminum, are provided in Table 8.1. Nine PZT BM500 patches with dimensions of 50 mm long, 50 mm wide and 1 mm thick, with mass density of 7650 kg/m^3 were used in this analysis. The material properties of PZT BM500 piezoceramic provided by Sensor Technology Limited of Collingswood, Ontario (2001), are given as:

$$[C^E]=\begin{bmatrix} 12.1 & 7.54 & 7.52 & 0 & 0 & 0 \\ 7.54 & 12.1 & 7.52 & 0 & 0 & 0 \\ 7.52 & 7.52 & 11.1 & 0 & 0 & 0 \\ 0 & 0 & 0 & 2.11 & 0 & 0 \\ 0 & 0 & 0 & 0 & 2.26 & 0 \\ 0 & 0 & 0 & 0 & 0 & 2.26 \end{bmatrix} \times 10^{10}\ [N/m^2] \qquad (8.22)$$

$$[e]=\begin{bmatrix} 0 & 0 & 0 & 0 & 0 & 12.3 \\ 0 & 0 & 0 & 0 & 12.3 & 0 \\ -5.4 & -5.4 & 15.1 & 0 & 0 & 0 \end{bmatrix}\ [C/m^2] \qquad (8.23)$$

$$[\varepsilon^S]=\begin{bmatrix} 8.11 & 0 & 0 \\ 0 & 8.11 & 0 \\ 0 & 0 & 7.349 \end{bmatrix} \times 10^{-9}\ [F/m] \qquad (8.24)$$

where $[C^E]$ is the elasticity matrix, $[e]$ is the piezoelectric matrix and $[\varepsilon^S]$ is the dielectric matrix. The commercial finite element program ANSYS was employed for modeling the response of pipes and the piezoelectric sensors. The three-dimensional coupled element (SOLID5) of ANSYS was used for modeling. The pipes were cantilevered (fully supported in one end, and free at the other end). The mesh density had 40 rows of element along the axial direction, 18 elements along the pipe's circumference, in each row, and two layers through the thickness, as shown in Figure (8.2a). The pipe was assumed to have been impacted at its free end by pendulum, which is simulated by applying a concentrated load with magnitude of 1000N applied in a time interval of 2.5μs. Figure (2d) shows the schematic plot of applied load. Different damage locations, sizes and stiffness reductions (as a damage form) were considered, which will be described in the following sections.

Table 8.1. Geometry and material properties of the pipe.

Outside diameter	273.5 mm
Wall thickness	9.3 mm
Length	2000 mm
Young's modulus	67×10^3 N/mm^2
Poisson ratio	ν=0.33
Mass density	2730 kg/m^3

Table 8.2. Comparison of the computed natural frequencies

Pipe Condition	Modes	FE (eigenvalue) solution (Hz)	FRF solution (Hz)	EMD solution
Healthy pipe	1	62.4	63.8	62.45
	2	339.1	332.1	332.28
	3	379.2	380.1	379.04
Damaged pipe (DL2)	1	62.3	63.7	62.41
	2	333.1	326.6	326.91
	3	377.1	376.3	376.59

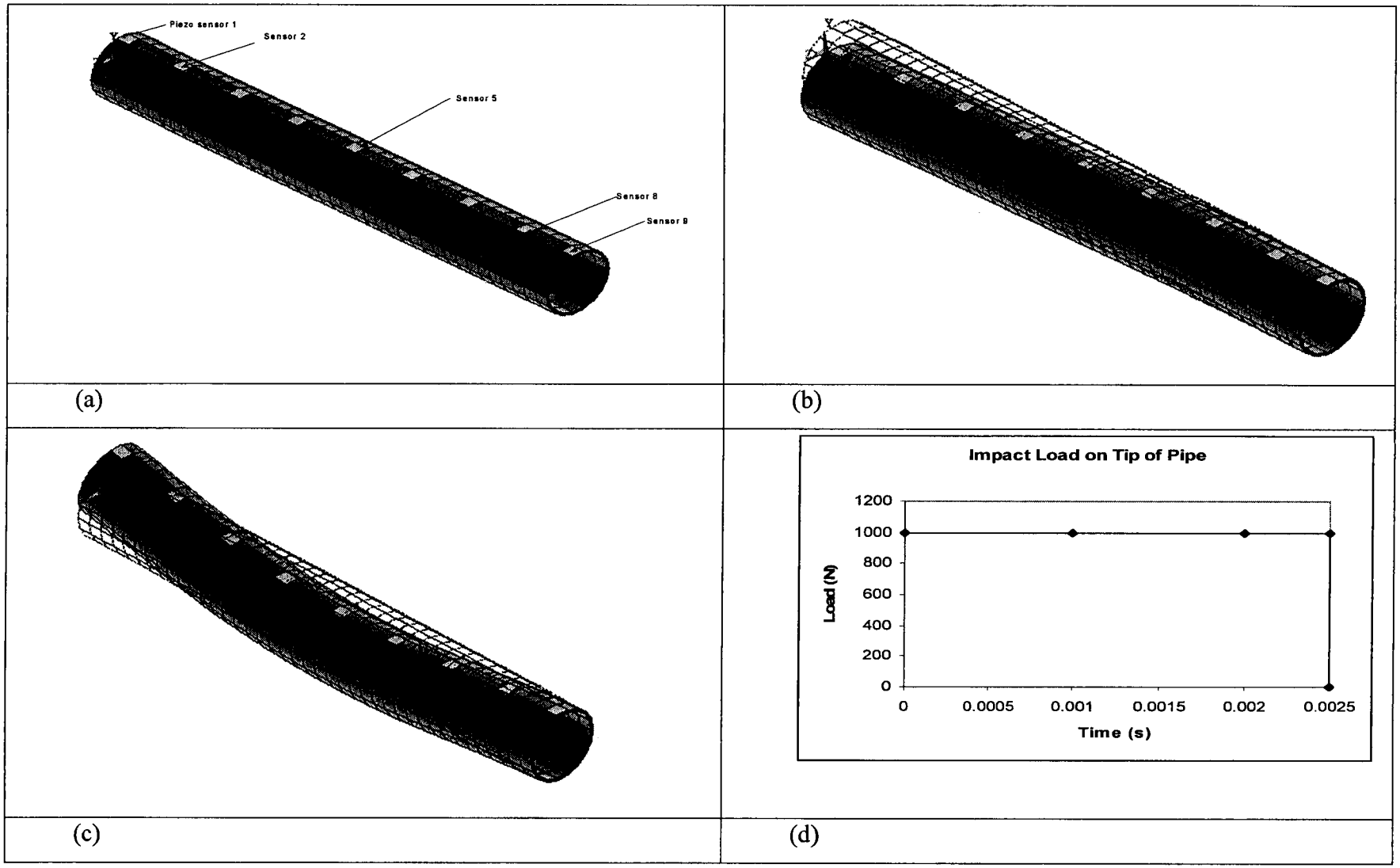

Figure 8.2. Dynamic response of the pipe; (a) FEM mesh, (b) First vibration mode, (c) second vibration mode.

8.7.1 Case 1: Dynamical response of piezoelectric sensors for different damage locations

To evaluate the integrity of the proposed methodologies, three different cantilevered aluminum pipes, each having a damage at different locations along their length, were considered. This form of damage is assumed to result from corrosion, and the subsequent reduction of material at that location. This is simulated by removing one layer (interior layers) element within two rows (i.e., a 100 mm width) off the mesh forming the pipe. The defects are assumed to be located in mid-distance between sensors 2 and 3, sensors 4 and 5, and sensors 7 and 8. These damage locations are referenced as DL1, DL2 and DL3, hereafter. The comparison of the natural frequencies obtained by the FEM (eigenvalue) analysis with those obtained from the frequency response function (FRF) and Empirical Mode decomposition analysis of the sensors for the healthy and damaged pipes (DL2) are tabulated in Table 8.2. Moreover, the first and second mode shapes for the healthy pipe are shown in Figures 8.2(b) and (c). As indicated in Table 8.2, a relatively close agreement among the results obtained from the three approaches is attained, indicating that the sensors' response from a modal analysis could be effectively used to evaluate the dynamic behavior of the system, since there are distinct differences between the two signals. Typical FRF response curves of one of the sensors (sensor 5) for the healthy and damaged pipes are also shown in Figure 8.3. Figure 8.4 illustrates the FRF response curves of sensor 5 for the pipes having damage at three locations (DL1, DL2 and DL3). The response of sensors 2, 4 and 7 when damage located in location 2 (DL2) is illustrated in Figure 8.5. A careful examination of the FRF responses shown in Figures 8.4 and 8.5 indicates that identical piezoelectric sensors, mounted under a similar condition on a pipe, would respond differently depending on the presence and location of damage in the substrate. Figure 8.6 shows calculation of the first and second natural frequencies based on EMD calculations for sensor 6 for the case of DL2. This is a significant observation, in that health monitoring of pipeline systems could be effectively achieved by using an array of piezoelectric transducers. The following section will provide justification for this statement.

Furthermore, wavelet analysis was also applied to the three cases. Specifically, the db4 wavelet and wavelet packet were used to conduct the analyses. Detailed wavelet responses obtained through the analysis of sensor 4 for the healthy and DL2 damaged pipeline cases are shown in Figures 8.7(a) and 8.7(b), respectively; similarly, the information obtained for the wavelet packet analysis is shown in Figures 8.8(a) and 8.8(b). The Empirical Mode Decomposition (EMD) was also applied to the all cases. Detailed results of EMD for calculation of IMFs of sensor 3 for healthy pipe and sensor 6 for DL1 are shown in Figures 8.9(a) and (b). Notice that the wavelet methodology adopted here involves a multi-resolution analysis for a piece of data windowed by shifted and scaled wavelets generated from the so-called "mother wavelet" (Wickerhauser, 1994). Only the higher-resolution details were used to make the above observation. Therefore, to detect a potential damage at a particular point in time would only require a small portion of data neighboring that particular time. This is an attractive feature of this approach and an effective means for on-line heath monitoring of pipelines.

As seen from Figures 8.8 and 8.9, the initial signal has been decomposed to its IMFs and baby wavelets. One could reach the original signal by inversing the process.

The energies components obtained by the FFT, EMD, WT and WPT and EMD are tabulated in Table 8.3. In this table, the WT and WPT energy components are evaluated based on the db3 wavelet at the 4^{th} level decomposition. In the case of the WT approach, the $d_4^a(t)$ and $d_4^d(t)$ component of energies shows sensitivity to damage. However, in the case of the WPT approach, the $d_4^1(t)$ component of energy exhibits more sensitivity to damage.

Figure 8.10 illustrates the damage signatures (damage energy indices evaluated based on the EMD, FFT integration, WT and WPT methodologies at the damage locations) as a function of the sensor number mounted along the axial direction of the pipe for the case where the damage is located in location 2 (DL2). It is observed that all four approaches could detect the defect locations within a range of a pair of sensors. However, it is noted that the WT, WPT and EMD methodologies could predict the damage location more accurately than the FFT methods (i.e. the differences in the energy indices from the sensors have much larger margin in WT and

WPT than in the other methods). The results also confirm the suitability of PZT sensors and their sensitivity in detecting damage in pipelines.

Figure 8.11 (a) illustrates the damage indices based on EMD, WT and WPT as a function of sensor number for the case where the damage is located in location (DL1). Figure 8.11(b) shows the damage indices based on EMD and WPT for the case where the damage is located in location (DL2).

Table 8.3. Comparison of the computed energies for FFT, WT and WPT for the damage case DL2.

Method	Components	$E_{healthy}$ (0-0.25 s)	$E_{damaged}$ (0-0.25 s)	Change (%)
FFT	—	394.2	2426.2	515.5
WT	$d_4^a(t)$	1.2687×10^{-5}	3.9225×10^{-3}	30816.7
	$d_4^d(t)$	8.6086×10^{-7}	2.5979×10^{-5}	2917.8
	$d_3^d(t)$	6.0146×10^{-5}	1.5819×10^{-4}	163.0
	$d_2^d(t)$	5.0762×10^{-5}	8.3846×10^{-5}	65.2
	$d_1^d(t)$	7.2237×10^{-5}	1.2242×10^{-4}	69.5
WPT	$d_4^1(t)$	8.6086×10^{-7}	2.5979×10^{-5}	2917.8
	$d_4^2(t)$	4.6565×10^{-5}	5.9677×10^{-5}	28.2
	$d_4^3(t)$	1.3367×10^{-5}	9.8914×10^{-5}	640.0
	$d_4^4(t)$	8.7762×10^{-6}	1.6786×10^{-5}	91.3
	$d_4^5(t)$	6.8594×10^{-6}	1.3166×10^{-5}	91.9
	$d_4^6(t)$	1.7970×10^{-5}	1.7382×10^{-5}	3.3
	$d_4^7(t)$	1.6655×10^{-5}	3.6173×10^{-5}	117.2
	$d_4^8(t)$	2.8572×10^{-7}	3.6739×10^{-7}	28.6
EMD	-	0.0115	1.0039	8629.56

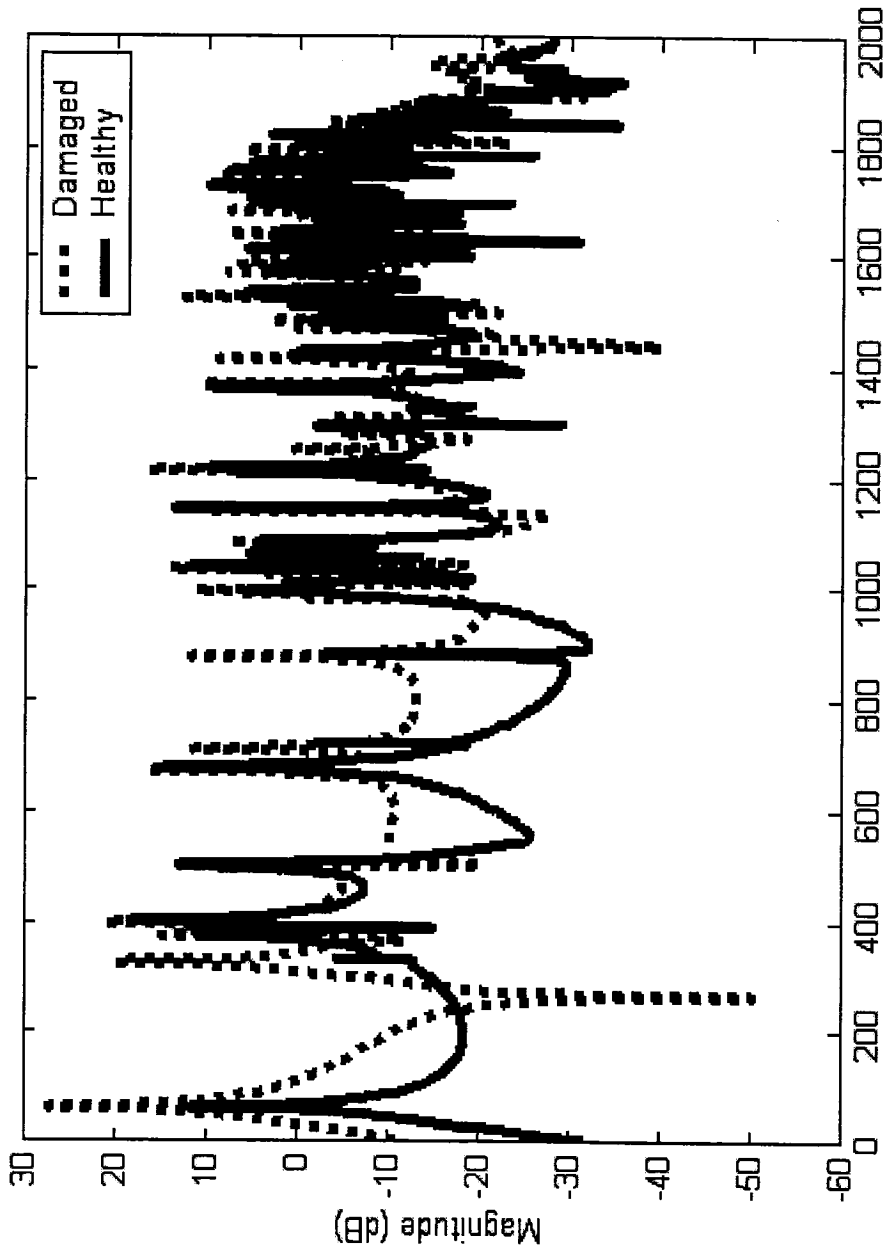

Figure 8.3. Typical FRF response curves of sensor 5 for the healthy and damaged pipes.

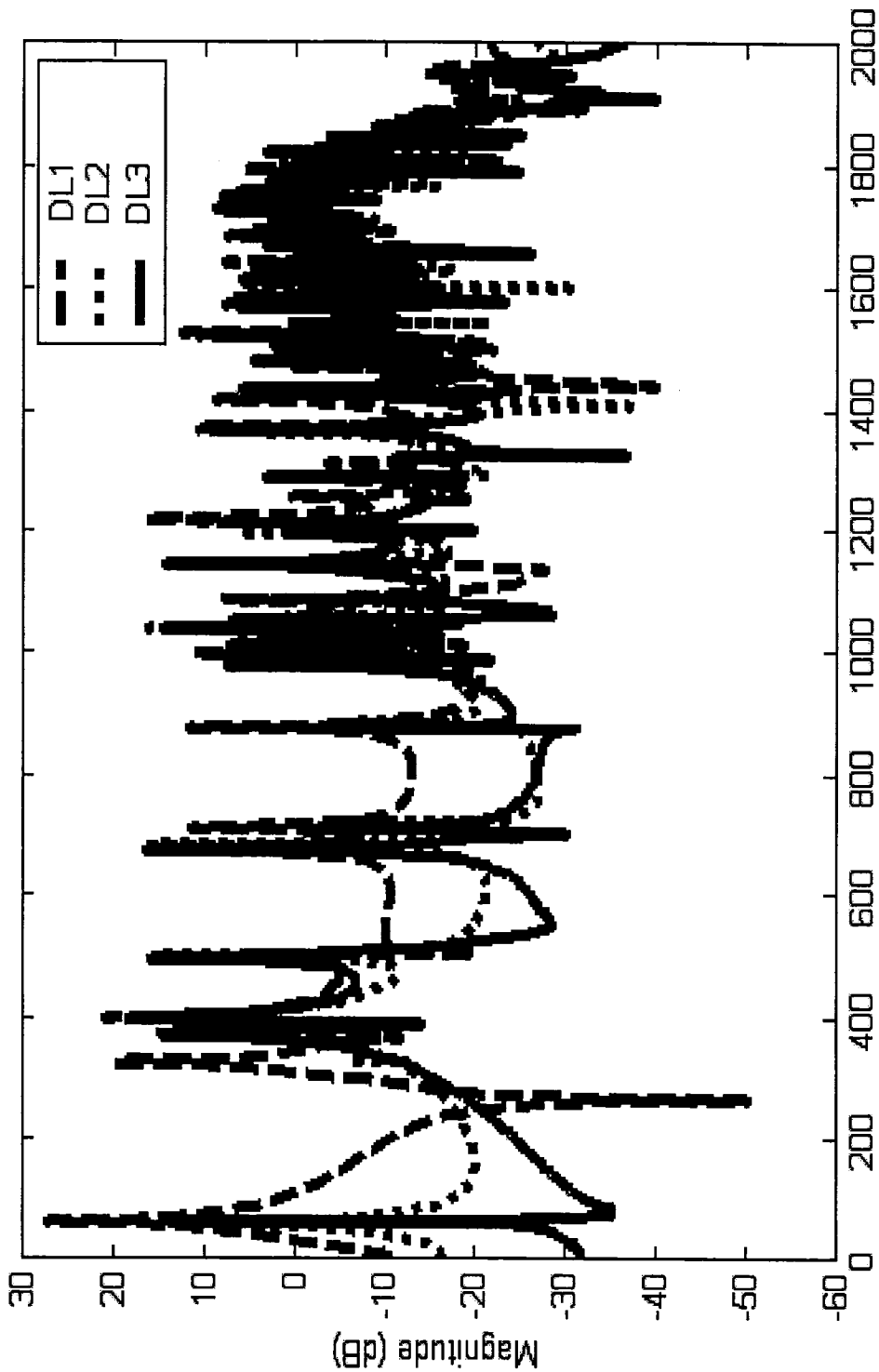

Figure 8.4. Comparison of FRF response for sensor 5 at the damage cases DL1, DL2 and DL3.

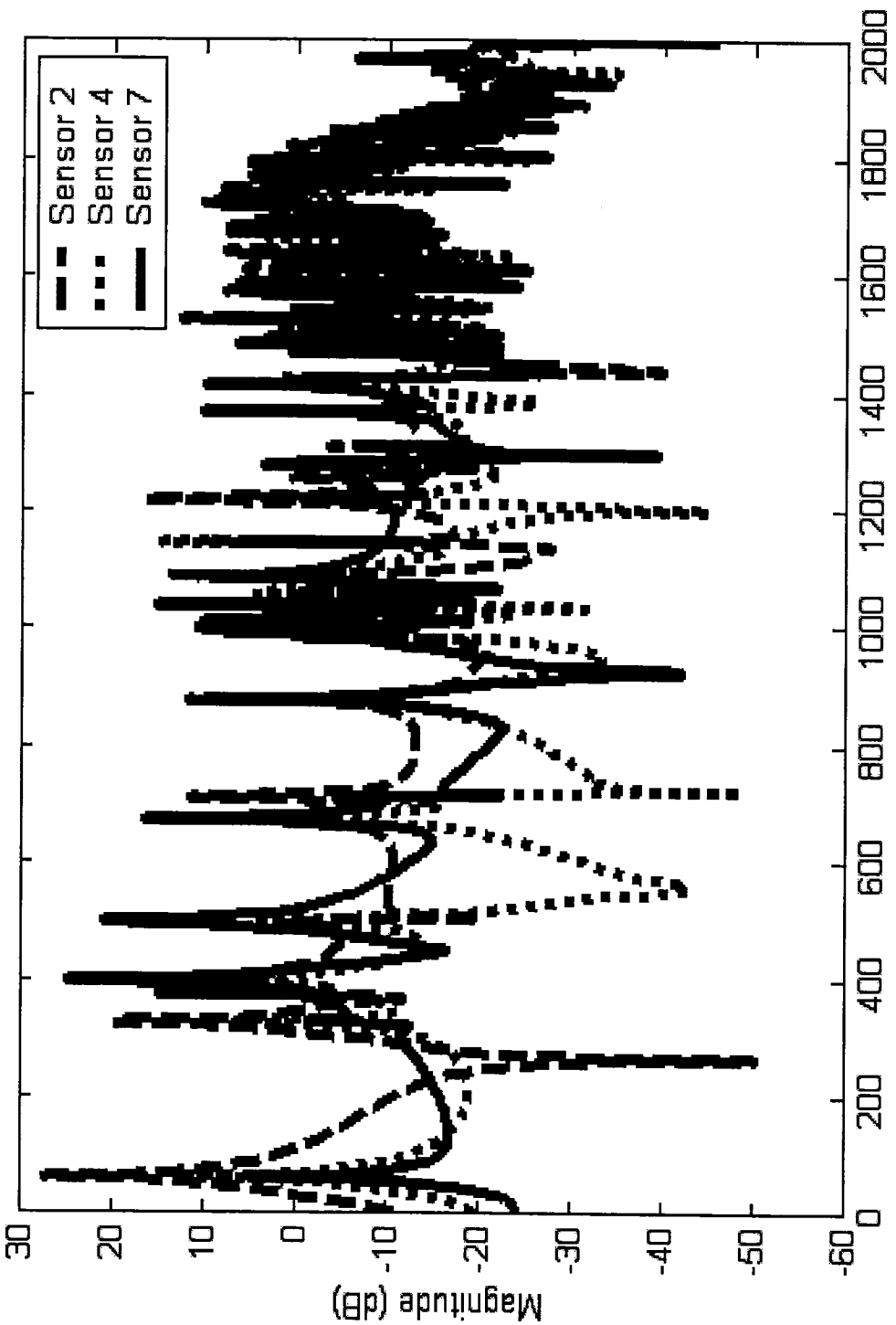

Figure 8.5. Comparison of FRF response for sensors 2, 4 and 7 at the damage case of DL2.

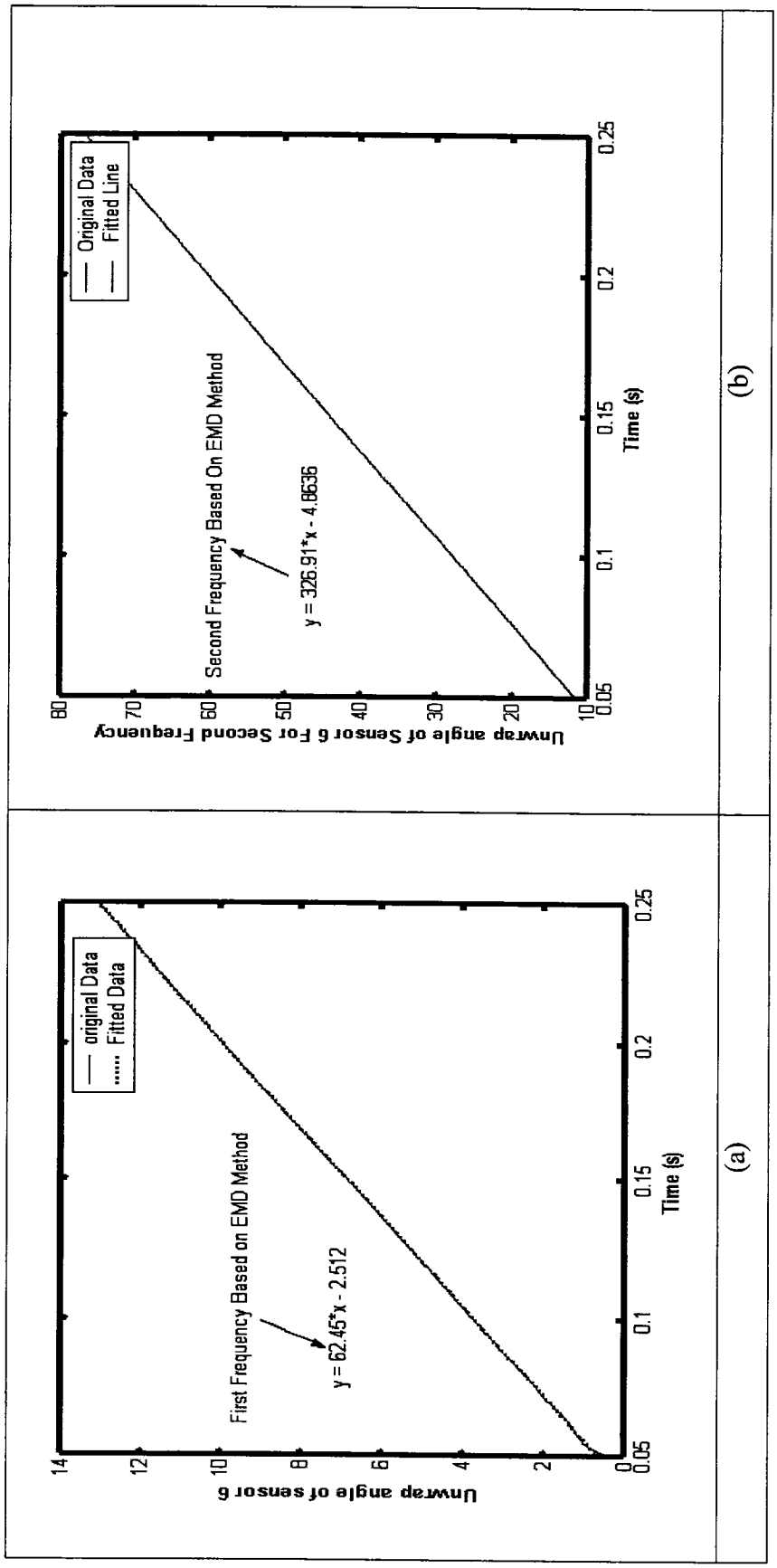

Figure 8.6. Empirical Mode Decomposition (EMD) for calculating first and second natural frequency based on first IMF.

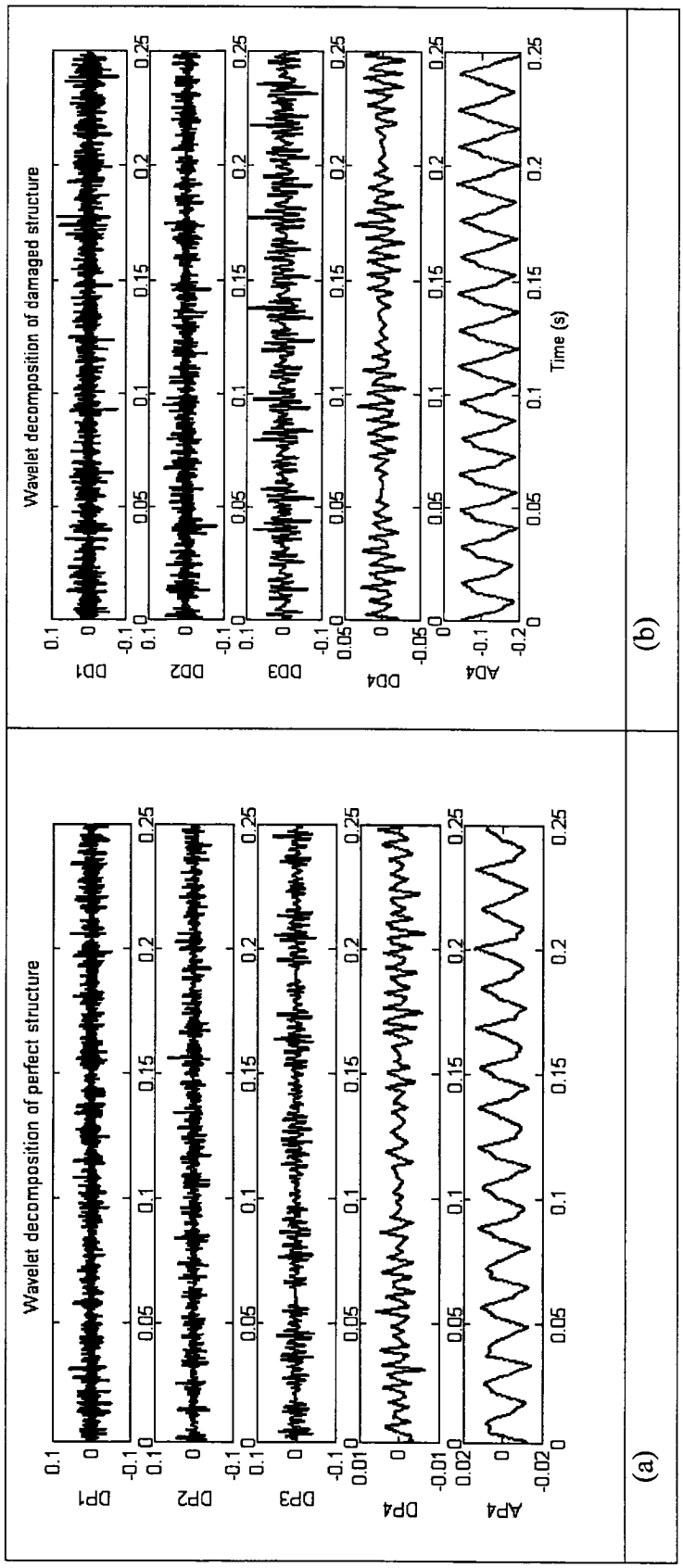

Figure 8.7. Wavelet simulation of (a) healthy pipe, (b) damaged pipe (at DL2).

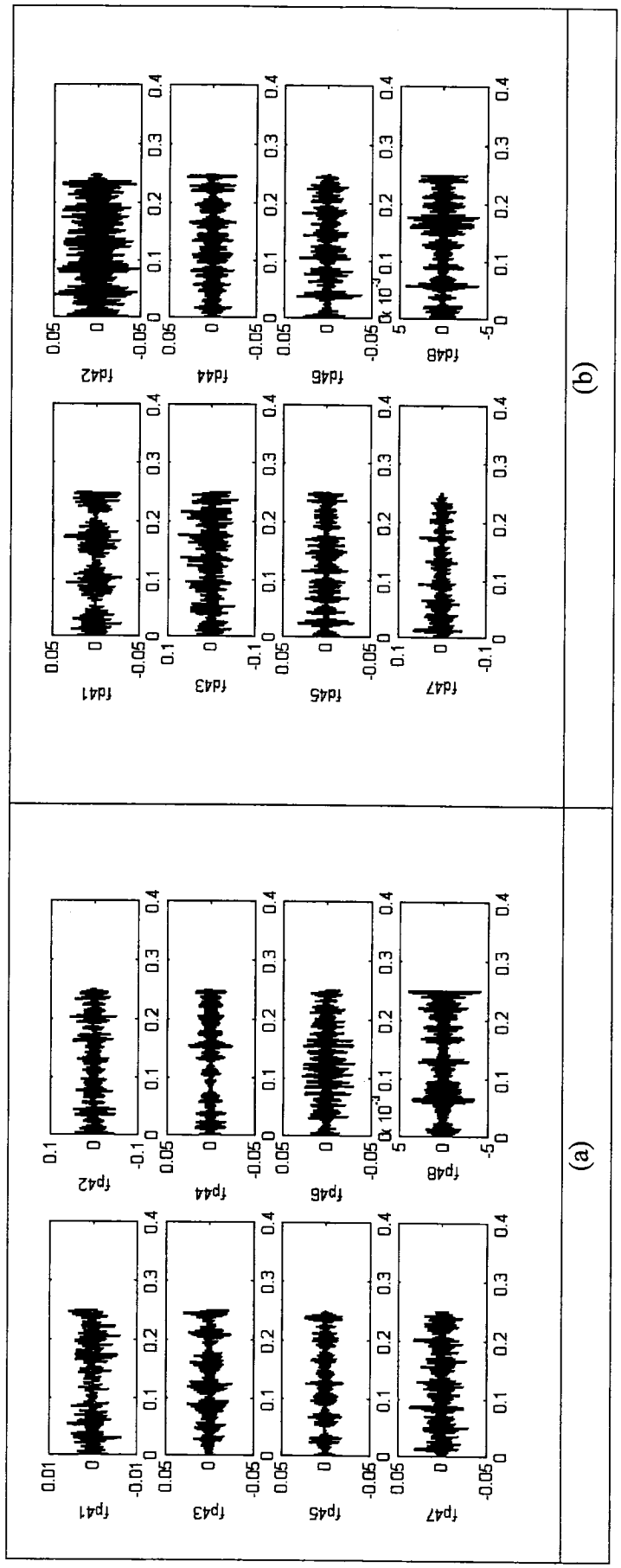

Figure 8.8. Wavelet packet simulation of (a) healthy pipe, (b) damaged pipe (at DL2).

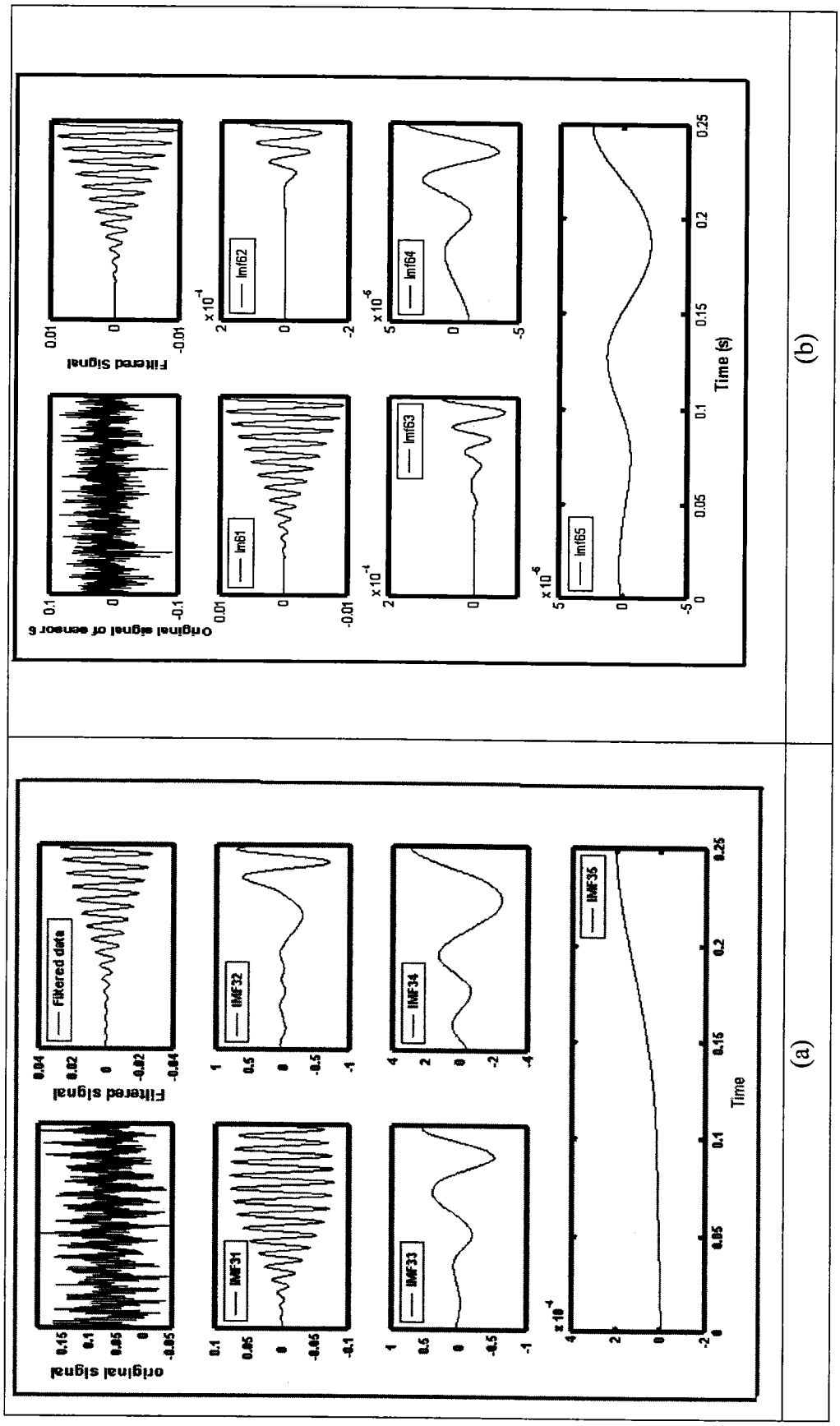

Figure 8.9. Empirical Mode Decomposition (EMD) of (a) healthy pipe for sensor 3, (b) Sensor 6.

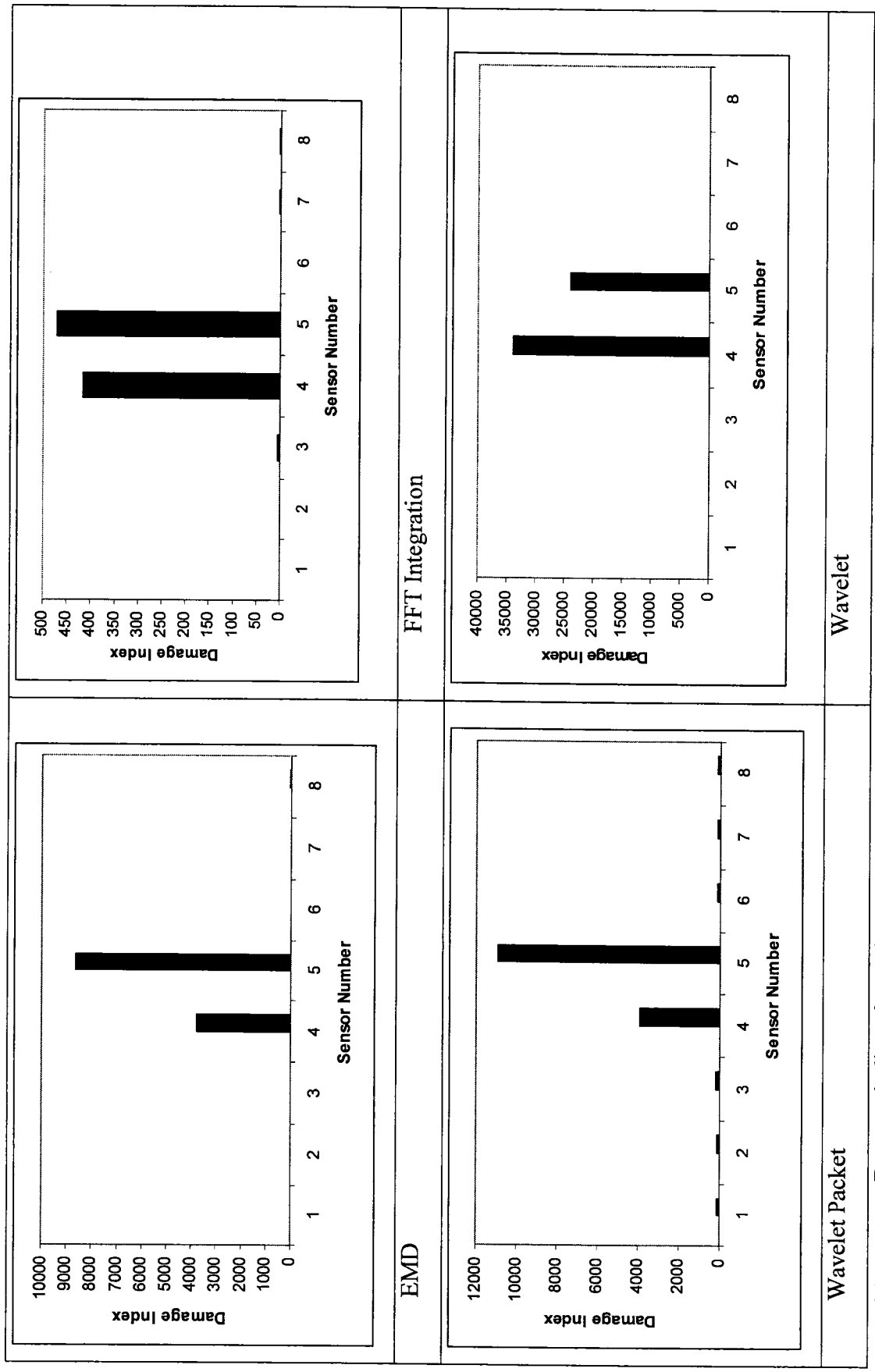

Figure 8.10. Damage indices for various percentiles of degradation based on the four methodologies (DL2).

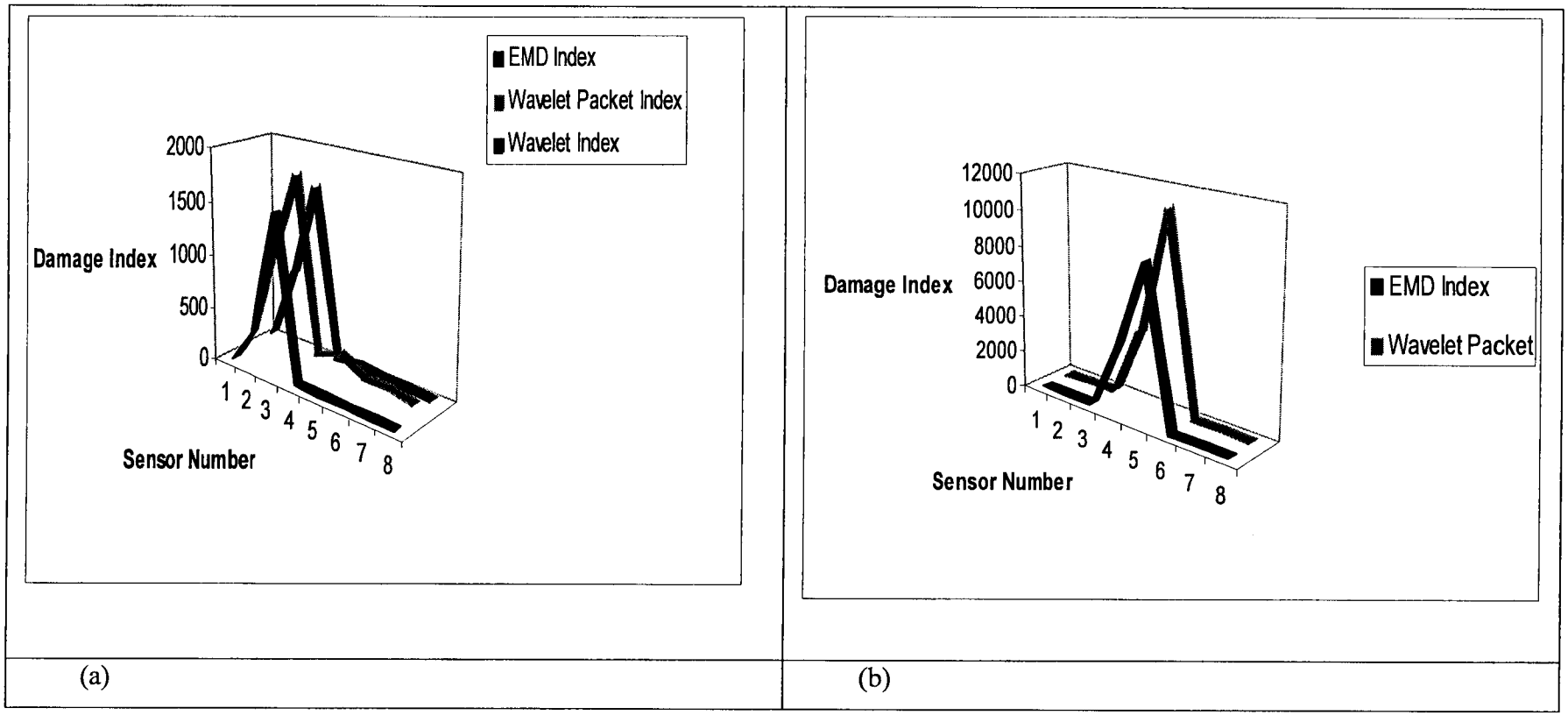

Figure 8.11. (a) Damage index at the damage location DL1 based on EMD,WT and WPT (b) Damage index at the damage location DL2 based on EMD and WPT.

8.7.2 Case 2: Detection of damage due to reduction in flexural rigidity

To further examine the integrity and sensitivity of the selected methodologies, this case study examines a pipe having reduced flexural rigidity in its mid-span, between sensors 4 and 5. This effect was simulated by reducing the Young's modulus of the two rows of elements at the pipe's mid-span. The reduction in flexural rigidity ranges from 10% to 50%, representing different intensities of damage. The comparison of FRF response for the cases of 10%, 30% and 50% reduction in rigidity is plotted in Figure 8.12. The comparison of the damage indices evaluated by EMD, WT and WPT methodologies are illustrated in Figure 8.13. The damage indices are clearly increased near the location where the pipe's rigidity is decreased. As it is clear seen from Figure 8.13, EMD method shows approximately linear function for damage index compare as WT and WPT method.

To summarize, as it is seen from the results of the case studies, the Fourier Transform method and the associated FFTs carry strong *a-priori* assumptions about the source data, such as the linearity and stationariness of the data. Signals associated to natural phenomena are essentially nonlinear and non-stationary. The accommodation of this fact in FFT-based analysis often involves using more data samples to assure acceptable convergence and non-algorithmic procedural steps for the interpretation of FFT results. Wavelet-based analysis may yield some improvement over the FFT because it can handle non-stationary data; however, it retains the limitation of requiring the data set to be linear. Wavelet methods may also prove inadequate, because notwithstanding the fact that wavelet is well-suited for analyzing data with gradual frequency changes, its non-locally adaptive approach causes "leakage". This leakage can spread frequency energy over a wider range, removing definition from data and giving it an overly smooth appearance. Only recently has an alternative view for mechanics, the Hilbert view, and the associated processing tool, the Empirical Mode Decomposition, been proposed.

The HHT, however, allows direct algorithmic analysis of nonlinear and non-stationary data functions by using an engineering and *aposteriori* data processing method, namely an Empirical Mode Decomposition (EMD). This method enables one to perform unconstrained decomposition of the source data function into a finite set of Intrinsic Mode Functions (IMFs) that can be effectively analyzed by the classical Hilbert Transform, thus making the HHT devoid of the FFT limitations.

8.8 Conclusions

Access to an effective health monitoring system is an important aspect of pipeline maintenance. The availability of an accurate and reliable damage detection system can significantly reduce the life-cycle cost of a pipeline system. This research introduced a new health monitoring approach based on sensing of vibration response of a pipe using smart piezoelectric transducers, and then evaluating the vibration response of the pipe using the data obtained by the transducers. In conjunction with the use of three-dimensional piezoelectric FE analysis, a novel approach was proposed for evaluating the "damage energy indices" established based on the Fast Fourier transform, Empirical Mode Decomposition (EMD) and have been compared with wavelet transform methodologies. The damage indices proposed in this paper can reveal the location of the defect. Case studies were considered to evaluate the integrity of the proposed methodologies. For this, cantilevered pipes, having various forms of defects, were considered. The defects were assumed to be at various locations, having different intensities (i.e., in the form of reduction of wall thickness to simulate a reduction in stiffness due to presence of corrosion). The numerical results confirm that the proposed approaches could effectively identify the existence and intensity of defects in the pipes. Among the FFT energy, FFT integration, Empirical Mode decomposition (EMD), wavelet energy and wavelet packet energy methodologies, the EMD and wavelet transform proved to be the most sensitive and effective methods in detecting the location and EMD is to be the intensity of the best method for finding the severity of damage.

8.9 Acknowledgement

The financial support of the Killam Foundation, in the form of a Doctoral Scholarship to the first author is gratefully acknowledged. We also acknowledge the support of the Atlantic Innovation Fund awarded to the second author.

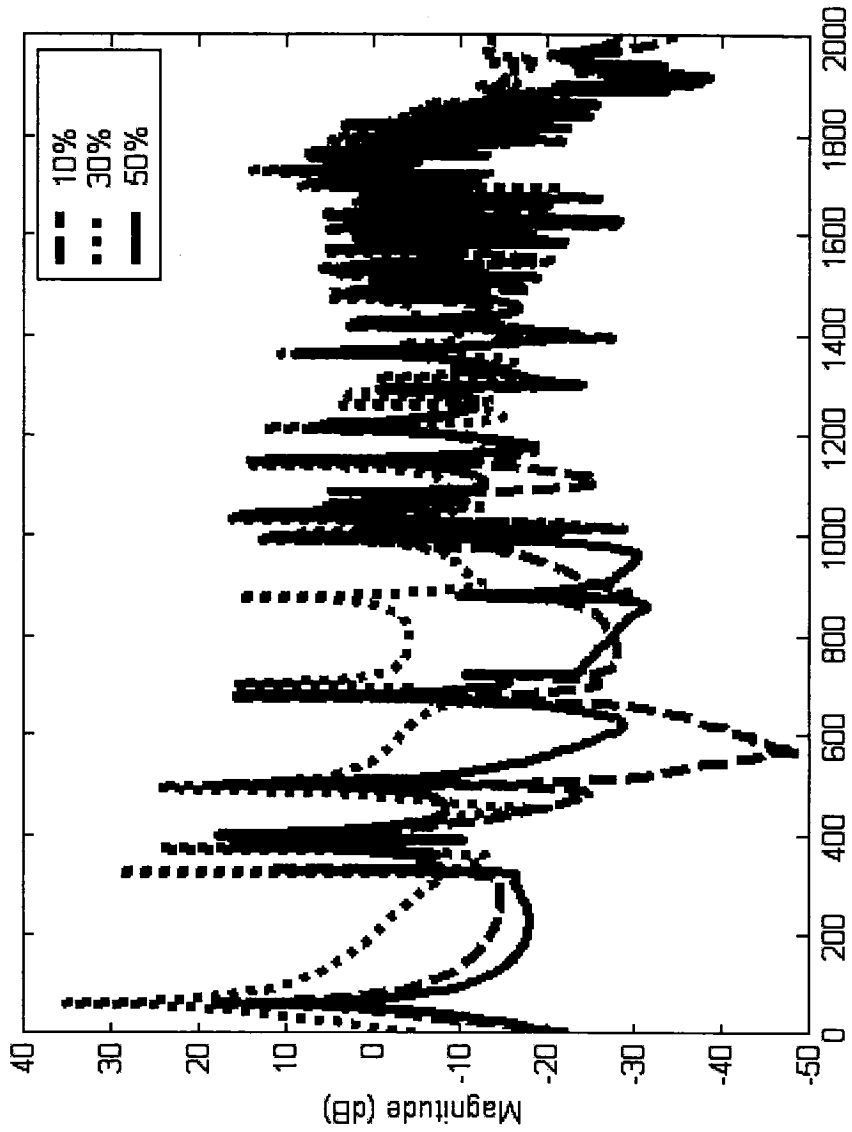

Figure 8.12. Comparison of the FRF responses for the pipe with 10%, 30% and 50% reduction in its flexural rigidity.

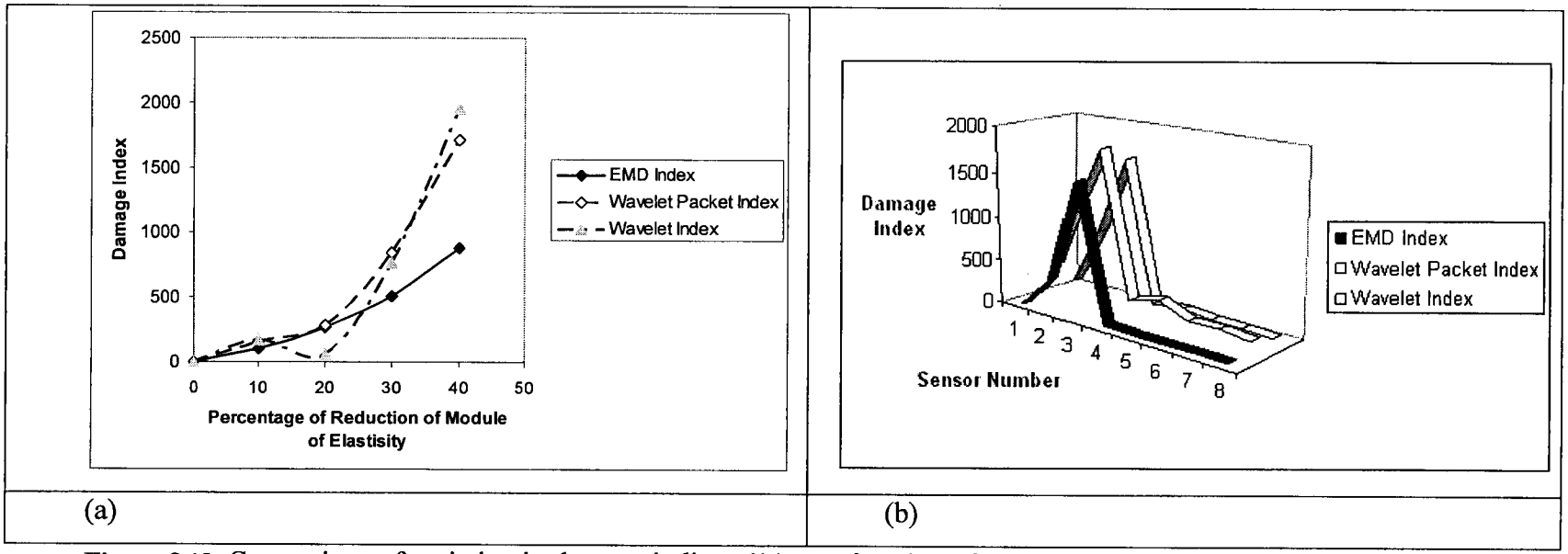

Figure 8.13. Comparison of variation in damage indices ((a) as a function of axial direction for sensor #4, and (b) as a function of sensor number) for the pipe with reduction in its flexure rigidity obtained by the FFT integration, WT and WPT methods (DL1).

8.10 References

Ayres, J. W., Lalande, F., Chaudhry, Z. and Rogers, C. A.., (1998). Qualitative impedance-based health monitoring of civil infrastructures, Smart Mater. Struct. 7: 599-605.

Cheraghi N., Zou G. P. and Taheri F., (2005), Piezoelectric-Based Pipeline Damage Assessment Using Fourier and Wavelet Analyses, International Journal of Computer-Aided Civil and Infrastructure Engineering, 20: 369-382.

Fuller, C. R., Snyder, S. D., Hansen, C. H. and Silcox, R. J., (1990). Active control of interior noise in model aircraft energies using piezocermatic actuators", Paper 90-3922, AIAA 13th Aeroacoustics Conference, Tallahassee, FL

Huang, K., (1998a). A nondestructive instrument bridge safety inspection system (NIBSIS) using a transient load. US patent No. 09=210.693.

Huang, N.E, Shen, Z., Long, S.R., Wu, M.C., Shih H.H., Zheng Q., Yen N-C, Tung C.C., and Liu H.H., (1998b). The empirical mode decomposition and Hilbert spectrum for nonlinear and non-stationary time series analysis. Proceedings of the Royal Society of London—Series A, 454: 903–995.

Huang N.E., Shen Z., and Long S.R., (1999). A new view of nonlinear water waves: the Hilbert spectrum. Annual Review of Fluid Mechanics, 31: 417– 457.

Rao, S.S., and Sunar, M., (1994). Piezoelectricity and its use in disturbance sensoring and control of flexible structures: a survey. Appl. Mech. Rev., 47: 113-136.

Reber, K., Beller, M. and Uzelac, N. I., (2002). How do defect assessment methods influence the choice and construction of in-line inspection tools, Proceeding of the 4th International Pipeline Conference: 2039-2044, Calgary, Alberta.

Santamarina, J. C., and Dante, F., (1998). Introduction to Discrete Signal and Inverse Problems in Civil Engineering. ASCE Press, Virginia, USA.

Sensor Technology Limited (2001) www.sensortech.ca.

Silcox, R. J., Lefebvre, S., Metcalf, V. L., Beyer, T. B. and Fuller, C. R., (1992). "Evaluation of piezoceramic actuators for control of aircraft interior noise", Proceedings of the DGLR/AIAA 14th Aeroacoustics Conference, Aachen, Germany, Number AIAA 92-02-091,pp 542-551.

Sun, F. P., Chaudhry, Z., Rogers, C. A., Majumdar, M. and Liang, C., (1995). "Automated real-time structure health monitoring via signature pattern recognition", Smart Structures and Material Conference (San Diego, California), Proc. SPIE 2443: 236-47.

Sun, Z. and Chang, C. C., (2002) Structural damage assessment based on wavelet packet transform", ASCE Journal of Structural Engineering, 128(10): 1354-1361.

Tseng, K. K. H., Soh, C. K., Gupta, A. and Bhalla, S., (2000). "Health monitoring of civil infrastructure using smart piezoceramic transducers", Proc. 3nd Int. Conf. On Computational Methods for Smart Structures and Materials Conf. (Madrid, Spain, June 2000), 153-62.

Wickerhauser, M. V., (1994). Adapted Wavelet Analysis from Theory to Software, A K Peters, Ltd., Wellesley, MA.

Wilkie, G. H., Elam, T. J., and Engen, D. L., (2002). Comparison of crack detection in-line inspection tools, Proceedings of the 4th International Pipeline Conference, Calgary, Alberta.

Yang, J.N., Lei, Y., Pan, S., and Huang, N.E., (2003) System identification of linear structures based on Hilbert-Huang spectral analysis. Part 1: normal modes, Earthquake engineering and structural dynamics, 32: 1443-1467.

Zou, Y., Tong, L. and Steven, G. P., (2000). Vibration-base model-dependent damage (delamination) identification and health monitoring for composite structures-a review, Journal of Sound and Vibration 230(2): 357-378.

Chapter 9

A NOVEL APPROACH FOR DETECTION OF DAMAGE IN ADHESIVELY BONDED JOINTS IN PLASTIC PIPES BASED ON VIBRATION METHOD USING PIEZOELECTRIC SENSORS

N. Cheraghi, M. Riley and F. Taheri

Publication Status: Submitted to publish at Journal of strain Analysis, May 2006

9.1 ABSTRACT

The use of dynamic response to identify damage and its location in civil engineering structures has been an increasing research focus in the recent years. Most of the available vibration-based damage assessment methods developed till now require modal properties that are obtained via the traditional Fourier Transform. Unfortunately, the Fourier-based modal properties, such as the natural frequencies, mode shapes, etc., have been reported to be insensitive to structural damage and hence are not regarded as suitable damage indicators.

This paper discusses the application of piezoelectric sensors used for evaluation of the integrity of adhesive bonded joints in PVC plastic pipes. A systematic experimental investigation was carried out to demonstrate the integrity of the proposed method in detecting damage in the adhesively bonded joints.

Besides the commonly used methods, a newly emerging time-frequency method, namely the Empirical Mode decomposition (EMD), was also employed. Two Novel "Damage indices" were developed based on the evaluation of vibration signal through piezoelectric sensors with the use of the Empirical Mode decomposition and Fast Fourier integration induced energies. The results have been compared to the available damage index method based on the wavelet packet transformation (WPT), which will be used in the literature review.

As it will be seen, the damage indices could effectively detect the integrity of adhesively bonded joints. Moreover, the energy indices could distinguish the differences among various loads of debonding in the joints.

9.2 Introduction

Adhesively bonded joints, as a primary structural joining method, could be a very efficient method in producing a light weight alternative for joining structural components. There are several advantages in using adhesively bonded joints over the conventional mechanically fastened joints. These include: the involvement of fewer parts; achievement of full load transfer can readily be achieved; the joint would be more fatigue resilient; a complete sealed joint can be obtained as well as a stiffer connection; the joint would be lighter weight with a smoother contour; and, the resulting joint would also be corrosion resistance with minimal stress concentration, since no holes would be present.

However, such joints also have their own disadvantages, such as: the environmental effects can adversely affect the adhesive; limited joint thickness can be achieved; only shear loading is acceptable; the joint cannot be readily disassembled; and, unwanted thermal residual stresses could be generated. As a result, new and improved design methods are needed to account for all influencing parameters. Adhesively bonded joints are also quite susceptible to the surface preparation, which in turn could directly influence the bond integrity. This has required changes in engineering and trade skills for producing quality joints, particularly in regards to surface preparation. Surface preparation is the key for obtaining a high quality adhesively bonded joints. It should be noted that one of the primary problems is that the inspection of the bondline integrity is not a trivial task.

The bondline integrity issue has been a significant "Achilles heel" in the outright acceptance of adhesively bonded joints in most industries. Therefore, the manufacturing processes have been refined to ensure the joint quality. Nevertheless, long-term joint degradation cannot be satisfactorily guaranteed following a damage (i.e. damage resulting impact or corrosion). The two questions to be asked are: how can the quality of the bondline be assessed non-destructively after years of service?

and, does the bondline properties change significantly with time?'. Unfortunately, the currently available Nondestructive Inspection (NDI) techniques do not provide the answers.

A brief discussion of the various NDI techniques available for defect detection in adhesively bonded joints will therefore be first presented to provide the reader with a background to some of the issues involved.

Visual Inspection

Apart from unaided visual inspection, which could only identify some obvious defects, simple magnification can identify quite small surface defects. A dye penetrant can be used to enhance the visualization of adhesive free edge crack. Visual inspection of bondline in free edges would also provide some assessment of the resin flow characteristics. The basic visual inspection method is inexpensive and simple, requiring relatively low skill, but it necessitates access to a clean surface, and the method is only suitable for detecting surface damages. The dye penetrant enhancement technique does, however, contaminate the surface to be inspected, so the component will require both pre- and post-cleaning.

Another visually enhanced inspection technique is that used to check for leaks in sealed structure like pipes, pressure vessels and honeycomb/skin composite panels. The technique is also known as the hot water leak test However, after using the hot water leak test the component requires radiography inspection to disclose any trapped water.

Impedance method

The impedance technique measures the response of the surface of a component to a low-frequency vibration, and is good at detecting debonds. However, a couplant may be required to ensure surface contact. The Fokker Bondtester Guyott et al (1990) is a well-known example of impedance NDI.

Ultrasonic

The implementation of ultrasonic inspection can range from inexpensive (~$3000) to quite costly ($300,000) in terms of the required equipment. The method can provide details of depth and size of the damage, or full details of the topography of sub-surface defects. There are two principal techniques: (i) the pulse-echo (A-scan) and (ii) the through transmission (C-scan); either one is commonly used (B-scan is also another variation of the C-scan ultrasonic scanning technique). Both A- and C-scan techniques measure changes in sound attenuation (amplitude or energy loss) of a reflected or transmitted sound wave. This energy loss is due to the mechanical vibration of the damaged region, and thus, the resulting changes in the attenuation of the transmission.

Acoustic emission

Acoustic emission techniques are based on the operator or an automated equipment detecting changes in sound from a light impact or elastic wave energy disturbances due to crack growth in the component. The component is generally loaded in some manner to initiate damage or grow an existing damage. This loading produces the internal sound from the local adhesive fracture. These emitted sound waves are frequently termed "stress waves". If the damage does not grow, then it cannot be detected. Detection of disbonds in metallic adherend bonded joints is also difficult due to the poor stress wave attenuation in the metal.

Acoustic/sonic (acoustic transmission)

The acoustic transmission technique was developed from a combination of the ultrasonic and acoustic methods to study subtle defects in composite structures, in particular, the strength loss due to moisture absorption and fatigue. It has been used to determine the bondline strength of adhesively bonded joints [Wegmna et al, 1992]. However, this and its indirect measurement of the interlaminar shear strength of composite are still under development. The technique requires an ultrasonic pulse be induced as a stress wave.

This stress wave would then produce acoustic emissions if under the stress the material forms micro cracks.

Microwave

Microwave NDI can be used mainly on non-metallic materials to determine the degree of moisture content through the measurement of microwave absorption. The technique requires two-sided access to the component and the shielding of the metal parts. Operator safety is also a concern, and the component must be cleaned prior to inspection. The application of microwave NDI techniques to adhesively bonded joints has had a very limited success.

Thermography

Thermography is an NDI technique that is used to essentially measure the infrared radiation response of a structure. Thermal energy dissipation (infrared radiation) produces a thermograph. A thermograph is a series of isothermal contour lines that maps the surface temperature, and this information can then be related to the in-plane stress field. When defects are present in the form of traction-free surfaces, then the rate at which thermal energy dissipates is reduced. The methods of applying the heat to the structure are: (i) passive, which uses a heat gun, and (ii) active, that resulting from vibration, which is produced due to the internal friction at the damage site. The resulting heat pattern can be measured in real time with an infrared camera and computer system. These results are in a far-field form and can be related directly to the component stress state [Bakis et al, 1989].

Interferometry

The use of light and its reflective properties to identify defects is the basis of interferometry. There are three basic techniques: Moire, holography and shearography.

Interferometric techniques provide a record of the defects, but are generally not portable. They are very sensitive techniques and show how the structure reacts under loading. However, they do require expensive equipment and need skilled operators

and interpreters. Moire interferometry is used to measure both in-plane and out-of plane displacement (shadow Moire), holographic interferometry measures purely out-of-plane displacement, and shearography measures the first derivative of the out-of-plane displacement, or the slope of the deformation.

Leaky lamb wave

Obliquely orientated acoustic waves have shown a mode change at ply interfaces and adhesive bondlines. These modified acoustic waves travel parallel to the ply interface and bondline. Their properties are affected by the resin-rich layer between plies and the adhesive layer properties. Delaminations and debonds have been easily identified as a result of interrogating the transmitted acoustic wave. Small changes in the adhesive properties (weak bonds) are not presently detectable in a reliable manner. However, the so-called "kissing bond delaminations" or debonds that have intimate contact between the two free surfaces) can be reliably detected using this leaky lamb wave technique [Bakis et al, 1989].

In this research a vibration based method for evaluation of adhesively bonded joints is proposed. Signals collected from any kind of sensors mounted on a structure (from piezoelectric sensors, in our study) cannot be directly analyzed to provide useful conclusions about the damage, unless the damage intensity is very high. The signal should be processed in order to extract useful information about the structural parameters and damage. The signal is often transformed to different domains in order to better interpret the physical characteristics inherent in the original signal. The original signal can be reconstructed by performing inverse operation on the transformed signal without any loss of data. The popular methods in signal processing for SHM applications include the Fourier, Wavelet and Hilbert-Huang Analyses. Each of these methods can be distinguished from each other by the method of mapping the signal and each has its own advantages in terms of applicability for analyzing specific data type.

This paper presents the application of piezoelectric sensors used for the evaluation of the integrity of adhesively bonded joints in PVC plastic pipes based on the analysis of the output voltage of piezoelectric sensors resulting from a vibration excitation.

9.3 FFT-BASED DAMAGE DETECTION METHOD

The Fourier Transform (FFT) based methodology relies on vibration data obtained through various sensors located on various locations of a structure. If there is more than one defect located in between two sensors, the methodologies, at its present status, cannot distinguish one defect from the other one. However, the methodologies can detect muti-defects, as long as each defect is located in between a pair of sensors. This may be considered as a serious drawback in some cases.

It is proposed that the integral of the amplitude of the FRF evaluated over various frequency ranges could be used as a critical quantity, hereafter referred to as, the "damage index". The selected frequency intervals should be such that their limits bound the natural frequencies of the original undamaged system, because these are the regions most sensitive to the changes in response to the damage.

It should be noted that there is no mathematical reasoning as to why the integration of the Fourier term at the location of damage produces a large value. Indeed, if one looks at the time-domain data, there would not be any noticeable change in the signal (with the exception of a minor shift in the signal at the damage location). Nevertheless, the observation of the behaviour of this integration quantity would enable one to detect damage in a system. This integral is defined by:

$$I_x = \int_{-\infty}^{+\infty} |X(\omega)| d\omega \tag{9.1}$$

Where $X(\omega)$ is the Fourier response of the piezoelectric output sensor (voltage) in the time domain. The damage index of integration is defined as

$$FRF\ I_\omega = \left| \frac{I_x^{Damaged} - I_x^{Healthy}}{I_x^{Healthy}} \right| \times 100 \tag{9.2}$$

where $I_x^{Damaged}$ and $I_x^{Healthy}$ are the integrals of pipe's signals at the damaged and undamaged (healthy) state, respectively.

9.4 WAVELET-BASED DAMAGE DETECTION METHOD

The wavelet packets consist of a set of linearly combined wavelet functions. A wavelet packet function is identified by three indices, $\psi^i_{j,k}(t)$, where integers i , j and k are the modulation, scale and translation parameter, respectively, such that:

$$\psi^i_{j,k}(t) = 2^{j/2}\psi^i(2^j t - k) \tag{9.3}$$

where t is time.

The wavelets ψ^i are obtained from the following recursive relationships,

$$\begin{aligned} \psi^{2i}(t) &= \sqrt{2}\sum_{k=-\infty}^{\infty} h(k)\psi^i(2t-k) \\ \psi^{2i+1}(t) &= \sqrt{2}\sum_{k=-\infty}^{\infty} g(k)\psi^i(2t-k) \end{aligned} \tag{9.4}$$

Note that the first wavelet is identified as the mother wavelet function, represented by:

$$\psi^0(t) = \varphi(t),\ \psi^1(t) = \psi(t) \tag{9.5}$$

where $h(k)$ and $g(k$ [Sun et al, 2002] are the discrete filters quadrature, or the mirror filters associated with the scaling function $\varphi(t)$ and the mother wavelet function $\psi(t)$.

It should be noted that any measurable and square-integratable function can be decomposed into wavelet packet component functions. The decomposition process is a recursive filter-decimation operation. The decomposed wavelet packet component signal, $f^i_j(t)$, can be expressed by a linear combination of wavelet packet functions $\psi^i_{j,k}(t)$ as follows,

$$f^i_j(t) = \sum_{k=-\infty}^{\infty} c^i_{j,k}\psi^i_{j,k}(t) \tag{9.6}$$

where $c^i_{j,k}$ is the wavelet packet coefficients and can be obtained by:

$$c^i_{j,k} = \int_{-\infty}^{\infty} f(t)\psi^i_{j,k}(t) \tag{9.7}$$

In above $f(t)$ is the original time domain signal, which in our case is the output voltage of piezoelectric sensors. Each component in the wavelet packet decomposition (WPD) tree can be viewed as the output of a filter tuned to a particular basis function, thus the whole tree can be regarded as a filter bank. At the top of the WPD tree (the lower decomposition level), the WPD would yield a good resolution in time domain, but a poor resolution in the frequency domain. On the other hand, at the bottom of the WPD tree (higher decomposition level), the WPD would yield a good resolution in the frequency domain, but a poor resolution in the time domain. For the purpose of structural health monitoring, frequency domain information tends to be more important and thus a high level of the WPD is often required to detect the minute changes in the signals.

After the identification of WPD, the task would be the determination of the decomposed signals, to be used for the structural condition assessment. By numerically analyzing a three-span bridge [Sun and Chang 2002] demonstrated, that wavelet packet component energies were the parameters sensitive to changes in the structure, and that they could be used as structural condition signatures. These component energies were defined as,

$$E_j^i = \int_{-\infty}^{\infty} f_j^i(t)^2 dt \tag{9.8}$$

It can be shown that, when the mother wavelet is semi-orthogonal or orthogonal, the signal energy, E_f, would be the summation of the j^{th} level component energies, as follows:

$$E_f = \int_{-\infty}^{\infty} f^2(t)dt = \sum_{i=1}^{2j} E_j^i \tag{9.9}$$

Since each wavelet packet component contains information of the signal in a specific time-frequency window, hence the magnitude of the component energy could vary quite significantly.

9.5 Mathematical Description of Hilbert Huang Transform (HHT)

The Hilbert-Huang Transform (HHT) method was proposed by [Huang et al, 1998]. It consists of two procedures: (i) an Empirical Mode Decomposition (EMD), and (ii) a Hilbert Spectral Analysis. With EMD, any complicated data set can be decomposed into a finite and often a smaller number of intrinsic mode functions.

In this method the signal is decomposed into intrinsic mode functions (IMFs) using the empirical mode decomposition (EMD) method, such that each IMF admits a well-behaved Hilbert transform. The Hilbert transform is applied to each intrinsic mode function in order to produce decomposition of the signal in the frequency-time domain. This approach is also referred to as the Hilbert-Huang spectral analysis (HHSA) and it is applicable to any non-stationary signal [Huang et al 1998 and 1999]. In this paper, the EMD method proposed by [Huang et al, 1998 and 1999] is used to decompose the measured response signal (in the case of our investigation, the output voltage of the piezoelectric sensors), into IMFs that would admit a well-behaved Hilbert transform. Based on the EMD, the modal response of each mode can be extracted from output voltage of a piezoelectric sensor.

The procedure of EMD starts with constructing the upper and lower envelopes of the signal by spline-fitting and then the averages (mean) of both envelopes are computed. The signal is then subtracted from the mean; this process is referred to as the sifting process. By repeating the sifting process until the resulting signal becomes a monocomponent; that is, the up-crossing or (down-crossing) of zero would result in one local peak or trough, this indicating that the number of up-crossings, or down-crossings of zero is equal to the number of peaks or troughs. The resulting monocomponent signal admits a well-behaved Hilbert transform and it is referred to as an IMF. The original signal is then subtracted from the IMF and the repeated sifting process is applied to the remaining signal to obtain another IMF. The process is repeated to obtain n IMFs, i.e.

$$x(t) = \sum_{j=1}^{n} c_j(t) + r_n(t) \tag{9.10}$$

in which $c_j(t)$ (j= 1,2, . . . ,n) are the IMFs of the measured signal, $x(t)$, and $r_n(t)$ is the residue, that can be the mean trend of the signal or a constant. Such a process is referred to as the EMD method [Huang et al,1998]. It has been shown by [Huang et al, 1998 and 1999] that the characteristics of the signal can be extracted through the behavior of the IMFs, and the EMD is applicable to non-stationary or nonlinear signals. Based on the EMD approach described above, the first IMF would contain the highest frequency contents of the signal. During the EMD process, a specified frequency, referred to as the intermittency frequency ω_{int}, can be prescribed, such that the resulting IMF will have frequencies higher than ω_{int}, as demonstrated by Huang [5]. This is accomplished by removing the data that have frequencies lower than ω_{int}, from the IMFs, by a straightforward counting process.

At this juncture, a new damage index is proposed, which is based on the first (IMFs) of the EMD procedures, which is obtained by decomposing a measured time domain transform function of the output voltage obtained through piezoelectric sensors, in response to the impact load applied to the structure by a hammer. The energy of first (IMFs) and the proposed damage index is defined by:

$$E = \int_0^{t_0} (IMF)^2 dt \tag{9.11}$$

$$DI_{mn} = \left| \frac{E_{mn}^{Healthy} - E_{mn}^{Damaged}}{E_{mn}^{Healthy}} \right| \times 100 \tag{9.12}$$

In the above equation, m is the sensor's number or the considered degree of freedom of the structure, n is the mode shape number and (IMF) is the first calculated intrinsic mode function of the signal which has been passed through band-pass criterion.

9.6 Experimental Set-up and Instrumentation

There were three different test specimens that were used to evaluate the integrity of the proposed approach in condition assessment of an the adhesively

bonded joint in the PVC pipes. The pipes were IPEX 6" dia PVC sewer pipes, with the section properties reported in Table 9.1. The procedure used to prepare the bonded joints was as follows:

- The pipe sections were cut to the appropriate length using a band saw.
- The surface of the bonding regions was cleaned with isopropyl alcohol to remove dirt.
- IPEX XIRTEC 7 primer was applied to the bonding regions.
- IPEX XIRTEC 11 PVC cement was then applied to the bonding regions.
- The two sections of pipe were slid into one another.
    - For fully bonded pipe the pipe were continuously rotated for approximately 40-60 sec. to ensure that the adhesive was distributed uniformly.
    - For the partially debonded pipe joints, the two pipe sections were carefully inserted into one another to ensure the debonded section (the portions with no adhesive), would not touch one another.
- The pipes were stood up vertically to cure, for a period of 2 hours, to ensure the cement did not run into the unbonded section.

Using the above procedure, three test specimens containing different levels of damage were manufactured. The damage (debond) extents are tabulated in Table 9.1.

Table 9.1: level of Damage in Test Specimens

Test Specimen	**Damage Present**
1	No Damage (Fully Bonded)
2	¾ Circumference Bonded
3	½ Circumference Bonded

The piezoelectric patches implemented in this investigation were QP15N PZT QuickPack strain sensors available from Mide Technology Corporation (Medford, MA). These patches were bonded to the surface of the pipe at the joint region, using

the West System's two-part epoxy. The rationale for the positioning will be explained in the following section. Once the patches were positioned, they were cured for approximately 12 hours under a vacuum, at 20in Hg, to remove air voids and ensure a strong bond. On the test specimens containing damage, piezoelectric sensors were positioned at the center of the damaged section of the joint and at 180^0 around the circumference from that sensor. For the fully bonded pipe, there was only one sensor bonded at the center of the joint.

9.6.1 Preliminary Investigation

Once the bonded joint was cured, a preliminary study was conducted to determine the optimal placement of the piezoelectric sensors. The preliminary study involved monitoring the pipe response with accelerometers for the varying degrees of damage, as noted in Table 9.1, as well as a joint that was just tightly fit, but with no adhesive applied. From the recorded data of the sensors, the natural frequencies were determined and quick modal analysis were performed. It was found that when the sensor was positioned near the joint, minor changes in the natural frequencies were observed (even for the unbonded joint). However, considerable variation in the frequencies (especially in the circumferential mode were observed, when the sensor was positioned on the joint.

9.6.2 Experimental Apparatus and Equipment

To detect the presence of a damage in the adhesively bonded PVC pipe joints, the dynamic response of the pipes were monitored at the joint location using a simply supported beam set-up, as shown in Figure 9.1. The supports of the pipes were setup using 6" cast iron flanges that were fastened to a massive steel platform. In order to fit the pipe section to the supports, a larger IPEX 6" PVC Blue Brute water pipes were milled out to fit tightly over the ends of the pipes. Once the Blue Brute piping sections were fitted to the ends of the pipes, they were clamped into the flanges, as shown in Figure 9.2.

The responses of the piezoelectric sensors were continuously monitored with a multipurpose PCI DT3010 data acquisition card, manufactured by Data Translation

(MA, USA), using a differential channel configuration. The data acquisition programs used to monitor the piezoelectric responses was developed in VEE Pro, which is a visual programming software. 40,000 data points were monitored for each test at a rate of 10 kHz. The computer was equipped with the use of a power conditioner, which helps remove the excessive noise from the system.

The loading of the specimens was applied with a PCB Piezotronics 086B01 impulse hammer. The impulse hammer response was monitored continuously using a DT-24EZ data acquisition card, also manufactured by Data Translation (MA, USA), with a single ended channel configuration. The data acquisition programs used to monitor the impulse hammer response was developed in LabVIEW, with the use of DT-LV Link, which is a software that allows LabVIEW to communicate with the Data Translation products. The signal of the impact hammer was monitored at the rate of 20,000 data at 10Hz. The response of the impulse hammer (being in mV), was amplified with the use of a PCB Piezotronics Inc. series 790 power amplifier. The power amplifier also eliminated most of the noise from the impulse hammer response signal.

9.6.3 Experimental Procedure

Every experiment was conducted by starting the data acquisition systems, then impacting the desired location with the impulse hammer. Three tests were performed for each experimental set-up, to ensure consistency and reproducibility of the results. To ensure all test results were processed in the same time scale, the time lag between the time of impact and the piezoelectric response was measured. The method used to determine the time lag was to monitor both signals with a differential channel set-up, which was performed using a single data acquisition computer. Continuously monitoring the piezoelectric sensor and the impulse hammer responses allowed for the two signals to be monitored simultaneously. It was determined that with this set-up the magnitude of the impulse load would be acquired incorrectly, and as a result this method was not implemented in the full experimental investigation.

To determine the parametric effects of the system, a total of 24 tests were conducted on each specimen. The test parameters that were varied through the

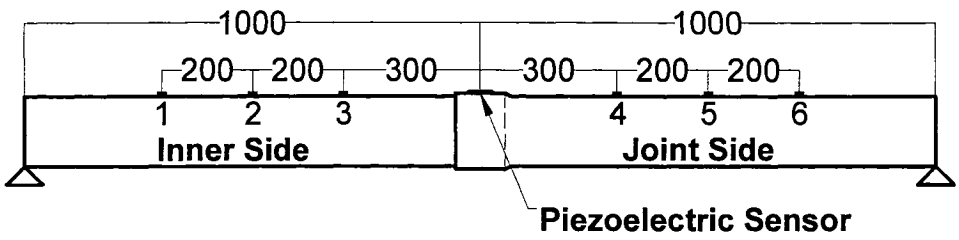

(a)

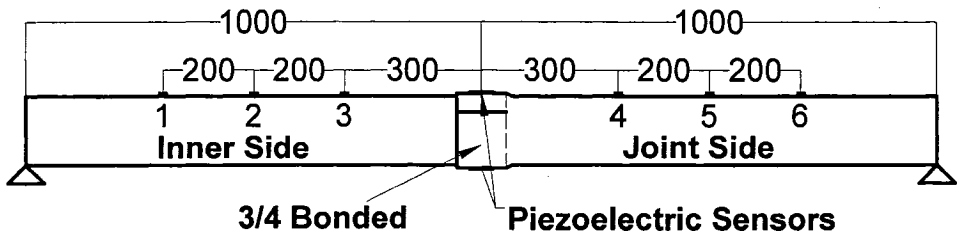

(b)

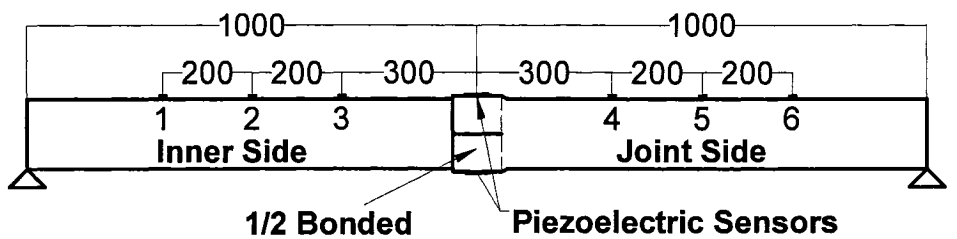

(c)

Figure 9.1: Experimental Test Set-up for Adhesively Bonded Pipe Joints (a) Fully Bonded Joint, (b) ¾ Bonded Joint, (c) ½ Bonded Joint

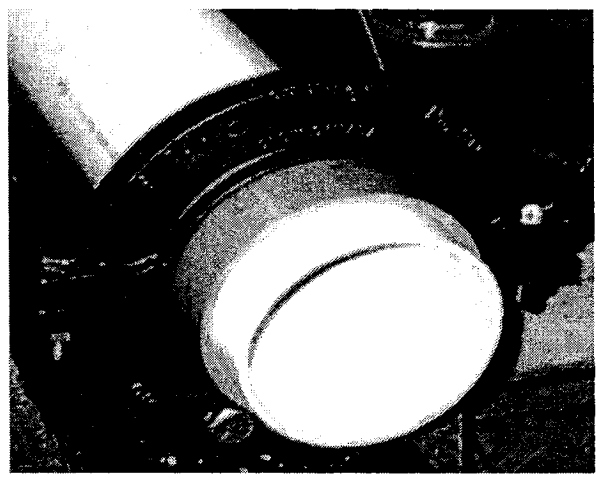

Figure 9.2: Support System for the Adhesively Bonded Pipe Joints

experiments included the load location, support tightness, and debond location. The influence of the loading location on the results were verified by impacting the pipes at six different locations along the length and three locations on each side of the joint as shown in Table 9.2.

Table 9.2: Impulse Hammer Impact Locations (The numbers are in reference to Figure 9.1)

Impact Location Number	Impacted Side	Distance From Joint Center
1	Bottom Side	300 mm
2	Bottom Side	500 mm
3	Bottom Side	700 mm
4	Top Side	300 mm
5	Top Side	500 mm
6	Top Side	700 mm

The fixture tightness was adjusted by varying the torque of the bolts clamping the flange to the pipe section. The two torques used in tightening the supports are shown in Table 9.3.

Table 9.3: Support Fixture Tightness

Fixture Tightness Number	Fixture Bolt Torque
1	84 N.m
2	43.4 N.m

The debonded section of the damaged pipes, or the sensor was located on the fully bonded pipe, was placed in two different positions to determine if the location of the damage affected the damage index (see Table 9.4).

An overview of the various set-up configurations considered is shown in Table 9.5.

9.6.4 Data Processing Methods

Once all tests were completed the results were processed using the MATLAB software. The following procedures were followed:

Table 9.4: Sensor/Debond Experimental Locations

Debond Location Identification Number	Position of Disbond
1	Top
2	Bottom

Table 9.5: Test Set-up Configurations (The Numbers are with reference to Tables 9.2 through 9.4)

Test Number	Parameters (Fixture Tightness, Sensor Location, Impact Location)	Test Number	Parameters (Fixture Tightness, Sensor Location, Impact Location)
1	1,1,1	13	1,2,1
2	1,1,2	14	1,2,2
3	1,1,3	15	1,2,3
4	1,1,4	16	1,2,4
5	1,1,5	17	1,2,5
6	1,1,6	18	1,2,6
7	2,1,1	19	2,2,1
8	2,1,2	20	2,2,2
9	2,1,3	21	2,2,3
10	2,1,4	22	2,2,4
11	2,1,5	23	2,2,5
12	2,1,6	24	2,2,6

9.6.4.1 Removal of Non-Response Data

Due to the experimental procedure, the reduced data had to be filtered and all non-response data removed. Appropriate MATLAB codes were written to remove the non-response data of the piezoelectric sensors for the fully bonded joint and the damaged joints, respectively. Note that, the only difference in the files was the presence of the additional data from the extra sensor used in the damaged pipe joints. The first step in removing the non-response data was to read the experimental response file into the MATLAB programs. The first value greater then the noise level was then located and a set number of data points prior to this value were kept, where the number of points retained was dependent on the time lag. The rest of the data prior to this point, which were considered as non response data (those between time of test initiate and the onset of the actual impact), was removed.

The final step was to remove the non-response data at the end of the file, which was determined visually, having known of the free vibration period of the system.

9.6.4.2 Response of Piezoelectric Sensors for Fully Bonded Pipe

Due to the fully bonded pipe containing only a single piezoelectric sensor, tests were conducted with the sensor located on the top and bottom of the joint. This allowed for the full comparison of all test results since the damaged pipes had two piezoelectric sensors. To save on the preceding computational efforts, the test results for the fully bonded joints were merged according to similar data structure, that is load location and support tightness. This was performed by the MATLAB code, which stored the test results for test set-up 1 and 13, 2 and 14, etc. in the same variables. This stored the response files for the fully bonded pipe in the same format as the damaged pipes, which had the results for sensors on the top and bottom of the joint.

9.6.4.3 Impulse Hammer Response Processing

The removal of the zero state data included removing all the non-response data at the start and end of the test. The start of the test was determined by finding the position where the impulse hammer voltage surpassed a set value, (in these cases, 0.1 volts). The test was then deemed to have started 2 points in time before this value was surpassed, which was found by visually inspecting the results. The actual loading response of the impulse hammer was found to last for approximately 1.5 msec, with the vibration response lasting for approximately 20 msec.

9.6.4.4 Evaluation of Frequency Response Functions (FRF's)

In order to properly analyze the data, the frequency response functions for each individual test is required. For this investigation the frequency response functions were the ratio of the piezoelectric sensors Fourier spectrum divided by the impulse hammer Fourier spectrum.

A MATLAB code was developed to filter the piezoelectric sensor responses, using the Butterworth band pass filter and convert time domain data to frequency

domain. The program is based on the 8192-point fast Fourier transform (FFT) of the piezoelectric sensors, as well as the impulse load function.

The last stage of the process was to calculate the transform matrix, which computed the FRF of the responses. This program normalized the piezoelectric FFT with respect to the impulse load FFT, as described earlier.

9.7 Experimental Results

The frequency response functions, wavelet and EMD analyses of all tests were carried out determined using a MATLAB code that was developed for this research. For all cases, the damage indices were evaluated relative to the undamaged state, as well as to the proceeding state.

9.7.1 Typical Responses

A typical time-history response and corresponding Fourier spectrum for a top surface bonded piezoelectric sensor are shown in Figures 9.3 and 9.4, respectively.

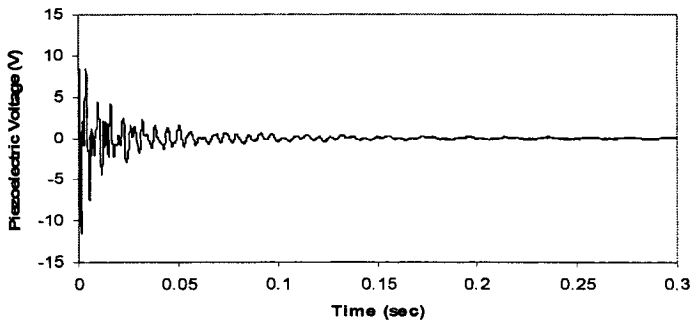

Figure 9.3: Typical Top Surface Bonded Piezoelectric Sensor Time History Response

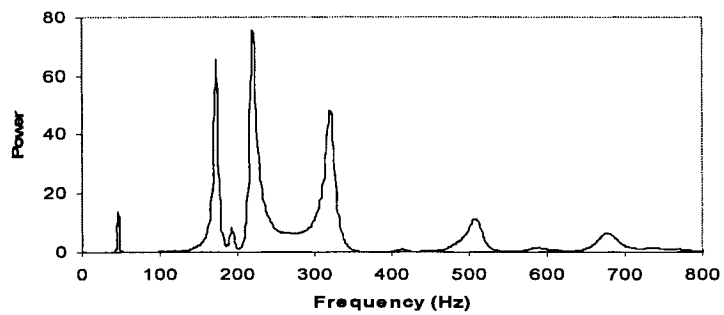

Figure9.4: Typical Fourier Spectrum for Top Surface Bonded Piezoelectric Sensor

Figure 9.5 shows comparison of the frequency response function for the three different degrees of damage.

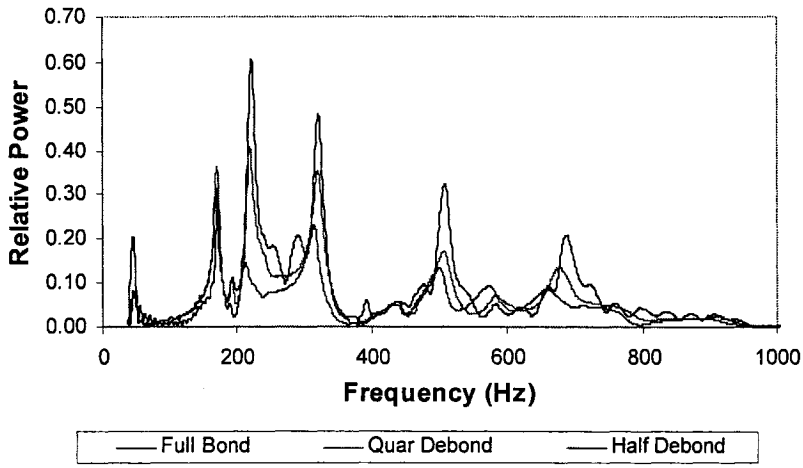

Figure 9.5: Typical Frequency Response Function for Varying Degrees of Damage in Adhesively Bonded PVC Pipe Joint for Top Sensor

Visual inspection of Figure 9.5 reveals that damage is present in the quarter- and half-debonded joint by noticing the significant frequency shifts in most of the natural frequencies. This, however, would not give any indication of the degree of damage within the system.

9.7.2 Influence of Sensor Location

An efficient SHM system is the one with minimum the requirement for complicated and expensive equipment. It would be more desirable to have a robust system that would use as few sensors as possible. It would be most desirable if only one sensor could be used to detect the presence of damage. The best system would then be the one that would use only one sensor, and that one would not have to locate the sensor on the damage region.

The FFT, Wavelet, and EMD damage indices are shown in Figure 9.6 for the two sensors on the half-bonded pipe joint for tests 1-6, respectively. These results are for the case when sensor 1 is located on the disbond section of the joint, and sensor 2 on the bonded section of the joint.

As can be seen from Figure 9.6, the sensor location relative to the damage location does not significantly affect the capability of the system to detect the damage. However, depending on the location of the excitation, varying index magnitudes were observed, as will be discussed in a later section. Also of note is the consistency of the results among the individual sensors for the two conditions monitored. In general, sensors which are located in the inner side (see Figure 9.1) produces more consistent index values.

9.7.3 Degree of Damage

In general, in adhesively bonded joints, damage initiation becomes more likely as the bonded system ages. Therefore, it is of paramount importance, not only to have the capability to determine the presence of damage, but also be able to monitor its growth. In order to verify the integrity and extent of capabilities of the proposed methods, specimens with varying degrees of damage were tested and compared. Figure 9.7 shows the results of the damage indices produced by the three approaches for varying degrees of damage, relative to the zero state damage.

9.7.3.1 Comparison of Damage Indices

Figure 9.8 shows comparison of damage indices for damage in adhesively bonded joints. The Figure shows the indices obtained for the sensors placed on the bonded and debonded regions. It can be seen that the EMD method produced damage indices with larger magnitude than the other two approaches.

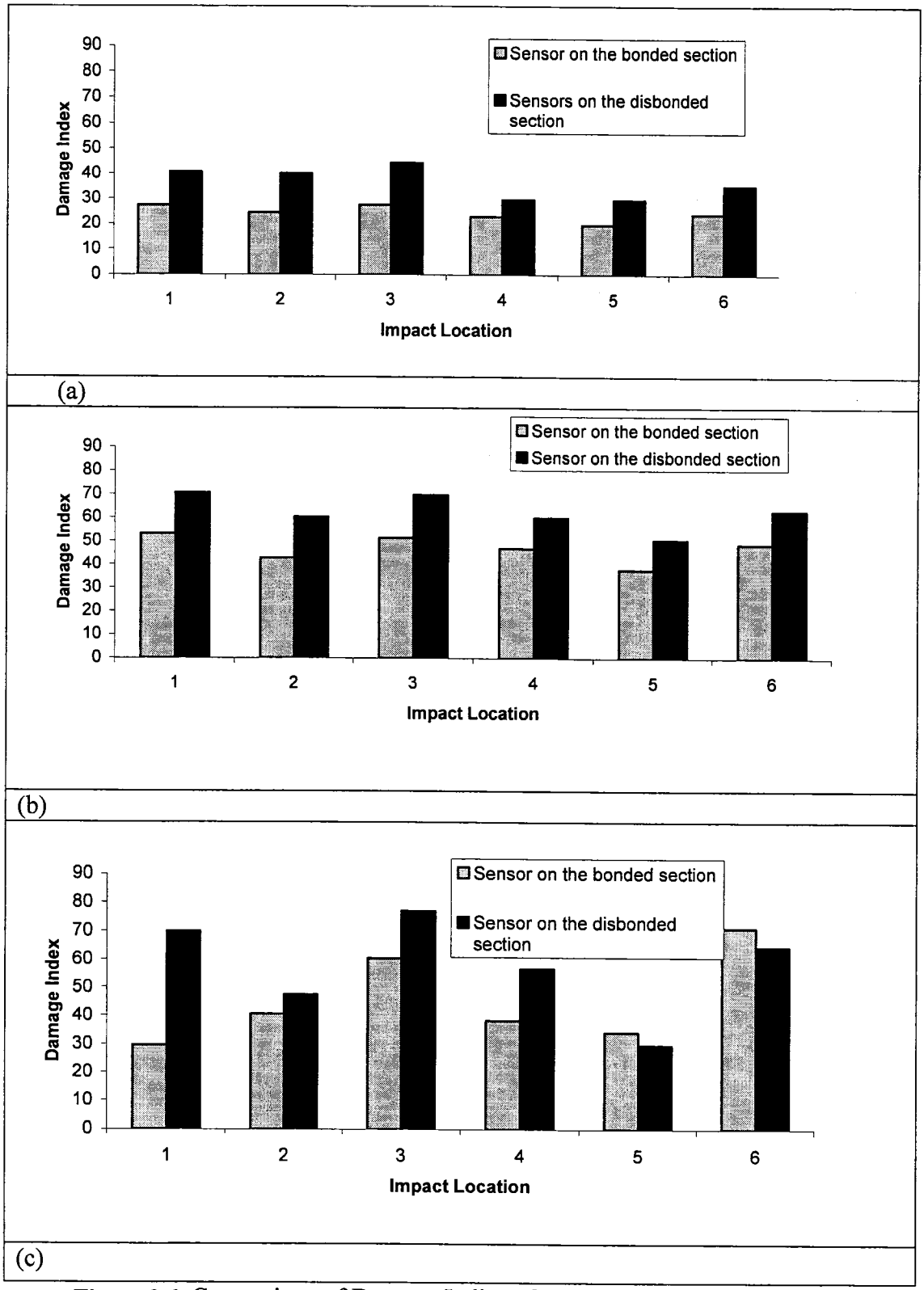

Figure 9.6: Comparison of Damage Indices for Sensors 1 and 2 of the ¾ bonded Joint (a) FFT Index, (b) EMD Index, and (c) Wavelet Index

9.7.4 Influence of Support Condition

During the service life of structures, their boundary conditions may change due to various circumstances. Therefore, it is of great importance to determine whether the proposed methodology could detect the potential changes in the piping system's boundary condition. To determine this influence, two different clamping pressures were applied to the supports as reported earlier in Table 9.3. Figure 9.9 shows the results for sensor 1, data recorded by for the quarter-disbonded joint, for the two different support conditions considered in this investigation.

As the results in Figure 9.9 indicate, the support condition has minor influence on the resulting damage indices. Nonetheless, it further illustrates the robustness of the proposed damage detection system. It is observed that the stiffer the support condition, the more pronounced the damage indices; however, the patterns observed for both support conditions are more or less the same, especially when the wavelet method is employed.

9.8 Conclusions

Access to an effective health monitoring system is an important issue when adhesive bonded joints are used in piping systems. The availability of an accurate and reliable damage detection system can significantly reduce the life-cycle cost of a bonded joint system, especially in piping systems.

This paper introduced a new health monitoring approach based on sensing of the vibration response of bonded joints in PVC pipes using smart piezoelectric transducers. Two novel approaches were proposed for evaluating the "damage energy indices". One was established based on the Fast Fourier transform and the other one based on the Empirical Mode Decompositions (EMD). The results were also compared with a wavelet damage index. The damage indices could distinguish the perfect bonded joint versus the variably disbonded joints. For this, simply supported pipes, having a joint with varying degree of disbond (half and quarter disbond), were constructed. The comparison of the experimental results with those produced by the proposed approaches confirmed the capability of the approaches. An important aspect

of the proposed approach is its robustness, in that if requires the vibration signals from only one sensor. Moreover, it was shown that the sensors located on the debonded section was more sensitive to the disband, hence produced more discrete damage indices, thus more accurate predictions.

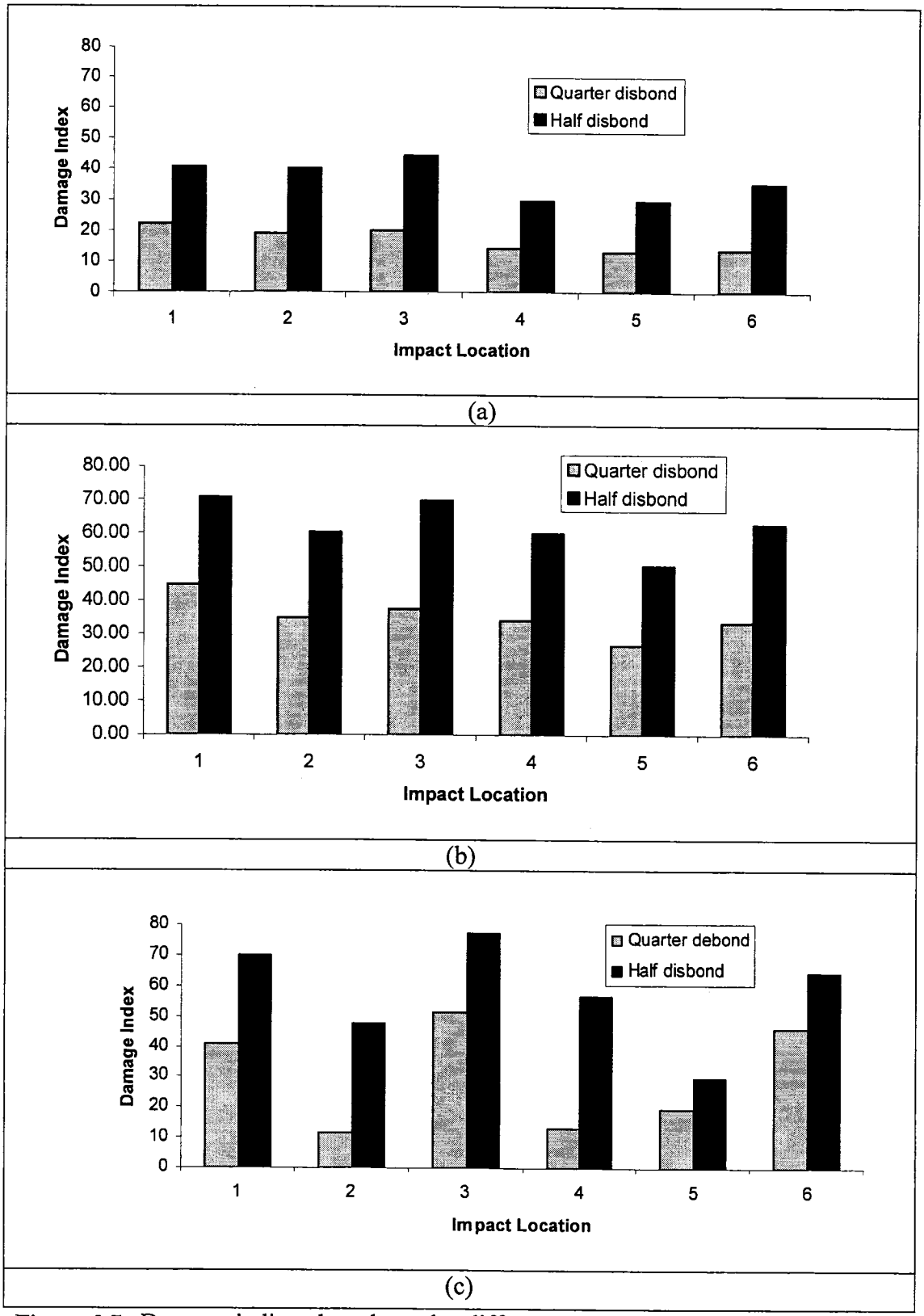

Figure 9.7: Damage indices based on the different methods for different degree of disbond: (a) FFT, (b): Wavelet and (c) EMD.

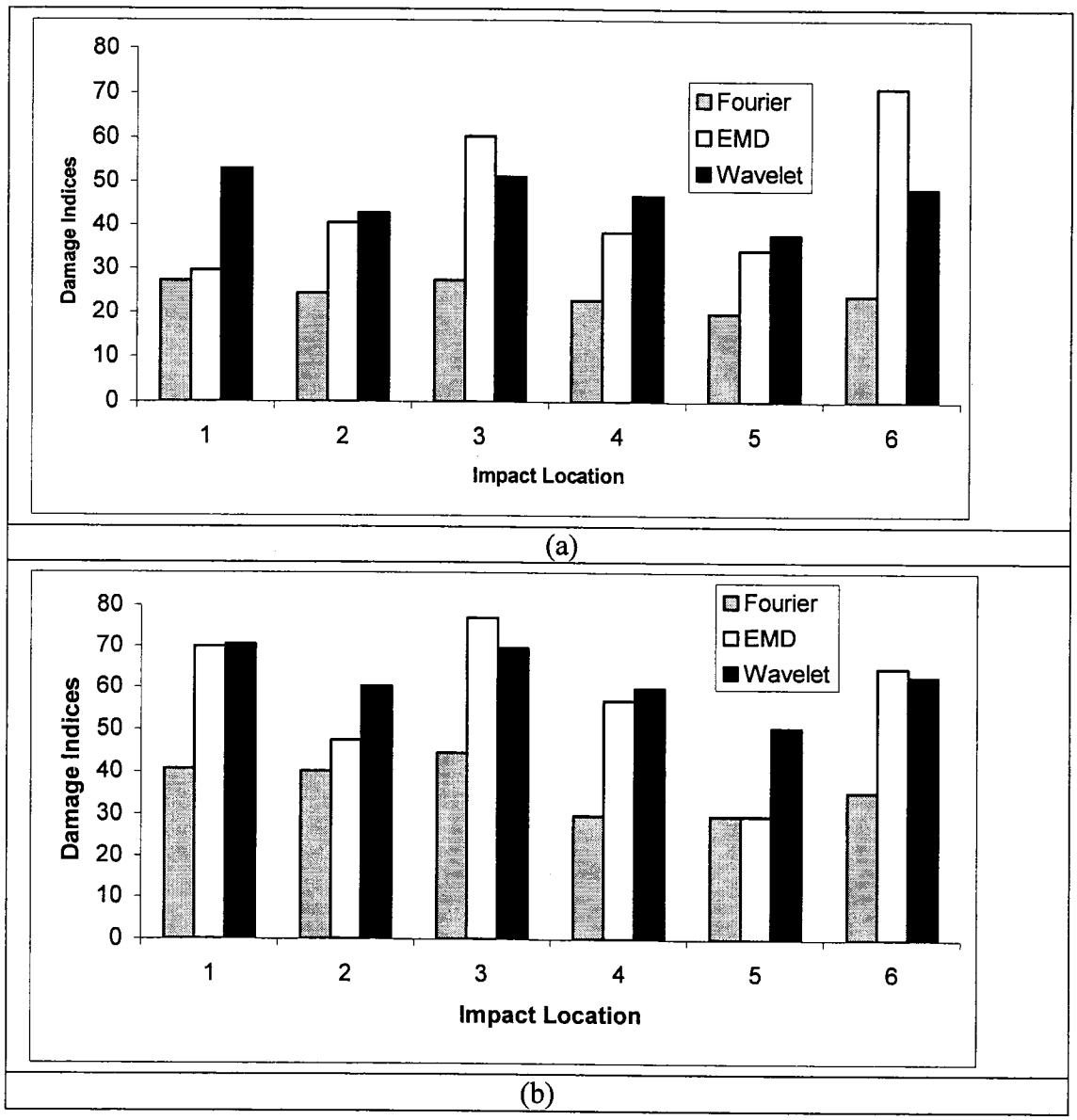

Figure 9.8: Comparison of the damage indices of bonded and debonded sensor with different method : (a) sensors located on the bonded region and (b) sensors located on the disbonded region

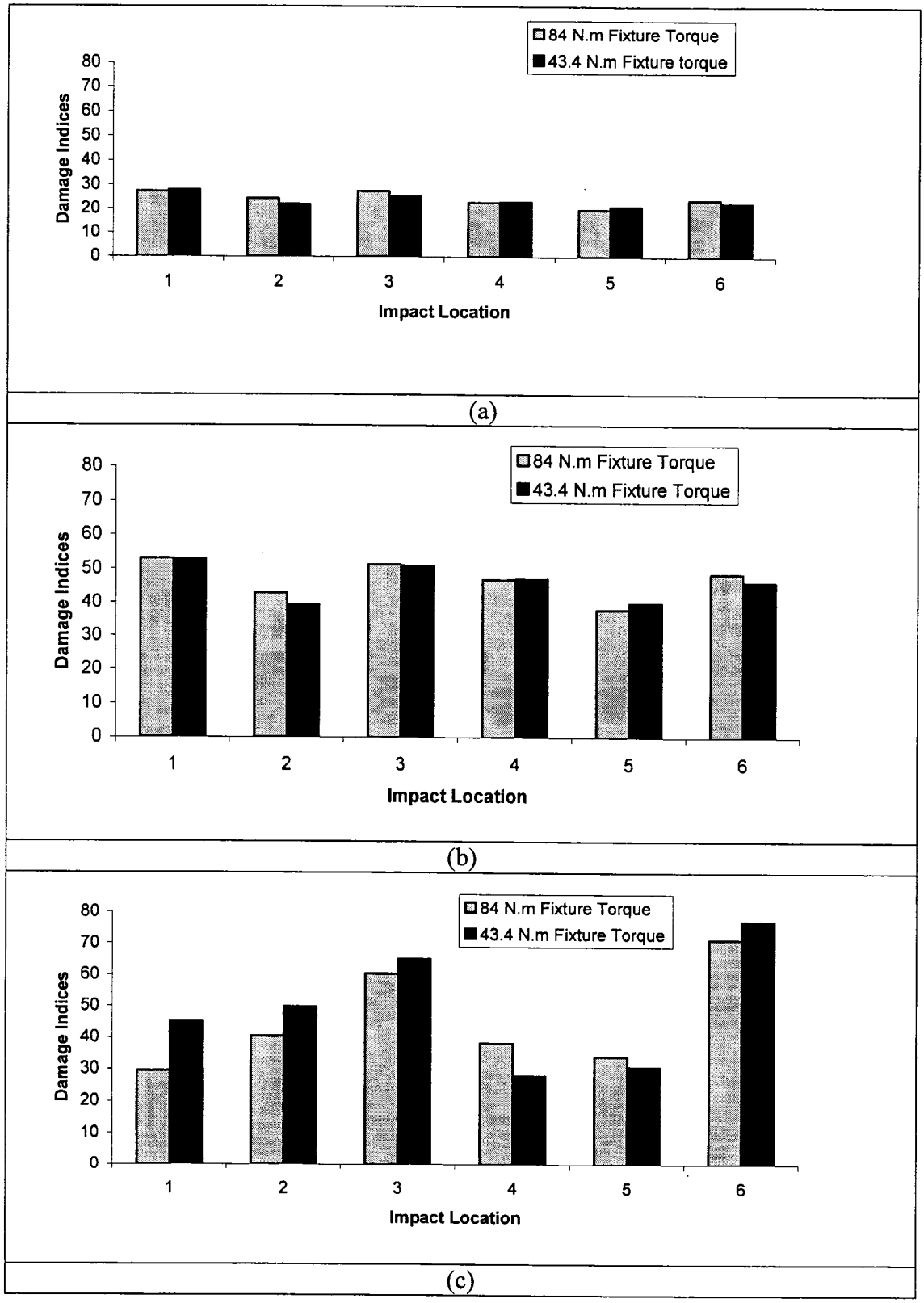

Figure 9.9: Comparison of the damage indices for different degree of support condition: (a) FFT, (b) Wavelet and (c) EMD

9.9 References

Guyott C.C.H; Adams. R. D, "Use of the Fokker Tester Joints with Varying Adhesive Thickness", Proceedings of the institution of Mechanical Engineering, Part B: Management and Engineering, n1, V201, P41-49

Wegman RF, Tullos TR. Nondestructive inspection, Chapter 11. Handbook of adhesive bonded structural repair. Park Ridge, NJ: Noyes Publ. 1992.

Bakis CE, Reifsnider KL. "Adiabatic Thermoelastic Measurements," Section VIIB of *Manual on Experimental Methods for Mechanical Testing of Composites*, R.L. Pendleton and M.E. Tuttle, Eds., Soc. for Experimental Mechanics, Bethel, PA, 1989.

Bar-Cohen Y, Mal AK. Nondestructive inspection and quality control- end-product Nondestructive evaluation of adhesive-bonded composite joints. Section 9. Adhesives and sealants, vol. 3, Engineered materials handbook, Cleveland, OH: ASM Int., 1990. p. 777-84.

Z. Sun and C. C. Chang " Structural Damage Assessment Based on Wavelet Packet Transform", Journal of Structural Engineering, 128(10), 1354-1361, 2002.

Huang, N.E, Shen, Z., Long, S.R., Wu, M.C., Shih H.H., Zheng Q., Yen N-C, Tung C.C., and Liu H.H. "The empirical mode decomposition and Hilbert spectrum for nonlinear and non-stationary time series analysis". Proceedings of the Royal Society of London—Series A, 1998, 454: 903–995.

Huang N.E., Shen Z., and Long S.R. A new view of nonlinear water waves: the Hilbert spectrum. Annual Review of Fluid Mechanics 1999, 31: 417– 457.

Huang, K. A nondestructive instrument bridge safety inspection system (NIBSIS) using a transient load. US patent No. 09=210.693, 1998

Chapter 10

Conclusions

10.1 Conclusions

This dissertation presented a set of new methodologies and approaches for damage detection and structural health monitoring. The procedure is based on recording the vibration response of the healthy structure, and the structure in its damage state, through piezoelectric sensors, followed by evaluating the so called "damage energy indices" through various signal analysis applications.

The application of the proposed methodology applied to various PVC pipe structures, revealed the following:

1) The Empirical Mode Decomposition (EMD) in conjunction with the Hilbert-Huang transform proved to be an effective tool for system identification.

2 (a) The proposed approach for calculating the damping of PVC pipes based on empirical mode decomposition was found to be very efficient in conjunction with the output voltage of piezoelectric sensors. It was noticed that although both pure time-domain method (i.e., LDA) and pure frequency-domain method (i.e., HPB) could produce consistent and acceptable results, the mixed time-frequency methods (i.e., HTA, EMD and MBA) produced more acceptable results. Therefore, the time-frequency domain approaches summarized above are recommended for evaluating the damping property of such highly damped materials.

(b) The Hilbert-Huang spectral analysis method could be effectively used for the identification of the dynamic characteristics of multi-DOF structural systems. A formulation was developed for evaluating the stiffness, and mass matrices of the

systems, as well as the mode shapes, and damping matrices were developed based on the measured free vibration-time histories of displacements of all degrees of freedom.

(c) Based on the Hilbert-Huang spectral analysis, the natural frequencies and damping ratios of the system could be effectively calculated based on the data collected through only one single sensor used for measuring the free vibration-time history of the system (conversely, only at one single location).

3) One can effectively establish the presence of damage and its location by using the proposed damage index based on the empirical mode decomposition and first intrinsic mode function.

4) The proposed approaches for damage detection based on wavelet, wavelet packet, FFT energy and FFT integration were found to be accurate enough to locate damage location and its intensity. Among the mentioned methodologies, the wavelet transform proved to be the most sensitive methods in detecting the location of the damage.

5) In comparing the above proposed damage indices with that based on EMD, the EMD and wavelet transform proved to be the most sensitive and effective methods in detecting damage location, and EMD proved to be the most effective method for finding the severity of damage.

6 (a) The proposed approaches for damage detection in pipe joints were found to be a very economical, efficient, and user-friendly capable of producing excellent results. The proposed approach used the time history response captured by piezoelectric sensors and the Fourier analysis, as well as the energy-based damage indices to identify the degradation of an adhesively bonded joint.

b) In the adhesively bonded pipe joints, the optimal location for the piezoelectric sensor was found to be situated directly on the joint. The proposed damage detection system, could effectively determine the presence of damage, as

well as a quantitative measure of its severity. It was also found that the sensor could be located anywhere on the joint and good result could still be obtained. Moreover, the ability of this method to detecting damage was not influenced by the location of the excitation force, damage location, or the support conditions. More pronounce, it was found that for the given set-up a more pronounced damage index was found when the following conditions hold:

a) More rigid support conditions

b) And the sensor was located in the vicinity of the damage. The later one would however be impractical in real applications.

(c) With the proposed damage detection method, it was found that only a single sensor would be all that is required to produce practical results. In the case of the adhesively bonded joints, a single sensor could be located on the joint to produce good results even though it may not be located directly on the damaged section.

10.2 Recommendations for Future Work

The work performed in this thesis produced a methodology for health monitoring of structures based on the proposed damage indices based on vibration signals obtained through piezoelectric sensor. The damage detection method that was implemented in this thesis showed excellent results for the condition considered within laboratory scaling. However, this applicability of the proposed method should be verified when applied to real structures, so that the influence of loading under natural conditions, as well as the environmental effects could be verified.

Today, the biggest challenge in structural health monitoring is to find a way to monitor the structures without instrumenting and interfering with the structure. Therefore, application of such instruments like the laser Doppler vibrometer should be explored in the future.

References

Adams, R. D., Cawley, P., Pye, C. J. and Stone, B. J., 1978, "A vibration technique for nondestructively assessing the integrity of structures," *Journal of Mechanical Engineering Science*, Vol. 20, pp. 93–100.

Adeli, H., (2001), "Neural networks in civil engineering: 1989-2000", *Computer-Aided Civil and Infrastructure Engineering*, 16(2), pp. 126-142.

Aktan, A. E., Lee, K. L., Chuntavan, C., and Aksel, T., 1994, "Modal Testing for Structural Identification and Condition Assessment of Constructed Facilities," in *Proc. of 12th International Modal Analysis Conference*, pp. 462–468.

Allen, J. B., and Rabiner, L. R., (1977), "A Unified Approach to Short-time Fourier Analysis and Synthesis," *Proc. IEEE*, Vol. 65, No. 11, pp. 1558-1564

Allik, H. & Hughes, T. J. R., 1970, 'Finite element method for piezoelectric vibration', *International Journal for Numerical Methods in Engineering*, 2:151–157.

Ayres, J. W., Lalande, F., Chaudhry, Z. and Rogers, C. A., 1998. "Qualitative impedance-based health monitoring of civil infrastructures", *Smart Mater. Struct.* 7, 599-605.

B. Jawerth and W. Sweldens, An overview of wavelet based multiresolution analysis,*SIAM Rev.*,36 (1994), pp. 377–412.http://cm.bell-labs.com/who/wim/papers/papers.html.

Bakis CE, Reifsnider KL. "Adiabatic Thermoelastic Measurements," Section VIIB of *Manual on Experimental Methods for Mechanical Testing of Composites*, R.L. Pendleton and M.E. Tuttle, Eds., Soc. for Experimental Mechanics, Bethel, PA, 1989.

Balis Crema, L., Castellani, A., and Coppotelli, G., 1995, "Generalization Of Non Destructive Damage Evaluation Using Modal Parameters," in *Proc. of the 13th International Modal Analysis Conference*, pp. 428–431.

Bar-Cohen Y, Mal AK. Nondestructive inspection and quality control- end-product Nondestructive evaluation of adhesive-bonded composite joints. *Section 9. Adhesives and sealants, vol. 3, Engineered materials handbook*, Cleveland, OH: ASM Int., 1990. p. 777-84.

Begg, R. D., Mackenzie, A. C., Dodds, C. J., and Loland, O., 1976, "Structural Integrity Monitoring Using Digital Processing Of Vibration Signals," in *Proc. 8th Annual Offshore Tech. Conf.*, pp. 305–311.

Bendat, J. S. & Piersol, A. G. 1986 *Random data: analysis and measurement procedures*, 2nd edn.New York: Wiley.

Bhalla, 2000. "Smart system based automated health monitoring of structure", Master of Engineering Dissertation Nanyang Technological University, Singapore.

Boashash, B. 1992 Estimating and interpreting the instantaneous frequency of a signal. I. Fundamentals.*Proc. IEEE* 80, 520–538.

Bracewell, R. (1999) *The Fourier Transform and Its Applications,* 3rd ed. McGraw-Hill, New York:.

Brincker, R., Kirkegaard, P. H., Anderson, P., and Martinez, M. E., 1995, "Damage Detection In An Offshore Structure," in *Proc. of the 13th International Modal Analysis Conference*, pp. 661–667.

Brockwell, P. J. & Davis, R. A. 1991 *Time series: theory and methods*. New York: Springer.

Cawley, P. and Adams, R. D., 1979, "The Locations Of Defects In Structures From Measurements Of Natural Frequencies," *Journal of Strain Analysis*, Vol. 14, No. 9, pp. 49–57, 1979.

Chance, J., Tomlinson, G. R., and Worden, K., 1994, "A Simplified Approach To The Numerical And Experimental Modeling Of The Dynamics Of A Cracked Beam," in *Proc. of the 12th International Modal Analysis Conference*, pp. 778–785.

Chattopadhyay, A., Li, J. & Haozhong, G., 1999, 'Coupled thermo-piezoelectric-mechanical model for smart composite laminate', *AIAA Journal*, 37(12).

Chen, H., Tsai, K., Qi, G., Yang, J., and Amini, F., (1995), "Neural Network for Structure Control", *Journal of Computing in Civil Engineering*, 9(2), pp. 168-176.

Chen, S.-H., Wang, Z.-D. & Liu, X.-H., 1997, 'Active vibration control and suppression for intelligent structures', *Journal of Sound and Vibration*, 200(2):167–177.

Chen, Y., and Swamidas, A. S. J., 1994, "Dynamic Characteristics And Modal Parameters Of A Plate With A Small Growing Surface Crack," in *Proc. of the 12th International Modal Analysis Conference*, pp. 1155–1161.

Cheraghi N., Zou G. P. and Taheri F., (2005), Piezoelectric-Based Pipeline Damage Assessment Using Fourier and Wavelet Analyses, *International Journal of Computer-Aided Civil and Infrastructure Engineering*, 20: 369-382.

Chiang L., Russell E. and Braatz R., (2001), "Fault Detection and Diagnosis in Industrial Systems", *Springer Verlag*.

Cobb, R. G., and Liebst, B. S., 1997a, "Structural Damage Identification Using Assigned Partial Eigenstructure," *AIAA Journal*, Vol. 35, No. 1, pp. 152-158.

Cohen, L. 1995 *Time-frequency analysis*. Englewood Cliffs, NJ: Prentice-Hall.

Coppolino, R. N. and Rubin, S., 1980, "Detectability of Structural Failures in Offshore Platforms by Ambient Vibration Monitoring," in *Proc. 12th Annual Offshore Tech.Conf.*, 101–110.

Crawley, E. F. & de Luis, J., 1987, 'Use of piezoelectric actuators as elements of intelligent structures', *AIAA Journal*, 25(10):1373–1385.

Crohas, H., and Lepert, P., 1982, "Damage-Detection Monitoring Method For Offshore Platforms Is Field-Tested," *Oil & Gas Journal*, Feb., Vol. 22, pp. 94–103.

Daubechies, I., (1992), "*10 Lectures on Wavelets*", Capital City Press.

Dellomo, M., (1999), 'Helicopter gearbox fault detection: a neural network based approach', *Journal of Vibration and Acoustics, Transactions of the ASME*, 121(3), pp 265-272.

Deng, Y., Wang W., Qian C., and Dai, D. (2001) _Boundary-processing technique in EMD method and Hilbert transform. _*Chinese Science Bulletin*, 46(3):954–961.

DeVore, Ronald A.; Jawerth, Bjorn; Lucier, Bradley J., 1992 "Image compression through wavelet transform coding", IEEE Transactions on Information Theory, Vol 38, pp. 719-746.

Doebling, S. W., Farrar, C. R., Prime, M. B., and Shevitz, D. W., 1996a, "Damage Identification and Health Monitoring of Structural and Mechanical Systems

from Changes in their Vibration Characteristics: A Literature Review", *Los Alamos National Laboratory report LA-13070-MS.*

Doebling, S. W., Hemez, F. M., Peterson, L. D., and Farhat, C., 1997b, "Improved Damage Location Accuracy Using Strain Energy-Based Mode Selection Criteria," *AIAA Journal*, Vol. 35, No. 4, pp. 693-699.

Dong C., Zhang, P. Q., Feng, W. Q., and Huang, T. C., 1994, "The Sensitivity Study Of The Modal Parameters Of A Cracked Beam," in *Proc. of the 12th International Modal Analysis Conference*, pp. 98–104.

Drazin, P. G. 1992 *Nonlinear systems*. Cambridge University Press.

Duggan, D. M., Wallace, E. R., and Caldwell, S. R., 1980, "Measured and Predicted Vibrational Behavior of Gulf of Mexico Platforms," in *Proc. 12th Annual Offshore Tech.Conf.*, pp. 92–100.

Eer Nisse, E. P., 1967, 'Variational method for electroelastic vibration analysis', *IEEE Transactions On Sonics And Ultrasonics*, 14(4):153–160.

Ewins, D. J., 1984, *Modal Testing: Theory and Practice*, John Wiley and Sons, New York.

Fahey S. O'F. and Pratt J. (1998a) "Frequency Domain Modal Estimation Techniques", *Experimental Techniques*, 33-37, September/October.

Fahey S. O'F. and Pratt J. (1998b) "Time Domain Modal Estimation Techniques", *Experimental Techniques*, 45-49, November/December.

Farrar, C. R., and Jauregui, D. V., 1996, "Damage Detection Algorithms Applied To Experimental And Numerical Modal Data From The I-40 Bridge," *Los Alamos National Lab report LA-13074-MS.*

Flandrin, P., Rilling, G. and Goncalves, P. (2004) _Empirical mode decomposition as a filter bank._ *IEEE Signal Processing Letters*, 11(2):112–114.

Forward, R., 1981, 'Electronic damping of orthogonal bending modes in a cylindrical mast experiment', *AIAA Journal of Spacecraft*, 18(1):11–17.

Fox, C. H. J., 1992, "The Location Of Defects In Structures: A Comparison Of The Use Of Natural Frequency And Mode Shape Data," in *Proc. of the 10th International Modal Analysis Conference*, pp. 522–528.

Friswell, M. I., Penny, J. E. T., and Wilson, D. A. L., 1994, "Using Vibration Data And Statistical Measures To Locate Damage In Structures," *Modal Analysis: The International Journal of Analytical and Experimental Modal Analysis*, Vol. 9, No. 4, pp. 239–254.

Fuller, C. R., Snyder, S. D., Hansen, C. H. and Silcox, R. J., (1990). Active control of interior noise in model aircraft energies using piezocermatic actuators", Paper 90-3922, *AIAA 13th Aeroacoustics Conference, Tallahassee, FL*

Giurgiutiu, V. and Rogers, C. A., 1997. "Electromechanical (E/M) impedence method for structural health monitoring and non-destructive evaluation", *Proc. 1st Int. Workshop on Structural Health Monitoring (California: Stanford University),* 433-44.

Giurgiutiu, V. and Rogers, C. A., 1998. "Recent advancements in the electro-mechanical (E/M) mpedance method for structural health monitoring and NDE", *Smart Structures and Materials Conf. (San Diego, California), Proc. SPIE* 3329, 536-47.

Goswami, J., and Chan, A., (1999), "*Fundamentals of Wavelets*: Theory, Algorithms and Applications", Wiley-Interscience.

Gudmundson, P., 1982, "Eigenfrequency Changes Of Structures Due To Cracks, Notches, or Other Geometrical Changes," *Journal of the Mechanics and Physics of Solids*, Vol. 30, No. 5, pp. 339–353.

Ha, S. K., Keilers, C. & Chang, F. K., 1992, 'Finite element analysis of composite structures containing distributed piezoceramic sensors and actuators', *AIAA Journal,* 30(3):772–780.

Hahn, S.J. (1996) "The Hilbert transform of the product $a(t)\cos(\omega_0 t + \phi_0)$" *Bulletin of the Polish Academy of Science*, 1996, **44**(1), 75–80.

Hammond, C.E. and Doggett, R.V. (1975) "Determination of Subcritical Damping by Moving-Block/ Random Applications" *National Aeronautics and Space administration symposium on Flutter Testing Techniques, NASA* **CP-415**, 59-76.

Han, C., Guo, H., Wang, C , Fan. D, and Sang, H. (2003) Multiscale edge detection based on EMD. *High technology letters (Chinese version)*, 6:13–17.

Haykin, S., (1998). "*Neural Networks: A Comprehensive Foundation (2nd Edition)*", Pearson Education.

Harris, Michael C.; Blotter, Jonathan D, 2005.; Sommerfeldt, Scott D.; De Bree, Hans-Elias, "Nearfield acoustic holography using energy-based measurements", Proceedings of the ASME International Design Engineering Technical Conferences and Computers and Information in Engineering Conference - DETC2005, Vol.1A, pp. 39-43.

Hearn, G. and Testa, R. B., 1991, "Modal Analysis For Damage Detection In Structures," *Journal of Structural Engineering*, Vol. 117, No. 10, pp. 3042–3063.

Hera A., and Hou Z., (2003). "Application of Wavelet Approach for ASCE Structural Health Monitoring Benchmark Studies", *ASCE Journal of Engineering Mechanics Vol.* 130, No. 1, pp. 96-104.

Hera, A. and Hou, Z., (2003), "Detecting Progressive Damage by Wavelet Approach", *Journal of Sound and Vibration*, (submitted)

Heyliger, P., Pei, K. C. & Saravanos, D., 1996, 'Layerwise mechanics and finite element model for laminated piezoelectric shells', *AIAA Journal*, 34(11):2353–2360.

Hilbert-Huang Transform to the analysis of molecular dynamic simulations. *J. Phys. Chem.*, A (107): 4869–4876.

Hong, C.-H. & Chopra, I., 1999, 'Modeling and validation of induced strain actuation of composite coupled plates', *AIAA Journal*, 37(3).

Hou, Z., Noori S. and Amand, St. R., (2000). "A Wavelet-Based Approach for Structural Damage Detection", *ASCE Journal of Engineering Mechanics,* Vol. 126, pp. 667-683.

Hu, N. and Fukunaga, H., (2001). "Structural damage identification using piezoelectric sensors", *Advanced Nondestructive Evaluation for Structural and Biological Health Monitoring, Proc. of SPIE*, 4335,371-382.

Huang et al, (1998), "The Empirical Mode Decomposition Method and the Hilbert Spectrum for Non-linear and Non-stationary Time Series Analysis", *Proc. R. Soc. Lond* , Vol. 454, pp. 903-995.

Huang N.E., Shen Z., and Long S.R. (1999) "A new view of nonlinear water waves: the Hilbert spectrum". *Annual Review of Fluid Mechanics*, **31,** 417– 457.

Huang, K. A nondestructive instrument bridge safety inspection system (NIBSIS) using a transient load. US patent No. 09=210.693, 1998.

Huang, W., Shen, Z., Huang, N.E., and Fung, Y.C. (1998) Engineering analysis of biological variables: An example of blood pressure over 1 day. *Proc. Natl. Acad. Sci. USA*, 95:4816–4821.

Huang, W., Shen, Z., Huang, N.E., and Fung, Y.C. (1999) Nonlinear indicial response of complex nonstationary oscillationsas pulmonary hypertension responding to step hypoxia. *Proc. Natl. Acad. Sci. USA*, 96:1834–1839.

Hughes, T. J. R., 1987, *The Finite Element Method, Prentice-Hall International Editions.*

Hunt, D. L., Weiss, S. P., West, W. M., Dunlap, T. A., and Freemeyer, S. R., 1990, "Development and implementation of a shuttle modal inspection system," *Sound and Vibration.*

Hwang, W. S. & Park, H. C., 1993, 'Finite element modeling of piezoelectric sensors and actuators', AIAA Journal, 31(5):930–937.

Iglasias, A.M. (2000) Investigating Various Modal Analysis Extraction Techniques to Estimate Damping Ratio. Masters thesis, Department of Mechanical Engineering, Virginia Polytechnic Institute and State University, Blacksburg, Virginia.

Imregun M. (1991) "A Comparison of SDOF and Global MDOF Modal Analysis Techniques when applied to a Lightly-Damped Linear Structure", *Proceedings of the International Modal Analysis Conference*, 435-441.

Jian, X. H., Tzou, H. S., Lissenden, C. J. and Penn, L. S., (1997). "Damage detection by piezoelectric patches in a free vibration method", *Journal of Composite Materials*, 31(4), 345-359.

Jawerth, Bjorn; Sweldens, Wim, 1994, "Overview of wavelet based multiresolution analyses", SIAM Review, Vol 36, No. 3, pp. 377-412.

Juneja, V., Haftka, R. T., and Cudney, H. H., 1997, "Damage Detection and Damage Detectability: Analysis and Experiments," *Journal of Aerospace Engineering*, Vol. 10, No. 4, pp. 135-142.

K¨oppe, H., Gabbert, U. & Tzou, H. S., 1998, 'On three-dimensional layered shell elements for the simulation of adaptive structures', *in Proceedings of the Euromech 373 Colloquium: Modeling and Control of Adaptive Mechanical Structures - Preprint, ADAMES, University of Magdeburg.*

Kam, T. Y. and Lee, T. Y., 1992, "Detection Of Cracks In Structures Using Modal Test Data," *Engineering Fracture Mechanics*, Vol. 42, No. 2, pp. 381–387.

Karnopp, D.C., Margolis, D.L., and Rosenberg, R.C. (2000) *System Dynamics: Modeling and Simulation Of Mechatronic Systems*, Third Edition, John Wiley & Sons, Inc., Canada.

Keilers, C. H. J. and Chang, F. K., (1995a). "Identifying delamination in composite beams using built-in piezoelectrics: Part I-experiments and analysis", *Journal of Intelligent Materials Systems and Structures*, 6, 649-663.

Keilers, C. H. J. and Chang, F. K., (1995b). "Identifying delamination in composite beams using built-in piezoelectrics: Part II-an identification method", *Journal of Intelligent Materials Systems and Structures*, 6, 664-672.

Keilers, C. H. J. and Chang, F. K., 1993. "Damage detection and diagnosis of composite using bull-in piezoceramics", *Proceeding of SPIE-The International Society for Optical Engineering Smart Structures and Intelligent Systems*, 1917, 1009-1015.

Kenley, R. M. and Dodds, C. J., 1980, "West Sole WE Platform: Detection of Damage by Structural Response Measurements," in *Proc. of the 12th Annual Offshore Tech. Conf.*, pp. 111–118.

Kerezsi, B., and Howard, I., (1995), "Vibration Fault Detection of Large Turbo-generators using Neural Networks", *IEEE International Conference on Neural Networks - Conference Proceedings*, 1, pp. 121-126.

Kim, J.-H., Jeon, H.-S., and Lee, C.-W., 1992, "Application Of The Modal Assurance Criteria For Detecting And Locating Structural Faults," in *Proc. 10th International Modal Analysis Conference*, pp. 536–540.

Ko, J. M., Wong, C. W., and Lam, H. F., 1994, "Damage Detection In Steel Framed Structures By Vibration Measurement Approach," in *Proc. of 12th International Modal Analysis Conference*, pp. 280–286.

Koh, C. G., See, L. M., and Balendra, T., 1995, "Damage Detection of Buildings: Numerical and Experimental Studies," *Journal of Structural Engineering-ASCE*, Vol. 121, No. 8, pp. 1155-1160.

Kondo, I. and Hamamoto, T., 1994, "Local Damage Detection Of Flexible Offshore Platforms Using Ambient Vibration Measurements," in *Proc. of the 4th International Offshore and Polar Engineering Conf.*, Vol. 4, pp. 400–407.

Lam, H. F., Ko, J. M., and Wong, C. W., 1995, "Detection of Damage Location Based on Sensitivity Analysis," in *Proc. of the 13th International Modal Analysis Conference*, pp. 1499–1505.

Lam, H.F., Katafygiotis, L.S., and Mickleborough N.C., (2004), "Application of a Statistical Model Updating Approach on Phase I of the IASC-ASCE Structural Health Monitoring Benchmark Study", *Journal of Engineering Mechanics*, Vol 130, No. 1, pp. 34-48.

Lazan, B.J. (1968) *Damping of Materials and Members in Structural Mechanics*, Pergamon Press, Oxford, UK.

Lee, H.-J. & Saravanos, D. A., 1996, 'Coupled layerwise analysis of thermopiezoelectric composite beams', *AIAA Journal*, 34(6):1231–1237.

Lei et al, (2003), "An Enhanced Statistical Damage Detection Algorithm Using Time Series Analysis", *Proceedings of the 4th International Workshop on Structural Health Monitoring*, Stanford, CA, USA.

Lerch, R., 1990, 'Simulation of piezoelectric devices by two- and three-dimensional finite elements', *IEEE Transactions on Ultrasonics, Ferroelectrics, and Frequency Control* , 37(3):233– 247.

Liang , Y., Zhou, C., and Wang Z., (1997), "Identification of restoring forces in non-linear vibration systems based on neural networks", *Journal of Sound and Vibration*, 206(1), pp 103-108.

Lifshitz, J. M. and A. Rotem, 1969, "Determination Of Reinforcement Unbonding Of Composites By A Vibration Technique," *Journal of Composite Materials*, Vol. 3, pp. 412–423.

Loh, C.H., Wu, T.C., and Huang, N.E. (2001) Application of EMD+HHT method to identify near-fault ground motion characteristics and structural responses. *BSSA, Special.*

Loix, N., Piefort, V. and Preumont, A., 1998, 'Modeling aspects of active structures with collocated piezoelectric actuators and sensors', Benelux Quarterly *Journal on Automatic Control (Journal a),* 39(1).

Loland, O. and Dodds, J. C., 1976, "Experience in developing and operating integrity monitoring system in north sea," in *Proc. of the 8th Annual Offshore Tech. Conf.*, pp. 313–319.

Long, S. R., Huang, N. E., Tung, C. C., Wu, M. L., Lin, R. Q., Mollo-Christensen, E. and Yuan, Y. 1995 The Hilbert techniques: an alternate approach for non-steady time series analysis. *IEEE Geoscience Remote Sensing Soc. Lett.* **3**, 6–11.

Lus, H., Betti, R., Longman, R.W. (1999). "Identification of Linear Structural Systems using Earthquake-Induced Vibration Data", *Journal of Earthquake Eng and Structural Dynamics,* Vol. 28, pp.1449 –1467.

Majumdar, P.M. and Suryanarayan, 1988. "Flexural vibrations of beams with delaminations", *Journal of Sound and Vibration* 195, 977-993.

Mallat S., 1999. *Wavelet Tour of Signal Processing (Wavelet Analysis & Its Applications)*, 2nd Edition, Academic Press, California, USA.

Mathsoft. http://www.mathsoft.com/wavelets.html.

Mayes, R. L., 1992, "Error Localization Using Mode Shapes–An Application To A Two Link Robot Arm," in *Proc. 10th International Modal Analysis Conference*, pp. 886–891.

Mayes, R. L., 1995, "An Experimental Algorithm For Detecting Damage Applied To The I-40 Bridge Over The Rio Grande," in *Proc. 13th International Modal Analysis Conference*, pp. 219–225.

Melhem, H. and Kim, H., 2003. "Damage detection in concrete by Fourier and wavelet analysis", *ASCE Journal of Engineering Mechanics*, 129(5), 571-577.

Migliori, A., Bell, T. M., Dixon, R. D., and Strong, R., 1993, "Resonant Ultrasound Non-Destructive Inspection," *Los Alamos National Laboratory report LA-UR-93-225.*

Mindlin, R. D., 1974, 'Equations of high frequency vibrations of thermopiezoelectric crystal plates', *International Journal of Solids Structure*, 10:625–637.

Moetakef, M. A., Joshi, S. P. & Lawrence, K. L., 1996, 'Elastic wave generation by piezoceramic patches', *AIAA Journal*, 34(10):2110–2117.

Moetakef, M. A., Lawrence, K. L., Joshi, S. P. & Shiakolas, P. S., 1995, 'Closed-form expressions for higher order electroelastic tetrahedral elements', *AIAA Journal*, 33(1):136–142.

Monkhouse R.S.C., Wilcox P.W., Lowe M.J.S., Dalton R.P., and P. Cawley. "The rapid Monitoring of Structures using Interdigital Lamb Wave Transducers." *Smart Materials and Structures*, v.9, 2000, 304-309.

Morassi, A., Rovere, N., 1997, "Localizing a Notch in a Steel Frame from Frequency Measurements," *Journal of Engineering Mechanics-ASCE*, Vol. 123, No. 5, pp. 422-432.

Naghipour M., Zou GP. and Taheri F. (2005) "Evaluation of Vibration Damping of GRP reinforced Glulam Composite Beams". *ASCE Journal of Engineering Mechanics, in press.*

Narkis, Y., 1994, "Identification Of Crack Location In Vibrating Simply Supported Beams," *Journal of Sound and Vibration*, Vol. 172, No. 4, pp. 549–558.

Nataraja, R., 1983, "Structural integrity monitoring in real seas," in *Proc. 15th Annual Offshore Tech. Conf.*, pp. 221–228.

Nelles, O., (2000), "*Nonlinear System Identification: From Classical Approaches to Neural Networks and Fuzzy Models*", Springer-Verlag.

Newland, D. E., 1993. An Introduction to Random vibrations, spectral and wavelet analysis, John Wiley & Sons, Inc., New York.

NISA (2004) V.12, Engineering Mechanics Research Corporation, Troy, MI.

Nunes, J.C., Bouaoune, Y., Delechelle, E., Niang, O., and Bunel,P.H. (2003) Image analysis by bidimensional empirical mode decomposition. *Image and Vision Computing*, 21:1019–1026.

Nwosu, D. I., Swamidas, A. S. J., Guigne, J. Y., and Olowokere, D. O., 1995, "Studies On Influence Of Cracks On The Dynamic Response Of Tubular T-Joints For Nondestructive Evaluation," in *Proc. of the 13th International Modal Analysis Conference*, pp. 1122–1128.

Paget, C. A., Grondel, S. and Delebarre, C., 2003. "Damage assessment in composites by Lamb waves and wavelet coefficients", *Smart Materials and Struct.*, 12, 393-402.

Pandey A. K. and Biswas, M., 1995, "Damage Diagnosis of Truss Structures by Estimation of Flexibility Change," *Modal Analysis – The International Journal of Analytical and Experimental Modal Analysis*, Vol. 10, No. 2, pp. 104-117.

Pandey, A. K., and Biswas, M., 1994, "Damage Detection In Structures Using Changes In Flexibility," *Journal of Sound and Vibration*, Vol. 169, No. 1, pp. 3–17.

Pandey, A. K., Biswas, M., and Samman, M. M., 1991, "Damage Detection From Changes In Curvature Mode Shapes," *Journal of Sound and Vibration*, Vol. 145, No. 2, pp. 321–332.

Penny, J. E. T., Wilson, D. A. L., and Friswell, M. I., 1993, "Damage Location In Structures Using Vibration Data," in *Proc. of the 11th International Modal Analysis Conference*, Vol. 1923, n pt 2, pp. 861–867.

Peterson, L. D., Doebling, S. W., and Alvin, K. F., 1995, "Experimental Determination Of Local Structural Stiffness By Disassembly Of Measured Flexibility Matrices," in *Proc. of 36th AIAA/ASME/ASCE/AHS/ASC Structures, Structural Dynamics, and Materials Conference*, pp.2756–2766, AIAA-95-1090-CP.

Phillips, S.C., Gledhill, R.G., Essex, J.W., and Edge, C.M. (2003) Application of theTitchmarsh. EC (1948) *Introduction to the Theory of Fourier Integrals*. Oxford University Press.

Piefort, V. & Henrioulle, K., 2000, 'Modelling of smart structures with colocated piezoelectric Actuator/Sensor pairs: Influence of the in-plane components', *5th International Conference on Computational Structures Technology, Leuven, Belgium.*

Preumont, A., 1997, *Vibration Control of Active Structures* - An Introduction, Kluwer Academic Publishers, Dordrecht, The Netherlands.

Qin, S. R. and Zhong, Y. M., 2004. "Research on the unified mathematical model for FT, STFT and WT and its applications", *Mechanical Systems and Signal Processing*, 18, 1335-1347.

R. A. DeVore and B. J. Lucier, Wavelets, Acta Numerica, 1 (1991), pp. 1–56.

Rao, S. S. & Sunar, M., 1993, 'Analysis of distributed thermopiezoelectric sensors and actuators in advanced intelligent structures', *AIAA Journal*, 31(7):1280–1286.

Rao, S.S., and Sunar, M. (1994) "Piezoelectricity and its use in disturbance sensoring and control of flexible structures: a survey." *Appl. Mech.* Rev., 47, 113-136.

Ratcliffe, C. P., 1997, "Damage Detection Using a Modified Laplacian Operator on Mode Shape Data," *Journal of Sound and Vibration*, Vol. 204, No. 3, pp. 505-517.

Rayleigh L. (1945) *Theory of sound* (two volumes). New York: Dover Publications, re-issue, second edition.

Reber, K., Beller, M. and Uzelac, N. I., (2002). How do defect assessment methods influence the choice and construction of in-line inspection tools, *Proceeding of the 4th International Pipeline Conference: 2039-2044, Calgary, Alberta.*

Reddy, J. N., 1984, *Energy and Variational Methods in Applied Mechanics*, John Wiley & sons.

Richardson, M. H. and Mannan, M. A., 1992, "Remote Detection And Location Of Structural Faults Using Modal Parameters," in *Proc. of the 10th International Modal Analysis Conference*, pp. 502–507.

Richart, F.E. Jr., Hall, J.R., and Woods, R.D. (1970) *Vibration of Soils and Foundation.* Prentice-Hall, Inc., Englewood Cliffs, N. J.

Rioul, O., and Vetterli, M., (1991), "Wavelets and Signal Processing", *IEEE SP Magazine* 8(4), pp. 14-38.

Rizos, P. F., Aspragathos, N., and Dimarogonas, A. D., 1990, "Identification Of Crack Location And Magnitude In A Cantilever From The Vibration Modes," *Journal of Sound and Vibration*, Vol. 138, No. 3, pp. 381–388.

Rytter, A., 1993, "Vibration based inspection of civil engineering structure," *Ph. D. Dissertation*, Department of Building Technology and Structural Engineering, Aalborg University, Denmark.

Saadat S., (2003), "Structural Health Monitoring and Detection of Progressive and Existing Damage using Artificial Neural Networks-Based System Identification", *PhD Dissertation, http://www.lib.ncsu.edu/theses/available/etd-03052003-025350/*

Saitoh, M. and Takei, B. T., 1996, "Damage Estimation and Identification of Structural Faults Using Modal Parameters," in *Proc. of the 14th International Modal Analysis Conference*, Dearborn, MI.

Salawu, O. S. and Williams, C., 1994, "Damage Location Using Vibration Mode Shapes," in *Proc. of 12th International Modal Analysis Conference*, pp. 933–939.

Salawu, O. S. and Williams, C., 1995, "Bridge Assessment Using Forced-Vibration Testing," *Journal of Structural Engineering*, Vol. 121, No. 2, pp. 161–173.

Salawu, O. S., 1995, "Nondestructive Assessment Of Structures Using The Integrity Index Method Applied To A Concrete Highway Bridge," *Insight*, Vol. 37, No. 11, pp. 875–878.

Salawu, O. S., 1997a, "Detection of Structural Damage Through Changes in Frequency: A Review," *Engineering Structures*, Vol. 19, No. 9, pp. 718-723.

Salawu, O. S., 1997b, "An Integrity Index Method for Structural Assessment of Engineering Structures Using Modal Testing," *Insight*, Vol. 39, No. 1, pp. 33-37.

Samanta, B., Al-Balushi, K., and Al-Araimi, S., (2004), "Bearing Fault Detection Using Artificial Neural Networks and Genetic Algorithm", *Eurasip Journal on Applied Signal Processing*, 2004(3), pp 366-377.

Samanta, B., Ray, M. C. & Bhattacharyya, R., 1996, 'Finite element model for active control of intelligent structures', *AIAA Journal*, 34(9):1885–1893.

Sanders, D., Kim, Y. I., and Stubbs, R. N., 1992, "Nondestructive Evaluation Of Damage In Composite Structures Using Modal Parameters," *Experimental Mechanics,* Vol. 32, pp. 240–251.

Santamarina, J. C., and Dante, F., (1998). Introduction to Discrete Signal and Inverse Problems in Civil Engineering. *ASCE Press*, Virginia, USA.

Saravanos, D. A., 1997, 'Mixed laminate theory and finite element for smart piezoelectric shell structure', *AIAA Journal*, 35(8):1327–1333.

Saravanos, D. A., 2000, 'Passively damped laminated piezoelectric shell structures with integrated electric networks', *AIAA Journal*, 38(7).

Schwartz, M., Bennett, W. R. & Stein, S. 1966 *Communications systems and techniques*. New York: McGraw-Hill.

Sensor Technology Limited (2001) www.sensortech.ca.

Shekel, J. 1953 'Instantaneous' frequency. *Proc. IRE* 41, 548.

Silcox, R. J., Lefebvre, S., Metcalf, V. L., Beyer, T. B. and Fuller, C. R., (1992). "Evaluation of piezoceramic actuators for control of aircraft interior noise", *Proceedings of the DGLR/AIAA 14th Aeroacoustics Conference, Aachen, Germany*, Number AIAA 92-02-091,pp 542-551.

Skjaeraek, P. S., Nielsen, S. R. K., and Cakmak, A. S., 1996b, "Identification of Damage in Reinforced-Concrete Structures from Earthquake Records: Optimal Location of Sensors," *Soil Dynamics and Earthquake Engineering*, Vol. 15, No. 6, pp. 347-358.

Skjaerbaek, P. S., Nielsen, S. R. K., and Cakmak, A. S., 1996a, "Assessment Of Damage In Seismically Excited RC-Structures From A Single Measured Response," in *Proc. of the 14th International Modal Analysis Conference*, pp. 133–139.

Smith, S. W. and Beattie, C. A., 1991a, "Model Correlation and Damage Location for Large Space Truss Structures: Secant Method Development and Evaluation", *NASA report NASA-CR-188102.*

Soh, C. K., Tseng, K. K. H, Bhalla, S. and Gupta, A., 2000. "Performance of smart piezoceramic transducers in health monitoring of RC bridge", *Smart Mater. Struct.* 9, 553-42.

Sohn, H., Farrar, C., Hunter, H.. and Worden, K., (2001b), "Applying the LANL Statistical Pattern Recognition Paradigm for Structural Health Monitoring to Data from a Surface-Effect Fast Patrol Boat". *Los Alamos National Laboratory Report, LA-13761-MS.*

Sohn. H., Farrar, C., Hunter, N., Worden, K., (2001a), "Structural Health Monitoring using Statistical Pattern Recognition Techniques", *Journal Dyn. Sys. Meas.& Control, Trans. ASME*, Vol. 23, No. 4, pp. 706-711.

Sonti, V. R. and Jones, J. D., 1996. "Dynamic effects of piezoactuators on the cylindrical shell response", *AIAA Journal*, 34(4), 795-801.

Srinivasan, M. G. and Kot, C. A., 1992, "Effects Of Damage On The Modal Parameters Of A Cylindrical Shell," in *Proc. of the 10th International Modal Analysis Conference,* pp. 529–535.

Staszewski, W. J., (1998), "Structural and Mechanical Damage Detection Using Wavelets", *The shock and Vibration Digest,* Vol. 30, pp. 457-472.

Stubbs, N. and Osegueda, R., 1990a, "Global Non-Destructive Damage Evaluation In Solids," *Modal Analysis: The International Journal of Analytical and Experimental Modal Analysis*, Vol. 5, No. 2, pp. 67–79.

Stubbs, N. and Osegueda, R., 1990b, "Global Damage Detection In Solids–Experimental Verification," *Modal Analysis: The International Journal of Analytical and Experimental Modal Analysis*, Vol. 5, No. 2, pp. 81–97.

Stubbs, N., and Kim, J. T., 1996, "Damage Localization in Structures without Baseline Modal Parameters," *AIAA Journal*, Vol. 34, No. 8, pp. 1644-1649.

Stubbs, N., Broome, T.H., and Osegueda, R., 1990, "Nondestructive Construction Error Detection In Large Space Structures," *AIAA Journal*, Vol. 28, No. 1, pp. 146–152.

Stubbs, N., J.-T. Kim, and Topole, K., 1992, "An Efficient And Robust Algorithm For Damage Localization In Offshore Platforms," in *Proc. ASCE Tenth Structures Congress*, pp. 543–546.

Stubbs, N., J.-T. Kim, and Topole, K., 1992, "An Efficient And Robust Algorithm For Damage Localization In Offshore Platforms," in *Proc. ASCE Tenth Structures Congress*, pp. 543–546.

Suleman, A. and Goncalves, M. A., 1995, 'Optimization issues in application of piezoelectric actuators in panel flutter control', IDMEC-Instituto Superior Tecnico, Departamento de Engenharia Mecanica, 1096 Codex, Portugal.

Suleman, A. & Venkayya, V. B., 1995b, 'A simple finite element formulation for a laminated composite plate with piezoelectric layers', *Journal of Intelligent Material Systems and Structures*, 6:776–782.

Sun, F. P., Chaudhry, Z., Rogers, C. A., Majumdar, M. and Liang, C., (1995). "Automated real-time structure health monitoring via signature pattern recognition", *Smart Structures and Material Conference (San Diego, California), Proc. SPIE 2443*: 236-47.

Sun, Z. and Chang, C. C., (2002) Structural damage assessment based on wavelet packet transform", *ASCE Journal of Structural Engineering*, 128(10): 1354-1361.

Sunar, M. and Rao, S. S., 1996, 'Distributed modeling and actuator location for piezoelectric control systems', *AIAA Journal*, 34(10):2209–2211.

Sunar, M. and Rao, S. S., 1997, 'Thermopiezoelectric control design and actuator placement', *AIAA Journal*, 35(3):534–539.

Tasker, F.A. and Chopra, I. (1990) "Assessment of Transient Analysis Techniques for Rotor Stability Testing" *Journal of the American Helicopter Society*, **35** (1), 39-50.

Tiersten, H. F., 1967, 'Hamilton's principle for linear piezoelectric media', *in Proceedings of the IEEE*, pp. 1523–1524.

Titchmarsh, E. C. 1948 *Introduction to the theory of Fourier integrals*. Oxford University Press.

Toksoy, T. and Aktan, A. E., 1994, "Bridge-Condition Assessment By Modal Flexibility," *Experimental Mechanics*, Vol. 34, pp. 271–278.

Topole, K. G. and Stubbs, N., 1995a, "Nondestructive Damage Evaluation of a Structure from Limited Modal Parameters," *Earthquake Engineering and Structural Dynamics*, Vol. 24, No. 11, pp. 1427-1436.

Topole, K. G. and Stubbs, N., 1995b, "Nondestructive Damage Evaluation in Complex Structures from a Minimum of Modal Parameters," *Modal Analysis – The International Journal of Analytical and Experimental Modal Analysis*, Vol. 10, No. 2, pp. 95-103.

Tracy, J. J. and Pardoen, G. C., 1989, "Effect Of Delamination On The Natural Frequencies Of Composite Laminates," *Journal of Composite Materials*, Vol. 23, pp. 1200–1215.

Tseng, K. K. H., Soh, C. K., Gupta, A. and Bhalla, S., (2000). "Health monitoring of civil infrastructure using smart piezoceramic transducers", Proc. 3nd *Int. Conf. On Computational Methods for Smart Structures and Materials Conf. (Madrid, Spain, June 2000),* 153-62.

Tzou, H. S. & Tseng, C. I., 1990, 'Distributed piezoelectric sensor/actuator design for dynamic measurement/control of distributed parameter systems: a piezoelectric finite element approach', *Journal of Sound and Vibration*, 138(1):17–34.

Tzou, H. S. & Tseng, C. I., 1991, 'Distributed modal identification and vibration control of continua: Piezoelectric finite element formulation and analysis', Transactions of the ASME, *Journal of Dynamic Systems, Measurement and Control*, 113:500–505.

Tzou, H. S. & Ye, R., 1996, 'Analysis of piezoelastic structures with laminated piezoelectric triangle shell elements', *AIAA Journal*, 34(1):110–115.

Vandiver, J. K., 1975, "Detection of Structural Failure on Fixed Platforms by Measurement of Dynamic Response," in *Proc. of the 7th Annual Offshore Tech. Conf.*, pp. 243–252.

Vandiver, J. K., 1977, "Detection of Structural Failure on Fixed Platforms by Measurement of Dynamic Response," *Journal of Petroleum Technology*, Vol 29, March, pp. 305–310.

Ville, J., (1948), " Theorie et application de la notion de signal analytical", *Cables et Transmissions* 2A-1, pp. 61-74.

Villemure, I., Ventura, C. E., and Sexsmith, R. G., 1996, "Impact and Ambient Vibration Testing to Assess Structural Damage in Reinforced Concrete Beams," in *Proc. of the 14th International Modal Analysis Conference*, Dearborn, MI.

Vincent, B., Hu, J., and Hou, Z. (1999), "Damage Detection Using Empirical Mode Decomposition Method and a Comparison with Wavelet Analysis",

Proceedings of the Second International Workshop on Structural Health Monitoring, Stanford, pp. 891-900.

Wang, W. and Zhang, A., 1987, "Sensitivity analysis in fault vibration diagnosis of structures," in *Proc. of 5th International Modal Analysis Conference*, pp. 496–501.

Wavelet digest. http://www.wavelet.org.

Wegman RF, Tullos TR. Nondestructive inspection, *Chapter 11. Handbook of adhesive bonded structural repair.* Park Ridge, NJ: Noyes Publ. 1992.

West, W. M., 1984, "Illustration Of The Use Of Modal Assurance Criterion To Detect Structural Changes In An Orbiter Test Specimen," in *Proc. Air Force Conference on Aircraft Structural Integrity*, pp. 1–6.

Whitham, G. B. 1975 *Linear and nonlinear waves*. New York: Wiley.

Whittome T. R., and Dodds, C. J., 1983, "Monitoring Offshore Structures by Vibration Techniques," in *Proc. of Design in Offshore Structures Conference*, pp. 93–100.

Wickerhauser, M. V., (1994). *Adapted Wavelet Analysis from Theory to Software*, A K Peters, Ltd., Wellesley, MA.

Wilkie, G. H., Elam, T. J., and Engen, D. L., (2002). Comparison of crack detection in-line inspection tools, *Proceedings of the 4th International Pipeline Conference, Calgary, Alberta.*

Wojnarowski, M. E., Stiansen, S. G., and Reddy, N. E., 1977, "Structural integrity evaluation of a fixed platform using vibration criteria," in *Proc. 9th Annual Offshore Tech.Conf,* pp. 247–256.

Worden, K., Allen, D., Sohn, H., Stinematers, D. and Farrar C., (2002). "Extreme Value Statistics for Damage detection in Mechanical Structures", *Los Alamos National Laboratory Report, LA-13903-MS.*

Wowk, V., 1991, *Machinery Vibration Measurement and Analysis*, McGraw Hill, Inc. New York.

Xu Y.L., and Chen J. (2004) "Structural Damage Detection Using Empirical Mode Decomposition: Experimental Investigation", *Journal of engineering mechanics*, 130, 1279-1288.

Yang J.N., Lei Y., Pan S., and Huang N. (2003) "System identification of linear structures based on Hilbert-Huang spectral analysis. Part 1: normal modes", *Earthquake engineering and structural dynamics*, 32, 1443-1467.

Yang, J., and Lei, Y., (2000), "System Identification of Linear Structures Using Hilbert Transformation and Empirical Mode Decomposition", *Proceedings of 18th International Modal Analysis Conference, A Conference on Structural Dynamics, San Antonio* I, pp. 213-219.

Yang, J.N., and Lei, Y. (2000) Identification of civil structures with non-proportional damping In Smart Structures and Materials 2000: Smart Systems for Bridges, Structures and Highways. *Proceedings of SPIE, 3988, Newport Beach, CA,* 284–294.

Yang, J.N., Lei, Y., Lin, S., and Huang, N.E. (2004) Identification of natural frequencies and damping of in situ tall buildings using ambient wind vibration data, *Journal of engineering mechanics*, 130:570-577.

Yang, J.N., Lei, Y., Pan, S., Huang, N., (2003), "System Identification of Linear Structures based on Hilbert-Huang Spectral Analysis. Part II: Complex Modes", *Earthquake Engineering & Structural Dynamics*, Vol. 32, No. 10, pp. 1533-1554.

Yang, Z., Qi, D., and Yang, L. (2004) A novel approach for detecting pitch based on Hilbert-Huang Transform. *Technical Report, Sun Yat-sen University.*

Yang, Z., Qi, D., and Yang, L. (2004) A novel automated detection of spindles from seepages based on Hilbert-Huang transform. *Technical Report, Sun Yat-sen University.*

Yao, G. C. C. and Chang, K. C., 1995, "A Study of Damage Diagnosis from Earthquake Records of a Steel Gable Frame," *Journal of the Chinese Institute of Engineers*, Vol. 18, No. 1, pp. 115-123.

Yoshida, I. (2001) Damage detection using Monte Carlo filter based on non-Gaussian noises. *Proceedings of the 8th International Conference on Structural Safety and Reliability, CD ROM.* Royal Swet & Zeitling: the Netherlands, 8pp.

Yuen, K., Beck, J., Katafygiotis, L.S., (2002), "Probabilistic Approach for Modal Identification using Non-stationary Noisy Response Measurements Only", *Earthquake Engineering and Structural Dynamics*, Vol. 31, pp. 1007-1023.

Yuen, M. M. F., 1985, "A Numerical Study of The Eigenparameters Of A Damaged Cantilever," *Journal of Sound and Vibration*, Vol. 103, pp. 301–310.

Z. Sun and C. C. Chang " Structural Damage Assessment Based on Wavelet Packet Transform", *Journal of Structural Engineering*, 128(10), 1354-1361, 2002.

Zhang, Z. and Atkan, A. E., 1995, "The Damage Indices For Constructed Facilities," in *Proc. Of the 13th International Modal Analysis Conference*, pp. 1520–1529.

Zhou, X., Chattopadhyay, A. and Haozhong, G., 2000, 'Dynamic responses of smart composites using a coupled thermo-piezoelectric-mechanical model', *AIAA Journal*, 38(10).

Zienkiewicz, O. C., 1971, The *Finite Element Method in Engineering Science*, Mc Graw-Hill, Maidenhead.

Zimmerman, D. C. and Smith, S.W., 1992, "Model Refinement and Damage Location for Intelligent Structures," from *Intelligent Structural Systems*, H.S. Tzou and G.L. Anderson, Eds., Kluwer Academic Publishers, pp. 403–452.

Zou, Y., Tong, L. and Steven, G. P., (2000). Vibration-base model-dependent damage (delamination) identification and health monitoring for composite structures-a review, *Journal of Sound and Vibration* 230(2): 357-378.